

VU Research Portal

The dynamic organization of the bacterial photosynthetic light-harvesting complexes: fluorescence microspectroscopy

Rutkauskas, D.

2006

document version

Publisher's PDF, also known as Version of record

[Link to publication in VU Research Portal](#)

citation for published version (APA)

Rutkauskas, D. (2006). *The dynamic organization of the bacterial photosynthetic light-harvesting complexes: fluorescence microspectroscopy*.

General rights

Copyright and moral rights for the publications made accessible in the public portal are retained by the authors and/or other copyright owners and it is a condition of accessing publications that users recognise and abide by the legal requirements associated with these rights.

- Users may download and print one copy of any publication from the public portal for the purpose of private study or research.
- You may not further distribute the material or use it for any profit-making activity or commercial gain
- You may freely distribute the URL identifying the publication in the public portal ?

Take down policy

If you believe that this document breaches copyright please contact us providing details, and we will remove access to the work immediately and investigate your claim.

E-mail address:

vuresearchportal.ub@vu.nl

The dynamic organization of the
bacterial photosynthetic light-
harvesting complexes: fluorescence
microspectroscopy

Danielis Rutkauskas

The research described in this thesis was financially supported by the Netherlands Organization for Scientific research (NWO)

This thesis was reviewed by

Prof. R. J. Cogdell, University of Glasgow, UK

Prof. A. Freiberg, University of Tartu, Estonia

Prof. J. Knoester, University of Groningen, The Netherlands

Dr. E. Peterman, Vrije Universiteit, Amsterdam, The Netherlands

Prof. R. van Grondelle, Vrije Universiteit, Amsterdam, The Netherlands

cover design by Nina Petropoulea
printed by PrintPartners Ipskamp B.V., Enschede

VRIJE UNIVERSITEIT

**The dynamic organization of the bacterial photosynthetic
light-harvesting complexes: fluorescence
microspectroscopy**

ACADEMISCH PROEFSCHRIFT

ter verkrijging van de graad Doctor aan
de Vrije Universiteit Amsterdam,
op gezag van de rector magnificus
prof.dr. T. Sminia,
in het openbaar te verdedigen
ten overstaan van de promotiecommissie
van de faculteit der Exacte Wetenschappen
op donderdag 19 januari 2006 om 15.45 uur
in de aula van de universiteit,
De Boelelaan 1105

door

Danielis Rutkauskas

geboren te Vilnius, Litouwen

promotor: prof.dr. R. van Grondelle

to my family

肩つぶり
そろそろのぼれ
富士の山

little snail,
inch by inch,
climb Mount Fuji!
(Kobayashi Issa)

Contents

Abbreviations	ix
1. Introduction	11
2. Experimental setup	35
3. Fluorescence spectral fluctuations of single LH2 complexes from <i>Rhodospseudomonas acidophila</i> strain 10050	53
4. Fluorescence spectroscopy of conformational changes of single LH2 complexes	69
5. Dynamics of the emission spectrum of a single LH2 complex: interplay of slow and fast nuclear motions	97
6. Comparative study of spectral flexibilities of bacterial light-harvesting complexes: structural implications	123
7. Spectral trends in the fluorescence of single bacterial light-harvesting complexes: experiment and modified Redfield simulation	147
8. Conformational relaxation of single bacterial light-harvesting complexes	166
Summary	179
Samenvatting	183
Nawoord	187

Abbreviations

3D	three-dimensional
ADP	adenosine diphosphate
APD	avalanche photodiode
APS	aminopropyltriethoxysilane
ATP	adenosine triphosphate
BChl	bacteriochlorophyll
Car	carotenoid
CCD	charge-coupled device
CW	continuous wave
cyt	cytochrome
FL	fluorescence
FLN	fluorescence line narrowing
FLP	fluorescence peak wavelength
fwhm	full width at half of the maximum
GWI	glass-water interface
H-bond	hydrogen bond
He-Ne	helium-neon
IR	infrared
LDAO	lauryldimethylamine oxide
LH1	core light-harvesting complex 1
LH2	peripheral light-harvesting complex 2
LHC	light-harvesting complex
M	magnification
NA	numerical aperture
NADPH	nicotinamide adenine dinucleotide phosphate
NI	National Instruments
P	special pair
PC	personal computer
PLL	poly-L-lysine
PR	participation ratio
PS	photosystem
PSI	photosystem 1
PSII	photosystem 2
PSU	photosynthetic unit

PzS	piezo scanner
Q	quinone
RC	reaction center
RT	room temperature
S/N	signal-to-noise ratio
SDFP	standard deviation of fluorescence peak wavelength
SPCM	single photon counting module
STD	standard deviation
Ti:S	titanium sapphire
VC	video camera
WT	wild type
ZPL	zero phonon line

Introduction

PHOTOSYNTHESIS

In plants, algae and certain types of bacteria, the process of photosynthesis results in the consumption of atmospheric carbon dioxide, that is used to synthesize carbohydrates, and the release of molecular oxygen as a by-product (oxygenic photosynthesis). Other types of bacteria use light energy to create organic compounds without producing oxygen (anoxygenic photosynthesis). Photosynthesis plays a vital role in the food chain on earth since, by reducing carbon dioxide to carbohydrates, it provides the energy required for the sustenance of virtually all life, as well as the molecular oxygen necessary for the survival of oxygen-consuming organisms. In addition, the fossil fuels currently burned to provide energy for human activity were produced by ancient photosynthetic organisms. It also has a large net value in the carbon dioxide flow from and to the atmosphere since through photosynthesis, carbon dioxide is reduced to carbohydrates and is returned to the atmosphere by microbial, plant and animal metabolism, and by biomass combustion.

For capturing solar light and subsequently converting this energy to forms more convenient for metabolic processes, photosynthetic organisms have dedicated molecular machineries. The initial stages in the chain of interactions among these machineries are governed by light-harvesting complexes (LHCs) – protein complexes non-covalently binding a number of pigment molecules absorbing light. A protein scaffold performs a coordinating function and tunes the spectroscopic properties of the bound pigments. At room temperature (RT) proteins are rather mobile entities performing movements of different amplitude and over a broad range of time scales. In this thesis we present an attempt to illustrate and analyze the dynamics of the pigment-protein interaction caused by spontaneous protein fluctuations. We do this by monitoring the evolution of fluorescence (FL) spectra of single LHCs. Comparison with a model allows us to draw conclusions about the character of protein motions.

Photosynthetic process

Carbohydrates are the end product of a series of physical and chemical reactions starting with the absorption of a light photon (Whitmarsh and Govindjee 1999). These reactions occur in and adjacent to the photosynthetic membrane that forms closed spaces in the cell volume. Thus, molecular players in the reactions are either embedded in the lipid bilayer, freely diffuse at the inner (lumen or periplasm) or outer (stroma or cytoplasm) side of the membrane, or their diffusion is restricted to two dimensions inside the membrane.

Light absorption is accomplished by pigments, *e.g.* chlorophylls and carotenoids, which, together with the scaffolding protein, form the LHCs. LHCs together with the reaction center (RC) and some other particles constitute a photosystem (PS). After a pigment in a LHC absorbs an incident photon, excitation energy is rapidly (on a picosecond time scale) transferred among the pigments of LHC and between different LHCs and is finally captured by the RC (van Grondelle, *et al.* 1994). This triggers a complicated sequence of electron and proton transfer reactions down the energy gradient that starts with electron transfer across the membrane inside the RC. These events leading to the net production of

compounds rich in free chemical energy – adenosine triphosphate (ATP) and nicotinamide adenine dinucleotide phosphate (NADPH) (or NADH), are traditionally called “light reactions”. ATP and NADPH contribute further to the synthesis of carbohydrates from carbon dioxide according to Calvin cycle that occurs at the outside of the photosynthetic membrane and which is independent of the light reactions.

This very general picture of photosynthetic phenomenon is applicable to all photosynthetic organisms. The specifics of the process, however, differ for different classes of organisms. The broadest classification is made according to the ability of photosynthetic organisms to evolve oxygen – thus oxygenic and anoxygenic photosynthesis. Oxygenic are plants, algae and certain types of bacteria (*e.g.* cyanobacteria), while some other bacteria are anoxygenic.

Oxygenic photosynthesis

In oxygenic photosynthetic organisms, two different membrane-embedded PSs – photosystem II (PSII) and photosystem I (PSI) – work concurrently but in series. In light PSII oxidizes water, thus producing molecular oxygen, and with mediation of cytochrome *bf* (cyt *bf*) it feeds electrons to the PSI, which in turn reduces NADP⁺ to NADPH. The transfer of a single electron from water to NADP⁺ involves about 30 metal ions and 7 organic cofactors. Protons are released in the lumen during the oxidation of water and are transported across the membrane into the lumen in the course of electron transfer from PSII to PSI, thus creating an electrochemical gradient across the photosynthetic membrane. The energy stored in this electrochemical potential is used by a membrane-bound ATP synthase to form ATP from adenosine diphosphate (ADP).

Anoxygenic photosynthesis

Anoxygenic photosynthetic bacteria differ from oxygenic organisms in that each species has only one PS. In some photosynthetic bacteria the RC of this PS is similar to that of PSII and in others to the one of PSI. In this thesis we are concerned with LHCs of anoxygenic non-sulphur purple bacteria. We illustrate the electron transfer path of *Rhodobacter (Rh.) sphaeroides*, which is one of these organisms. The RC of this bacterium has been resolved by means of X-ray crystallography (Allen, *et al.* 1987) and it is similar to the RC of plant PSII. After the special pair (P) in the RC (an excitonically coupled pair of bacteriochlorophyll a molecules) receives electronic excitation from the LHC, P is oxidized and an electron is transferred to the quinone (Q) on the opposite (cytoplasmic) side of the membrane (Figure 1). After a second charge separation, 2 protons from the cytoplasm are taken up to form the doubly reduced Q – QH₂, which subsequently detaches from the RC and diffuses inside the membrane to the adjacent cytochrome *bc*₁ (cyt *bc*₁) complex. Cyt *bc*₁ oxidizes QH₂ and transfers electrons to a water-soluble electron carrier, the cytochrome *c*₂ (cyt *c*₂). The latter reduces the oxidized primary donor P⁺ (in oxygenic photosynthesis P⁺ would strip electrons through a number of mediators from water, thus producing oxygen). Q freely diffuses inside the membrane until it encounters the RC. The two protons of QH₂ are

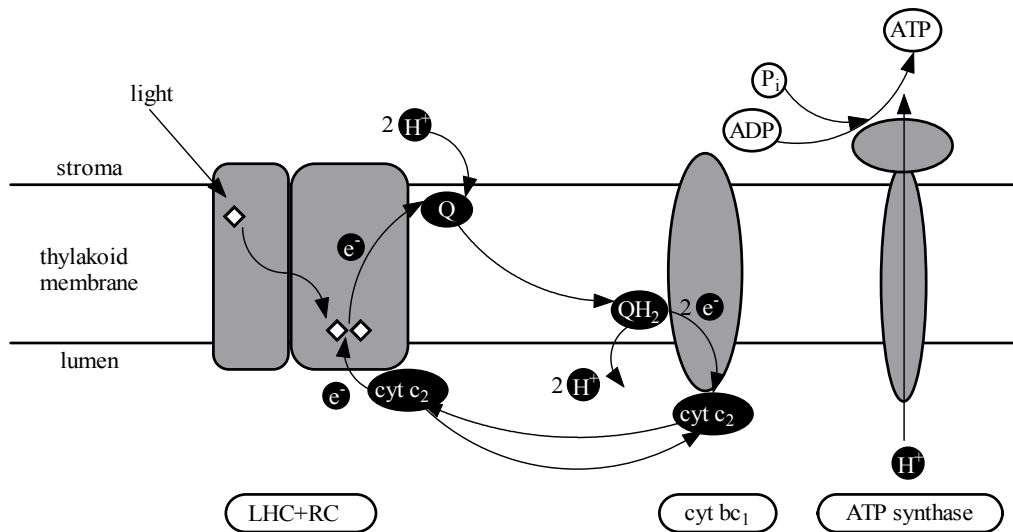
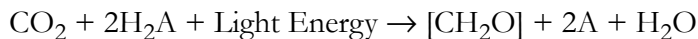


Figure 1. Overview of the photosynthetic apparatus and its function in purple bacteria.

released in the lumen thus contributing to the electrochemical proton gradient across the membrane. In this way the electron transfer chain is closed and the net result of the reaction is the production of an electrochemical gradient that is utilized by ATP synthase to form ATP from ADP.

Summarizing, the overall equation of photosynthesis encompassing both light and dark reactions is frequently written as:



Here A can be either oxygen, sulphur, or even an organic compound and the equation describes oxygenic or anoxygenic photosynthesis, respectively.

PHOTOSYNTHETIC LIGHT-HARVESTING

Bacteriochlorophylls

Bacteriochlorophylls (BChls) are the central pigments of the photosynthetic bacteria and have some of the highest extinction coefficients among organic molecules (in the order of $10^5 \text{ cm}^{-1}\text{M}^{-1}$) (Hoff and Ames 1991). They function as antenna pigments in the LHCs and as accessory and P chromophores in the RC. All BChls are derivatives of the parent compound porphyrin but differ in the functional group substitution (Senge and Smith 1995). There exists a number of types of BChls with trivial names alphabetically ranging from BChl *a-g*, the most abundant in photosynthetic bacteria being BChl *a* and *b*. The molecular structure of BChl *a* is shown in Figure 2. The extensive conjugated π -electron system of the porphyrin ring gives rise to the intense absorption bands of BChls. The arrow

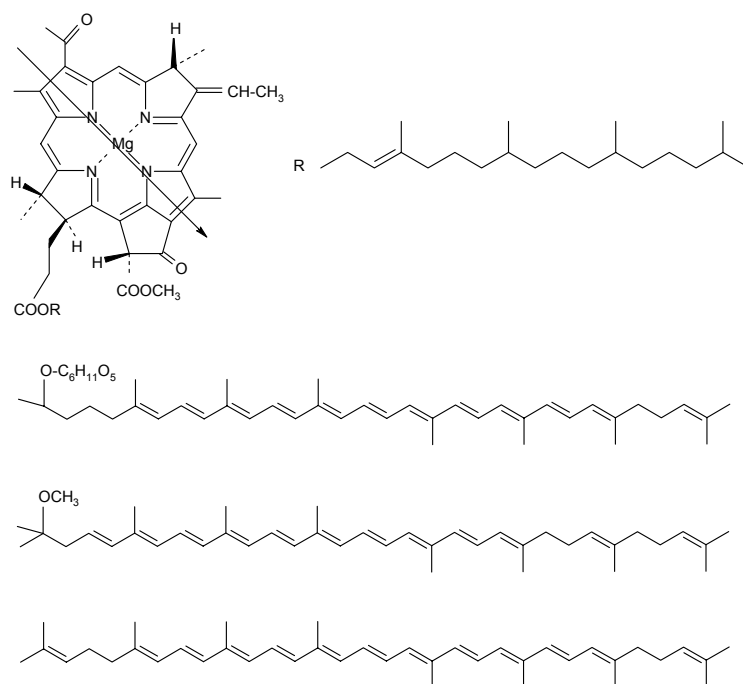


Figure 2. Structures of pigments occurring in bacterial LHCs. From top to bottom: BChl *a*, rhodopin glucoside (found in LH2 of *Rps. acidophila*), spheroidene (LH2 of *Rb. sphaeroides*), and lycopene (LH2 of *Rs. molischianum*).

indicates the approximate direction of the Q_y transition dipole moment that is in the plane of the ring. The Q_x transition dipole is also in the ring plane and perpendicular to the Q_y transition dipole, whereas the Soret band consists of several transitions. The absorption spectrum of BChl *a* in solution is shown in Figure 3. It exhibits three pronounced intense absorption bands corresponding to the three transitions. The near infrared absorption band

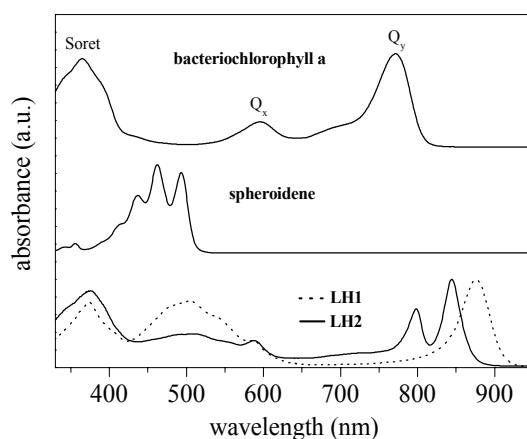


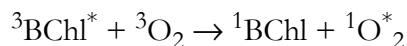
Figure 3. RT absorption spectra of BChl *a* in a mixture of polar solvents (Frigaard, *et al.* 1996), spheroidene in hexane, and isolated LH2 and LH1 complexes of *Rb. sphaeroides*.

associated with the Q_y transition peaks around 770 nm. In the violet/ultraviolet spectral region an absorption band peaking around 365 nm is due to the Soret transitions. A third, less pronounced band at 595 nm is caused by the Q_x transition. It has to be noted that the infrared absorption of free BChl *a* in solution is blue-shifted relative to that of a “monomeric” BChl *a* molecule in the B800 ring of LH2 complex (see below) by about 30 nm, which is attributed to the protein-pigment interactions in the latter.

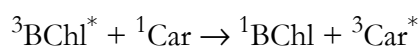
Carotenoids

Carotenoids (Cars) are another important group of photosynthetic pigments. At variance to BChls, they are linear molecules and exhibit much more structural diversity: ~600 different Cars have been isolated from natural sources. Most of them are composed of a C_{40} hydrocarbon backbone containing a series of conjugated double bonds (Britton 1985). The number of these double bonds ranges from 7 to 13 for Cars found in photosynthetic organisms. They also differ by the modifications of the basic linear structure (*e.g.* cyclic end groups, methyl side groups). Figure 2 contains a few examples of Cars found in bacterial LHCs. Due to the presence of substituted functional groups the theoretical description of electronic states of Cars is complicated and it is usually approximated by that of the corresponding polyenes (Christensen 1999). The transition to the lowest excited state S_1 is optically forbidden since S_1 has the same symmetry as the ground state S_0 . The absorption spectrum of Car molecules is dominated by the transition to the symmetry allowed higher-energy S_2 state (extinction coefficient of this transition is probably somewhat higher but similar to that of BChls – in the order of $10^5 \text{ cm}^{-1}\text{M}^{-1}$) (Britton 1995). The S_1 state is populated only by rapid internal conversion from the S_2 state, occurring with a subpicosecond rate, and in turn it relaxes to the ground state within a few picoseconds (Polivka and Sundström 2004). The exact values of S_1 and S_2 lifetimes depend on the length and structure of the Car. Cars function as complimentary absorbers in the blue-green spectral region not covered by BChls (see Figure 3). Although their lifetimes are short, there are very efficient energy transfer pathways from Cars to BChls and the latter act as terminal excitation energy acceptors (Sundström, *et al.* 1999).

Apart from the light-harvesting function even more important is the photoprotective action of Cars (Sheer 2003). Singly excited BChl has a finite probability of intersystem crossing to the triplet state that is energetically high enough to react with oxygen in its triplet ground state thus promoting it to the singlet state:



Singlet oxygen is highly reactive and can be damaging for biological material. Thus it is imperative to prevent this sensitization of oxygen, and that is what Cars are capable of doing by accepting BChl triplet excitation:



Since the triplet excited state energy of Car is lower than that of singlet excited oxygen, the formation of the latter is prohibited.

Finally, Cars also have an important structural role. Some LHCs do not assemble in the absence of Cars. Moreover, removing Cars from the intact complexes causes those complexes to disassemble (Frank and Cogdell 1996).

Structure of bacterial LHCs

In 1995 the structure of the LH2 complex of *Rhodospseudomonas (Rps.) acidophila* was resolved with 2.5 Å resolution by Cogdell and co-workers (McDermott, *et al.* 1995). The 2.4 Å structure of *Rhodospirillum (Rs.) molischanum* by Michel and Schulten and co-workers followed in 1996 (Koepeke, *et al.* 1996). The structure of LH2 of *Rps. acidophila* was recently refined to 2.0 Å resolution (Papiz, *et al.* 2003). Only an 8.5 Å resolution electron microscopy projection map could be obtained for the LH1 complex from a two dimensional crystal of reconstituted LH1 of *Rs. rubrum* (Karrasch, *et al.* 1995). Based on this low resolution map and polypeptide sequence homology with the LH2 of *Rs. molischanum* (Zuber and Brunisholz 1991), an accurate model of LH1 of *Rb. sphaeroides* has been constructed (Hu and Schulten 1998). Similarly, with the help of homology modelling, a model for LH2 of *Rb. sphaeroides* was made by using the known structure of LH2 of *Rps. acidophila* (Hu, *et al.* 1998). A structure of an LH1 complex including the RC from *Rps. palustris* became recently available at 4.8 Å resolution (Roszak, *et al.* 2003).

From the established structures and models it appears that both LH2 and LH1 complexes are highly symmetric circular aggregates of a number of pigments (BChls and

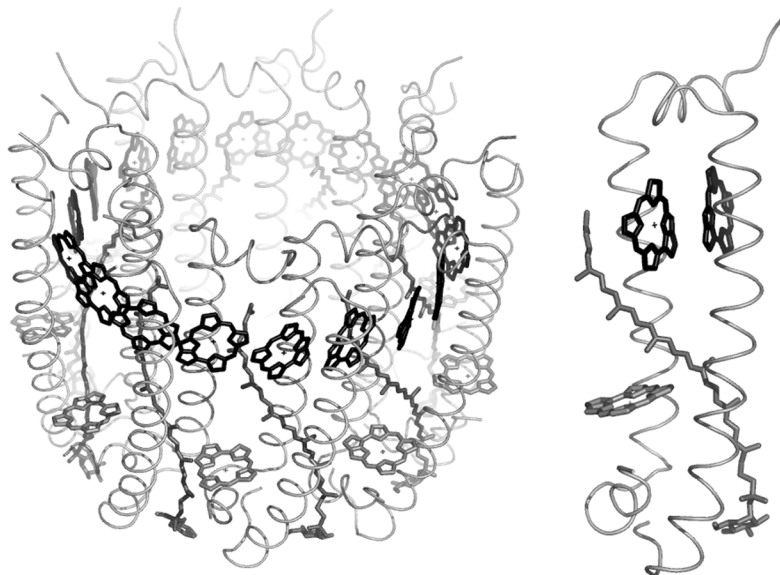


Figure 4. The structure of LH2 of *Rps. acidophila* and of its dimeric subunit. The B850 ring of BChls *a* is depicted in black, B800 – grey, Cars – dark grey, and protein – light grey.

Cars) in a scaffold of transmembrane protein alpha helices. The recurring structural motif is the basic dimeric subunit consisting of two alpha helices (although in *Rps. viridis*, for example, there exists an additional polypeptide) and a number of pigment molecules depending on the type of the complex (see Figure 4).

As an example here we outline in greater detail the structure of LH2 of *Rps. acidophila* (see Figure 4). The complex consists of two concentric cylinders of nine alpha helices each: the α -polypeptide on the inside and β -polypeptide on the outside of the complex with a radius of 34 Å. Each pair of radially opposite alpha helices non-covalently binds three BChls *a* (see further), forming the $\alpha\beta$ -subunit. Two of these BChl *a* molecules are ligated through the Mg atoms of their bacteriochlorin ring to the histidine side chain of the α or β -polypeptide in the subunit. Nine of these BChl *a* pairs form a ring of tightly coupled pigments closer to the C-terminal (periplasmic membrane surface) with their molecular planes perpendicular to the membrane surface (or parallel to the symmetry axis of the complex). The Q_y transition dipole moments are approximately perpendicular and the Q_x parallel to the symmetry axis of the complex. This pigment ring is responsible for the intense absorption peaking at around 850 nm and is generically denoted B850. The B850 inter- and intra-subunit BChl *a*-BChl *a* centre-to-centre distances are very similar, about 9 Å. The other nine BChl *a* molecules form a ring 16.5 Å further into the membrane and closer to the N-terminal of the $\alpha\beta$ -subunit (cytoplasmic membrane surface). The BChls *a* are positioned between helices of the β -polypeptides with a centre-to-centre distance of about 21 Å. Each of these molecules is ligated through its Mg atom to the formylated α Met1 residue. This ring of BChl *a* molecules is responsible for the absorption band peaking at around 800 nm, hence its name – B800. The pigment planes in B800 are approximately parallel to the membrane surface. The major Car molecule is rhodopin glucoside with a measured BChl *a*/Car ratio of 3:2 (Freer, *et al.* 1996). One Car molecule runs from the N-terminal side of one $\alpha\beta$ -subunit to the C-terminal side of the next one, making van der Waals contacts with the B800 bacteriochlorin ring of the former subunit and the α -B850 bacteriochlorin ring of the latter. There is also some evidence for the presence of the second Car molecule but it has not been fully resolved.

Another crystallographically resolved LH2 complex from *Rs. molischianum* is generally very similar to that of *Rps. acidophila*. The most conspicuous difference is that it exhibits eightfold symmetry instead of ninefold. Also the planes of the B800 BChls *a* are 90° rotated compared to *Rps. acidophila* resulting in a significantly weaker coupling between the B800 BChls *a*. Furthermore the B800 macrocycles are tilted away from the membrane plane by about 30°.

The LH1 complex of *Rb. sphaeroides* is modelled as consisting of 16 $\alpha\beta$ -subunits each binding a pair of BChls *a* and one Car molecule. This ring of BChls *a* is responsible for the absorption peaking at around 875 nm and is accordingly named B875. The overall diameter of the LH1 complex is 118 Å thus large enough to enclose the RC and fulfil its function of the terminal LHC in the chain of excitation migration. The LH1 does not contain a pigment ring analogous to B800 in LH2.

Photosynthetic unit

A universal motive both in bacterial and plant photosynthesis is that the light reactions leading to a stable primary charge separation occur in the photosynthetic unit (PSU), consisting of the RC and LHCs. This charge separation leading to subsequent reactions occur as long as P of the RC can be electronically excited. However, the absorption cross section of the RC is relatively small, so when it is exposed to direct sunlight it cannot reach the maximum possible turn-over rate (about 1kHz). Thus the function of LHCs is to absorb photons and funnel the excitation energy to the RC. Such an arrangement also economizes the organism's metabolic energy for the biosynthesis since it is less costly to synthesize relatively small proteins providing the scaffold for the antenna pigments than to produce many copies of the large RC and its associated electron transfer proteins.

A fragment of the proposed organization of the purple non-sulphur bacterial PSU of *Rb. sphaeroides* is shown in Figure 5 with the relevant energy transfer time constants (Hu, *et al.* 1998). It consists of the RC and the LH1, core antenna complex, directly surrounding the RC. Around the LH1 complex there is a number of peripheral antenna complexes – LH2s. In some species such as *Rps. acidophila* and *Rps. palustris* there exists a third kind of complex – LH3, that is similar to LH2 but has a shifted absorption maximum due to a different pattern of hydrogen bonding. All of these antenna complexes are embedded in the membrane (however for some organisms LHCs can be water soluble pigment-protein complexes). The number of LH2s and LH3s in PSU varies and is dependent on growth conditions such as light intensity and temperature (Aagaard and Siström 1972). The PSU exhibits a pronounced energetic hierarchy: LH3 absorbs light of the highest energy at around 800 and 820 nm, LH2 complexes that surround LH1 absorb maximally at around 800 and 850 nm; and LH1 that surrounds the RC absorbs the lowest energy around 875 nm. This energetic cascade serves to funnel the excitation energy from the LH3 and LH2

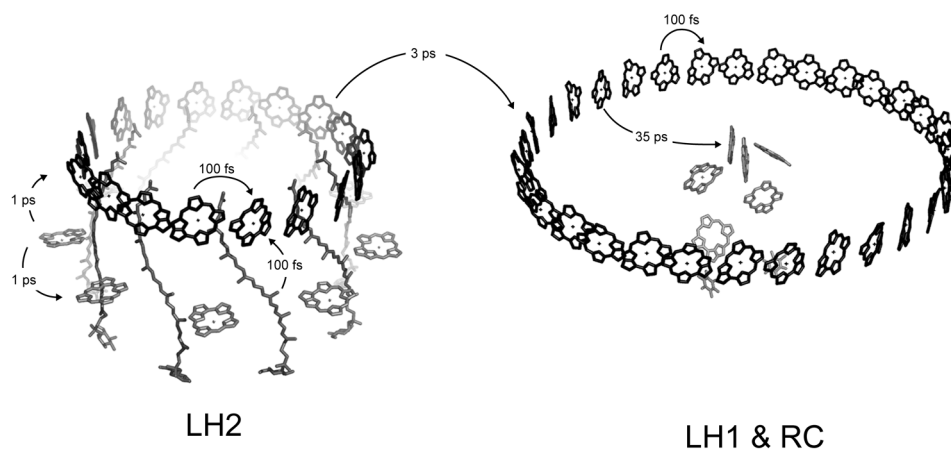


Figure 5. A scheme of the bacterial PSU with relevant energy transfer time constants. Courtesy of Dr. E. Papagiannakis and Dr. M.Vengris.

through LH1 to the RC. The overall yield of absorbed energy transfer to the RC is close to unity (~95%) and occurs in ≤ 100 ps (Fleming and van Grondelle 1997). This efficient energy transfer is facilitated by the favourable coplanar position of the pigment rings in the peripheral and core LHCs imbedded in the membrane. Depending on the excitation conditions a number of intermediate intra- and inter-complex energy transfer steps occur between different pigment sites within the B800 ring, energy relaxation in B850, within one complex from B800 to B850, from LH2 to LH2, from LH2 to LH1 and finally from LH1 to RC (Sundström, *et al.* 1999). All relevant transfer times have been measured and estimated theoretically making assumptions of various degree of complexity. Some of the energy transfer times are outlined in Figure 5.

To describe the excited state dynamics in such a system of coupled pigments has been a major scientific issue during the last decade. Depending on the investigated system and experimental conditions at least two limiting cases have been defined: incoherent Förster hopping between weakly interacting chromophores vs. the molecular exciton description for “strongly” coupled chromophores, in which the time evolution of the excited state occurs via phonon-induced relaxation between exciton states. In bacterial LHCs both of these regimes are encountered: hopping between distant pigments of the B800 ring and exciton relaxation in the B850 ring of tightly coupled BChls *a*. It is surprising how subtle quantum mechanical effects are elegantly utilized in bacterial photosynthesis. For example, the excitonic splitting of energy levels of B850 ring improves the donor-acceptor spectral overlap in the B800 to B850 energy transfer thus increasing the efficiency of this transfer step (Hu, *et al.* 2002).

PROTEIN MOVEMENTS IN SINGLE-MOLECULE EXPERIMENTS

Since long proteins have been characterized as “screaming and kicking” (Weber 1975) to emphasize the fact that they are not rigid entities. The different sets of coordinates that protein atoms acquire in the course of their movements are called “conformations” or “conformational substates”, and the known crystal structures are only averages of different conformations. Conformational substates are associated with certain values of the potential energy of the system. Transitions between conformations occur by crossing the potential energy barriers of different magnitude (Frauenfelder, *et al.* 1991). The distribution of barrier height leads to a wide variety of movement amplitudes and time scales (Careri, *et al.* 1979, Wagner 1983). In a LHC these motions cause a modulation of the pigment-protein interaction and consequently also of the electronic structure of the pigment aggregates occurring in LHCs. As explained in the next section, protein motions define the shape of corresponding FL spectral profile. Slow protein motions are the cause of changes of the so-called static disorder of pigment electronic transition energies, while fast protein motions occurring during the excitation/emission process constitute the homogeneous line broadening.

The investigation of protein motions is aggravated by the inevitable ensemble averaging

in a bulk sample. Although the initial state of many molecules can be synchronized by, for example, a laser pulse, the subsequent relaxation process, available for observation, is the result of many different contributions. In contrast, single-molecule techniques allow for the investigation of the spontaneous evolution of individual molecules of interest. The objective of the present work is to investigate “natural” conformational changes of bacterial LHCs; therefore single-molecule FL spectroscopy is the appropriate technique. The feasibility of such investigations was demonstrated in the RT polarized FL experiments that were interpreted in terms of an elliptical absorber and emitter with ellipticity and directions of the principal axis varying as a result of the B800 and/or B850 distortion destroying the rotational symmetry and traveling around the ring on a timescale of seconds (Bopp, *et al.* 1999). Spectral diffusion of the B800 band of LH2 was observed in low temperature experiments, and was also attributed to structural alterations (van Oijen, *et al.* 2000).

ELECTRONIC STRUCTURE OF THE B850 RING

Effective Hamiltonian description

To understand the way a pigment-protein aggregate serves the light-harvesting function requires knowledge of the electronic properties of its excited states. An B850-like ring is composed of a number of pigments in close proximity. Thus, the electronic properties of the ring can not be regarded merely as the sum of the responses of the individual chromophores. Rather, they have to be considered as a result of all pigments operating collectively.

A number of theoretical attempts aimed to establish the energy level scheme and the corresponding distribution of oscillator strengths. Due to the large size of the system, *ab initio* calculations have not been feasible so far and different authors employed methods ranging in their complexity from the semiempirical intermediate neglect of differential overlap model parameterised for spectroscopy (INDO/S) (Cory, *et al.* 1998) to an effective Hamiltonian representation based on the point dipole treatment (Hu, *et al.* 1997, Novoderezhkin, *et al.* 1999), the more sophisticated point monopole treatment (Sauer, *et al.* 1996), or a quantum mechanical consistent-force-field/ π -electron (QCFF/PI) approach (Alden, *et al.* 1997). Qualitatively all these approaches produce the same results. The INDO/S is advantageous in that it does not assume any adjustable parameters while the rest of the models do. With a certain accuracy the latter can be equivalently represented by the effective Hamiltonian of the whole system, which is by far more illustrative and easy to comprehend. Essential features of such an effective Hamiltonian description are the energies of the local electronic excited states of and the interaction between individual pigments. These unknown parameters are adjusted so that the effective Hamiltonian approach reproduces the results of the semiempirical calculation.

It is illustrative to consider the interaction inside the chromophore dimer first, since in the B850 ring, although intra- and inter-subunit distances between pigments are similar, the

interaction within the $\alpha\beta$ -subunit is stronger than between pigments from neighbouring subunits due to the different relative orientations of the BChl chlorin rings. Thus the B850 ring can be considered to consist of a number of not only structural but also electronic dimers. The electronic structure of the whole ring will then result from the interaction of these dimers and will reflect the characteristics of the dimer.

The result of the Coloumbic interaction between the dipole moments of the two molecules is that the dimer can be excited to two states of different energy (van Amerongen, *et al.* 2000), which are named excitonic states. The splitting between them equals twice the coupling energy, and the relative magnitude of the dipole strength of these states depends on the position and orientation of the two transition dipole moments: for “head-to-tail” dimer the lowest energy transition is strongly allowed, while for “sandwiched” configuration the highest energy transition is allowed. The conclusion is that the excitonic interaction, depending on the geometry of the system, shifts and changes the outlook of the absorption spectrum.

Generalization to a larger number of interacting pigments is rather straightforward (Hu, *et al.* 1997): the resulting excited states of the system are assumed to be linear combinations of the products of individual molecular states with only one of the molecules excited. System eigenfunctions and corresponding eigenenergies are obtained by diagonalizing the Hamiltonian matrix:

$$H_{ij} = \delta_{ij}\epsilon_i + V_{ij} \quad (1)$$

where ϵ_i are molecular excitation energies, and V_{ij} the matrix elements of the dipole-dipole interaction between molecules i and j , expressed as:

$$V_{ij} = C \left(\frac{\vec{d}_i \cdot \vec{d}_j}{r_{ij}^3} - \frac{3(\vec{r}_{ij} \cdot \vec{d}_i)(\vec{r}_{ij} \cdot \vec{d}_j)}{r_{ij}^5} \right) \quad (2)$$

The resulting excited state scheme consists of two excitonic bands (see Figure 6). The specific number of states in each band depends on the number of interacting molecules in the ring. In the case of *R. molishianum* there are 8 interacting dimers and each of the bands contains 8 states. In each band, however, 6 of these states are doubly degenerate (have identical energies). The two degenerate states that are just above the lowest one possess all oscillator strength. Since the sum of oscillator strengths of all excitonic states has to be equal to the sum of all individual oscillator strengths of constituent chromophores, these two strongly allowed excitonic states are equally superradiant and their oscillator strengths equal almost 8 times that of the monomer. The corresponding transition dipole moments lie in the plane of the ring and are orthogonal to each other.

The results of these calculations are obtained assuming perfect circular symmetry. In reality, pigments interact not only with each other but also with their protein scaffold. The intrinsic disorder of the protein causes differences in the pigment transitions or site



Figure 6. Exciton band structure of LH2 of *Rs. molischianum*. Adapted from (Cory, *et al.* 1998).

energies, which is commonly referred to as static energetic disorder. This static disorder is introduced by assuming random deviations of the pigment transition energies taken from a Gaussian distribution of a certain width. Each realization of these random deviations will generate different excitonic eigenfunctions and eigenvalues. Averaged over a number of

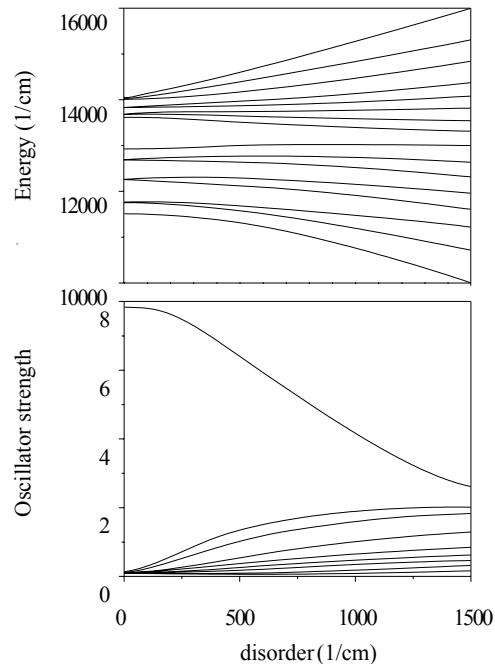


Figure 7. Effect of the static energetic disorder on splitting and redistribution of oscillator strength between exciton levels. Adapted from (Hu, *et al.* 1997). The three lowest exciton states are depicted by thick lines.

realizations, the effect of energetic disorder is shown in Figure 7: the energetic degeneracy of exciton states is removed, which redistributes the oscillator strength between excitonic states – the two strongly allowed states lend some of their oscillator strength to the lowest one. The exciton level splitting and redistribution of oscillator strength increases with larger energetic disorder.

Superradiance experiments on LH2 and LH1 at low temperature (Monshouwer, *et al.* 1997) demonstrated that the concept of energetic disorder corresponds to the real-life situation: after exciton relaxation only the lowest excitonic state would be populated (higher states are not thermally populated at low temperature), and in the case there was no disorder, according to the ideal excitonic picture, this state would exhibit no FL. However, experimental evidence shows that, on the contrary, even at low temperature, LH2 and LH1 are not only fluorescent but superradiant: the oscillator strength of the fluorescent state equals 2-3 times that of a single BChl.

Origin of static disorder

The commonly accepted reason for the appearance of static energetic disorder is the interaction of a pigment with its surrounding protein: since proteins are in many aspects glass-like, intrinsically disordered systems, it is not unreasonable to expect that pigment-protein interactions are also heterogeneous. Below are listed some of the documented modes of BChl-protein interactions:

- a) local protein environment:
 - i) point charges;
 - ii) hydrogen bonding (H-bonding);
 - iii) axial ligation;
- b) structural changes of the chromophore itself:
 - i) rotation of the C2 acetyl group;
 - ii) distortion of porphyrin macrocycle.

(Cogdell, *et al.* 2002).

Calculations indicate that structural distortions of the molecular macrocycle may lead to absorption red-shifts in the order of 100 nm in extreme cases (Barkigia, *et al.* 1988). The rotation of an acetyl group out of the plane of the BChl *a* molecule causes a blue shift of an absorption of up to 20 nm for the Q_y transition if the torsion angle assumes values of $\pm 90^\circ$ (Gudowskanowak, *et al.* 1990, Hanson, *et al.* 1987). H-bonding to the acetyl group of BChl *a* is calculated to red-shift the absorption of Q_y by 6 nm, while H-bonding to the keto group causes a blue shift of the same magnitude (Hanson, *et al.* 1987).

In fact, the factors listed in the first group can be the origin of the structural effects in the second part of the list. For example H-bonds to the peripheral groups of BChl *a* and axial ligation to the Mg^{2+} ion are supposed to be the cause of structural distortion of the molecular macrocycle (Scheidt and Lee 1987). The impact of H-bonds was confirmed in experiments applying site-directed mutagenesis (Fowler, *et al.* 1994). Mutation of either one or both of the α Tyr+13(44) and α Tyr+14(45) residues in the case of *Rb. sphaeroides* LH2

caused progressive blue shifts of the absorption bands by 11 and 26 nm, respectively, which were associated with the breaking of H-bonds to the acetyl groups of one or both B850 BChls *a*. Interpretation of these results, however, is not straightforward – it is clear that mutation brings about spectral changes although it is not apparent what is the exact mechanism of such a change. The pure effect of H-bond removal is too insignificant to account for the observations, and consequently the observed spectral changes are most likely caused by structural changes of the BChl molecule – such as rotation of the acetyl group or a distortion of the macrocycle. Furthermore, the alteration of wild-type residues possibly introduces side effects unrelated to the H-bond removal.

Using the modified Redfield theory to calculate the FL profile

The shape of the FL profile is an experimentally observable that reflects the underlying electronic state of the system of interest and consequently also the corresponding structural conformation. Since we are primarily concerned with possible structural changes of circular antenna complexes, the consideration of mechanisms underlying the spectral profile form, are of interest. It has been recently suggested that FL profile shape is determined by the exciton self-trapping due to polaron formation accounting for the observable broad and strongly red-shifted FL spectrum at low temperature (Freiberg, *et al.* 2003). However, in the absence of an adequate quantitative polaron model and having observed rather subtle relationship between the spectral parameters calling for a quantitative description we utilize the modified Redfield theory to describe excitation dynamics and spectra. This model takes into account the excitonic interactions between pigments, the static disorder of pigment electronic transition energies, and the coupling of electronic transitions to nuclear motions, which is the cause of the dynamic disorder (Mukamel 1995, Zhang, *et al.* 1998).

The dynamic disorder in the site representation implies that either the electronic transition energies of the chromophores, or the couplings between them are modulated by fast intra- or intermolecular nuclear motions, collectively termed – phonons. These nuclear motions occur during the absorption/FL and thus have an impact on the absorption/emission properties. Furthermore, a specific realization of the static disorder sets the transition energies at a given moment in time. As the term “static” implies, this set of transition energies does not change during the characteristic absorption/FL times, but it will change on a much longer timescale because of the reorganization of equilibrium nuclear positions. A subtle interplay between the static and the dynamic disorder determines the shape of the spectral profile.

In the FL profile calculation first the exciton eigenvalues (transition frequencies ω_k) and the corresponding eigenfunctions (or wavefunction amplitudes c_n^k , which represent participation of the n th site in the k th exciton state) are calculated by diagonalizing the one-exciton Hamiltonian with a certain realization of the static disorder for the pigment electronic transition energies. Then in the framework of the Redfield theory, FL profile is expressed as (Meier, *et al.* 1997, Zhang, *et al.* 1998):

$$\begin{aligned}
\text{FL}(\omega) &= \omega \sum_k P_k \mathbf{d}_k^2 \text{Re} \int_0^{\infty} e^{i(\omega - \omega_k)t + i2\lambda_{kkkk}t - \mathbf{g}_{kkkk}^*(t) - R_{kkkk}t} dt \\
\mathbf{d}_k &= \sum_n c_n^k \mathbf{d}_n \\
R_{kkkk} &= - \sum_{k' \neq k} R_{k'k'kk}
\end{aligned} \tag{3}$$

where P_k is the steady state thermal population, \mathbf{d}_k is the transition dipole moment, \mathbf{g}_{kkkk} is the spectral line broadening function, and λ_{kkkk} is the reorganization energy of the k th exciton state. Obviously, \mathbf{d}_k depends on the realization of the static disorder by means of the wavefunction amplitudes c_n^k . So does P_k since it depends on the magnitude of the energetic splitting between the exciton states, which is determined by the static (by means of the transition frequencies ω_k) and dynamic (due to reorganization effects – see below) disorder.

Generally $R_{kk'k''k''}$ is a (Redfield) tensor and its different components describe various dissipative terms. For example $R_{kkk'k'}$ is the rate constant of the population transfer from the k' th state to the k th state, and is given by:

$$\begin{aligned}
R_{kkk'k'} &= \\
& -2\text{Re} \int_0^{\infty} \hat{W}(\omega_{kk'}, t) \{ \mathbf{g}_{kk'k'k'}''(t) - \{ \mathbf{g}_{k'kk'k'}'(t) - \mathbf{g}_{k'kkk}''(t) + 2i\lambda_{k'kk'k'} \} \\
& \times \{ \mathbf{g}_{k'k'kk}''(t) - \mathbf{g}_{kkkk}''(t) + 2i\lambda_{k'k'kk} \} \} dt \\
\hat{W}(\omega_{kk'}, t) &= \\
& \exp \{ -i\omega_{kk'}t - \mathbf{g}_{kkkk}(t) - \mathbf{g}_{k'k'k'k'}(t) + 2\mathbf{g}_{k'k'kk}(t) + 2i(\lambda_{k'k'kk} - \lambda_{k'k'k'k'})t \}
\end{aligned} \tag{4}$$

where $\omega_{kk'} = \omega_k - \omega_{k'}$.

Consequently R_{kkkk} in formula (3) is the sum of all the transfer-rate constants from the k th state to all other exciton states – *i.e.*, it is the rate of the exciton relaxation from the k th state. Including this term into the calculation of the FL profile implies that the relaxation-induced broadening of each exciton state is taken into account by its inverse lifetime, *i.e.*, R_{kkkk} .

The line broadening function and the reorganization energy can be further expressed in terms of the spectral density function in the exciton representation:

$$\begin{aligned}
g_{kk'k''k'''}(t) &= \\
& - \int_{-\infty}^{\infty} \frac{1}{2\pi\omega} C_{kk'k''k'''}(\omega) \left[\coth \frac{\omega}{2k_B T} (\cos \omega t - 1) - i(\sin \omega t - \omega t) \right] d\omega \\
\lambda_{kk'k''k'''} &= - \lim_{t \rightarrow \infty} \frac{d}{dt} \text{Im} \{ g_{kk'k''k'''}(t) \} = \int_{-\infty}^{\infty} \frac{1}{2\pi\omega} C_{kk'k''k'''}(\omega) d\omega \quad (5)
\end{aligned}$$

The spectral density in the exciton representation is expressed by means of the spectral density in the site representation as:

$$\begin{aligned}
C_{kk'k''k'''}(\omega) &= \sum_n c_n^k c_n^{k'} c_n^{k''} c_n^{k'''} C(\omega) \\
C(\omega) &= 2\lambda_0 \frac{\omega\gamma_0}{\omega^2 + \gamma_0^2} + \sum_{j=1,2,\dots} 2\lambda_j \omega_j^2 \frac{\omega\gamma_j}{(\omega_j^2 - \omega^2)^2 + \omega^2 \gamma_j^2} \\
\lambda_j &= S_j \omega_j \\
\lambda &= \int_{-\infty}^{\infty} \frac{1}{2\pi\omega} C(\omega) d\omega = \lambda_0 + \sum_{j=1,2,\dots} \lambda_j \quad (6)
\end{aligned}$$

where λ is the reorganization energy, and S_j is the Huang-Rhys factor of the j th vibrational mode in the site representation. λ_0 and γ_0 are the coupling and the damping parameters of the Brownian oscillator; ω_j , λ_j , and γ_j are the frequency, the coupling, and the damping constants of the high frequency vibrations.

In general the spectral density function in the site representation is a tensor with components representing diagonal (modulation of pigment site energies) and off-diagonal (modulation of couplings between pigments) coupling of nuclear modes to pigment electronic transitions, as well as all possible correlations between these couplings. In our model we assume pigment sites with identical and independent diagonal couplings – thus the spectral density tensor in the site representation is reduced to a scalar with no site-related indexing. Such an approach does not require introducing experimentally inaccessible spectral density components and at the same time it reproduces the overall effect of phonon coupling.

The first part of Equation 6 implies that the diagonal phonon coupling in the site

representation results in both diagonal and off-diagonal coupling in the exciton basis. Equation 5 shows that in the exciton representation the diagonal coupling causes the homogeneous broadening of the exciton states, through the line broadening function g_{kkkk} . The zero phonon line (ZPL) position of the k th exciton state is $\omega_k - \lambda_{kkkk}$ and the first moment of the FL from the k th exciton state is $\omega_k - 2\lambda_{kkkk}$; thus the diagonal coupling also affects the position of the exciton levels (and the splitting between them) and the FL spectral lines. Furthermore, the off-diagonal coupling in the exciton representation causes excitation relaxation between the exciton levels (Equation 4).

The interplay of the static and the dynamic disorder results from the fact that the line broadening function g_{kkkk} and the reorganization shift λ_{kkkk} are proportional to the participation ratio (PR) of the k th exciton state $PR_k = \sum_n (c_n^k)^4$ (Equations 5 and 6), which depends on the realization of the static disorder through the wavefunction amplitudes c_n^k . Furthermore, although in the expression of the spectral density in the site representation the phonon coupling constants are fixed, the spectral density in the exciton representation is dependent on the PR value of the exciton state. Consequently, the effective phonon coupling to exciton state causes different broadenings and reorganization shifts for each of exciton states depending on the realization of the static disorder.

From the calculations it appears that the FL profile shape and position are determined by a few characteristic regimes of excitonic splitting and effective phonon coupling. They both depend on the realization of the static disorder and correlate well with the magnitude of the PR values of the three lowest exciton states, which due to thermal population contribute to the spectral profile.

For realizations with relatively small PR values, the exciton structure is not significantly different from the case of an ideally homogeneous ring. The lowest exciton state $k = 0$ borrows only little dipole strength from the higher states $k = \pm 1$ and the energetic splitting between the lowest and higher states is not large enough to prevent the population of these higher states. Thus the thermally weighted contribution to the overall spectral profile mainly results from the $k = \pm 1$ exciton states that are on the higher energy side and consequently are also broadened due to the exciton relaxation. Therefore, the resulting FL profile is blue-shifted and broadened.

Realizations resulting in intermediate PR values, correspond to Hamiltonian eigenvalues associated with an increase of the splitting between the exciton levels and their red shift (Figure 7). This lowers the population of the higher $k = \pm 1$ exciton states. The lowest $k = 0$ exciton state borrows more of the dipole strength from the higher ones. The combined effect of these two factors is that the lowest exciton state contributes more to the spectral profile. Augmented PR values cause a further red shift of the exciton states induced by the larger effective phonon coupling. The result is a relatively narrow spectral profile with intermediate spectral peak position.

Finally, realizations with large PR values correspond to an exciton structure strongly affected by the static disorder. It induces a large splitting between and the red shift of the exciton levels and lends even more dipole strength to the lowest exciton state. Therefore,

predominantly the lowest exciton state is populated and contributes to the FL. Furthermore, a large PR value of the $k = 0$ state increases the effective phonon coupling, broadening and shifting this exciton level even further to the red. The resulting FL profile is broadened and red-shifted.

IN THIS THESIS

The aim of the present work is to investigate slow conformational changes of bacterial LHCs by monitoring single-molecule FL spectral evolution at physiological temperatures. The rationale for such an experimental plot follows from what has been discussed in the preceding sections. The FL profile shape and position are indicative of the underlying energy level structure that in turn is connected to the realization of the static disorder of the pigment site energies. The changes of the realization of this disorder are associated with the rearrangement of equilibrium nuclear positions or, in other words, the conformational state of the pigment-protein complex. The concept of energetic disorder is a phenomenological way of associating possible structural changes with the observable FL spectral evolution. Such an approach does not reveal the specifics of the microscopic structural changes, instead it allows for the most general and systematic description of the electronic structures associated with different conformations of the pigment-protein complex.

The second chapter presents a thorough description of an experimental setup developed and utilized to obtain experimental data – sequences of FL spectra of single immobilized LHCs.

The third and the fourth chapters are respectively a brief and an extended version of the description and analysis of the experimental results obtained for LH2 of *Rps. acidophila*. Sequences of FL spectra of single LH2s were measured at ambient and elevated temperatures with the aim to destabilize the ring structure. The measurements were performed with different excitation intensities in order to examine the occurrence of light-induced effects. For a number of measured complexes the FL peak position is found to evolve through a number of quasi-stable states of distinctly different magnitude. The extent of the spectral jumping is found to be weakly dependent on the sample temperature but much more conspicuously variable with the excitation intensity, leading to the conclusion that the observed spectral jumping is, at least partially, light-induced. The observed spectral changes are hypothesized to be associated with conformational changes of the pigment-protein. The thermal energy released in the complex under intense excitation due to radiationless energy relaxation pathways enhances the probability of conformational changes, thus leading to the observed dependency of the frequency of spectral jumping on excitation intensity. From the comparison of the temporal traces of different spectral fit parameters we also conclude the existence of a correlation between the changes of those parameters: a spectral shifting either to the blue or to the red from the intermediate position is found to be associated with spectral broadening, an observation interpreted in terms of a model based on a modified Redfield theory.

The fifth chapter presents a more thorough theoretical description of the model used to interpret the changes of the spectral profile shape. We utilize the phenomenological description based on the concept of different realizations of the static disorder of the pigments' electronic transition energies and therefore different regimes of energetic shifting and broadening of the exciton states induced by phonon coupling. It is further investigated, how different limiting cases of the static energetic disorder are associated with different scenarios of excitation evolution in the framework of the density matrix formalism.

In the sixth chapter we provide a statistical comparison of the frequency of spectral jumping of different types of LHCs. We built cumulative histograms of occurrences of spectral jumping using a definition of spectral jump that takes into account not only the spectral changes between adjacent points in the time trace but also overall spectral trends. Different kinds of complexes are compared based on datasets obtained with two different excitation wavelengths. We present a microscopic interpretation of the observed differences of spectral flexibility based on the documented microscopic factors determining pigment site energies.

The seventh chapter is a comparative study of spectral trends of different types of LHCs. Instead of comparing averages of spectral profiles with spectral peak position within a narrow interval as was done in the preceding chapters, we built histograms of averages of spectral fwhm or asymmetry corresponding to values of spectral peak wavelength. Such a presentation is more apt for comparison. Correlations of spectral parameters could be quantitatively interpreted for LH2 of *Rps. acidophila*, *Rb. sphaeroides* and *Rs. molischianum* and LH1 complex of *Rb. sphaeroides*.

The eighth chapter investigates the pigment-protein conformational relaxation; this occurs after a spectral jump, when the excitation is switched off and the complex is allowed to evolve at its natural pace. After a dark period of certain duration the excitation is switched on again to verify whether the complex has evolved. This cycle is repeated a number of times. It turns out that in significant number of cases complexes undergo spectral evolution from the destabilized states.

REFERENCES

- Aagaard, J., and Sistrom, W. R. (1972) Control of synthesis of reaction center bacteriochlorophyll in photosynthetic bacteria. *Photochem. Photobiol.* 15, 209-&.
- Alden, R. G., Johnson, E., Nagarajan, V., Parson, W. W., Law, C. J., and Cogdell, R. J. (1997) Calculations of spectroscopic properties of the LH2 bacteriochlorophyll-protein antenna complex from *Rhodospirillum rubrum*. *J. Phys. Chem. B.* 101, 4667-4680.
- Allen, J. P., Feher, G., Yeates, T. O., Komiya, H., and Rees, D. C. (1987) Structure of the reaction center from *Rhodospirillum rubrum* R-26 – the protein subunits. *Proc. Natl. Acad. Sci. U.S.A.* 84, 6162-6166.
- Barkigia, K. M., Chantranupong, L., Smith, K. M., and Fajer, J. (1988) Structural and theoretical models of photosynthetic chromophores – implications for redox, light-absorption properties and vectorial electron flow. *J. Am. Chem. Soc.* 110, 7566-7567.

- Bopp, M. A., Sytnik, A., Howard, T. D., Cogdell, R. J., and Hochstrasser, R. M. (1999) The dynamics of structural deformations of immobilized single light-harvesting complexes. *Proc. Natl. Acad. Sci. U.S.A.* 96, 11271-11276.
- Britton, G. (1985) General carotenoid methods. *Method. Enzymol.* 111, 113-149.
- Britton, G. (1995) UV/visible spectroscopy. In Carotenoids. Britton, G., Liaaen-Jensen, S. and Pfander, H., Eds., Vol. 1B, Birkhauser Verlag, Basel.
- Careri, G., Fasella, P., and Gratton, E. (1979) Enzyme dynamics – statistical physics approach. *Ann. Rev. Biophys. Bioeng.* 8, 69-97.
- Christensen, R. L. (1999) The electronic states of carotenoids. In The photochemistry of carotenoids. Frank, H. A., Young, A. J., Braun, M. and Cogdell, R. J., Eds., Kluwer, Dordrecht.
- Cogdell, R. J., Howard, T. D., Isaacs, N. W., McLuskey, K., and Gardiner, A. T. (2002) Structural factors which control the position of the Q_y absorption band of bacteriochlorophyll a in purple bacterial antenna complexes. *Photosynth. Res.* 74, 135-141.
- Cory, M. G., Zerner, M. C., Xu, X. C., and Shulten, K. (1998) Electronic excitations in aggregates of bacteriochlorophylls. *J. Phys. Chem. B.* 102, 7640-7650.
- Fleming, G. R., and van Grondelle, R. (1997) Femtosecond spectroscopy of photosynthetic light-harvesting systems. *Curr. Op. Struct. Biol.* 7, 738-748.
- Fowler, G. J. S., Sockalingum, G. D., Robert, B., and Hunter, C. N. (1994) Blue shifts in bacteriochlorophyll absorbency correlate with changed hydrogen-bonding patterns in light-harvesting 2 mutants of *Rhodobacter sphaeroides* with alterations at alpha-Tyr-44 and alpha-Tyr-45. *Biochem. J.* 299, 695-700.
- Frank, H. A., and Cogdell, R. J. (1996) Carotenoids in photosynthesis. *Photochem. Photobiol.* 63, 257-264.
- Frauenfelder, H., Sligar, S. G., and Wolynes, P. G. (1991) The energy landscapes and motions of proteins. *Science.* 254, 1598-1603.
- Freer, A., Prince, S., Sauer, K., Papiz, M., Hawthornthwaite, A. M., McDermott, G., Cogdell, R., and Isaacs, N. W. (1996) Pigment-pigment interactions and energy transfer in the antenna complex of the photosynthetic bacterium *Rhodospirillum rubrum*. *Structure.* 4, 449-462.
- Freiberg, A., Rätsep, M., Timpmann, K., Trinkunas, G., and Woodbury, N. W. (2003) Self-trapped excitons in LH2 antenna complexes between 5 K and ambient temperature. *J. Phys. Chem. B.* 107, 11510-11519.
- Frigaard, N. U., Larsen, K. L., and Cox, R. P. (1996) Spectrochromatography of photosynthetic pigments as a fingerprinting technique for microbial phototrophs. *Fems Microbiol. Ecol.* 20, 69-77.
- Gudowskanowak, E., Newton, M. D., and Fajer, J. (1990) Conformational and environmental effects on bacteriochlorophyll optical spectra – correlations of calculated spectra with structural results. *J. Phys. Chem.* 94, 5795-5801.
- Hanson, L. K., Thompson, M. A., and Fajer, J. (1987) Environmental effect of properties of chlorophylls *in vivo*. Theoretical models. In Progress in photosynthesis research. Biggins, J., Ed., Martinus Nihoff, Dordrecht.
- Hoff, A. J., and Ames, J. (1991) Visible absorption spectroscopy of chlorophylls. In Chlorophylls. Sheer, H., Ed., CRC Press, Boca Raton.
- Hu, X., and Schulten, K. (1998) Model for the light-harvesting complex I (B875) of *Rhodobacter sphaeroides*. *Biophys. J.* 75, 683-694.
- Hu, X. C., Damjanovic, A., Ritz, T., and Schulten, K. (1998) Architecture and mechanism of the

- light-harvesting apparatus of purple bacteria. *Proc. Natl. Acad. Sci. U.S.A.* 95, 5935-5941.
- Hu, X. C., Ritz, T., Damjanovic, A., Autenrieth, F., and Schulten, K. (2002) Photosynthetic apparatus of purple bacteria. *Q. Rev. Biophys.* 35, 1-62.
- Hu, X. C., Ritz, T., Damjanovic, A., and Schulten, K. (1997) Pigment organization and transfer of electronic excitation in the photosynthetic unit of purple bacteria. *J. Phys. Chem. B.* 101, 3854-3871.
- Karrasch, S., Bullough, P. A., and Ghosh, R. (1995) The 8.5-Angstrom projection map of the light-harvesting complex-I from *Rhodospirillum rubrum* reveals a ring composed of 16 subunits. *EMBO J.* 14, 631-638.
- Koepke, J., Hu, X. C., Muenke, C., Schulten, K., and Michel, H. (1996) The crystal structure of the light-harvesting complex II (B800-850) from *Rhodospirillum rubrum*. *Structure.* 4, 581-597.
- McDermott, G., Prince, S. M., Freer, A. A., Hawthornthwaite, A. M., Papiz, M. Z., Cogdell, R. J., and Isaacs, N. W. (1995) Crystal structure of an integral membrane light-harvesting complex from photosynthetic bacteria. *Nature.* 374, 517-521.
- Meier, T., Chernyak, V., and Mukamel, S. (1997) Femtosecond photon echoes in molecular aggregates. *J. Chem. Phys.* 107, 8759-8780.
- Monshouwer, R., Abrahamsson, M., van Mourik, F., and van Grondelle, R. (1997) Superradiance and exciton delocalization in bacterial photosynthetic light-harvesting systems. *J. Phys. Chem. B.* 101, 7241-7248.
- Mukamel, S. (1995) Principles of Nonlinear Optical Spectroscopy, Oxford University Press, New York.
- Novoderezhkin, V., Monshouwer, R., and van Grondelle, R. (1999) Exciton (de)localization in the LH2 antenna of *Rhodobacter sphaeroides* as revealed by relative difference absorption measurements of the LH2 antenna and the B820 subunit. *J. Phys. Chem. B.* 103, 10540-10548.
- Papiz, M. Z., Prince, S. M., Howard, T., Cogdell, R. J., and Isaacs, N. W. (2003) The structure and thermal motion of the B800-850 LH2 complex from *Rps. acidophila* at 2.0 Å over-circle resolution and 100 K: new structural features and functionally relevant motions. *J. Mol. Biol.* 326, 1523-1538.
- Polivka, T., and Sundström, V. (2004) Ultrafast dynamics of carotenoid excited states – from solution to natural and artificial systems. *Chem. Rev.* 104, 2021-2071.
- Roszak, A. W., Howard, T. D., Southall, J., Gardiner, A. T., Law, C. J., Isaacs, N. W., and Cogdell, R. J. (2003) Crystal structure of the RC-LH1 core complex from *Rhodospseudomonas palustris*. *Science.* 302, 1969-1972.
- Sauer, K., Cogdell, R. J., Prince, S. M., Freer, A., Isaacs, N. W., and Scheer, H. (1996) Structure-based calculations of the optical spectra of the LH2 bacteriochlorophyll-protein complex from *Rhodospseudomonas acidophila*. *Photochem. Photobiol.* 64, 564-576.
- Scheidt, W. R., and Lee, Y. J. (1987) Recent advances in the stereochemistry of metallotetrapyrroles. In *Structure and Bonding*. Buchler, J. W., Ed., Vol. 64, Springer-Verlag, Berlin.
- Senge, M. O., and Smith, K. M. (1995) Biosynthesis and structures of the bacteriochlorophylls. In *Anoxygenic photosynthetic bacteria*. Blankenship, R. E., Madigan, M. T. and Bauer, C. E., Eds., Kluwer academic publishers, Dordrecht.
- Sheer, H. (2003) The pigments. In *Light-harvesting antennas in photosynthesis*. Green, B. R. and Parson, W. W., Eds., Kluwer academic publishers, Dordrecht.
- Sundström, V., Pullerits, T., and van Grondelle, R. (1999) Photosynthetic light-harvesting: reconciling dynamics and structure of purple bacterial LH2 reveals function of photosynthetic unit. *J. Phys. Chem. B.* 103, 2327-2346.

- van Amerongen, H., Valkunas, L., and van Grondelle, R. (2000) Photosynthetic excitons, World Scientific, Singapore.
- van Grondelle, R., Dekker, J. P., Gillbro, T., and Sundström, V. (1994) Energy-transfer and trapping in photosynthesis. *Biochim. Biophys. Acta.* 1187, 1-65.
- van Oijen, A. M., Ketelaars, M., Köhler, J., Aartsma, T. J., and Schmidt, J. (2000) Spectroscopy of individual light-harvesting 2 complexes of *Rhodospseudomonas acidophila*: diagonal disorder, intercomplex heterogeneity, spectral diffusion, and energy transfer in the B800 band. *Biophys. J.* 78, 1570-1577.
- Wagner, G. (1983) Characterization of the distribution of internal motions in the basic pancreatic trypsin-inhibitor using a large number of internal NMR probes. *Q. Rev. Biophys.* 16, 1-57.
- Weber, G. (1975) Energetics of ligand binding to proteins. *Adv. Protein Chem.* 29, 1-83.
- Whitmarsh, J., and Govindjee (1999) The photosynthetic process. In Concepts in photobiology: photosynthesis and photomorphogenesis. Singhal, G., Renger, G., Sopory, S., Irrgang, K.-D. and Govindjee, Eds., Narosa Publishers, New Delhi.
- Zhang, W. M., Meier, T., Chernyak, V., and Mukamel, S. (1998) Exciton-migration and three-pulse femtosecond optical spectroscopies of photosynthetic antenna complexes. *J. Chem. Phys.* 108, 7763-7774.
- Zuber, H., and Brunisholz, R. A. (1991) Structure and function of antenna polypeptides and chlorophyll-protein complexes: principles and variability. In Chlorophylls. Sheer, H., Ed., CRC, Boca Raton, FL.

Experimental setup

A significant part of this Ph.D. project consisted of building the confocal fluorescence (FL) microscopy setup for detection and spectral analysis of single light-harvesting complexes (LHCs). Single-molecule detection is possible due to a combination of several factors: localized excitation and efficient signal collection, nanometer precision positioning, well directed and tunable-wavelength laser excitation, low-noise high-quantum-yield detection, efficient optical filtering of reflected excitation light, and powerful computer interface enabling automation and thus acquisition of massive data amounts without labor-consuming and error-prone human interference.

As important as state-of-the-art hardware and software setup is the sample stability. We could improve it to an unprecedented level: single molecules were fluorescent at physiological temperature during several minutes, and the sample was fit for measurement for days. This enabled us to fulfil the best case scenario of this project, and record phenomena that were difficult to observe.

In this chapter is given a step-by-step description of the optical and mechanical setup, followed by a separate section on sample cooling and deoxygenation.

OPTO-MECHANICAL SETUP

An overall scheme of the setup is shown in Figure 1. It consists of three main parts: the excitation branch, the microscope with a mounted sample cell, and the detection branch. The overall optical signal path can be described as follows: a collimated excitation beam is reflected by a dichroic mirror into the objective that focuses light on a single molecule of interest, the FL signal is collected by the same objective, passes through the dichroic mirror, and is reflected onto a tube lens that focuses it onto the confocal pinhole; the light is then recollimated by another lens and reflected for focusing onto a single photon counting module (SPCM), based on an avalanche photodiode (APD) or passed onto a grating, dispersed and focused onto a charge-coupled device (CCD) camera chip to acquire spectra.

Excitation

For excitation we implemented two options – either a tunable-wavelength (700-900 nm) titanium sapphire (Ti:S) laser system (Coherent, Mira 900) producing femtosecond pulses with 76 MHz repetition rate, or small, continuous wave (CW) helium-neon (He-Ne) laser (Melles Griot, 05SYR810-230) generating light at 594 nm. The Ti:S light is linearly polarized while the He-Ne has a random polarization. The excitation wavelength is selected by flipping a mirror and is directed towards the back port of the microscope with the mirror periscope that compensates for the height difference between the laserheads and the microscope. The laser beam is reflected into the upright objective with the corresponding dichroic mirror that has the property of reflecting relatively short wavelength light and transmitting longer wavelengths (see Figure 2). Since the two lasers produce different wavelengths, different dichroic mirrors are used for each of them (Chroma Technology

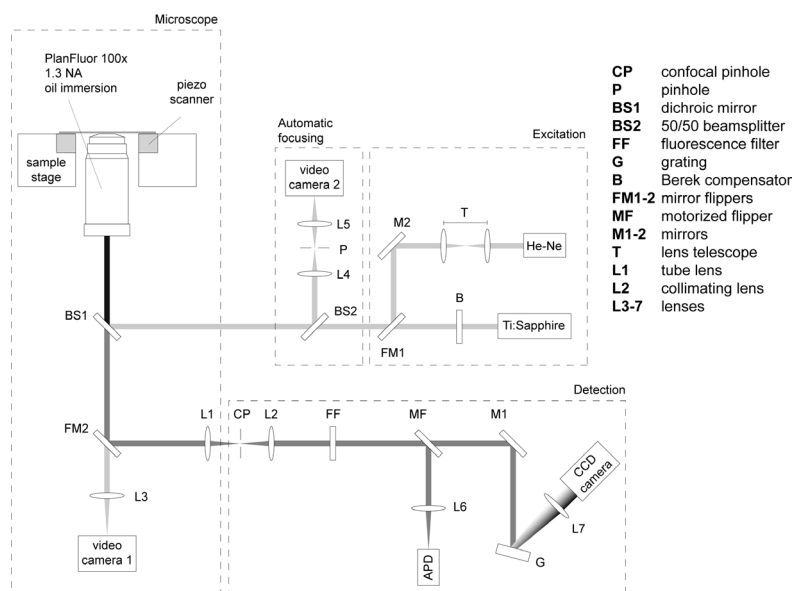


Figure 1. Optical scheme of the setup.

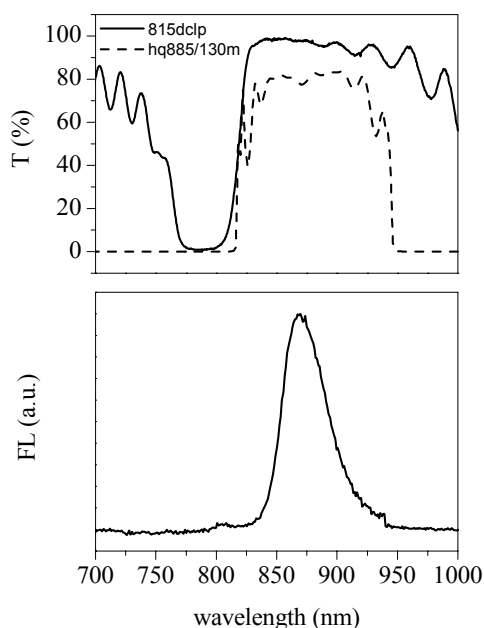


Figure 2. Example of fluorescence filter and dichroic mirror transmission profiles together with typical fluorescence spectrum of a light-harvesting complex.

Corp., 815dclp for 800 nm, and 605dext for 594 nm). The Ti:S beam passes through a Berek compensator (New Focus, 5540M) that is adjusted to render the light reflected from the dichroic circularly polarized to make the excitation of the complex, immobilized on a glass coverslip, independent of the orientation of excitonic dipole moments. It is not known what effect the microscope objective has on the polarization but it probably changes circularly polarized light to elliptical. In any case, even elliptical light is less orientationally selective than the linearly polarized one. In the case of He-Ne excitation, no additional modification is brought to the polarization of the beam since it is already random. The He-Ne beam passes through a telescope of two lenses that slightly decolimates the beam, which, as will be discussed below, was necessary for the compensation of objective achromatic aberration.

Microscope

The node part of the microscope, to a large extent determining its optical performance as a whole, is its objective. It consists of a number of optical elements of different refractive index material, specific radius of curvature and carefully positioned with respect to each other. The function of the objective is to focus the excitation light into the smallest area possible. Ideally – in the absence of optical aberrations – this focus area would be diffraction limited, that is, fundamentally limited by the physics of the wave-like nature of light. Modern design of the objectives approaches this limit very closely (see “Diffraction” section).

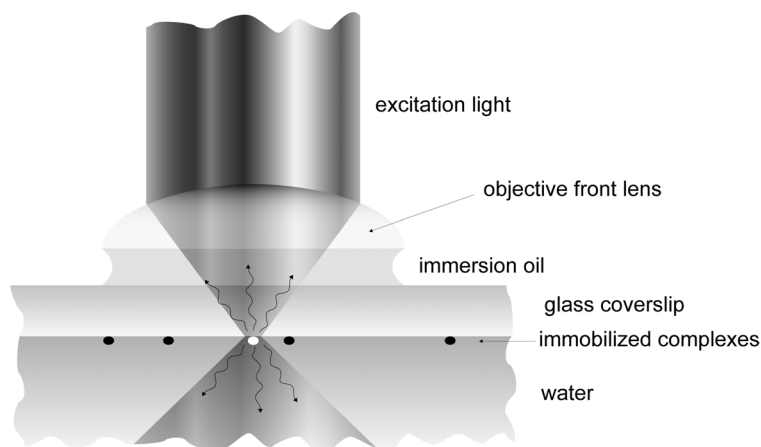


Figure 3. Focusing area.

We use the contemporary standard of the so-called infinity-corrected objective (Nikon, Plan Fluor 100 \times , 1.3 NA, oil immersion) that produces a collimated beam from a source at a focal distance (*i.e.*, it projects real image to infinity) unlike the old standard around which objectives were designed to form the real image of the object located between $1f$ and $2f$ (f – focal distance) at 160 mm distance.

Another function of the objective is to collect the sample FL light from the excitation area – that is, we utilize the widely spread so-called epi-illumination configuration, when the same objective has a two-fold function: that of excitation and collection of signal.

A close-up of the objective focal area is shown in Figure 3. Single complexes of interest are immobilized on a glass coverslip that forms the transparent basis of the sample cell. The upper lens of the objective is coupled to a glass coverslip through a layer of immersion oil, and the excitation light is focused onto a glass-water interface (GWI) thus enabling excitation of, and response collection from individual complexes. In the case of a high numerical aperture objective (NA = 1.3) the semi-aperture angle α (an angle between the most oblique light rays exiting the objective and the optical axis) is rather large: $NA = n \cdot \sin\alpha$, where n is the refractive index of the immersion medium (~ 1.52 for immersion oil), yielding $\alpha = 59^\circ$. This means that oblique light rays converge at rather oblique angles making the objective a sensitive element of the optical arrangement. It is designed for the situation when the refraction indexes of the immersion oil and the coverslip are the same – that is, there is no refraction of light rays propagating from the oil into the glass. Refractive index mismatch causes light rays that converge at different angles to propagate through different optical paths, resulting in optical phase differences and in a less than diffraction-

limited focal field distribution. Furthermore, the relative magnitude of the refractive indexes of the immersion oil and the coverslip glass depends on the excitation light wavelength and is also sensitive to temperature, making excitation and signal collection efficiency sensitive to experimental conditions.

Besides the main part – the objective – a microscope is not complete without some accessory opto-mechanical components such as a sample stage, an objective stage, which positions the objective along the optical axis, a tube lens forming the first real image of the object in the focus of the objective, and some means of directing the collected signal light onto the detection devices. All of these components can in principle be obtained separately and assembled together into a functioning microscope. We, however, chose for a commercially available biological microscope (Nikon, Eclipse TE300) that already contains all the aforementioned components although does not have the flexibility of custom design. In fact, microscope manufactures are very secretive about the details of their design so we do not possess information about the specific optical components and their disposition inside the microscope. It, however, provides an option of directing signal light onto different ports – front port video camera (VC) for focusing and side port for directing FL out of the microscope and onto detection devices.

Detection

FL filters

The confocal pinhole and the dichroic mirror are not sufficient to filter off all excitation light that is back-reflected from the GWI, and additional FL filters are required to remove residual background. The requirements for these filters are stringent since the aim is to record the whole FL spectrum of LHC, and the separation between the excitation wavelength (800 nm) and the wavelength of spectral maximum of FL varies between 40 and 70 nm depending on the species while the spectral full width at half of the maximum (fwhm) is 40-50 nm. Because of this, the rising edge of the filter transmission has to be quite steep. Dichroic mirror and FL filter transmission profiles together with a typical average spectrum are shown in Figure 2. The choices for the 800 nm excitation were a notch filter (Kaiser Optical Systems Inc., HNPF-800.0-1.0) or an interference barrier filter (Chroma Technology Corp., HQ885/130m) with maximum transmission of ~80% over a range of ~130 nm. With 594 nm excitation there is a larger separation between excitation and FL, and a glass filter with rather oblique rise of transmission profile is sufficient for this task (Edmund Optics Ltd, RG715). The drawback of the 594 nm excitation is that it generates a conspicuous background in the coverslip glass. A spectral measurement can be corrected for this by collecting and subtracting a background spectrum. In the case of image acquisition this problem can not be circumvented in such a way, and only a limited range of excitation intensities can be used to yield images with acceptable signal-to-noise ratio that can be analyzed for the occurrence of single complexes.

Detection devices

After passing through the FL filter the signal is directed onto either the APD (Perkin Elmer

Optoelectronics, SPCM-AQR-16) for image or the nitrogen-cooled back-illuminated deep depletion CCD camera (Princeton Instruments, Roper Scientific, Spec10: 100BR) for spectral acquisition. For spectral detection the FL light is dispersed with a grating (Optometrics LLC, HR600/1.0U 30SQ.X9.5mm) and focused onto a CCD chip with a circular lens. There is no commercial spectrograph implemented in order to reduce the number of optical elements and also to be able to custom-choose their characteristics – thus insuring the most efficient signal detection.

Scanning

In our experiments single-molecule detection involves the acquisition of an image of a surface area where molecules are immobilized. In confocal mode (as opposed to wide field) the data acquisition is serial rather than parallel, *i.e.*, only one point of the sample surface is analyzed at a time. Consequently, image acquisition must involve raster scanning in two perpendicular directions. In our setup we opted for the sample scanning option rather than the laser scanning, meaning that the laser beam is kept immobile, while the sample cell is translated relative to the beam, which insures the simplicity of the operation and the stability of the laser beam position focused on the sample surface. This is done with a piezo scanner (PzS) (Physik Instrumente, P-731.8C, E-710.4LC controller) of nanometer positioning precision. While the scanner is changing the position of the sample, the APD measures the corresponding FL signal intensity so that the position and intensity can be associated to produce a FL image. From the FL image the position of individual complexes can be identified and further investigated.

Synchronization of the experiment with the computer interface

The sequential procedure of data acquisition is the following (Figure 4): the PzS scans the area of the sample surface, and the SPCM-APD concurrently generates TTL pulses with the arrival of FL photons, producing a FL image; the image is analyzed for individual complexes by a software routine, coded using the National Instruments (NI) IMAQ library; the cycle of spectral acquisition is then initiated: the PzS positions an individual complex over the exciting laser beam focus, and the CCD camera obtains sequences of FL spectra of that complex; after this is done for all the complexes in the scanned area, the PzS scans another sample surface area and the described procedure is repeated. After the area within the PzS reach is fully scanned, the sample stage is roughly pushed by a motorized actuator (New Focus, 8320, 8753 intelligent driver) to make a fresh part of the sample surface available for scanning. The setup is switched between the image and the spectral acquisition with a motorized mirror flipper (New Focus, 8892). Before each image and spectral series acquisition, if the quality of the focusing worsens due to mechanical or thermal drift, the objective is automatically repositioned for optimal focusing by a motorized rotator (New Focus, 8401M, 8753 intelligent driver) in combination with an IMAQ board (NI, single channel, analog, monochrome PCI-1407) that analyses the image of the reflected excitation light on a VC (see the “Compensating for the thermal drift” section).

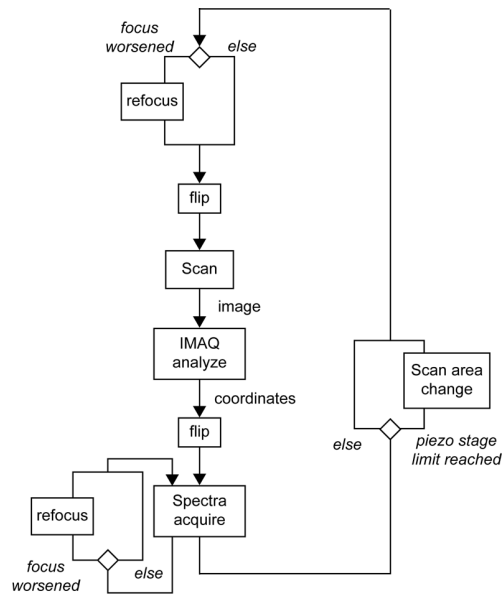


Figure 4. Flow diagram of experimental procedure.

The operation of electromechanical components and detection devices is synchronized by the personal computer (PC) as indicated in Figure 5. All devices are operated by a program coded in LabView 6.0 (NI). The CCD camera has a commercial WinSpec interface that is accessed from the LabView program using ActiveX technology.

The CCD camera controller is connected to the PC through the dedicated PCI card.

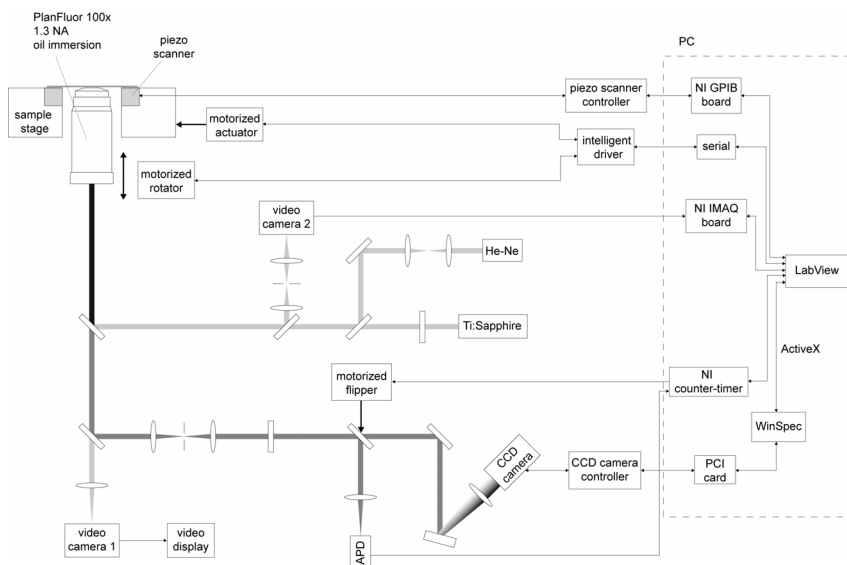


Figure 5. Controller and computer interface scheme of the setup.

TTL pulses of the SPCM-APD are counted with the counter-timer board (NI, PCI-6602). The PzS controller is connected to the PC through the NI PCI-GPIB card. The motorized rotator and actuator driver connects to the PC through a serial port. The motorized mirror flipper is positioned by TTL pulses provided by the counter-timer board.

THE ROLE OF THE PINHOLE

Diffraction

The wavelike nature of light and the finite dimensions of the optical element apertures, as well as of the laser beams, result in the limitation of the imaging quality due to diffraction. This implies that even a point source (in the absence of optical aberrations) is imaged by a lens as a three-dimensional (3D) pattern of electric field intensity of finite diffraction-limited characteristic size. The diameter of the first maximum of this pattern in lateral direction (Airy disk) is $1.22\lambda / \text{NA}$ (≈ 750 nm for $\text{NA} = 1.3$, $\lambda = 800$ nm), where λ is the excitation wavelength (Muller 2002). The fwhm of the image of a single LHC, which is essentially a scan of the focal area since the complex is much smaller than the probe, is 600 nm. The corresponding diameter of an Airy disk is 1200 nm. Hence, we come close to the theoretical minimum of the diffraction limited focus spot size.

Confocal principle

The confocal pinhole that is in an optical plane, conjugate to the focus of the objective, is the key element of the setup and gives it its name (Figure 1). It functions as a spatial filter for the light originating from the out-of-focus regions of the sample as shown in Figure 6 (Murthy 2001).

Not only the excitation focus is diffraction-limited but also the image of the fluorescing complex onto the confocal pinhole – even though a single complex can be regarded as a point source compared to the wavelength of light, its image is again a 3D pattern similar to the excitation focus. Taking into account the magnification (M) of the objective, the diameter of the pinhole that would allow the whole of the Airy disk of the complex image to pass, is $1.22\lambda M / \text{NA}$ (≈ 80 μm for $\text{NA} = 1.3$, $\lambda = 870$ nm, and $M = 100$) (Muller 2002). In our setup we use a 75 μm pinhole.

Optical sectioning and resolution

The pinhole enables the so-called optical sectioning – the signal is collected only from a thin layer of the sample at a time. A different layer is chosen by changing the axial position of the focus. The resolution of the microscope, *i.e.*, its ability to distinguish two adjacent objects, also depends on the size of the pinhole, although after a certain limit the reduction of the pinhole size hardly improves the resolution (Wilson 1995). In this case of single-molecule detection, the optical sectioning capability is not so important since the sample is intrinsically much thinner than the focal volume in axial direction: widely separated isolated complexes are dispersed on a coverslip and for the detection the focus is positioned onto

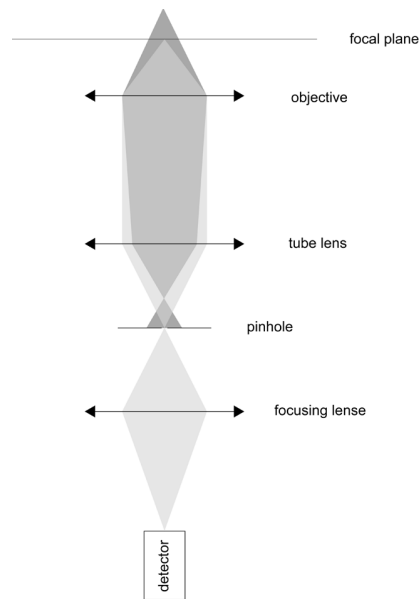


Figure 6. Confocal principle.

individual complex at a time. Nor spatial resolution is crucial, since complexes can be placed with arbitrary spacing. However, the presence of a pinhole significantly reduces the background of reflected excitation light.

EFFICIENCY CONSIDERATIONS

Collection and detection efficiencies

The amount of FL photons that are detected after all the signal processing depends on several factors:

- in epi-configuration, the objective collection efficiency is given by $k = \frac{1}{2}(1 - \cos\alpha)$ (Muller 2002), where α is the semiaperture angle. In our case $k = 25\%$;
- the microscope objective has a limited transmission; in the region of 800-950 nm we measured a fairly constant transmission of the Nikon PlanFuor objective of $\sim 60\%$;
- the FL signal travels through the microscope experiencing losses at the dichroic mirror, the optical element directing it to a proper port, the tube lens, the confocal pinhole, the FL filters, and other lenses and mirrors.

A rough estimate for overall throughput is $\sim 10\%$. Furthermore, detection devices – APD and CCD – have wavelength-dependent quantum efficiencies of output signal generation. For the APD this ranges from 60-25% and for the CCD from 85-55% in the 800-950 nm wavelength region. Hence, the total detection efficiency is probably about 5%.

The specified dark noise of the APD is < 20 counts/s, while the CCD dark current is $0.01 e^-/p/s$ at $-100^\circ C$ and the system read noise $< 5 e^-$ rms at 100 kHz readout frequency.

Since for spectral acquisition the FL signal is dispersed onto a number of detecting pixels, the signal level requirement is more demanding than in the case of image acquisition. A typical LHC FL spectrum covers the range of 800-950 nm. CCD pixels are binned to yield a resolution better than 1 nm. Thus, the spectral range of interest consists of 150 “superpixels”. The readout noise of a superpixel is the same as that of a pixel, and the total readout noise of the spectrum amounts to $\sim 750 e^-$. What should be the signal level for a reasonable spectrum is a rather philosophical question. From daily experience, spectra with an integral area of 5000-10000 counts can be considered “nice”. Taking into account the final estimated signal collection efficiency this requires 10^5 - $2 \cdot 10^5$ photons/s to be emitted by a single complex.

Expected signal levels

With the typical excitation intensity of 1 μW at 800 nm, assuming Gaussian laser beam profile and diffraction-limited focus size, the LH2 complex of *Rhodospseudomonas (Rps.) acidophila* absorbs $\sim 1 \cdot 10^7$ photons/s (Rutkauskas, *et al.* 2004). Its FL quantum yield is 10% (Monshouwer, *et al.* 1997), but the emission is reduced to a few percent by the formation of triplets, yielding about 10^5 FL photons emanating the complex, which is just enough to record single complex spectra with an integration time of 1 s (see previous section).

OPERATION ROUTINES

Focusing of the objective

Prior to any kind of microscope operation, the objective has to be positioned with its focus on the GWI with the immobilized single complexes (see Figure 3). The focus position is monitored by the reflection of excitation light on a small VC (Watec America Corp., Watec LCC-902K) mounted at the front port of the microscope (Figure 7). The dichroic mirror is deliberately designed to be $<100\%$ reflective for the excitation light, and a fraction of the excitation light, reflected from the GWI, is transmitted. The lens is positioned to focus the collimated beam onto a VC chip, which is at a fixed position. Since the objective is infinity-corrected, it produces a collimated beam of reflected light only when the optical source is at its focal distance. However, even though the apparent source of the reflected excitation light is at the focal distance, it superimposes on the GWI only when the excitation laser beam is collimated. That is – a bright image on the VC indicates objective focusing excitation light on the GWI only when the excitation laser beam is well collimated. If, for example, the excitation beam is converging, the objective forms an image closer than the focal distance. The GWI serves as a mirror, and an imaginary source is formed opposite to the real one relative to the GWI. Moving the objective to position the imaginary source at a focal distance, yields a collimated beam of reflected light (Figure 8). This means that although the VC reads optimal focus, in fact, the excitation laser beam is not focused on the GWI. Similarly, when the beam is diverging, the objective has to be in the position shown in

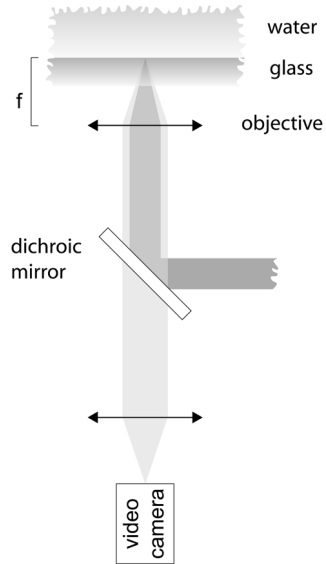


Figure 7. Focusing by the reflection of the excitation from the glass-water interface. f denotes the focal distance of the objective. The exciting laser beam is depicted by dark grey and the reflected light – by light grey.

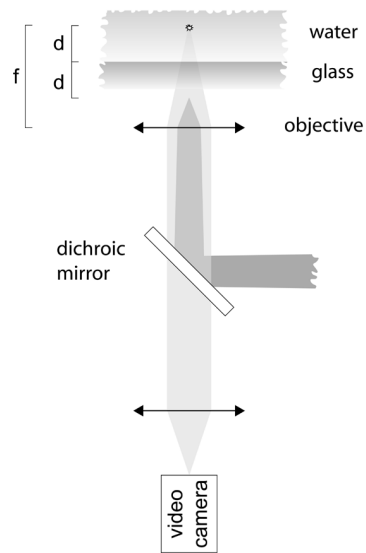


Figure 8. Monitoring of the decollimated converging excitation beam. The small star represents an imaginary optical source. It is at the same distance from but on the other side of the glass-water interface as the real image of the excitation beam.

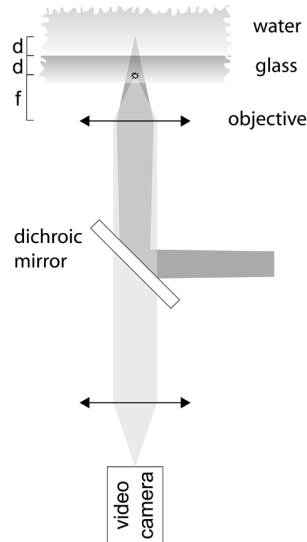


Figure 9. Monitoring of the decollimated diverging excitation beam. The small star represents a real optical source. The excitation beam is shown to propagate and focus beyond the glass-water interface only for explanation. This would-be focus spot is at the same distance from but on the other side of the glass-water interface as the real optical source of the reflected excitation light.

Figure 9, to yield a collimated beam of reflected light. Again, the laser beam focus does not rest on the GWI. To conclude, only when the excitation laser beam is collimated, can the focusing condition be monitored on the VC. Keeping this in mind, the Ti:S laser beam is inserted into the objective without modification since it is well-collimated.

Alignment of confocal pinhole and detectors

The collimating lens after the confocal pinhole is positioned to produce a collimated beam of 800 nm reflected light when the excitation light at this wavelength is focused onto the GWI. The confocal pinhole and detection devices can be aligned with different probes – polystyrene fluorescent beads, a concentrated sample of immobilized LHCs, or even a bulk solution of a fluorescent dye. Polystyrene beads can be easily immobilized on a glass surface by adding a little bit of salt into the solution. However, there are no commercially available beads optimal in the near infrared (IR) region. Although the red-most available kind of 1 μm beads can still be detected very easily even when exciting with 800 nm light, 1 μm is comparable to the focal area dimension and thus too large for a precise alignment. A better probe is a layer of LHCs immobilized on a glass surface and washed with oxygen-free buffer. In the absence of oxygen, such preparation is quite stable and can be used for alignment. Finally, a bulk solution of any fluorescent dye with properly selected absorption can serve as a probe for optical adjustments. Upon objective focusing onto an GWI, the FL signal originates mainly from the area of the first significant maximum of the focus pattern, and the confocal pinhole can be positioned in a plane conjugate to the fluorescent source.

Compensating for the objective achromatism

The chromatic aberration of the lens is the dependence of the focal distance on the light wavelength. Nikon PlanFlour objective is presumably corrected for chromatic aberration at two wavelengths (481.1 nm and 656.3 nm), which does not guarantee identical focal distances for 800 nm and 594 nm, our two excitation wavelengths. In practice, the focuses at these two wavelengths are longitudinally separated to a larger extent than can be tolerated, keeping in mind the stringent distance requirements in the focal area (defocusing by a fraction of a micron reduces the signal detectably). Thus, once the objective is positioned for optimal FL signal collection (collimated 800 nm beam focused onto the GWI) the 594 nm beam has to be decollimated to bring the focal volume onto the GWI. The beam is decollimated to obtain maximum signal from a sample of immobilized LHCs in deoxygenated environment. Note that in such a situation the reflected 594 nm light is not projected onto a VC as a tight focus because the optical source of the reflected light is not at a focal distance of the objective for that wavelength (reflected light is not collimated by the objective). For the routine positioning of the objective with 594 nm excitation wavelength we use an additional small VC as is explained in the next section.

Compensating for the thermal drift

During prolonged periods of time, the GWI and the objective drift relative to each other, which worsens the quality of excitation and signal collection. It is possible to correct for this automatically by monitoring the intensity of the reflection from the GWI. Most of the excitation light reflected from the GWI is reflected by the dichroic mirror back down the excitation pathway. Part of the reflection is diverted by the beamsplitter in the excitation branch (Figure 1). This diverted reflection is focused onto a pinhole (not to be confused with the confocal pinhole) and after passing the pinhole focused onto a VC. The pinhole is positioned to yield the maximum integral intensity on the VC when the excitation light is properly focused onto the GWI. Changes of this focusing will cause the reflected light to focus differently on the pinhole, and consequently different amount of light will pass through the pinhole. Hence, the light intensity detected by the VC is a direct measure of the focusing quality.

The microscope objective stage is attached to a motorized rotator; the latter, with the aid of a robust software algorithm brings the sample focus to optimum by associating the position of the rotator with the reflection intensity detected by the VC that is coupled to the video grabber board.

The pinhole can be positioned for optimal focus of any wavelength of excitation light – the automatic refocusing procedure can be realized for any excitation wavelength by simply manually adjusting the position of the pinhole. At the same time this scheme is an independent way of optimally focusing 594 nm excitation.

Wavelength end detection sensitivity calibration

The wavelength calibration is done by positioning an argon lamp (which has several narrow

emission lines at known wavelengths) over the drop of a milk emulsion on a coverslip and focusing the objective on an GWI. It is presumed that this creates a uniform light source at the focus of the objective so that the spectral line reading does not depend on the exact position of the lamp. The spectral calibration can also be used to fine-tune the axial position of the CCD camera – since the argon lamp spectrum around 840 nm has two closely spaced spectral lines, the CCD is adjusted to best resolve them.

FL sensitivity correction is obtained by reflecting light from a tungsten halogen lamp with a gold mirror (that has a flat reflection profile in the near IR spectral region of interest) again onto a drop of milk emulsion and recording the spectrum. For correction, the actual measurement has to be multiplied by the reciprocal of the correction spectrum.

SAMPLE PREPARATION

Sample cell

The functional scheme of the home-designed sample cell is shown in Figure 10. It consists of a standard 0.17 mm thickness, Ø25 mm circular glass coverslip (Harvard Apparatus Ltd., CS-25R) at the bottom, a teflon spacer of 0.7 mm thickness in the middle and a temperature controlling element on top. The cell is assembled by pressing these three elements tightly together with a threaded screw. The upper element is a closed cylinder with an empty volume; there are two inlets into this volume for the circulator bath and two capillary inlets traversing the cylinder and allowing access into the sample volume of the cell. Water can be circulated in the volume of the upper element by a cooling and heating thermostat (Fisher Scientific, polystat K6-3) making it possible to adjust the temperature of the cell. Although there is a temperature gradient in the cell, the temperature very close to the GWI is

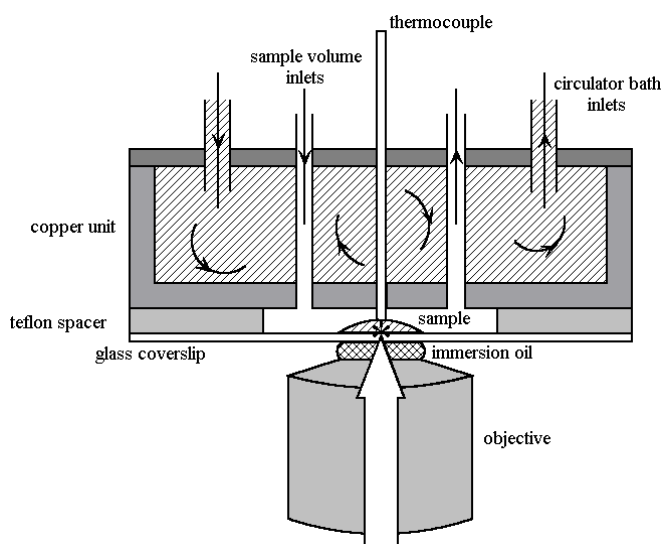


Figure 10. Sample cell.

measured with a thermocouple (Tempcontrol I.E.P. B.V., MTK-2, P610 indicator) traversing the heating element.

Single complexes are deposited by spreading a drop of 5 μ l of pM sample solution on a dry coverslip and allowing the complexes to immobilize during the time it takes to assemble the cell. Complexes that do not immobilize on the glass surface are removed from the sample cell by flushing it with a deoxygenated buffer.

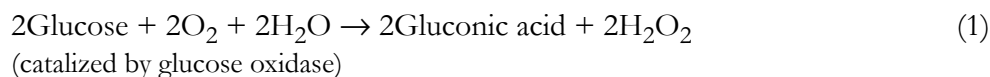
The option of temperature control was initially meant for increasing the temperature of the sample in order to destabilize it, but it turned out to be advantageous in the opposite sense – some of the measured samples were not stable enough to conduct any meaningful measurement at ambient temperature although decrease of temperature down to 5° C made them suitable for measurement for at least a day.

Oxygen removal

If the singlet excited bacteriochlorophyll (BChl) molecule in the LHC crosses to the triplet state, it can sensitize molecular oxygen which then becomes a highly reactive free radical and can cause severe damage to the LHC leading to its photobleaching. In practise, the survival time of a single LHC under illumination is significantly reduced in the presence of oxygen. In the course of the setup development we were lucky to detect images of LH2 of *Rps. acidophila* in a buffer containing LDAO in contact with natural atmosphere. Though the complexes were not stable enough for spectral measurements, they still produced distinct images. On the contrary, other species in a different detergent did not yield similar images, which initially led to the false idea of radically different stabilities, or different strength of adherence to the treated glass surface of different kinds of complexes. However, it turned out that it is probably a different detergent micelle permeability to oxygen that caused these differences in sample stability. Consequently, although carotenoid molecules in LHCs quench BChl triplets, oxygen probably still receives some of the BChl triplet excitations or a different mechanism of excitation trap formation in LHC ring causes quenching of LHC FL (Law and Cogdell 1998). Regardless of the actual mechanism, oxygen removal significantly prolongs the lifetime of the complexes.

We designed and built a special chamber for the deoxygenation of the sample buffer. Gaseous nitrogen can be flown through the chamber with the buffer in a controlled way, while the buffer is agitated with a magnetic spinner. Initial fast flow exponentially reduces the amount of oxygen in the atmosphere above the buffer and subsequent slow flow reduces the concentration of oxygen originating from the buffer to any desired extent. This way, the concentration of oxygen in the buffer can be diminished in ~0.5 h to levels undetectable by an electrolytic oxygen meter (Cyberscan 100 Do, Eutech Instruments Pte Ltd.). Furthermore, residual oxygen can be removed by dissolving minute amounts of $\text{Na}_2\text{S}_2\text{O}_4$ without opening the chamber after the oxygen removal with nitrogen flow.

An alternative to physical oxygen removal is a three component oxygen scavenger consisting of glucose oxidase, catalase and glucose (Bopp, *et al.* 1999, Ha, *et al.* 1999, Harada, *et al.* 1990). The reaction mechanism of this system is:



The net reaction:



Reaction (1) occurs faster with an optical β -D-glucose isomer.

All three components were obtained from Sigma-Aldrich Chemie B.V. 100 times concentrated water stock solutions of glucose oxidase and catalase were frozen to -80°C for storage. Thawed stock solutions were added to the buffer together with the powder glucose to adjust the final concentrations to $200\ \mu\text{g}/\text{ml}$ of glucose oxidase, $35\ \mu\text{g}/\text{ml}$ of catalase, and $7.5\ \text{mg}/\text{ml}$ of glucose. Closing the chamber and quickly creating a nitrogen atmosphere enables the preservation of an oxygen-free solution.

Excessive nitrogen gas pressure pushes the oxygen-free buffer directly from the deoxygenation chamber through the assembled sample cell, removing the access sample and submerging single complexes immobilized on a glass surface in oxygen-free environment.

Sample immobilization

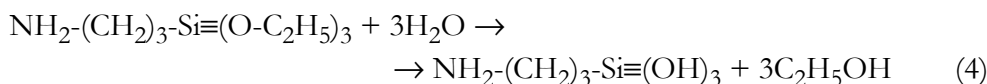
Prior to any meaningful data acquisition, isolated LHCs have to be immobilized on a surface. There are at least a few different techniques of doing that.

One widely spread way, also popular in atomic force microscopy, is the use of a mica substrate. A freshly cleaved mica sheet is atomically flat and right after cleavage it is also completely clean. Furthermore, mica is naturally slightly negatively charged. So LHCs are attracted to its surface either through interaction of their polar or charged residues or by means of the positively charged protein N terminus. However, we did not take advantage of this option because mica is a rather fragile substance and using it as a base of a sample cell is problematic for mechanical reasons. Moreover, it has limited optical transparency, a different reflection index than the immersion oil and it exhibits anisotropic polarization properties. Consequently, as was laid out earlier in this chapter, it causes a refractive index mismatch which seriously impairs the efficiency of excitation and signal collection. A different configuration is possible with a piece of mica sheet on a glass coverslip with immobilized complexes on a surface facing downwards. This method however does not work, because even a small piece of mica sheet can not be pressed to the glass surface close enough – that is, to focus on a mica-water interface (with immobilized complexes) the objective focus has to penetrate a layer of water with a thickness of a few microns which is sufficient to render the measurement totally inefficient. Furthermore, even if mica could be close enough to the coverslip, in such configuration flushing the sample with deoxygenated

buffer would be problematic.

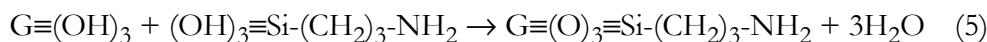
Therefore we chose for a different approach. Aminopropyltriethoxysilane (APS) or poly-L-lysine (PLL) (Sigma-Aldrich Chemie B.V.) can be deposited on a glass surface to form a “carpet” of positively charged (at neutral pH) amino groups that are capable of forming non-covalent bonds with pigment-protein complexes.

Protocols of glass silanization are described in (Arkles, EBSiences, Fishelson, *et al.* 2001, Pierce). The routine consists of dipping the glass in 2-5% APS solution, rinsing it with water or organic solvent, drying and possibly curing for some time in the oven. APS $\text{NH}_2\text{-(CH}_2\text{)}_3\text{-Si}\equiv\text{(O-C}_2\text{H}_5\text{)}_3$ deposition on the glass surface occurs in several stages. In the first stage it undergoes hydrolysis over O-C bond:



Reaction in equation 4 takes place with transient amounts of water in organic solution, mixture of water and organic solvent, or water solution of APS. The presence of water is essential for hydrolysis.

In the second stage, reaction of condensation occurs, during which the hydrolysed APS reacts with hydroxyl groups on a glass surface:



In equation 5 APS forms covalent bonds to the glass. For the reaction 5 to occur, the glass surface has to be first treated with the “piranha” (a mixture of concentrated sulfuric acid and hydrogen peroxide) and then with the NaOH solution to form hydroxyl groups on the surface (Fishelson, *et al.* 2001).

PLL is a polymer of lysine amino acid with a side chain containing one amino group. The coating procedure is straightforward (Sigma product sheet): coverslips are mounted in a teflon mini-rack (Molecular Probes Europe B.V.) and submerged for 5 min in a 0.01% PLL deionised water solution. No prior glass processing is involved. Treated coverslips are rinsed with copious amounts of deionised water and submerged in it for storage. Before use they are dried with a stream of gaseous nitrogen.

Although it is recommended to clean the glass before depositing the PLL or the APS, in practice we experienced that this step does not result in any more efficient immobilization. Furthermore, piranha and NaOH treatment in the case of APS could also be omitted, moreover that it often makes the glass “dirtier”, probably because the glass quality is insufficient to undergo etching with a concentrated acid or base. Following the entire procedure is probably crucial for achieving a homogeneous and reproducible coating, but this is not relevant for our purposes.

REFERENCES

- Arkles, B. Silane coupling agent chemistry. <http://www.unitedchem.com/>.
- Bopp, M. A., Sytnik, A., Howard, T. D., Cogdell, R. J., and Hochstrasser, R. M. (1999) The dynamics of structural deformations of immobilized single light-harvesting complexes. *Proc. Natl. Acad. Sci. U.S.A.* 96, 11271-11276.
- EBSiences. <http://www.ebsciences.com/histology/t8100sec.htm>.
- Fishelson, N., Shkrob, I., Lev, O., Gun, J., and Modestov, A. D. (2001) Studies on charge transport in self-assembled gold-dithiol films: conductivity, photoconductivity, and photoelectrochemical measurements. *Langmuir*. 17, 403-412.
- Ha, T. J., Ting, A. Y., Liang, J., Caldwell, W. B., Deniz, A. A., Chemla, D. S., Schultz, P. G., and Weiss, S. (1999) Single-molecule fluorescence spectroscopy of enzyme conformational dynamics and cleavage mechanism. *Proc. Natl. Acad. Sci. U.S.A.* 96, 893-898.
- Harada, Y., Sakurada, K., Aoki, T., Thomas, D. D., and Yanagida, T. (1990) Mechanochemical coupling in actomyosin energy transduction studied by *in vitro* movement assay. *J. Mol. Biol.* 216, 49-68.
- Law, C. J., and Cogdell, R. J. (1998) The effect of chemical oxidation on the fluorescence of the LH1 (B880) complex from the purple bacterium *Rhodospirillum rubrum*. *Febs Lett.* 432, 27-30.
- Monshouwer, R., Abrahamsson, M., van Mourik, F., and van Grondelle, R. (1997) Superradiance and exciton delocalization in bacterial photosynthetic light-harvesting systems. *J. Phys. Chem. B.* 101, 7241-7248.
- Muller, M. (2002) Introduction to confocal fluorescence microscopy, Shaker publishing, Maastricht.
- Murthy, D. B. (2001) Fundamentals of light microscopy and electronic imaging, Wiley-Liss.
- Pierce. <http://www.piercenet.com/files/TR0001dh4-Attach-to-glass-cleavable.pdf>.
- Rutkauskas, D., Novoderezhkin, V., Cogdell, R. J., and van Grondelle, R. (2004) Fluorescence spectral fluctuations of single LH2 complexes from *Rhodospirillum rubrum* strain 10050. *Biochemistry*. 43, 4431-4438.
- Wilson, T. (1995) The role of the pinhole in confocal imaging systems. In Handbook of biological confocal microscopy. Pawley, J. B., Ed., Plenum Press, New York.

Fluorescence spectral fluctuations of single LH2 complexes from *Rhodospseudomonas acidophila* strain 10050

Danielis Rutkauskas, Vladimir Novoderezhkin, Richard J. Cogdell, and Rienk van Grondelle

ABSTRACT

We have investigated the energy landscape of the bacterial photosynthetic peripheral light-harvesting complex 2 of purple bacterium *Rhodospseudomonas acidophila* by monitoring sequences of fluorescence spectra of single LH2 assemblies, at room temperature, with different excitation intensities as well as at elevated temperatures, utilizing a confocal microscope. The fluorescence peak wavelength of individual complexes was found to abruptly move between quasi-stable levels differing by up to 30 nm. These spectral shifts either to the blue or to the red were accompanied by a broadening and decrease of the intensity of the fluorescence spectrum. The frequency and size of these fluorescence peak movements were found to increase linearly with excitation intensity. Using the modified Redfield theory, changes in the realization of the static disorder accounted for the observed changes in spectral shape and intensity. Long lifetimes of the quasi-stable states suggest large free energy barriers between the different realizations.

INTRODUCTION

Photosynthetic pigment-protein complexes play a decisive role in the collection of solar energy and the transfer of electronic excitation energy to the photosynthetic reaction center, where a charge separation is initiated (van Grondelle 1985, van Grondelle, *et al.* 1994). Since a high-resolution structure of the peripheral light-harvesting complex 2 (LH2) of the photosynthetic bacterium *Rhodospseudomonas (Rps.) acidophila* has become available (McDermott, *et al.* 1995, Papiz, *et al.* 2003), the molecule has played a key role in aiding our current understanding of photosynthetic light-harvesting (Cogdell, *et al.* 1996, Hu, *et al.* 2002, Robert, *et al.* 2003, Sundström, *et al.* 1999). LH2 of *Rps. acidophila* is a highly symmetric ring of nine protein-pigment subunits, each containing two helical transmembrane polypeptides, the α -polypeptide on the inner and the β -polypeptide on the outer side of the ring. The hydrophobic terminal of the protein binds a ring of 18 tightly coupled bacteriochlorophyll (BChl) molecules with a center-to-center distance of less than 1 nm between neighboring pigments. This ring is responsible for the intense absorption of LH2 at 850 nm (B850 ring). A second ring of nine weakly interacting BChls is located in the polar region of the protein and is largely responsible for the absorption around 800 nm (B800 ring).

From the detailed study of the spectroscopic and energy transfer properties of LH2, a consistent physical picture of the complex has emerged (Alden, *et al.* 1997, Hu, *et al.* 1997, Sauer, *et al.* 1996, Scholes and Fleming 2000, Wu, *et al.* 1997). All basic spectroscopic features can be understood on the basis of a model that includes both intrinsic disorder and excitonic coupling between the pigments ($\sim 300 \text{ cm}^{-1}$ for neighboring BChls in the B850 ring and $\sim 30 \text{ cm}^{-1}$ for adjacent pigments in the B800 ring). Via introduction of relaxation between the elements of the so-called density matrix, the dynamics of vibrational and electronic coherence and excitation energy transfer have been described in great detail.

On the basis of room- and low-temperature single-molecule experiments, it has been proposed that the LH2 ring can deviate from the ideally circular structure (Bopp, *et al.* 1999, Ketelaars, *et al.* 2001, Matsushita, *et al.* 2001, van Oijen, *et al.* 1999). Room-temperature (RT) polarized fluorescence (FL) experiments were interpreted in terms of an elliptical absorber and emitter with ellipticity and directions of the principal axis varying as a result of the B800 and/or B850 distortion that destroys the rotational symmetry, traveling around the ring on a time scale of seconds (Bopp, *et al.* 1999). The anomalously large splitting of the two major orthogonal excitonic transitions observed in low-temperature polarized FL excitation spectra was attributed to a modulation of the coupling strength in the B850 ring that was asserted to be associated with an elliptical deformation (Ketelaars, *et al.* 2001, Matsushita, *et al.* 2001, van Oijen, *et al.* 1999). Spectral diffusion of the B800 band of LH2, observed in the low-temperature experiments, was also attributed to structural alterations (van Oijen, *et al.* 2000). These spectral fluctuations of different magnitudes occurring on different time scales were associated with the hierarchical structure of the protein conformational landscape (Hofmann, *et al.* 2003). Smaller ellipticities of 0.95-0.91 were found in AFM measurements

of loosely packed LH2s in membrane, and were probably partly due to an interplay of the disrupting tip and stabilizing lipid environment effects (Scheuring, *et al.* 2001). On the other hand, isolated LH2s in the scaffold of detergent molecules clearly deviated from a ringlike shape (Hong, *et al.* 2004). In general, the observed variation of the spectral and functional properties of LH2 suggests that the complex can undergo a variety of deformations. It is reasonable to assume that such dynamic structural alterations also underlie the pattern of the static disorder of pigment site energies that play a key role in understanding the spectroscopic and energy transfer properties of LH2.

In the work presented here, we investigate these dynamic fluctuations under physiological conditions, as manifested by the time evolution of the FL spectrum. To do so, we have acquired series of FL spectra of single LH2 complexes at RT and elevated temperatures with various excitation intensities.

MATERIALS AND METHODS

Sample preparation and immobilization

Isolated LH2 complexes were immobilized on a standard microscope coverslip treated with a 0.01% poly-l-lysine (PLL, Sigma) solution. The coverslip was used as a base for a home-designed, hermetic, temperature-controlled sample cell.

Purified LH2 complexes of *Rps. acidophila* were prepared as described previously (Cogdell and Hawthornthwaite 1993, Halloren, *et al.* 1995). The sample stock solution of 0.62 μM LH2 in buffer of 20 mM Tris (pH 8.0) and 0.1% lauryldimethylamine oxide (LDAO) was kept at -80°C prior to being thawed. It was diluted in the same buffer in two steps by a factor of $2 \cdot 10^4$. A 20 μl drop of a 33 pM LH2 solution was placed on the coverslip, and the sample cell was assembled. After a few minutes, the cell volume was washed with deoxygenated, 0.1% LDAO-containing buffer, thus removing the access sample and submerging the immobilized single molecules in an oxygen-free environment. Oxygen was thoroughly removed from the buffer by flowing gaseous nitrogen and by agitating the buffer with a magnetic spinner to a level that cannot be detected with an electrolytic oxygen meter.

Experimental setup

FL images and spectra were acquired with a confocal microscope based on a commercial inverted microscope (Nikon, Eclipse TE300). The excitation source was a titanium sapphire laser system (Coherent, Mira 900) producing 3 ps, 800 nm pulses with a repetition rate of 76 MHz. A dichroic beam splitter (Chroma Technology Corp., 815dclp) reflected the laser beam into the objective lens (Nikon, Plan Fluor 100 \times , 1.3 NA, oil immersion), focusing the excitation light onto the glass-water interface in the sample cell to a diffraction-limited spot (fwhm of ~ 600 nm). The intensities used in the experiments (from 0.13 to 1.6 kW/cm^2 or equivalently 500 nW to 6 μW) represent the values at this interface. The emission was filtered with a 100 μm pinhole and single 130 nm interference filter (Chroma Technology

Corp., HQ885/130m).

The sample cell was mounted on a closed loop two-dimensional piezo stage (Physik Instrumente, P-731.8C) controlled by a digital four-channel controller (Physik Instrumente, E-710.4LC).

To obtain images, emission was detected with a Si avalanche photodiode (APD) single photon-counting module (SPCM-AQR-16, Perkin-Elmer Optoelectronics) and counter timer board (National Instruments, PCI-6602). Spectra were acquired by dispersing the FL onto a liquid nitrogen-cooled back-illuminated charge-coupled device (CCD) camera chip (Princeton Instruments, Roper Scientific, Spec10: 100BR). CCD pixels were binned along the spectroscopic axis to yield a resolution of <1 nm. FL detection in both image and spectral acquisition modes was indiscriminate of signal polarization. The polarization sensitivity of the detection due to the dispersing element was not explicitly taken into account. However, because of a wide angle of acceptance of the high numerical aperture objective, we expect the effect of polarization sensitivity to be small.

Images and spectra

A FL image is acquired by continuously sweeping the piezo stage over the laser focus with a frequency of 3 Hz while its position in the perpendicular direction is changed by 100 nm for each line; the FL signal is concomitantly detected with an APD. Images are then constructed by associating the piezo stage coordinate with the corresponding intensity. The scanning covers a $10 \mu\text{m} \times 10 \mu\text{m}$ area. After the coordinates of bright particles are determined, the piezo stage is positioned to bring the particle into the focus of the objective, and after the mode is switched to a spectroscopic one, a series of FL spectra is collected for 2 min with an integration time (0.5-2 s) that is dependent on the excitation power and the sample temperature. At higher excitation intensities and lower temperatures, shorter integration times are sufficient for the collection of the spectra with a satisfactory signal-to-noise ratio. The excitation intensity and the ambient conditions remain unchanged during the acquisition.

Data analysis

For a quantitative analysis, the acquired spectra are fitted with a skewed Gaussian function, using a non-linear Levenberg-Marquardt fitting method. The expression for the skewed Gaussian function is

$$F(\lambda) = \Delta + A \exp(-\ln(2)[\ln(1 + 2b(\lambda - \lambda_m)/\Delta\lambda)/b]^2)$$

where Δ is the offset, A the amplitude, λ_m the FL peak wavelength (FLP), $\Delta\lambda$ the width, and b the skewness.

The fwhm of the spectrum is calculated from the width and the skewness. Consequently, by fitting each spectrum from a series, we obtain the time traces of the amplitude, the fwhm, and the FLP with the corresponding confidence margins.

RESULTS

The primary objective of this study was to investigate if we could observe fluctuations of peak wavelength, width, and intensity of emission spectrum of single LH2 complexes as a measure of structural dynamics, which can occur in this complex. This was achieved by collecting series of single-molecule FL spectra at RT and variable excitation intensity as well as at elevated temperatures. In total, close to 1000 molecules were studied under various ambient conditions. Intrinsic (*i.e.*, measured with a low excitation power) fluctuations proved to be insignificant on the time scale of our experiment (2 min). However, increasing the excitation power introduced prominent spectral jumps and changes in the spectral shape and intensity of the emission. To a smaller extent, the same effect could be detected in experiments at elevated temperatures (28 and 35° C), though the stability of the LH2 complexes was decreased significantly.

Earlier experiments (Bopp, *et al.* 1999) have shown that the survival time of the illuminated LH2 complexes strongly depends on the presence of oxygen in the environment. We observed that irreversible photobleaching of an oxygen-containing sample took place over the course of seconds or tens of seconds, and even when kept in the dark, the oxygen-containing preparation degraded in a few hours at RT. On the other hand, careful removal of oxygen from the ambient prolonged the bright state of single LH2s to minutes or even tens of minutes in some cases, and the sample remained suitable for measurements for 2 days. For the reasons given above, all the single-molecule measurements presented in this work were carried out on oxygen-free samples.

Images

An example of a raw FL image of LH2 assemblies immobilized on a PLL-treated coverslip is shown in Figure 1. Each image is 100 pixels \times 100 pixels (0.1 μm per pixel). The pixel integration time is 3 ms. The excitation intensity at 800 nm is 3.5 μW . The background is ≤ 10 counts/pixel, and the maximum intensity is 87 counts/pixel. Although particles appear to be similar in integral intensity, in reality they are distributed over a range of 1300-2500

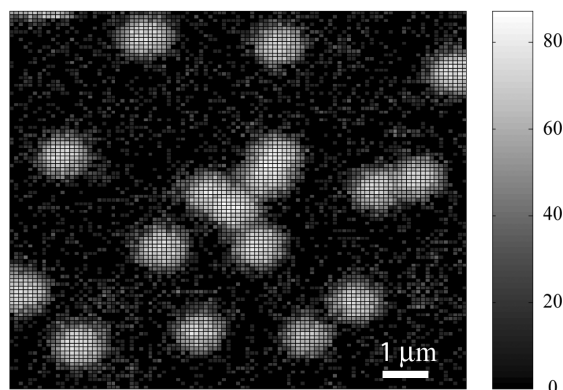


Figure 1. FL image of single LH2 complexes.

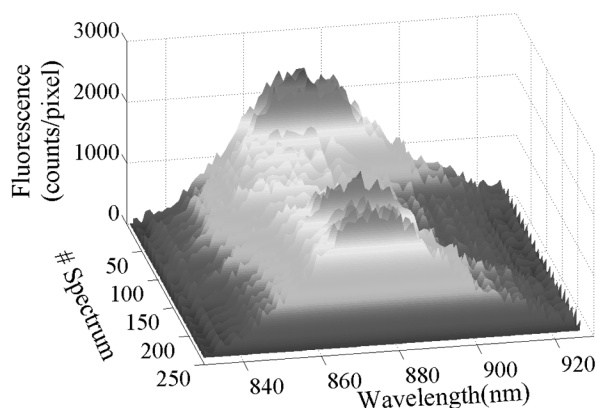


Figure 2. Series of FL spectra of a single LH2.

counts, which is probably partly due to the polarization effects of the excitation absorption and emission (since single complexes are immobilized on an atomically non-flat glass surface) and partly to the tendency of the emission intensity to fluctuate. We also do not exclude the possibility of observing aggregated complexes or adjacent complexes appearing as one particle. To make sure that we monitor only single LH2s, excessively bright particles are discarded and spectral measurements are carried out on molecules constituting the bulk of the intensity distribution.

FL spectra

A typical series of FL spectra of a single LH2 enabling the observation of the spectral diffusion is presented in Figure 2. It results from a sequence of 240 single LH2 spectra via summation of each 10 consecutive spectra for clarity. The spectrum integration time is 0.5 s, and the excitation intensity at 800 nm is 6 μ W. In this experiment, the FL amplitude and the FLP diffuse dramatically. Spectra at the beginning of the series have a relatively high amplitude and an intermediate FLP, whereas in the course of the measurement, the amplitude subsides with the FLP shifting to the blue; both parameters recover at the end of the series. Notably, the width of a single complex FL spectrum is comparable with that of the bulk spectrum (data not shown).

FLP traces

FLP time traces of four individual particles are shown in Figure 3. The spectrum integration time is 0.5 s, and the excitation intensity at 800 nm is 6 μ W. Though acquired with the same excitation intensity and ambient conditions, the traces are qualitatively different. The FLP fluctuates weakly in Figure 3A, while panels B and C of Figure 3 demonstrate notable spectral jumps to the blue and to the red relative to the initial FLP value, respectively. Interestingly, the FLP abruptly jumps between the various levels of almost constant magnitude, and even more remarkably, it regains a value close to the initial one before the end of the trace. Unexpectedly, the complex spends a number of seconds in each of the

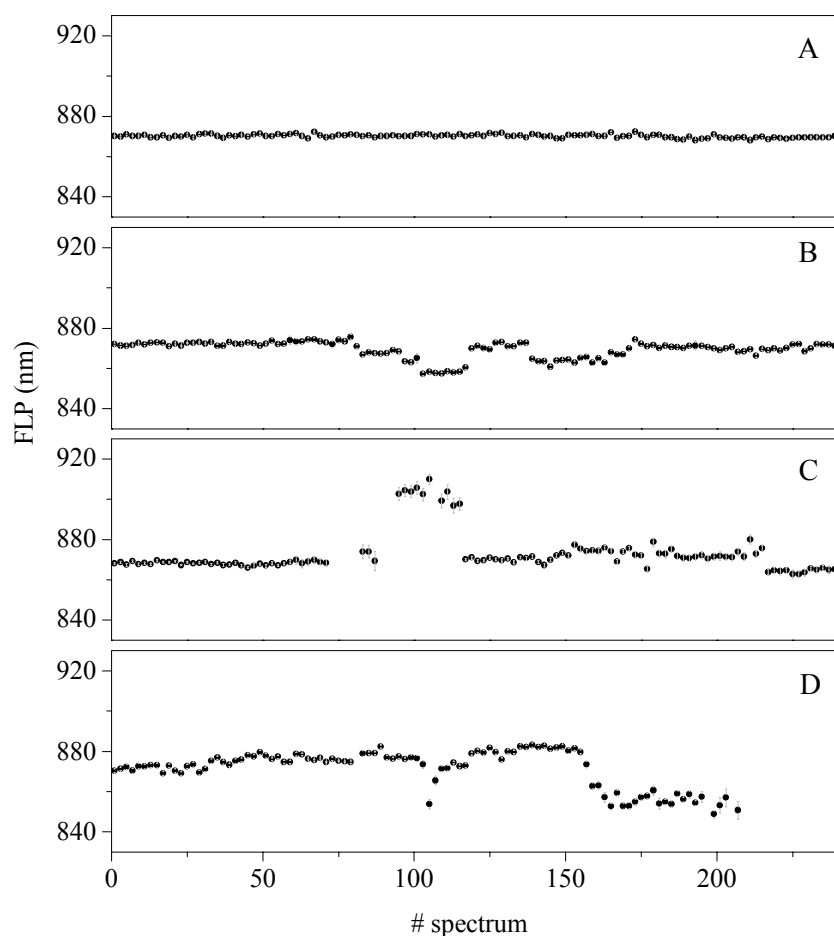


Figure 3. FLP time traces of four individual LH2s. Various spectral diffusion scenarios: (A) relatively constant FLP, (B) spectral jumps to the blue, (C) spectral jump to the red, and (D) spectral jumps to both the red and blue. Only every third data point is presented for clarity.

stable states before it moves to a different state. Figure 3D shows spectral diffusion in both directions. The spectrum of a single particle first drifts to longer wavelengths, then abruptly jumps to the blue, and finally settles at a FLP that is shifted to the blue by ~ 15 nm relative to the initial FLP, preventing the unambiguous classification of this particle as one that performs a spectral jump in one direction. We note that these conspicuous spectral jumps are in many cases reversible, and the initial FLP value (or a value close to it) is regained (Figure 3B,C). For other particles, the initial FLP is not recovered before photobleaching occurs (Figure 3D) (or rather an apparent photobleaching; we have observed the recovery of the emission of some complexes after dark periods of more than 2 min, data not shown). From Figure 3C, it appears that the LH2 bleaching does not occur as a single event; after the complex enters a dark state for a few seconds, its emission reappears with a different FLP. On the other hand, the spectral diffusion can occur without the temporary loss of the

radiative power, as shown in the Figure 3B. From all the particles measured with the excitation intensities in the range from 1.5 to 6 μW , $\sim 10\%$ exhibited the step-like character of the FLP traces.

Light-induced spectral fluctuations

In this work, we confine ourselves to a qualitative description of the spectral properties of the strongly fluctuating particles. A detailed account of the relevant statistics will be presented in the next Chapter. In summary, we observed that few spectral jumps of the single LH2 occur at low excitation intensity and RT, but the frequency of their occurrence increases with an increase in excitation intensity and to a much lesser extent with temperature elevation. Thus, spectral diffusion in our experiment is mostly light-induced. However, since the observed spectral jumps are reversible (Figure 3), we conclude that even with the highest excitation intensity used here, the LH2 complex is not driven into conformational states from which it can no longer escape. Instead, stronger excitation or an elevated temperature enables an exploration of a broader range of states in a finite span of the experimental time.

Some of the strongly fluctuating LH2 assemblies exhibited a strong correlation between the temporal changes of the FLP and the amplitude and/or between the FLP and the fwhm. We observed that these correlations might be either positive or negative; for example, some single LH2s display a negative jump of the FLP (blue shift) with a concomitant increase of the fwhm (negative correlation), and others undergo an increase in FLP (red shift) that is connected with an increment of the fwhm (positive correlation). Overall, we observe that if a particle undergoes significant spectral diffusion, accompanied by the correlated evolution of two or all three spectral fit parameters, then an FLP increase or reduction is associated with a spectral broadening and a decrease of radiative power.

In summary, the main observations made in our experiment are that abrupt light-induced jumps of FLP occur between levels distinctly different in magnitude, a complex dwells for a relatively long time in one of the quasi-stable states, and FLP jumps are accompanied by spectral broadening and a decrease in amplitude.

DISCUSSION

Excitation dynamics

After the B800 ring in the LH2 complex absorbs a photon, energy is transferred to the B850 BChl molecules in ~ 1 ps (Ma, *et al.* 1997, Salverda, *et al.* 2000) with a very high efficiency since the competing processes of FL and non-radiative decay are 3 orders of magnitude slower (Monshouwer, *et al.* 1997). Subsequently, exciton relaxation and excitation hopping will occur in the B850 ring, with a certain probability leading to FL.

When one considers that the molar absorption coefficient of LH2 at 800 nm is $2.3 \cdot 10^6 \text{ M}^{-1} \text{ cm}^{-1}$ (Alden, *et al.* 1997), a single complex will absorb $8.6 \cdot 10^6$ photons/s, if positioned in the center of the Gaussian laser beam, delivering 1 μW of continuous wave (CW)

excitation at 800 nm. The BChl triplet with a lifetime of 70 μ s (Monger, *et al.* 1976) is formed with a 2-15% yield (Cogdell, *et al.* 1981, Monger, *et al.* 1976) and is efficiently transferred to the carotenoid which has a triplet lifetime of \sim 10 μ s (Angerhofer, *et al.* 1995). This triplet is a very efficient trap of the singlet BChl excitations due to S-T annihilation. In the triplet-free state, the FL quantum efficiency is 10% (Monshouwer, *et al.* 1997). From the simple calculation with the above parameters, it follows that in the presence of the carotenoid triplet, the FL yield decreases by a factor of 200. The frequency of triplet formation is dependent on the triplet yield and excitation intensity. Thus, the resulting FL yield considering the presence of the triplet is dependent on the same parameters. The observed average FL count rate is \sim 8500 counts/s at an excitation intensity of 500 nW. With the estimated signal collection efficiency of 8%, we would expect to achieve this level of signal with a 9% (in the middle of the range of values; see above) triplet formation yield which corresponds to the resulting FL quantum efficiency of 2.5%.

This analysis implies that only a fraction of the absorbed excitation photons is re-emitted as FL. The remaining excitations either decay radiationlessly directly to the ground state, form a triplet, or are quenched by triplets. In either case, the absorbed excitation energy is eventually dissipated as heat, which leads to a temperature increase of the pigment surroundings. However, despite the large number of excitations produced in the system, we only seldom observe spectral changes. The complex appears to dwell for a relatively long time in one of the quasi-stable states, characterized by a specific peak wavelength, profile shape, and intensity of emission. We thus conclude that the free energy barriers separating those quasi-stable states must be large.

Local temperature increase is a plausible cause of the structural alterations that we will associate with a change in the realization of the static disorder of the electronic transition energies in the system that is in turn connected to particular spectral properties. Below, we develop a model that accounts for the observed changes in the spectral profile shape and peak wavelength position.

A quantitative description of single-molecule emission spectra

In our model of the B850 ring, we utilize the modified Redfield approach that incorporates excitonic interactions, static disorder of the electronic transition energies of the pigments, and strong coupling of the electronic transitions to nuclear motions (phonons). The coupling to the fast nuclear motions determines the optical line shape in both conventional (Mukamel 1995) and single-molecule spectroscopy (Jung, *et al.* 2002). Slow nuclear motions result in different equilibrium positions of the nuclear coordinates, *i.e.*, are associated with the evolution of the pigment-protein conformations on a microsecond to second time scale, and produce different realizations of the static disorder of the electronic transition energies (Dempster, *et al.* 2001). They are the cause of the inhomogeneous broadening of the bulk spectrum. Particular nuclear coordinates result in states of a single complex, characterized by a certain FLP and a spectral line shape. Thermally activated slow nuclear motions lead to the transitions between these states, observed as abrupt jumps in the FLP traces (Figure 3).

Here we will not consider the dynamics of such transitions, but restrict ourselves to the modeling of the FL line shapes for different realizations of the disorder.

The energies of the exciton levels are calculated by constructing and diagonalizing the one-exciton Hamiltonian. B850 BChls in the dimeric subunit of LH2 are assumed to have unperturbed transition energies of 12415 and 12215 cm^{-1} that were adjusted from a fit of a bulk spectrum. The nearest neighbor interaction energies inside the protein dimer and between pigments of adjacent dimers were taken to be 291 and 273 cm^{-1} , respectively (Sauer, *et al.* 1996). The static disorder of the transition energies was taken into account by introducing uncorrelated variations randomly taken from a Gaussian distribution with a fwhm of σ . The numerical diagonalization of the Hamiltonian (for each realization of the disorder) gives the energies of the exciton states, ω_k , and the wave function amplitudes, c_n^k , (participation of the n th pigment site in the k th exciton state).

The absorption and FL line shapes of the exciton states are calculated assuming strong exciton-phonon coupling (Zhang, *et al.* 1998). The homogeneous absorption line shape for the k th exciton state is expressed in terms of the line broadening function, g_k . The steady state Stokes shift of the emission maximum of the k th state is given by $2\lambda_k$, where λ_k is the reorganization energy of the k th exciton state. Both g_k and λ_k are related to the spectral density, $C_k(\omega)$, in the exciton basis, which is connected with the spectral density in the site representation, $C_n(\omega)$, through the fourth power of the wave function amplitudes, *i.e.*, $C_k(\omega) = \sum_n (c_n^k)^4 C_n(\omega)$. Here we have assumed that the phonon-induced modulation of the electronic transition is described by an uncorrelated diagonal disorder (not to be confused with static disorder). The $\sum_n (c_n^k)^4$ factor is also known as the participation ratio (PR), or inverse delocalization length of the k th exciton state. Thus, the phonon-induced broadening and the Stokes shift of the exciton level are dependent on the PR of that level.

The spectral density $C_n(\omega)$ is assumed to have the form of an overdamped Brownian oscillator (Mukamel 1995, Zhang, *et al.* 1998) with a coupling parameter λ and a relaxation time τ . In our model, λ and τ (as well as σ) are site-independent free parameters adjusted from the fit of the bulk absorption and FL spectra.

The model also regards the relaxation-induced broadening, *i.e.*, we suppose an additional homogeneous broadening of the exciton states given by their inverse lifetimes, $R_k = -\sum_{k'} R_{k'k'kk}$, where $R_{k'k'kk}$ is the rate of the $k \rightarrow k'$ transition calculated (Zhang, *et al.* 1998) in terms of g_k functions.

The RT bulk absorption and FL spectra of the B850 ring can be reproduced with the following parameter values: $\sigma = 370 \text{ cm}^{-1}$, $\lambda = 220 \text{ cm}^{-1}$, and $\tau = 70 \text{ fs}$. Introducing higher static and dynamic disorder values, *i.e.*, $\sigma = 450 \text{ cm}^{-1}$ and $\lambda = 370 \text{ cm}^{-1}$, improved even further a fit of the single-molecule FL spectra profiles.

Single LH2 FL profiles calculated for 150 realizations of the static disorder at RT are shown in Figure 4. The FLP are distributed over a range of values similar to the experimental data. However, since we do not have an explicit model to describe the dynamics of spectral jumping, the collection of calculated FLPs (Figure 4) does not

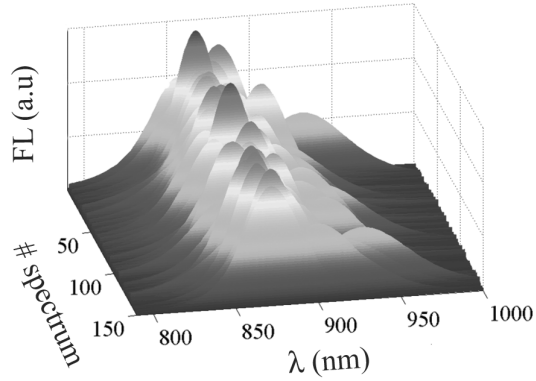


Figure 4. FL profiles calculated for 150 realizations of the disorder for a single LH2 complex at RT. represent temporal evolution of the spectrum.

Figure 5A-C contains three experimental profiles that are averages of all single-molecule FL spectra measured with an excitation intensity of $3.5 \mu\text{W}$ and peaking in intervals of 859-861, 869-871, and 889-891 nm. These average spectra have fwhm values of 53, 48, and 67

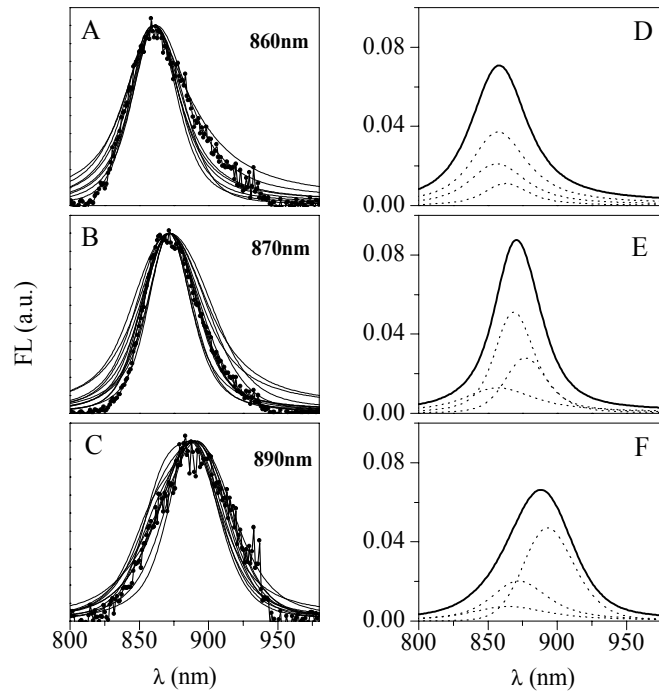


Figure 5. Experimental (points connected with the thick solid line) and calculated (solid thin line) FL profiles: (A) blue-shifted, (B) intermediate, and (C) red-shifted. (D-F) Three typical realizations of disorder resulting in FL profiles with different FLP, shown together with contributions from the three lowest exciton states (dashed lines). The spectra are not normalized for the comparison of their relative amplitudes (parameters of these three realizations are also given in Table 1).

Table 1. FLP and FL amplitudes of the three FL profiles shown in panels D-F of Figure 5, together with the corresponding PRs for the lowest exciton components ($k = 0, -1,$ and 1).

FLP (nm)	859	871	888
FL amplitude (a.u.)	0.077	0.094	0.070
PR ($k = 0$)	0.107	0.203	0.356
PR ($k = -1$)	0.098	0.139	0.157
PR ($k = 1$)	0.131	0.087	0.180

nm, respectively. The red-shifted spectrum (Figure 5C) is significantly broadened and has a pronounced short-wavelength wing. Spectra with the blue-shifted and intermediate FLP (panels A and B of Figure 5, respectively) feature a regular FL profile asymmetry, *i.e.*, a broader long-wavelength tail. Notably, the blue- and red-shifted spectra are broader than that with an intermediate FLP. For comparison, a number of calculated FL profiles corresponding to different realizations of the static disorder have been collected into three groups with their peak wavelengths belonging to narrow intervals of 859-862, 871-873, and 886-892 nm around the corresponding experimentally determined values. The average calculated FL profile has a maximum near 870 nm. Realizations with the FLP near this wavelength occur with the highest probability. Overlaying of experimental and simulated curves in Figure 5A-C shows that the model satisfactorily reproduces all the features of the experimental spectra.

The FL line shapes and their peak wavelengths are determined by a specific realization of the static disorder, which is related to a particular excitonic energy level structure. Typical patterns of such structure corresponding to the three experimentally measured FLP at 859, 871, and 888 nm (Figure 5A-C) are shown in panels D-F of Figure 5, respectively. The corresponding PRs of the exciton levels, shown in Figure 5D-F, are listed in Table 1. For a circular aggregate of N molecules, the $PR = 1/N$ for the lowest and $3/(2N)$ for the higher states in the absence of the disorder. In the case of the LH2 ring, $N = 18$ and the PR is calculated to be 0.056 and 0.083, respectively. Including the disorder results in a dramatic increase of the lowest state PR. For LH2 with a realistic value for the disorder, the $PR = 0.1$ - 0.15 for the higher states and 0.15 - 0.35 for the lowest state, with an increasing PR value for the red-shifted levels (Alden, *et al.* 1997, Novoderezhkin, *et al.* 1999, Novoderezhkin, *et al.* 1999, Novoderezhkin, *et al.* 2003). The phonon-induced broadening is related to a certain PR value; thus, the red-shifted excitonic levels are additionally broadened by an enhanced phonon coupling.

Table 1 and Figure 5D show that the blue-shifted FL profile corresponds to a relatively delocalized state. Indeed, the PRs for all three excitonic levels are relatively small and consequently must be associated with small contributions from specific sites, thus implying that the excitation is delocalized over different sites. Consequently, an excitonic structure of

these levels is not destroyed by the disorder. The lowest state is only weakly allowed (the corresponding band has a small amplitude) so that the RT emission originates mostly from the degenerate $k = \pm 1$ pair, giving rise to a blue-shifted FL.

Realization of a larger static disorder (Figure 5E and the second column in Table 1) results in a larger splitting between the $k = \pm 1$ levels so that the lower $k = -1$ state becomes more populated and more emissive as compared to the $k = 1$ state. However, both $k = -1$ and $k = 1$ levels still remain delocalized (PR = 0.087-0.139). The lowest $k = 0$ state becomes more localized (PR = 0.2), more radiant, and more red-shifted. Such an exciton structure is characteristic of the realizations with the FLP near the maximum of the bulk emission spectrum.

Figure 5F shows an example of a red-shifted FL profile. The exciton structure is strongly affected by the disorder, which induces a large splitting between the three lowest states. The PR value is relatively large for all the states and especially for the lowest one. Because of the large splitting between the exciton levels, the FL originates mostly from the lowest state. Its localized character (PR ≥ 0.35) gives rise to an increased phonon coupling, which leads to a significant broadening of the $k = 0$ level. Because of a larger Stokes shift, the emission is also further red-shifted.

Downhill exciton relaxation with a rate increasing for the higher levels is an additional line-broadening factor contributing to the width of the blue-shifted FL spectrum. In our model, $R_k = 16, 29, 44,$ and 57 ps^{-1} for the $k = 0, -1, 1,$ and -2 levels, respectively. The more pronounced relaxation broadening of the $k = \pm 1$ levels results in a larger width of the blue-shifted FL spectra (determined mostly by the $k = \pm 1$ emission). If the relaxational broadening was disregarded, a blue shift would always be accompanied by the narrowing of the FL profile. Indeed, the $k = \pm 1$ levels are narrower than the $k = 0$ levels, since the corresponding PR values, and consequently the phonon couplings, are smaller.

Calculated amplitudes of FL corresponding to the three typical realizations of disorder (Table 1) reproduce the experimentally observed decrease in spectral amplitude upon spectral jumping.

In summary, we have experimentally observed notable light-induced jumps in the FLP between the levels of distinctly different magnitude. Though spectral fluctuations were evidently light-induced, they did not signal the deterioration of the assembly, since jumps were reversible. We conclude that the excitation intensity drives the complex into conformational states, which are less accessible under dark conditions, but still intrinsic to the system.

The observed spectral jumps were accompanied by a broadening of the FL profile and a decrease in amplitude. We have qualitatively accounted for these effects by modeling the FL spectra with different realizations of the static disorder of pigment transition energies. However, our model does not encompass the dynamics of the spectral jumps. The observation that large spectral jumps occur with a very low probability with respect to the number of excitations received by the system leads us to conclude that large free energy barriers separate the states with distinctly different spectral properties.

REFERENCES

- Alden, R. G., Johnson, E., Nagarajan, V., Parson, W. W., Law, C. J., and Cogdell, R. J. (1997) Calculations of spectroscopic properties of the LH2 bacteriochlorophyll-protein antenna complex from *Rhodospseudomonas acidophila*. *J. Phys. Chem. B.* 101, 4667-4680.
- Angerhofer, A., Bornhauser, F., Gall, A., and Cogdell, R. J. (1995) Optical and optically detected magnetic resonance investigation on purple photosynthetic bacterial antenna complexes. *Chem. Phys.* 194, 259-274.
- Bopp, M. A., Sytnik, A., Howard, T. D., Cogdell, R. J., and Hochstrasser, R. M. (1999) The dynamics of structural deformations of immobilized single light-harvesting complexes. *Proc. Natl. Acad. Sci. U.S.A.* 96, 11271-11276.
- Cogdell, R. J., Fyfe, P. K., Barrett, S. J., Prince, S. M., Freer, A. A., Isaacs, N. W., McGlynn, P., and Hunter, C. N. (1996) The purple bacterial photosynthetic unit. *Photosynth. Res.* 48, 55-63.
- Cogdell, R. J., and Hawthornthwaite, A. M. (1993) Preparation, purification and crystallization of purple bacterial antenna complexes. Vol. 1, Academic Press, New York.
- Cogdell, R. J., Hipkins, M. F., MacDonald, W., and Truscott, T. G. (1981) Energy transfer between the carotenoid and the bacteriochlorophyll within the B-800-850 light-harvesting pigment-protein complex of *Rhodospseudomonas sphaeroides*. *Biochim. Biophys. Acta.* 634, 191-202.
- Dempster, S. E., Jang, S. J., and Silbey, R. J. (2001) Single molecule spectroscopy of disordered circular aggregates: a perturbation analysis. *J. Chem. Phys.* 114, 10015-10023.
- Halloren, E., McDermott, G., Lindsay, J. G., Miller, C., Freer, A. A., Isaacs, N. W., and Cogdell, R. J. (1995) Studies on the light-harvesting complexes from the thermotolerant purple bacterium *Rhodospseudomonas cryptolactis*. *Photosynth. Res.* 44, 149-155.
- Hofmann, C., Aartsma, T. J., Michel, H., and Köhler, J. (2003) Direct observation of tiers in the energy landscape of a chromoprotein: a single-molecule study. *Proc. Natl. Acad. Sci. U.S.A.* 100, 15534-15538.
- Hong, X., Weng, Y.-X., and Li, M. (2004) Determination of the topological shape of integral membrane protein light-harvesting complex LH2 from photosynthetic bacteria in the detergent solution by small-angle X-ray scattering. *Biophys. J.* 86, 1082-1088.
- Hu, X. C., Ritz, T., Damjanovic, A., Autenrieth, F., and Schulten, K. (2002) Photosynthetic apparatus of purple bacteria. *Q. Rev. Biophys.* 35, 1-62.
- Hu, X. C., Ritz, T., Damjanovic, A., and Schulten, K. (1997) Pigment organization and transfer of electronic excitation in the photosynthetic unit of purple bacteria. *J. Phys. Chem. B.* 101, 3854-3871.
- Jung, Y., Barkai, E., and Silbey, R. J. (2002) Current status of single-molecule spectroscopy: theoretical aspects. *J. Chem. Phys.* 117, 10980-10995.
- Ketelaars, M., van Oijen, A. M., Matsushita, M., Köhler, J., Schmidt, J., and Aartsma, T. J. (2001) Spectroscopy on the B850 band of individual light-harvesting 2 complexes of *Rhodospseudomonas acidophila* I. Experiments and Monte Carlo simulations. *Biophys. J.* 80, 1591-1603.
- Ma, Y. Z., Cogdell, R. J., and Gillbro, T. (1997) Energy transfer and exciton annihilation in the B800-850 antenna complex of the photosynthetic purple bacterium *Rhodospseudomonas acidophila* (Strain 10050). A femtosecond transient absorption study. *J. Phys. Chem. B.* 101, 1087-1095.
- Matsushita, M., Ketelaars, M., van Oijen, A. M., Köhler, J., Aartsma, T. J., and Schmidt, J. (2001) Spectroscopy on the B850 band of individual light-harvesting 2 complexes of *Rhodospseudomonas acidophila* II. Exciton states of an elliptically deformed ring aggregate. *Biophys. J.* 80, 1604-1614.
- McDermott, G., Prince, S. M., Freer, A. A., Hawthornthwaite, A. M., Papiz, M. Z., Cogdell, R. J., and

- Isaacs, N. W. (1995) Crystal structure of an integral membrane light-harvesting complex from photosynthetic bacteria. *Nature*. 374, 517-521.
- Monger, T. G., Cogdell, R. J., and Parson, W. W. (1976) Triplet states of bacteriochlorophyll and carotenoids in chromatophores of photosynthetic bacteria. *Biochim. Biophys. Acta*. 449, 136-153.
- Monshouwer, R., Abrahamsson, M., van Mourik, F., and van Grondelle, R. (1997) Superradiance and exciton delocalization in bacterial photosynthetic light-harvesting systems. *J. Phys. Chem. B*. 101, 7241-7248.
- Mukamel, S. (1995) Principles of Nonlinear Optical Spectroscopy, Oxford University Press, New York.
- Novoderezhkin, V., Monshouwer, R., and van Grondelle, R. (1999) Disordered exciton model for the core light-harvesting antenna of *Rhodospseudomonas viridis*. *Biophys. J.* 77, 666-681.
- Novoderezhkin, V., Monshouwer, R., and van Grondelle, R. (1999) Exciton (de)localization in the LH2 antenna of *Rhodobacter sphaeroides* as revealed by relative difference absorption measurements of the LH2 antenna and the B820 subunit. *J. Phys. Chem. B*. 103, 10540-10548.
- Novoderezhkin, V., Wendling, M., and van Grondelle, R. (2003) Intra- and interband transfers in the B800-B850 antenna of *Rhodospirillum rubrum*. Redfield theory modeling of polarized pump-probe kinetics. *J. Phys. Chem. B*. 107, 11534-11548.
- Papiz, M. Z., Prince, S. M., Howard, T., Cogdell, R. J., and Isaacs, N. W. (2003) The structure and thermal motion of the B800-850 LH2 complex from *Rps. acidophila* at 2.0 Å over-circle resolution and 100 K: new structural features and functionally relevant motions. *J. Mol. Biol.* 326, 1523-1538.
- Robert, B., Cogdell, R. J., and van Grondelle, R. (2003) The light-harvesting system of purple bacteria. In Light-harvesting antennas in photosynthesis. Green, B. R. and Parson, W. W., Eds., Vol. 13, Kluwer academic publishers, Dordrecht, Netherlands.
- Salverda, J. M., van Mourik, F., van der Zwan, G., and van Grondelle, R. (2000) Energy transfer in the B800 rings of the peripheral bacterial light-harvesting complexes of *Rhodospseudomonas acidophila* and *Rhodospirillum rubrum* studied with photon echo techniques. *J. Phys. Chem. B*. 104, 11395-11408.
- Sauer, K., Cogdell, R. J., Prince, S. M., Freer, A., Isaacs, N. W., and Scheer, H. (1996) Structure-based calculations of the optical spectra of the LH2 bacteriochlorophyll-protein complex from *Rhodospseudomonas acidophila*. *Photochem. Photobiol.* 64, 564-576.
- Scheuring, S., Reiss-Husson, F., Engel, A., Rigaud, J. L., and Ranck, J. L. (2001) High-resolution AFM topographs of *Rubrivivax gelatinosus* light-harvesting complex LH2. *EMBO J.* 20, 3029-3035.
- Scholes, G. D., and Fleming, G. R. (2000) On the mechanism of light harvesting in photosynthetic purple bacteria: B800 to B850 energy transfer. *J. Phys. Chem. B*. 104, 1854-1868.
- Sundström, V., Pullerits, T., and van Grondelle, R. (1999) Photosynthetic light-harvesting: reconciling dynamics and structure of purple bacterial LH2 reveals function of photosynthetic unit. *J. Phys. Chem. B*. 103, 2327-2346.
- van Grondelle, R. (1985) Excitation energy transfer, trapping and annihilation in photosynthetic systems. *Biochim. Biophys. Acta*. 811, 147-195.
- van Grondelle, R., Dekker, J. P., Gillbro, T., and Sundström, V. (1994) Energy-transfer and trapping in photosynthesis. *Biochim. Biophys. Acta*. 1187, 1-65.
- van Oijen, A. M., Ketelaars, M., Köhler, J., Aartsma, T. J., and Schmidt, J. (2000) Spectroscopy of individual light-harvesting 2 complexes of *Rhodospseudomonas acidophila*: diagonal disorder, intercomplex heterogeneity, spectral diffusion, and energy transfer in the B800 band. *Biophys. J.* 78, 1570-1577.
- van Oijen, A. M., Ketelaars, M., Köhler, J., Aartsma, T. J., and Schmidt, J. (1999) Unraveling the

electronic structure of individual photosynthetic pigment-protein complexes. *Science*. 285, 400-402.

Wu, H. M., Rätsep, M., Lee, I. J., Cogdell, R. J., and Small, G. J. (1997) Exciton level structure and energy disorder of the B850 ring and the LH2 antennal complex. *J. Phys. Chem. B* 101, 7654-7663.

Zhang, W. M., Meier, T., Chernyak, V., and Mukamel, S. (1998) Exciton-migration and three-pulse femtosecond optical spectroscopies of photosynthetic antenna complexes. *J. Chem. Phys.* 108, 7763-7774.

Fluorescence spectroscopy of conformational changes of single LH2 complexes

Danielis Rutkauskas, Vladimir Novoderezhkin, Richard J. Cogdell and Rienk van Grondelle

ABSTRACT

We have investigated the energy landscape of the bacterial photosynthetic peripheral light-harvesting complex 2 of purple bacterium *Rhodospseudomonas acidophila* by monitoring sequences of fluorescence spectra of single assemblies, at room temperature, with different excitation intensities as well as at elevated temperatures, utilizing a confocal microscope. The fluorescence peak wavelength of individual complexes was found to abruptly move between long-lived quasi-stable levels differing by up to 30 nm. The frequency and size of these fluorescence peak movements was found to increase linearly with the excitation intensity. These spectral shifts either to the blue or to the red were accompanied by a broadening and decrease of the intensity of the fluorescence spectrum. The probability for a particle to undergo significant spectral shift in either direction was found to be roughly the same. Using the modified Redfield theory the observed changes in spectral shape and intensity were accounted for by changes in the realization of the static disorder. Long lifetimes of the quasi-stable states suggest large energetic barriers between the states characterized by different emission spectra.

INTRODUCTION

Photosynthetic pigment-protein complexes play a decisive role in the collection of solar energy and the transfer of electronic excitation energy to the photosynthetic reaction center, where a charge separation is initiated (van Grondelle 1985, van Grondelle, *et al.* 1994). Since a high-resolution crystallographic structure of the peripheral light-harvesting complex 2 (LH2) of the photosynthetic bacterium *Rhodospseudomonas (Rps.) acidophila* has become available (McDermott, *et al.* 1995, Papiz, *et al.* 2003), the molecule has played a key role in aiding our current understanding of photosynthetic light-harvesting (Cogdell, *et al.* 1996, Hu, *et al.* 2002, Robert, *et al.* 2003, Sundström, *et al.* 1999). The LH2 of *Rps. acidophila* is a highly symmetric ring of 9 protein-pigment subunits, each containing 2 helical transmembrane polypeptides, the α -polypeptide on the inner and the β -polypeptide on the outer side of the ring. The hydrophobic terminal of the protein binds a ring of 18 tightly coupled bacteriochlorophyll (BChl) molecules with a center-to-center distance of less than 1 nm between neighboring pigments. This ring is responsible for the intense absorption of LH2 at 850 nm (B850 ring). A second ring of 9 weakly interacting BChls is located in the polar region of the protein and is largely responsible for the absorption around 800 nm (B800 ring).

From the detailed study of the spectroscopic properties of LH2, a consistent picture of energy levels and energy transfer in the complex has emerged (Alden, *et al.* 1997, Hu, *et al.* 1997, Novoderezhkin, *et al.* 1999, Novoderezhkin, *et al.* 2003, Sauer, *et al.* 1996, Scholes and Fleming 2000, van Grondelle and Novoderezhkin 2001, Wu, *et al.* 1997). All basic spectroscopic features can be understood on the basis of a model that includes both intrinsic pigment site energy disorder and excitonic coupling between the pigments (about 300 cm^{-1} for neighboring BChls in the B850 and about 30 cm^{-1} for adjacent pigments in the B800). By introducing relaxation between the elements of the so-called density matrix, the dynamics of vibrational and electronic coherence and excitation energy transfer have been described in great detail.

Based on room- and low-temperature single-molecule experiments it has been proposed that the LH2 ring can deviate from the ideally circular structure of the complex in crystal (Bopp, *et al.* 1999, Ketelaars, *et al.* 2001, Matsushita, *et al.* 2001, van Oijen, *et al.* 1999). The anomalously large splitting of the two major orthogonal excitonic transitions observed in low-temperature polarized fluorescence (FL) excitation spectra was attributed to a modulation of the coupling strength in the B850 ring that was asserted to be associated with an elliptical deformation (Ketelaars, *et al.* 2001, Matsushita, *et al.* 2001, van Oijen, *et al.* 1999). It was found that native membrane environment contributes significantly to stabilization of circular structure of bacterial light-harvesting complexes (Gerken, *et al.* 2003). Thus smaller ellipticities of 0.95-0.91 were found in AFM measurements of loosely packed LH2s in membrane, and were probably due to an interplay of the disrupting tip and stabilizing lipid environment effects (Scheuring, *et al.* 2001).

Room-temperature (RT) polarized FL experiments were interpreted in terms of an

elliptical absorber and emitter with ellipticity and directions of the principal axis varying as a result of the B800 and/or B850 distortion destroying the rotational symmetry and traveling around the ring on a timescale of seconds (Bopp, *et al.* 1999). Spectral diffusion of the B800 band of LH2, observed in the low-temperature experiments, was also attributed to structural alterations (van Oijen, *et al.* 2000). These spectral fluctuations of different magnitude occurring on different time scales were associated with a hierarchical structure of the protein conformational landscape (Hofmann, *et al.* 2003). In general, the observed variation of the spectral and functional properties of LH2 suggests that the complex can undergo a variety of deformations. It is in accordance with the widely expected notion of a protein as a complex system that is characterized by a rugged potential energy landscape with multiple barriers separating potential energy valleys associated with different conformational substates (Frauenfelder 2003). At RT protein possesses sufficient energy to migrate between different substates. Protein transitions from one substate to another can be also induced by repetitive laser excitation due to thermal energy released through radiationless deactivation channels after pigment absorption of excitation light. In a pigment-protein complex like LH2 spectral peak wavelengths and line shapes of absorption and FL spectra are partly determined by the pigment-protein interactions such as through the formation of hydrogen bonds (Fowler, *et al.* 1992, Olsen, *et al.* 1994). The latter are modulated by the structural changes of the protein and so are the spectra. For a phenomenological description of the underlying electronic mechanism of spectral changes it is reasonable to assume that dynamic structural alterations of the protein also underlie the pattern of the static disorder of the pigment site energies that play a key role in understanding of the spectroscopic and energy transfer properties of LH2.

In the present work we investigate these dynamic fluctuations under physiological conditions, as manifested by the time evolution of the FL spectrum. To do so we have acquired series of FL spectra of single LH2 complexes at room and elevated temperatures with various excitation intensities. We observed sudden moves of the peak wavelength of the emission spectrum of LH2; both the frequency and the magnitude of spectral jumps was found to depend on the excitation intensity. Spectral jumps to the blue and to the red occur with a similar probability and are associated with spectral broadening and lowering of the intensity. The observed spectral variations can be qualitatively interpreted by sudden changes in the realization of the static disorder.

MATERIALS AND METHODS

Sample preparation and immobilization

Isolated LH2 complexes were immobilized on a standard microscope coverslip (0.17 mm thickness) treated with 0.01% poly-L-lysine (PLL) (Sigma) solution for 5 minutes. The coverslip was used as a base for a home-designed, hermetic, temperature-controlled sample cell.

Purified LH2 complexes of *Rps. acidophila* were prepared as described earlier (Cogdell and Hawthornthwaite 1993, Halloren, *et al.* 1995). The sample stock solution of 0.62 μM LH2 in buffer of 20 mM Tris-HCl (pH 8.0) and 0.1% lauryldimethylamine oxide (LDAO) was kept at -80°C prior to thawing. It was diluted in the same buffer in two steps by a factor of $2 \cdot 10^4$. A 20 μl drop of 33 pM LH2 solution was added onto the coverslip, and the sample cell was assembled. After a few minutes the cell volume was washed with deoxygenated, 0.1% LDAO-containing buffer, thus removing the excess sample and submerging the immobilized single molecules in an oxygen-free environment. Oxygen was thoroughly removed from the buffer by flowing gaseous nitrogen and agitating it with a magnetic spinner to the level not detectable by electrolytic oxygen meter (Cyberscan 100 Do, Eutech Instruments Pte Ltd.). Buffer was inserted into the sample cell directly from the deoxygenation volume with excessive gaseous nitrogen pressure. In this procedure the use of chemical oxygen scavenger was avoided.

Experimental setup

FL images and spectra were acquired with a confocal microscope based on a commercial inverted microscope (Nikon, Eclipse TE300). A scheme of the setup is presented in Figure 1. The excitation source was a tunable-wavelength titanium sapphire laser system (Coherent, Mira 900) producing 3 ps, 800 nm pulses with a repetition rate of 76 MHz. A dichroic beam

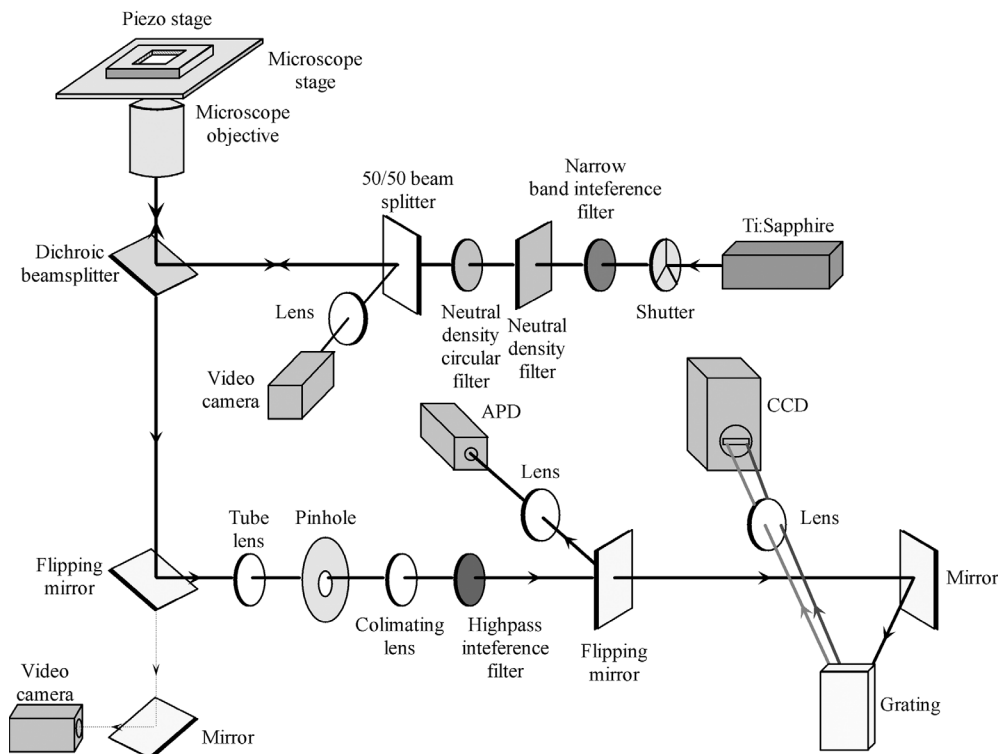


Figure 1. Optical scheme of the experimental setup.

splitter (Chroma Technology Corp., 815dclp) reflected the laser beam into an objective (Nikon, Plan Fluor 100×, 1.3 NA, oil immersion), focusing the excitation light onto a glass-water interface in the sample cell to a diffraction-limited spot (fwhm of ~600 nm). The intensities used in the experiments (from 0.13 to 1.6 kW/cm² or equivalently 500 nW to 6 μW) represent the values at this interface. Non-fluorescing immersion oil (Nikon) coupled the objective to the glass coverslip. The emission was collected with the same objective and spatially filtered by a 100 μm pinhole. Scattered excitation light was rejected with single 130 nm broad interference filter (Chroma Technology Corp., HQ885/130m).

The sample cell was mounted on a closed-loop two-dimensional piezo stage (Physik Instrumente, P-731.8C) controlled by a digital four-channel controller (Physik Instrumente, E-710.4LC).

To obtain images, emission was detected with Si avalanche photodiode (APD) single photon-counting module (SPCM-AQR-16, Perkin Elmer Optoelectronics) and counter timer board (National Instruments, PCI-6602). Spectra were acquired by dispersing the FL onto a liquid nitrogen-cooled back-illuminated charge-coupled device (CCD) camera chip (Princeton Instruments, Roper Scientific, Spec10:100BR) by a gold-coated grating (Optometrics LLC, HR600/1.0U 30SQ.X9.5mm). CCD pixels were binned along the spectroscopic axis to yield a resolution of < 1nm. The polarization sensitivity of the detection was found to be insignificant and thus no correction was required. The setup was switched between the image acquisition and spectroscopic modes by a motorized mirror flipper (New Focus, 8892M).

The longitudinal drift of the focus due to thermal flux in experiments at elevated temperature was eliminated by monitoring focus position with a monochrome video camera (Watec America Corp., Watec LCC-902K,) coupled to a video grabber board (National Instruments, PCI-1407) and translating the microscope objective with a motorized polarizer rotator (New Focus, 8401M, 8754 driver) to optimum position after an acquisition of each series of FL spectra.

An electrical shutter (Uniblitz, VS25S2S1, VMM-D1 driver) blocked the excitation light between the measurements.

Mirror and lens antireflection coatings were optimized for signal processing in near infrared.

Images and spectra

A FL image is acquired by continuously sweeping the piezo stage over the laser focus with the 3 Hz frequency while its position in the perpendicular direction is changed by 100 nm for each line; the FL signal is concomitantly detected with an APD. Image is then constructed by associating the piezo stage coordinate with the corresponding intensity. The scanning covers an area of 10 μm × 10 μm. Image is background-thresholded and excessively small, big, bright, weak, elongated or adjacent particles as well as particles bordering the edges of the image are discarded. The coordinates of remaining particles are determined, and the piezo stage is positioned to bring the particle into the focus of the

objective and after switching to the spectroscopic mode a series of FL spectra is collected for 2 min with an integration time (0.5-2 s) dependent on the excitation power and the sample temperature. At higher excitation intensities and lower temperature, shorter integration times are sufficient for the collection of the spectra with satisfactory signal to noise ratio. The excitation intensity and the ambient conditions remain unchanged during the acquisition.

Bulk spectra were measured with the same setup on assemblies immobilized on a treated coverslip from the stock solution of LH2.

The spectrofluorometer was wavelength-calibrated by referencing the known lines of Ar lamp spectrum, acquired by positioning the lamp over a milk emulsion layer on a cover-slip (creating a uniform light source) and focusing the microscope objective on the coverslip-water interface.

Detection sensitivity was calibrated with a tungsten halogen lamp, assuming that its emission spectrum is flat in the region of interest.

Software

The program communicating with the counter timer and video grabber boards, driving piezo stage, motorized flipper, electrical shutter, and motorized polarizer rotator was coded in the Labview environment. Commercial CCD camera software was accessed from the program, utilizing ActiveX technology.

Data analysis

For a quantitative analysis, the acquired spectra are fitted with a skewed Gaussian function, using a non-linear Levenberg-Marquardt fitting method. The expression for the skewed Gaussian function is

$$F(\lambda) = \Delta + A \exp(-\ln(2)[\ln(1 + 2b(\lambda - \lambda_m)/\Delta\lambda)/b]^2)$$

where Δ is the offset, A the amplitude, λ_m the FL peak wavelength (FLP), $\Delta\lambda$ the width, b the skewness. The fwhm of the spectrum is calculated from the width and the skewness. Consequently, by fitting each spectrum from a series we obtain the time traces of the amplitude, the fwhm, and the FLP with the corresponding confidence margins.

RESULTS

The primary objective of this study was to investigate if we could observe fluctuations of peak wavelength, width and intensity of emission spectrum of single LH2 complexes as a measure of structural dynamics, which can occur in this complex. This was achieved by collecting series of single-molecule FL spectra at RT and variable excitation intensity as well as at elevated temperature. In total close to 1000 molecules were studied at various ambient conditions. Intrinsic (*i.e.*, measured with low excitation power) fluctuations proved to be insignificant on the time scale of our experiment (2 min). However, increasing the excitation

power introduced prominent spectral jumps and changes in the spectral shape and intensity of the emission. To a smaller extent the same effect was detectable in experiments at elevated temperatures (28, 35° C). However, under these conditions the stability of the LH2 complexes was decreased significantly.

Earlier experiments (Bopp, *et al.* 1999) have shown that, the survival time of the illuminated LH2 complexes strongly depends on the presence of oxygen in the environment. We observed that irreversible photobleaching of an oxygen-containing sample took place in the course of seconds or tens of seconds and even when kept in the dark, the oxygen-containing preparation degraded in a few hours at RT. On the other hand, careful removal of oxygen from the sample ambient prolonged the bright state of single LH2s to minutes or even tens of minutes and the sample remained suitable for measurements for two days.

Furthermore, at relatively low excitation intensity (500 nW) only about 20% of the molecules entered a dark state in the course of 2 minutes. The remaining 80% stayed bright during the measurement, and their emission intensity fluctuated between levels of different magnitude. This is in contrast to the earlier study (Bopp, *et al.* 1997) where a larger fraction of particles bleached permanently or temporarily entered the dark state in a few seconds after the onset of the excitation – probably due to the remaining dissolved oxygen.

For the above reasons all of the single-molecule measurements presented in this work were carried out on the oxygen-free samples.

Images

An example of a raw FL image of immobilized LH2 assemblies is shown in Figure 2. The image consists of 100 pixels × 100 pixels, the pixel integration time is 3 ms. The excitation intensity at 800 nm is 3.5 μW. The background is ≤10 counts/pixel and the maximum intensity is 87 counts/pixel. Although particles appear to be of a similar integral intensity, in reality they are distributed over a range of 1300 to 2500 counts, which is probably partly due to the polarization effects of the excitation absorption and emission and partly to the

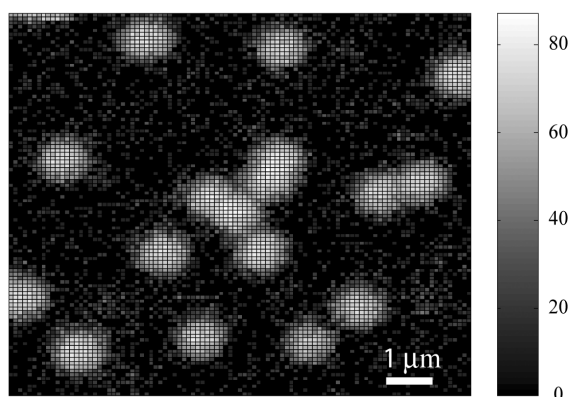


Figure 2. FL image of single LH2 complexes immobilized on a PLL treated coverslip.

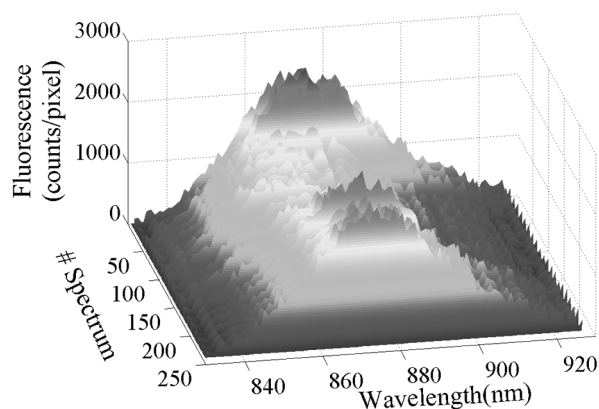


Figure 3. Series of FL spectra of a single LH2.

tendency of the emission intensity to fluctuate. The latter consideration is supported by the fact that at lower excitation intensity levels the distribution of the particle intensities is notably narrower. We also do not exclude the possibility of observing aggregated complexes or adjacent complexes appearing as one particle. To make sure that we monitor only single LH2s, excessively bright particles are discarded and spectral measurements are carried out on molecules which lie in the middle of the bulk of the intensity distribution.

FL spectra

A typical series of FL spectra of single LH2 enabling the observation of the spectral diffusion is presented in Figure 3. These results were obtained from a sequence of 240 single LH2 spectra, acquired at 20° C with 0.5 s integration time and excitation intensity of 6 μ W at 800 nm, by summing each 10 consecutive spectra for clarity. In this experiment, the

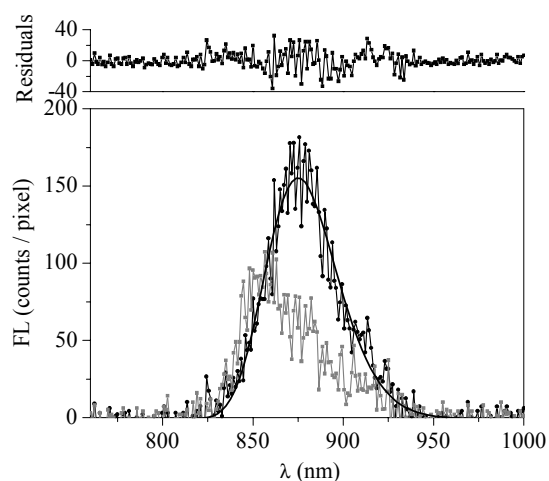


Figure 4. Comparison of two spectra from the original sequence in Figure 3: with intermediate FLP (black circles) and blue FLP (grey squares). The solid curve is the skewed Gaussian fit.

FL amplitude and the FLP diffuse dramatically, with the integral intensity ranging from 4000 to 10000 counts per original spectrum. Spectra at the beginning of the series have relatively high amplitude and intermediate FLP, whereas in the course of the measurement, the amplitude subsides with the FLP shifting to the blue; both parameters recover to values close to the initial ones at the end of the series. Notably, the width of a single complex FL spectrum is comparable with that of the bulk spectrum (data not shown). In Figure 4 two spectra from the same series are compared for the better demonstration of the spectral diffusion. In the same figure we show an example of a fit and the corresponding residuals.

FLP traces

The time course of the FLP of four individual particles is shown in Figure 5. The spectral integration time is 0.5 s, the excitation intensity at 800 nm is 6 μW and sample temperature

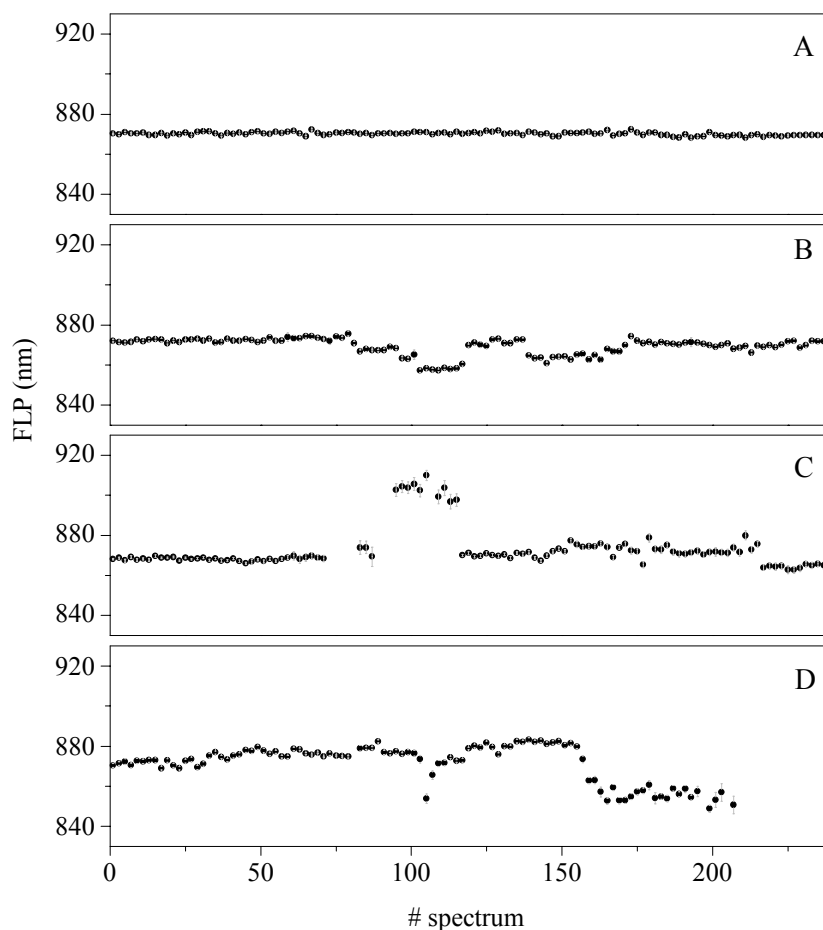


Figure 5. FLP time traces of four individual LH2s. Only every 3rd data point is presented to improve clarity. Various spectral diffusion scenarios: (A) insignificant diffusion, (B) spectral jumps to the blue, (C) spectral jump to the red, (D) spectral jumps both to the red and to the blue.

is 20° C. Though acquired with the same excitation intensity and ambient conditions, the traces are qualitatively different. The FLP fluctuates weakly in Figure 5A, while the panels B and C of Figure 5 demonstrate notable spectral jumps, respectively to the blue and to the red relative to the initial FLP value. Interestingly, the FLP abruptly jumps between the various levels of almost constant magnitude and even more remarkably, it regains a value close to the initial one before the end of the trace. Unexpectedly, the complex spends a number of seconds in each of the quasi-stable states before it transits to a different state. The trace in Figure 5D show spectral diffusion in both directions: the spectrum of this single complex first drifts to longer wavelengths, then abruptly jumps to the blue, to finally settle at a FLP, blue-shifted by ~15 nm relative to the initial FLP, preventing the unambiguous classification of this particle as performing a spectral jump in one direction. We note that these conspicuous spectral jumps are in many cases reversible, and the initial FLP value (or a value close to it) is regained (Figure 5B, C). For other particles the initial FLP is not recovered before photobleaching occurs (Figure 5D) (or rather an apparent photobleaching – we have observed the recovery of the emission of some complexes after dark periods longer than 2 min, data not shown). Careful inspection of the trace in Figure 5C reveals that the LH2 bleaching does not occur as a single event: after entering a dark state for a few seconds the emission of this complex reappears with a different FLP. On the other hand, the spectral diffusion can occur without temporary loss of the radiative power as is shown in the Figure 5B.

Spectral fluctuations of different magnitude and frequency were observed depending on the excitation intensity and sample temperature. These fluctuations can naturally occur in the system or they can be induced by elevated temperature or increased excitation intensity. To investigate these possibilities we have calculated various statistical properties of the obtained spectra.

Single-molecule average and bulk spectra

An average of all spectra measured at 20° C with 6 μ W excitation intensity is compared in Figure 6 with the 500 nW excitation bulk spectrum. The mean of the single-molecule spectra has the same FLP but is somewhat broader than the bulk spectrum. The broadening of the former is due to the contribution of the particles that underwent spectral shifts either to higher or lower wavelengths. The true bulk spectrum results from a contribution of a much larger number of single molecules, detected at different stages of evolution in their conformational landscape. Consequently, if the number of the available conformational states was the same for the molecules constituting the bulk and for the particles measured individually, then the bulk and the average spectra would have identical shape (provided sufficient statistics of single-molecule spectra measurements exists). The non-overlap of the two spectra (even given a limited number of single-molecule measurements) implies that the higher excitation intensity drives the molecules into conformational states less accessible or even unavailable in the dark.

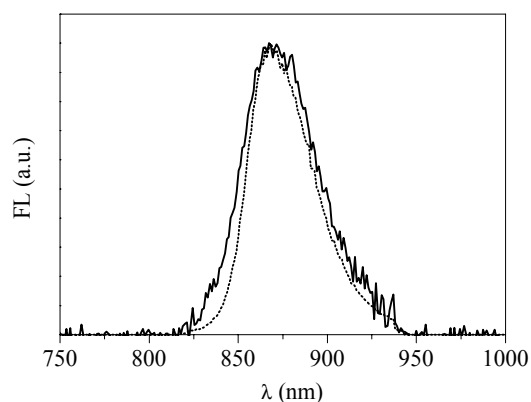


Figure 6. Comparison of the 500 nW excitation bulk spectrum (dotted curve) with the time and population average (solid curve) of single-molecule spectra, acquired with 6 μ W excitation.

Distributions of the FLP and the standard deviation of FLP

The excitation intensity and ambient temperature dependence of the observed spectral fluctuations is summarized in histograms of the FLP and the standard deviation of the FLP (SDFP) time traces (Figure 7). An FLP histogram represents the distribution of the peak wavelengths of all of the single-molecule spectra measured under particular experimental

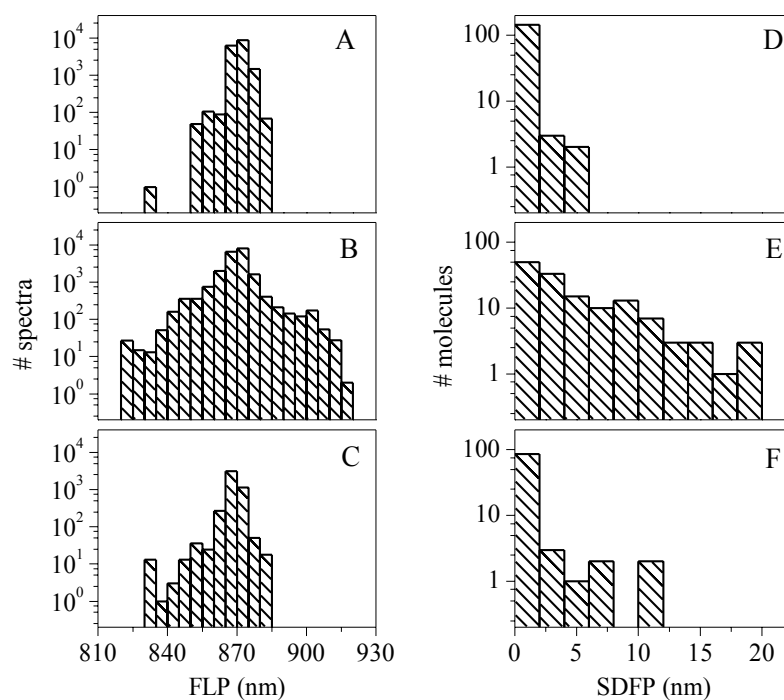


Figure 7. Distributions of FLP and SDFP: (A) and (D) 20° C and 500 nW excitation; (B) and (E) 20° C and 6 μ W; (C) and (F) 35° C and 500 nW.

conditions. SDFP was calculated for each particle with the original spectral integration time, and is indicative of the FLP fluctuation from the mean value for that particle. The SDFP distribution reflects the number of strongly fluctuating particles in the particular experimental population. The FLP distribution results partly from the particles having an intrinsically shifted spectrum and partly from the spectral fluctuations. Comparison of FLP histograms obtained at 20° C with 500 nW (Figure 7A) and 6 μ W (Figure 7B) excitation intensity reveals a broadening of the distribution with increasing excitation intensity. This broadening is due to an increased occurrence of significant spectral diffusion. Similarly, comparison of SDFP histograms acquired at 20° C with 500 nW (Figure 7D) and 6 μ W (Figure 7E) indicates notably larger number of particles exhibiting significant and/or frequent spectral jumps at higher excitation intensity. The temperature dependence of spectral fluctuations is also observable though less pronounced. At 35° C and 500 nW excitation (Figure 7F) the SDFP distribution is broader than at 20° C and the same excitation intensity (Figure 7D), but still much narrower than that, calculated from the measurement at 20° C and 6 μ W (Figure 7E). Similarly, the FLP distribution resulting from the measurement at 35° C and 500 nW excitation (Figure 7C) is broader than the one at 20° C and 500 nW (Figure 7A) but notably narrower than at 20° C and 6 μ W (Figure 7B). Thus, laser light-induced spectral fluctuations are more significant than those associated with experimentally feasible increases in temperature. At temperatures higher than 35° C the sample preparation deteriorated before the equilibration of the laser focus position could be achieved, thus rendering the collection of data not feasible.

Statistics of strongly fluctuating molecules

Table 1 summarizes overall numbers of measured particles and particles with large SDFP at different experimental conditions. The fraction of strongly fluctuating particles tends to increase with the excitation intensity. To classify spectral jumps we chose the negative or positive sign of the 3rd moment of the FLP time trace as a criterion of the spectral shift occurring either to the blue or to the red, respectively. The 3rd moment was chosen since it indicates the extent of the distribution of data values around the mean and its sign reflects the position of the majority of deviating data values with respect to the mean. It appears, that the number of the blue-shifting complexes is larger but of the same order of magnitude as that of the red-shifting assemblies. Considering the limited numbers of molecules used in our measurement we tentatively conclude that there exists roughly the same probability for a particle to undergo big spectral shift in either direction.

Similarly, elevation of temperature leads to the increase of the amount of strongly fluctuating particles. However, the quantitative relationship between the temperature and the overall number of spectrally diffusing particles is not clear. As in the measurements at high excitation intensity, it appears that there are more blue-shifting complexes. However, the temperature dependence of the ratio of the number of molecules jumping either to the red or to the blue cannot be envisaged either. Better measurement statistics at a larger number of temperature points is required for a quantitative assessment of the heating effect.

Table 1. Particles undergoing spectral fluctuation. Numbers of particles undergoing spectral shift to the blue or to the red are denoted “blue” and “red” respectively. The specific value of SDFP of 2.44 is obtained from the 500 nW excitation dataset. The major part of corresponding SDFP values is distributed in a narrow range but a small number of standard deviation values are distinctly separate from the rest (data not shown). The 2.44 value is the maximum of the main part of the distribution and thus thresholds the onset of significant spectral fluctuation.

	Experimental conditions						
Temperature (° C)	20	20	20	20	20	28	35
Excitation (μW)	0.5	1.5	2.5	3.5	6	0.5	0.5
Numbers of measured particles							
Total	149	124	128	119	138	120	94
SDFP > 2.44							
Total	2	23	32	30	58	8	5
Blue	2	18	17	18	45	4	4
Red	0	5	15	12	13	4	1

At the moment it can be concluded that a temperature effect takes place but it is much less notable than that associated with the increase of the excitation intensity.

Correlation analysis

Some of the light-harvesting assemblies exhibit a strong correlation between the temporal changes of the FLP and the amplitude or between the FLP and the fwhm (in the following analysis correlation is arbitrarily considered strong if its absolute value is in the 0.5-1 range). We observed that these correlations might be either positive or negative. For example there exist single LH2s that display a negative jump of the FLP with a concomitant increase of the fwhm (negative correlation); others undergo an increase of the FLP that is connected with the increment of the fwhm (positive correlation). Furthermore, some of the molecules are characterized by strong correlations between both pairs of parameters. Figure 8 presents an example of two individual LH2s with all three parameters progressing in time in a correlated manner. A spectral jump to the blue is accompanied by the increase of the fwhm and the decrement of the amplitude in Figures 8D-F. On the other hand, FLP jump to longer wavelengths is again associated with the increment of the fwhm and the reduction of the amplitude in Figures 8A-C.

Table 2 summarizes the statistics of particles with large SDFP, featuring strong positive or negative pair-wise (either FLP-amplitude or FLP-fwhm) correlations. It also lists the numbers of particles exhibiting a combination of pair-wise correlations: either positive FLP-amplitude and negative FLP-fwhm or negative FLP-amplitude and positive FLP-fwhm. Interestingly, we observed only a few occurrences of molecules indicating a different combination of pair-wise correlations. It appears from the table that the proportion of

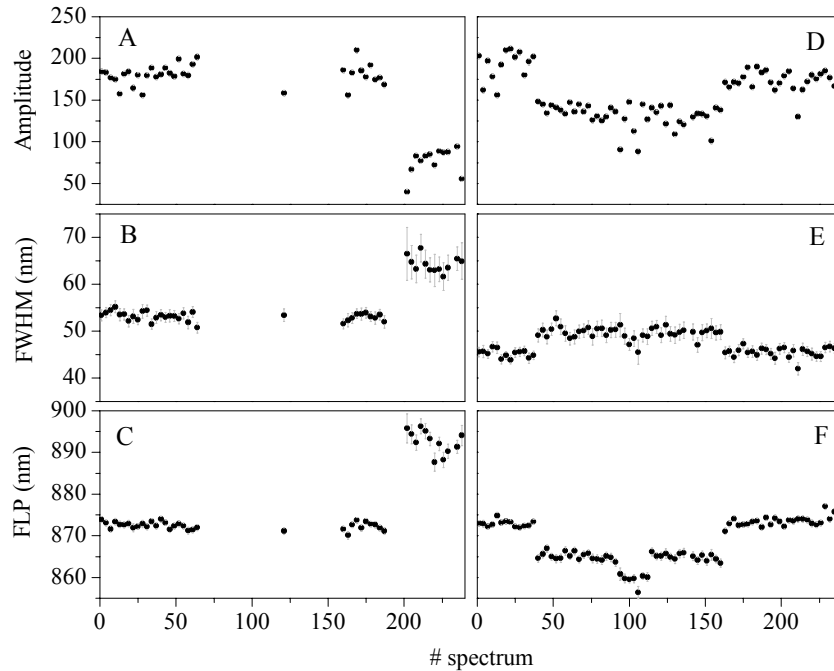


Figure 8. Correlated FLP, amplitude and fwhm traces of two individual LH2s: (A-C) spectral shift to the red; (D-F) spectral shift to the blue. Excitation intensity at 800 nm is 6 μW for (D-F) and 3.5 μW for (A-C).

strongly correlating particles relative to the number of strongly fluctuating ones is dependent on the excitation power and generally is significant.

Table 2 also contains information about the particles that show a combination of the pair-wise correlations and in addition exhibit a particular sign of the 3rd moment of the FLP time trace. It appears that most of the molecules with the positive FLP-amplitude and negative FLP-fwhm correlations have that sign negative; on the other hand, the negative FLP-amplitude and positive FLP-fwhm combination of the correlations corresponds very well with the 3rd moment being positive. This means that, for example, if the 3rd moment is negative, the FLP drops, spectrum broadens (since the FLP-fwhm correlation is negative, the fwhm has to increase with the reduction of the FLP) and subsides in intensity (since the amplitude-FLP correlation is positive, the decrease of the FLP means the declining amplitude). In fact the judgment by the 3rd moment in small number of cases does not coincide with the visual impression of the sign of the spectral jump. Effectively all the particles exhibiting double pair-wise correlation undergo spectral diffusion in the same direction. Overall, we observe that if a particle undergoes significant spectral diffusion, which is accompanied by the correlated evolution of all three spectral fit parameters, then FLP increase or reduction is associated with the spectral broadening and the loss of the radiative power. Furthermore, there exists a very good correspondence between a particle

Table 2. Molecules exhibiting strong correlations between spectral fit parameters. “Combination (blue shift)” refers to the number of particles that exhibit both amplitude-FLP and FLP-fwhm correlations with corresponding signs. Numbers in brackets point to the particles that in addition to both pair-wise correlations, have the negative 3rd moment of the FLP time trace. Similarly “Combination (red shift)” relates to the corresponding combination of correlations and particles with positive 3rd moment of the FLP time trace.

	Experimental conditions						
Temperature (° C)	20	20	20	20	20	28	35
Excitation (μW)	0.5	1.5	2.5	3.5	6	0.5	0.5
	Numbers of measured particles						
Total	149	124	128	119	138	120	94
SDFP > 2.44	2	23	32	30	58	8	5
	Numbers of correlating particles						
Amplitude-FLP positive	1	11	7	9	19	1	0
FLP-fwhm negative	0	7	5	6	13	1	3
Combination (blue shift)	0 (0)	6 (6)	3 (2)	5 (5)	11 (9)	0 (0)	0 (0)
Amplitude-FLP negative	0	3	3	13	7	2	1
FLP-fwhm positive	0	4	7	13	7	4	1
Combination (red shift)	0 (0)	3 (3)	2 (2)	11 (11)	5 (3)	2 (2)	0 (0)

having only strong positive FLP-amplitude or negative FLP-fwhm correlation and its tendency to exhibit big spectral shifts to the blue; similarly, merely negative FLP-amplitude or positive FLP-fwhm correlation is associated with the red-shifting.

A quantitative relationship between the number of the correlating particles and the excitation intensity is not evident from the data presented here, which is probably due to the limited statistics of our measurement. In fact, even at the highest excitation intensity, only about 10% of the particles exhibit strong correlations. Thus the occurrence of the correlated behavior is generally quite rare. Nevertheless, at the lowest excitation of 500 nW we observe no particles with two pair-wise correlations. Such correlating particles appear with the increase of the excitation intensity though the number of these particles does not increase monotonously with the excitation intensity. Fewer appear as the temperature is increased. Consequently, we are able to conclude that higher levels of excitation and to a lesser extent – increase of an ambient temperature, induce correlated behavior of the particles.

Statistics of spectral jumps

We further characterize the statistics of the spectral jumping by calculating the distributions

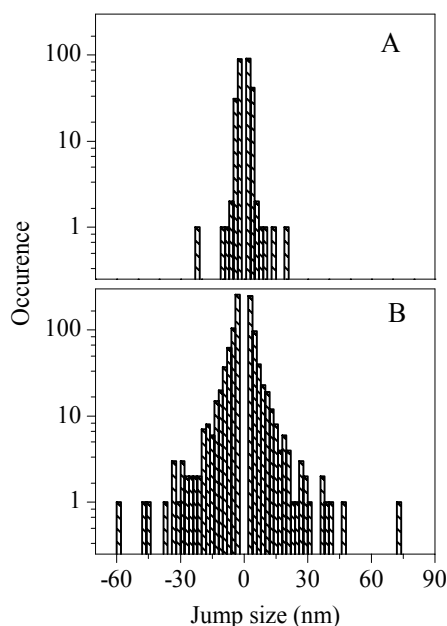


Figure 9. Occurrences of spectral jumps of a certain size, calculated over all FLP trajectories measured under the same experimental conditions. Excitation intensity: (A) $0.5 \mu\text{W}$; (B) $6 \mu\text{W}$.

of jumps of a certain magnitude over the whole population of complexes measured under the same experimental conditions. A threshold of the jump size is arbitrarily set to 2 nm. The magnitude of the jump is calculated between two adjacent points in FLP time trace. Prior to the calculation, points of the trace are pooled in bins to yield a time bin of 2 s, common to all the experimental data sets. In Figure 9 we show histograms of spectral jumps at excitation intensities of $0.5 \mu\text{W}$ and $6 \mu\text{W}$. Distributions of jump size broaden with excitation intensity resulting in exponential decay components of 0.97 ± 0.06 and -0.69 ± 0.05 , and 2.18 ± 0.04 and -2.25 ± 0.08 , respectively. Logarithmic representation of a particular jump size occurrence reveals rare cases of excessively large jumps. The number of such outlier spectral shifts notably increases with excitation intensity.

Finally, the threshold of the jump size was set to 5 nm, and the number of jumps greater than the limiting value was calculated for all the particles for each experimental population. The excitation intensity and temperature dependence of the average number of jumps per molecule is depicted in Figure 10. For the measurements at 20°C this number increases approximately linearly with the excitation, which is in agreement with a simple model regarding the transition between two spectrally different conformations of the protein as a local temperature-driven activation process. On the other hand, the increase of the temperature in the experiments with 500 nW excitation power leads to relatively small change of the frequency of spectral shifting. In fact, in our experiment the number of jumps at 35°C is smaller than that at 28°C , which is probably due to insufficient difference of temperature values. Temperature effect is too weak to obtain a consistent increase in the

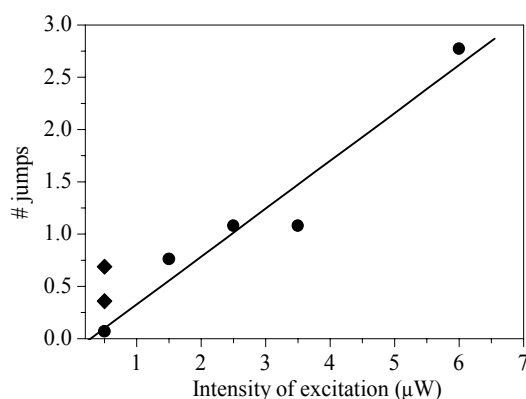


Figure 10. Intensity dependence of an average number of spectral jumps exceeding 5 nm calculated over different experimental populations of particles. Circle data points with a linear fit correspond to 20° C. Diamond data points are acquired with 500 nW excitation at two elevated temperature values: upper point at 28° C; lower point at 35° C.

number of spectral jumps with temperature increase of 7° C. Extrapolation of the experimental data linear fit to zero intensity of excitation indicates a vanishing average number of jumps at that intensity.

DISCUSSION AND MODELLING

After the B800 ring in the LH2 complex absorbs an excitation photon, energy is transferred to the B850 BChl molecules in about 1 ps (Ma, *et al.* 1997, Salverda, *et al.* 2000) with a very high efficiency since competing processes of FL and non-radiative decay are three orders of magnitude slower (Monshouwer, *et al.* 1997). Subsequently exciton relaxation and excitation hopping occur in the B850 ring, with a certain probability leading to FL.

Considering that the molar absorption coefficient of LH2 at 800 nm is $2.3 \cdot 10^6 \text{ M}^{-1} \text{ cm}^{-1}$ (Alden, *et al.* 1997), a single complex will absorb $8.6 \cdot 10^6$ photons/s, if positioned in the center of the Gaussian laser beam, delivering 1 μW of (continuous wave) CW excitation at 800 nm. The BChl triplet with a lifetime of 70 μs (Monger, *et al.* 1976) is formed with 2-15% yield (Cogdell, *et al.* 1981, Monger, *et al.* 1976) and is transferred to the carotenoid in ~20 ns (Angerhofer, *et al.* 1995). This transfer step is highly efficient due to a BChl triplet lifetime much longer than the transfer time. The carotenoid triplet, having a lifetime of ~10 μs (Angerhofer, *et al.* 1995), is a very efficient trap for the singlet BChl excitations due to S-T annihilation occurring in about 6 ps (Bradforth, *et al.* 1995), since the competing FL and radiationless relaxation processes are much slower. From the simple calculation with the above parameters, it follows that in the presence of the carotenoid triplet in the complex, FL is heavily quenched (is about 200 times weaker than in the triplet-free condition). Formation of a second triplet in the system is also prevented by the fast S-T annihilation: since the intersystem crossing for the BChl takes place in 50 ns (calculated from the triplet

yield of 0.02 (Monger, *et al.* 1976)) and radiative lifetime of 1 ns (Monshouwer, *et al.* 1997), due to fast S-T annihilation, probability of the second triplet formation is 0.0001. With 1 μ W excitation power it would take 0.1 ms to form the second triplet in the system, which is an order of magnitude longer than the lifetime of the carotenoid triplet.

In summary – the system will spend part of its time in a state with a carotenoid triplet, in which the FL is very weak, and part of the time it will be in the triplet-free state and re-emit with a 10% quantum efficiency (Monshouwer, *et al.* 1997). The resulting quantum efficiency is dependent on the excitation rate and the yield of triplet formation. Triplet formation frequency is dependent on triplet quantum yield and excitation intensity. Thus the resulting FL quantum efficiency is dependent on the same set of parameters. At 500 nW excitation intensity we observe FL count rate of about 8500 counts/s, which with the estimated signal collection efficiency of 8% corresponds to 9% triplet formation yield (value in the middle of the range cited above). This corresponds to the resulting FL quantum efficiency of 2.5%.

This analysis implies that only a small fraction of the absorbed excitation photons is reemitted as FL. The remaining excitations either decay radiationlessly directly to the ground state, form a triplet or are quenched by triplets. In these cases, the absorbed excitation energy is eventually dissipated as heat, which leads to local temperature increase of the pigment surroundings. The pigment-protein complex is characterized by multiple potential energy substates separated by energetic barriers and corresponding to different protein structural conformations. Local temperature increase is a plausible cause of the structural alteration of the protein: in the event of overheating protein is removed from its local energetic minimum and upon subsequent cooling due to heat diffusion it possibly arrives to a state with a different energetic minimum. The change in the protein conformation induces the change in the pigment-protein interaction, which is possibly manifested as spectral change.

From the above analysis of excitation energy dynamics and time traces of the FLP it appears that in spite of the large number of excitations dumped in the system in the form of heat, the complex appears to dwell for a relatively long time in one of the quasi-stable states, characterized by a specific peak wavelength, spectral shape and intensity of the emission. We thus conclude that the free energy barriers separating those quasi-stable states with distinctly different spectroscopic properties must be large.

The possible light-induced structural alterations and their effect on pigment-protein interactions we will associate on a phenomenological level with a change in realization of the static disorder of the electronic transition energies of pigments in the complex that is in turn connected to particular spectral properties. Below we develop a model that quantitatively describes the observed changes in the spectral profile shape and its position on the basis of this hypothesis.

A quantitative description of single-molecule emission spectra

In our model for the FL spectrum of a single B850 ring we utilize the modified Redfield approach that incorporates excitonic interactions, static disorder of the electronic transition

energies of the pigments, and strong coupling of the electronic transitions to nuclear motions (phonons) of the surrounding (protein) medium. The spectral line shape of the pigment-protein complex and its dynamics are determined by coupling of electronic transitions to a manifold of nuclear modes. Fast modes determine the optical line shape both in conventional (Mukamel 1995) and single-molecules spectroscopies (Dempster, *et al.* 2001). Slow nuclear motions are associated with the evolution of the pigment-protein conformation on a microsecond to second time scale and result in different equilibrium positions of the nuclear coordinates producing different realizations of the static disorder of the electronic transition energies (Koolhaas, *et al.* 1997). They are the cause of the inhomogeneous broadening of the bulk spectrum. Particular nuclear coordinates result in specific states for a single complex, characterized by a certain FLP and a line shape. Thermally activated slow nuclear motions lead to the transitions between these states, observed as abrupt jumps in the FLP traces (Figure 5). Here we will not consider the dynamics of such transitions, but restrict ourselves to the modeling of the FL line shapes for different realizations of the disorder.

The energies of the exciton levels are calculated by constructing and diagonalizing the one-exciton Hamiltonian. B850 BChls in the dimeric subunit of LH2 are assumed to have unperturbed transition energies of 12415 and 12215 cm^{-1} (Sauer, *et al.* 1996) that were adjusted from a fit of a bulk spectrum. The energies of interactions of pigments associated with proteins $1\alpha-1\beta$, $1\alpha-2\alpha$, $1\alpha-2\beta$, $1\beta-2\alpha$, $1\beta-2\beta$ (the same number denotes the same protein dimer, while different numbers denote neighboring dimers), were taken to be 291, -50, 12, 273 and -36 cm^{-1} respectively (Sauer, *et al.* 1996). The static disorder of the transition energies was taken into account by introducing uncorrelated variations randomly taken from a Gaussian distribution with a fwhm of σ . The numerical diagonalization of the Hamiltonian (for each realization of the disorder) provides the energies of the exciton states, ω_k , and the wavefunction amplitudes, c_n^k , (participation of the n th pigment site in the k th exciton state).

Relatively high excitation densities we apply in our experiment might produce more than one excitation in a single LH2 complex. We model the B850 ring with one-exciton Hamiltonian, since emission lifetime is ~ 1 ns (Monshouwer, *et al.* 1997) while much faster exciton annihilation occurs on a ps (Ma, *et al.* 1997) time scale thus making the FL signal contribution from two-exciton states negligible.

The absorption and FL line shapes of the exciton states are calculated assuming strong exciton-phonon coupling (Zhang, *et al.* 1998). The homogeneous absorption line shape for the k th exciton state is expressed in terms of the line broadening function, g_k . The steady-state Stokes shift of the emission maximum of the k th state is given by $2\lambda_k$, where λ_k is the reorganization energy. Both g_k and λ_k are related to the spectral density, $C_k(\omega)$, in the exciton basis, which is connected with the spectral density in the site representation, $C_n(\omega)$, through the fourth power of the wavefunction amplitudes, *i.e.*, $C_k(\omega) = \sum_n (c_n^k)^4 C_n(\omega)$. Here we have assumed that the phonon-induced fast modulation of the electronic transitions is described by an uncorrelated diagonal disorder (not to be confused with the

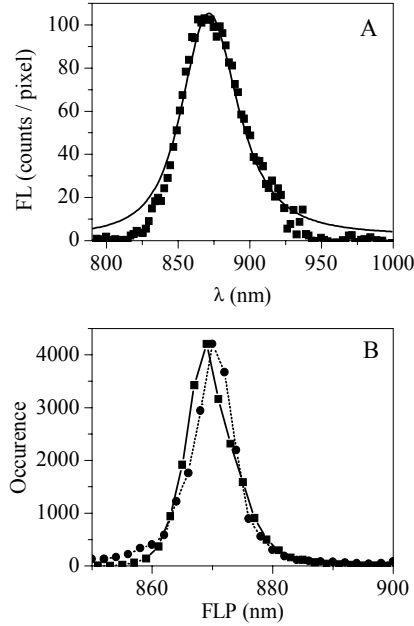


Figure 11. (A) An average in time and over experimental population of single-molecule spectra measured with $6 \mu\text{W}$ excitation intensity at 800 nm (squares) and calculated FL spectrum averaged over realizations of static disorder (solid line). (B) Distributions of FLP of single-molecule spectra measured with $6 \mu\text{W}$ excitation intensity at 800 nm (circles, dotted line to guide the eye) and simulated spectra, calculated with different realizations of disorder (squares, solid line).

static disorder). The $\sum_n (c_n^k)^4$ factor is also known as the participation ratio (PR), or inverse delocalization length of the k th exciton state. Indeed, the PR of the exciton state is relatively small only if all of the wavefunction amplitudes are small, which, due to the normalization condition guarantees approximately equal contributions from different sites and is indicative of excitation delocalization over different sites. On the other hand, again due to the normalization requirement, a large PR could result only from a few relatively large and the remaining small wavefunction amplitudes implying that the excitation is localized on a few sites predominantly contributing to the value of PR.

In summary, the phonon-induced broadening and the Stokes shift of each of the exciton levels is dependent on the PR of that level which in turn is dependent on the realization of the static disorder through the wavefunction amplitudes. Hence, the optical line shape and the peak wavelength are determined by the realization of the static disorder.

The spectral density $C_n(\omega)$ is assumed to have the form of an overdamped Brownian oscillator (Mukamel 1995, Zhang, *et al.* 1998) with the coupling parameter λ and relaxation time τ . In our model, λ and τ (as well as σ) are site-independent free parameters adjusted from the fit of the absorption and FL spectra. The RT single-molecule FL spectrum acquired with $6 \mu\text{W}$ excitation intensity and averaged in time and over particles together with the distribution of the FL peak wavelengths (Figure 11) can be reproduced with $\sigma =$

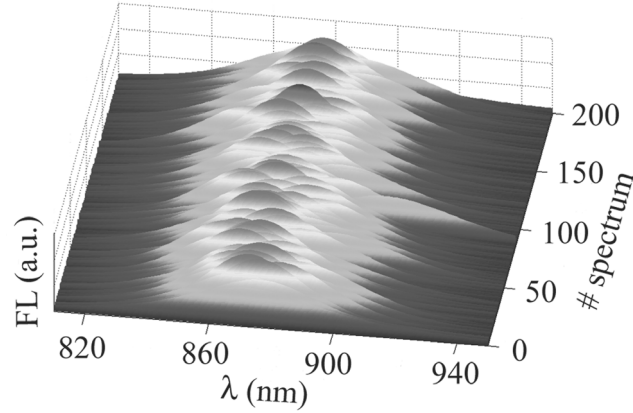


Figure 12. FL profiles of single LH2 calculated for 200 realizations of disorder at RT.

370 cm^{-1} , $\lambda = 390 \text{ cm}^{-1}$, and $\tau = 50 \text{ fs}$. Notably the RT absorption spectrum of the LH2 B850 band *in vivo* can be reproduced with the same σ and τ , and $\lambda = 220 \text{ cm}^{-1}$ (data not shown).

The model also takes into account the relaxation-induced broadening, *i.e.*, we suppose an additional homogeneous broadening of the exciton states given by their inverse lifetimes $R_k = -\sum_{k'} R_{k'k'kk}$, where $R_{k'k'kk}$ is the rate of the $k \rightarrow k'$ transition calculated (Zhang, *et al.* 1998) in terms of g_k functions.

Single LH2 FL profiles calculated for 200 realizations of the static disorder at RT are presented in Figure 12. The FLP is distributed over a range of values similar to the experimental data. However, since we do not have an explicit model to describe the dynamics of spectral jumping, the collection of calculated FLP values does not represent temporal evolution of the spectrum. The average of the calculated FL profiles has a maximum near 870 nm, which is the peak wavelength of the experimental bulk spectrum. Realizations with the FLP near this wavelength occur with the highest probability.

Figure 13 shows three experimental and corresponding simulated FL profiles with different peak wavelengths. Experimental curves are averages of all single-molecule FL spectra measured with $3.5 \mu\text{W}$ excitation intensity and featuring FLP in intervals of 859-861, 869-871 and 889-891 nm. These average spectra have respective fwhms of 53, 48 and 67 nm. Simulated profiles are averages of spectra calculated with different realizations of disorder and peaking in the same corresponding intervals. The red-shifted profile has a pronounced short-wavelength wing. Averages with blue-shifted and intermediate FLP feature a regular FL profile asymmetry, *i.e.*, a broader long-wavelength tail. Notably, the blue- and red-shifted experimental spectra are broader than that with the intermediate FLP. Overlaying of experimental and simulated spectra shows that the model satisfactorily reproduces many of the features observed in the experimental data. Typical blue and red-shifted simulated FL profiles also have lower intensity than the ones with the intermediate FLP (Rutkauskas, *et al.* 2004). Thus simulated spectra qualitatively reproduce the experimentally observed correlation between spectral peak wavelength shifts and spectral

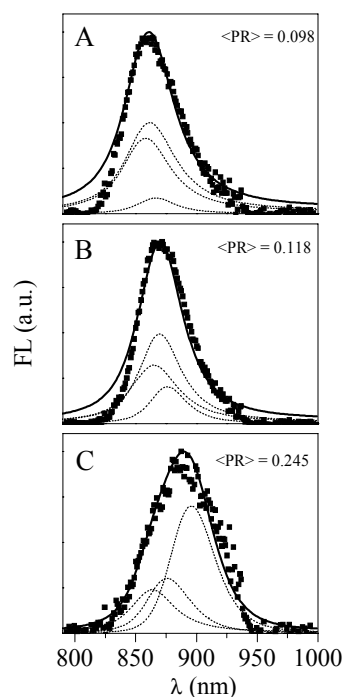


Figure 13. Three spectrally different average experimental (squares) and calculated (solid line) FL profiles: (A) blue-shifted, (B) intermediate, and (C) red-shifted. Calculated spectra are presented together with contributions from the three lowest exciton components (dotted lines).

broadening and diminishing intensity.

In the following we will comment on the mechanism, by which static disorder determines the spectral profile shape and peak wavelength. We found that simulated line shapes with different FLP correspond to a specific exciton structure (energy level scheme of exciton states), which in turn is associated with a particular pattern of static disorder. Contributions of the three lowest exciton states to the FL profiles with intermediate, blue- and red-shifted FLP are depicted by dotted lines in Figure 13. In this picture, a separate exciton level profile (as well as the whole FL profile) is an average over different realizations of static disorder that result in a FLP within a particular interval. Transition dipole strengths of exciton states are weighed with the steady-state populations of the corresponding exciton states. The three types of exciton structure presented in Figure 13 correspond to different degrees of excitation delocalization in all three exciton levels. The extent of delocalization can be characterized by an PR of an individual exciton state in the presence of a particular realization of disorder. For a circular aggregate of N molecules $PR = 1/N$ for the lowest and $3/2N$ for higher states in the absence of the static disorder. In the case of the LH2 ring, $N = 18$ and PR is calculated to be 0.056 and 0.083, respectively. Including the disorder results in a dramatic increase of PR of all states, especially of the lowest one. Even small disorder results in $PR = 0.09-0.1$ (depending on the realization of the disorder) of all three

states. A strongly disordered aggregate is conveniently characterized by a wavelength-dependent $PR(\lambda)$, defined as the PR average over the exciton states that result from different realizations of the static disorder and feature energies within a narrow interval around λ (Alden, *et al.* 1997, Novoderezhkin, *et al.* 1999). For example, for LH2, taking interaction energy 250-400 cm^{-1} with a realistic value of disorder of 300-450 cm^{-1} for a fwhm of the Gaussian distribution (Alden, *et al.* 1997, Novoderezhkin, *et al.* 1999), $PR(\lambda)$ is almost constant (0.1-0.12) throughout the absorption band (*i.e.*, in the region determined mostly by higher excitonic states), increases to 0.12-0.2 in the red edge, where the lowest state starts to contribute, and increases up to 0.3-0.4 in the very red edge due to the contribution of strongly red-shifted and localized lowest states (Alden, *et al.* 1997, Novoderezhkin, *et al.* 1999, Novoderezhkin, *et al.* 1999, Novoderezhkin, *et al.* 2003). Delocalization of the exciton states contributing to the steady-state FL is reflected in the thermally averaged PR, $\langle PR \rangle$, defined as an average of individual exciton state PR values weighed with steady-state populations of those states. $\langle PR \rangle$ values corresponding to blue, intermediate and red-shifted FLP are 0.098, 0.118 and 0.245, respectively, reflecting the increasingly localized character of the exciton states contributing to FL spectrum, when it shifts to the red.

Figure 13A reveals that the blue-shifted FL profile corresponds to a relatively delocalized exciton ($\langle PR \rangle < 0.1$) with its structure marginally affected by the presence of the static disorder. The lowest $k = 0$ state is only weakly allowed, so the RT emission originates mostly from the degenerate $k = \pm 1$ pair giving rise to a blue-shifted FL.

Notice that k -notation originates from the exciton wavenumbers of a circular aggregate without disorder. For a disordered antenna mixing of the zero-order wavefunctions produces more complicated exciton states, which cannot be characterized by k wavenumbers. On the other hand, exciton structure of antenna with intermediate values of disorder resembles that of the homogeneous aggregate: larger part of dipole strength is still concentrated in the two higher levels. Thus for the ease of discussion we persist in labeling exciton levels with k wavenumbers though they do not have the same meaning for homogeneous and for disordered aggregates.

Realizations of a larger static disorder (Figure 13B) result in a larger splitting between the $k = \pm 1$ levels, so that the lower $k = -1$ state becomes more populated and more emitting as compared to the $k = 1$. However, both $k = -1$ and $k = 1$ levels still remain delocalized ($PR(\lambda) = 0.09-0.11$ in the corresponding spectral region). The lowest $k = 0$ state becomes more emitting borrowing part of the dipole strength from higher levels through disorder-induced mixing of states. Due to this mixing the $k = 0$ state also becomes more localized. The contribution of the lowest state increases $PR(\lambda)$ in the long-wavelength region ($PR(\lambda) = 0.11-0.17$). The corresponding $\langle PR \rangle$ value is about 0.12. Such an exciton structure is characteristic of realizations with the FLP near the maximum of the average emission.

Figure 13C demonstrates an example of a red-shifted FL profile. Its exciton structure is strongly affected by the disorder, which induces large splitting between the three lowest states. The $PR(\lambda)$ value is large for all the states especially for the lowest one. Due to the

large splitting between the exciton states, the FL originates from the most populated lowest state, which is now strongly allowed and localized ($PR(\lambda) > 0.3$). Its localized character leads to a significant broadening and red shift of the FLP.

Red-shifted FL profiles correspond to a disorder-induced localization of exciton state on 3-4 pigments. Energetic shift of just one pigment in a ring will not lead to such strong localization since the remaining energetically equivalent and excitonically interacting pigments will give rise to delocalized excitonic state. On the other hand, random energetic shift of a larger number of pigments in the ring will be associated with significantly more pronounced destruction of delocalization of excitonic wavefunction and hence red shift of FL spectrum. Red-shift of a few pigments would also shift the overall spectral profile to the red without destruction of exciton delocalization. However, such shift would not be accompanied by the change of spectral shape since broadening of spectral profile is associated with increased localization.

Downhill exciton relaxation with a rate increasing for the higher levels is an additional line-broadening factor contributing to the width of the blue-shifted FL spectrum. In fact, “downhill” relaxation is a result of multiple pathways including both uphill and downhill excitation transfers. However, at finite temperature the downhill channel is always faster, so the higher states have shorter lifetimes. In our model $R_k = 16, 29, 44,$ and 57 ps^{-1} for $k = 0, -1, 1$ and -2 levels, respectively. It should be noted that the relaxation tensor in our modeling is different for different realizations of disorder. The inverse lifetimes R_k listed here are averages over disorder.

The more pronounced relaxation broadening of the $k = \pm 1$ levels results in a larger width of the blue-shifted FL spectra (determined mostly by the $k = \pm 1$ emission). Notice that disregarding the relaxational broadening, a blue shift would be always accompanied by the narrowing of the FL line, because the $k = \pm 1$ levels are narrower than the lowest one due to smaller PR values and, as a result, smaller phonon coupling. Omitting the relaxation, it would be impossible to interpret the observed broadening of the blue-shifted FL profile.

CONCLUSIONS

We have experimentally observed notable light-induced jumps of single LH2 FL spectrum peak wavelength between the levels of distinctly different magnitude. Though spectral fluctuations were evidently light-induced, they did not signal the deterioration of the assembly, since in most cases jumps were reversible. We conclude, that the intense excitation drives the complex into conformational states, which are less accessible in dark conditions, but still intrinsic to the system. The probability for a complex to undergo a large spectral jump either to longer or shorter wavelengths was found to be roughly the same. The number of spectral jumps was found to be linearly dependent on the excitation intensity, which is in agreement with a simple model regarding the transition between two spectrally different conformations of the protein as a local temperature-driven activation process.

The observed spectral jumps were accompanied by a broadening of the FL profile and

the decrease of amplitude. We have qualitatively accounted for these effects by modeling the FL with different realizations of the static disorder of pigment transition energies. However, our model does not encompass the dynamics of the spectral jumps. The observation that large spectral jumps occur with a very low probability with respect to the number of excitations received by the system, leads us to conclude that large free energy barriers separate the states with distinctly different spectral properties.

REFERENCES

- Alden, R. G., Johnson, E., Nagarajan, V., Parson, W. W., Law, C. J., and Cogdell, R. J. (1997) Calculations of spectroscopic properties of the LH2 bacteriochlorophyll-protein antenna complex from *Rhodospseudomonas acidophila*. *J. Phys. Chem. B* 101, 4667-4680.
- Angerhofer, A., Bornhauser, F., Gall, A., and Cogdell, R. J. (1995) Optical and optically detected magnetic resonance investigation on purple photosynthetic bacterial antenna complexes. *Chem. Phys.* 194, 259-274.
- Bopp, M. A., Jia, Y. W., Li, L. Q., Cogdell, R. J., and Hochstrasser, R. M. (1997) Fluorescence and photobleaching dynamics of single light-harvesting complexes. *Proc. Natl. Acad. Sci. U.S.A.* 94, 10630-10635.
- Bopp, M. A., Sytnik, A., Howard, T. D., Cogdell, R. J., and Hochstrasser, R. M. (1999) The dynamics of structural deformations of immobilized single light-harvesting complexes. *Proc. Natl. Acad. Sci. U.S.A.* 96, 11271-11276.
- Bradforth, S. E., Jimenez, R., van Mourik, F., van Grondelle, R., and Fleming, G. R. (1995) Excitation transfer in the core light-harvesting complex (LH1) of *Rhodobacter sphaeroides*: an ultrafast fluorescence depolarization and annihilation study. *J. Phys. Chem.* 99, 16179-16191.
- Cogdell, R. J., Fyfe, P. K., Barrett, S. J., Prince, S. M., Freer, A. A., Isaacs, N. W., McGlynn, P., and Hunter, C. N. (1996) The purple bacterial photosynthetic unit. *Photosynth. Res.* 48, 55-63.
- Cogdell, R. J., and Hawthornthwaite, A. M. (1993) Preparation, purification and crystallization of purple bacterial antenna complexes. Vol. 1, Academic Press, New York.
- Cogdell, R. J., Hipkins, M. F., MacDonald, W., and Truscott, T. G. (1981) Energy transfer between the carotenoid and the bacteriochlorophyll within the B-800-850 light-harvesting pigment-protein complex of *Rhodospseudomonas sphaeroides*. *Biochim. Biophys. Acta.* 634, 191-202.
- Dempster, S. E., Jang, S. J., and Silbey, R. J. (2001) Single molecule spectroscopy of disordered circular aggregates: a perturbation analysis. *J. Chem. Phys.* 114, 10015-10023.
- Fowler, G. J. S., Visschers, R. W., Grief, G. G., van Grondelle, R., and Hunter, C. N. (1992) Genetically modified photosynthetic antenna complexes with blueshifted absorbency bands. *Nature.* 355, 848-850.
- Frauenfelder, H. (2003) Complexity of proteins. In *Physics of biological systems: from molecules to species*, Springer-Verlag, Heidelberg.
- Gerken, U., Jelezko, F., Gotze, B., Branschadel, M., Tietz, C., Ghosh, R., and Wrachtrup, J. (2003) Membrane environment reduces the accessible conformational space available to an integral membrane protein. *J. Phys. Chem. B* 107, 338-343.
- Halloren, E., McDermott, G., Lindsay, J. G., Miller, C., Freer, A. A., Isaacs, N. W., and Cogdell, R. J. (1995) Studies on the light-harvesting complexes from the thermotolerant purple bacterium *Rhodospseudomonas cryptolactis*. *Photosynth. Res.* 44, 149-155.

- Hofmann, C., Aartsma, T. J., Michel, H., and Köhler, J. (2003) Direct observation of tiers in the energy landscape of a chromoprotein: a single-molecule study. *Proc. Natl. Acad. Sci. U.S.A.* 100, 15534-15538.
- Hu, X. C., Ritz, T., Damjanovic, A., Autenrieth, F., and Schulten, K. (2002) Photosynthetic apparatus of purple bacteria. *Q. Rev. Biophys.* 35, 1-62.
- Hu, X. C., Ritz, T., Damjanovic, A., and Schulten, K. (1997) Pigment organization and transfer of electronic excitation in the photosynthetic unit of purple bacteria. *J. Phys. Chem. B.* 101, 3854-3871.
- Jung, Y., Barkai, E., and Silbey, R. J. (2002) Current status of single-molecule spectroscopy: theoretical aspects. *J. Chem. Phys.* 117, 10980-10995.
- Ketelaars, M., van Oijen, A. M., Matsushita, M., Köhler, J., Schmidt, J., and Aartsma, T. J. (2001) Spectroscopy on the B850 band of individual light-harvesting 2 complexes of *Rhodospseudomonas acidophila* I. Experiments and Monte Carlo simulations. *Biophys. J.* 80, 1591-1603.
- Koolhaas, M. H. C., van der Zwan, G., Frese, R. N., and van Grondelle, R. (1997) Red shift of the zero crossing in the CD spectra of the LH2 antenna complex of *Rhodospseudomonas acidophila*: a structure-based study. *J. Phys. Chem. B.* 101, 7262-7270.
- Ma, Y. Z., Cogdell, R. J., and Gillbro, T. (1997) Energy transfer and exciton annihilation in the B800-850 antenna complex of the photosynthetic purple bacterium *Rhodospseudomonas acidophila* (Strain 10050). A femtosecond transient absorption study. *J. Phys. Chem. B.* 101, 1087-1095.
- Matsushita, M., Ketelaars, M., van Oijen, A. M., Köhler, J., Aartsma, T. J., and Schmidt, J. (2001) Spectroscopy on the B850 band of individual light-harvesting 2 complexes of *Rhodospseudomonas acidophila* II. Exciton states of an elliptically deformed ring aggregate. *Biophys. J.* 80, 1604-1614.
- McDermott, G., Prince, S. M., Freer, A. A., Hawthornthwaite, A. M., Papiz, M. Z., Cogdell, R. J., and Isaacs, N. W. (1995) Crystal structure of an integral membrane light-harvesting complex from photosynthetic bacteria. *Nature.* 374, 517-521.
- Monger, T. G., Cogdell, R. J., and Parson, W. W. (1976) Triplet states of bacteriochlorophyll and carotenoids in chromatophores of photosynthetic bacteria. *Biochim. Biophys. Acta.* 449, 136-153.
- Monshouwer, R., Abrahamsson, M., van Mourik, F., and van Grondelle, R. (1997) Superradiance and exciton delocalization in bacterial photosynthetic light-harvesting systems. *J. Phys. Chem. B.* 101, 7241-7248.
- Mukamel, S. (1995) Principles of Nonlinear Optical Spectroscopy, Oxford University Press, New York.
- Novoderezhkin, V., Monshouwer, R., and van Grondelle, R. (1999) Disordered exciton model for the core light-harvesting antenna of *Rhodospseudomonas viridis*. *Biophys. J.* 77, 666-681.
- Novoderezhkin, V., Monshouwer, R., and van Grondelle, R. (1999) Exciton (de)localization in the LH2 antenna of *Rhodobacter sphaeroides* as revealed by relative difference absorption measurements of the LH2 antenna and the B820 subunit. *J. Phys. Chem. B.* 103, 10540-10548.
- Novoderezhkin, V., Wendling, M., and van Grondelle, R. (2003) Intra- and interband transfers in the B800-B850 antenna of *Rhodospirillum rubrum*. Redfield theory modeling of polarized pump-probe kinetics. *J. Phys. Chem. B.* 107, 11534-11548.
- Olsen, J. D., Sockalingum, G. D., Robert, B., and Hunter, C. N. (1994) Modification of a hydrogen bond to a bacteriochlorophyll a molecule in the light-harvesting 1 antenna of *Rhodobacter sphaeroides*. *Proc. Natl. Acad. Sci. U.S.A.* 91, 7124-7128.
- Papiz, M. Z., Prince, S. M., Howard, T., Cogdell, R. J., and Isaacs, N. W. (2003) The structure and thermal motion of the B800-850 LH2 complex from *Rps. acidophila* at 2.0 Å over-circle resolution and 100 K: new structural features and functionally relevant motions. *J. Mol. Biol.* 326, 1523-1538.

- Robert, B., Cogdell, R. J., and van Grondelle, R. (2003) The light-harvesting system of purple bacteria. In *Light-harvesting antennas in photosynthesis*. Green, B. R. and Parson, W. W., Eds., Vol. 13, Kluwer academic publishers, Dordrecht, Netherlands.
- Rutkauskas, D., Novoderezhkin, V., Cogdell, R. J., and van Grondelle, R. (2004) Fluorescence spectral fluctuations of single LH2 complexes from *Rhodospseudomonas acidophila* strain 10050. *Biochemistry*. 43, 4431-4438.
- Salverda, J. M., van Mourik, F., van der Zwan, G., and van Grondelle, R. (2000) Energy transfer in the B800 rings of the peripheral bacterial light-harvesting complexes of *Rhodospseudomonas acidophila* and *Rhodospirillum rubrum* studied with photon echo techniques. *J. Phys. Chem. B*. 104, 11395-11408.
- Sauer, K., Cogdell, R. J., Prince, S. M., Freer, A., Isaacs, N. W., and Scheer, H. (1996) Structure-based calculations of the optical spectra of the LH2 bacteriochlorophyll-protein complex from *Rhodospseudomonas acidophila*. *Photochem. Photobiol.* 64, 564-576.
- Scheuring, S., Reiss-Husson, F., Engel, A., Rigaud, J. L., and Ranck, J. L. (2001) High-resolution AFM topographs of *Rubrivivax gelatinosus* light-harvesting complex LH2. *EMBO J.* 20, 3029-3035.
- Scholes, G. D., and Fleming, G. R. (2000) On the mechanism of light harvesting in photosynthetic purple bacteria: B800 to B850 energy transfer. *J. Phys. Chem. B*. 104, 1854-1868.
- Sundström, V., Pullerits, T., and van Grondelle, R. (1999) Photosynthetic light-harvesting: reconciling dynamics and structure of purple bacterial LH2 reveals function of photosynthetic unit. *J. Phys. Chem. B*. 103, 2327-2346.
- van Grondelle, R. (1985) Excitation energy transfer, trapping and annihilation in photosynthetic systems. *Biochim. Biophys. Acta*. 811, 147-195.
- van Grondelle, R., Dekker, J. P., Gillbro, T., and Sundström, V. (1994) Energy-transfer and trapping in photosynthesis. *Biochim. Biophys. Acta*. 1187, 1-65.
- van Grondelle, R., and Novoderezhkin, V. (2001) Dynamics of excitation energy transfer in the LH1 and LH2 light-harvesting complexes of photosynthetic bacteria. *Biochemistry*. 40, 15057-15068.
- van Oijen, A. M., Ketelaars, M., Köhler, J., Aartsma, T. J., and Schmidt, J. (2000) Spectroscopy of individual light-harvesting 2 complexes of *Rhodospseudomonas acidophila*: diagonal disorder, intercomplex heterogeneity, spectral diffusion, and energy transfer in the B800 band. *Biophys. J.* 78, 1570-1577.
- van Oijen, A. M., Ketelaars, M., Köhler, J., Aartsma, T. J., and Schmidt, J. (1999) Unraveling the electronic structure of individual photosynthetic pigment-protein complexes. *Science*. 285, 400-402.
- Wu, H. M., Rätsep, M., Lee, I. J., Cogdell, R. J., and Small, G. J. (1997) Exciton level structure and energy disorder of the B850 ring and the LH2 antennal complex. *J. Phys. Chem. B*. 101, 7654-7663.
- Zhang, W. M., Meier, T., Chernyak, V., and Mukamel, S. (1998) Exciton-migration and three-pulse femtosecond optical spectroscopies of photosynthetic antenna complexes. *J. Chem. Phys.* 108, 7763-7774.

Dynamics of the emission spectrum of a single LH2 complex: interplay of slow and fast nuclear motions

Vladimir I. Novoderezhkin, Danielis Rutkauskas, and Rienk van Grondelle

ABSTRACT

We have studied the relationship between the realizations of static disorder and the emission spectra observed for a single LH2 complex (Rutkauskas, *et al.* 2005). We show that the experimentally observed spectral fluctuations reflect realizations of the disorder in the B850 ring associated with different degrees of exciton delocalization and different effective coupling of the excitons to phonon modes. The main spectral features cannot be explained using models with correlated disorder associated with elliptical deformations of the ring. A quantitative explanation of the measured single-molecule spectra is obtained using the modified Redfield theory and a model of the B850 ring with uncorrelated disorder of the site energies. The positions and spectral shapes of the main exciton components in this model are determined by the disorder-induced shift of exciton eigenvalues in combination with phonon-induced effects (*i.e.*, reorganization shift and broadening, that increase in proportion to the inverse delocalization length of the exciton state). Being dependent on the realization of the disorder, these factors produce different forms of the emission profile. In addition, the different degree of delocalization and effective couplings to phonons determines a different type of excitation dynamics for each of these realizations. We demonstrate that experimentally observed quasi-stable conformational states are characterized by excitation energy transfer regimes varying from a coherent wave-like motion of a delocalized exciton (with a 100 fs pass over half of the ring) to a hopping-type motion of the wavepacket (with a 350 fs jumps between separated groups of 3-4 molecules) and self-trapped excitations that do not move from their localization site.

INTRODUCTION

Photosynthesis starts with the absorption of a solar photon by one of the light-harvesting pigment-protein complexes and transferring the excitation energy to the photosynthetic reaction center where a charge separation is initiated (van Grondelle, *et al.* 1994). These initial and ultrafast events have been extensively investigated in photosynthetic purple bacteria. The bacterial light-harvesting complexes comprise a number of packed pigments circularly arranged in a protein scaffold. The peripheral light-harvesting complex 2 (LH2) from *Rhodospseudomonas (Rps.) acidophila*, the crystal structure of which has been determined with high resolution (McDermott, *et al.* 1995, Papiz, *et al.* 2003), is a highly symmetric ring of 9 pigment-protein subunits, each containing 2 trans-membrane polypeptide helices and 3 bacteriochlorophyll (BChl) molecules, with the α -polypeptide on the inner and the β -polypeptide on the outer side of the ring. The hydrophobic terminal of the protein binds a ring of 18 tightly coupled BChl molecules with a center-to-center distance of less than 1 nm between neighboring pigments. This ring is responsible for the intense absorption of LH2 peaking at around 850 nm (B850 ring). A second ring of 9 weakly interacting BChls is located in the polar region of the protein and is responsible for the absorption around 800 nm (B800 ring).

From nonlinear spectroscopic studies a consistent physical picture of the excitation dynamics in the B850 ring has emerged (Hu, *et al.* 2002, Sundström, *et al.* 1999, van Grondelle and Novoderezhkin 2001). All basic spectroscopic features can be understood on the basis of a model that includes both the excitonic coupling between pigments and the disorder induced by nuclear motion. Strong excitonic interactions between the chromophores within the B850 ring tend to delocalize the excitation over a number of pigments, whereas the nuclear motions (slow conformational changes of the pigment-protein matrix, fast intra-pigment vibrations, and phonon modes) break the symmetry of the complex producing more localized states (Dahlbom, *et al.* 2001, Meier, *et al.* 1997, Novoderezhkin, *et al.* 1999). Conventional bulk experiments reveal the details of excitonic relaxation and excitation energy transfer dynamics on a fs/ps time scale, but these observations and conclusions are associated with an averaging over a large number of complexes with different realizations of the energetic disorder, which is manifested as inhomogeneous spectral line-broadening. On the other hand, although restricted to visualization of dynamics on ms/s time scale, single-molecule experiments circumvent this ensemble averaging.

Based on room- and low-temperature single-molecule experiments it has been proposed that the LH2 ring can deviate from the ideally circular structure (Bopp, *et al.* 1999, Ketelaars, *et al.* 2001, Matsushita, *et al.* 2001, van Oijen, *et al.* 1999). Room-temperature (RT) polarized fluorescence (FL) experiments were interpreted in terms of an elliptical absorber and emitter with ellipticity and directions of the principal axis varying as a result of the B800 and/or B850 distortion destroying the rotational symmetry and traveling around the ring on a timescale of seconds (Bopp, *et al.* 1999). The anomalously large splitting of the two major

orthogonal excitonic transitions observed in low-temperature polarized FL excitation spectra was attributed to a modulation of the coupling strength in the B850 ring that was asserted to be associated with an elliptical deformation (Ketelaars, *et al.* 2001, Matsushita, *et al.* 2001, van Oijen, *et al.* 1999). Spectral fluctuations of different magnitude observed on different time scales were associated with a hierarchical structure of the protein conformational landscape (Hofmann, *et al.* 2003). Smaller structural ellipticities were found for loosely packed LH2s in membranes, and were probably partly due to an interplay of the disrupting tip and stabilizing lipid environment (Scheuring, *et al.* 2001).

In general, the observed variation of the spectral and functional properties of LH2 suggests that the complex can undergo a variety of deformations or evolve through a number of conformational substates. It is reasonable to assume that such conformational substates or in other words realizations of nuclear coordinates underlie the pattern of the static disorder of pigment site energies and interaction energies between pigments that play a key role in our current understanding of the spectroscopic and energy transfer properties of LH2. In a recent experiment (Rutkauskas, *et al.* 2005, Rutkauskas, *et al.* 2004) we have observed a spectral evolution of LH2 between different conformations at RT occurring on a second time scale (corresponding to slow nuclear motions) and manifested by abrupt movements of the FL peak wavelength of individual LH2 complexes between long-lived quasi-stable levels differing by up to 30 nm. We accounted for these spectral fluctuations on the basis of the modified Redfield theory by modeling the FL profiles for different realizations of the static disorder of the pigment transition energies.

In this paper we study in greater detail the mechanism of how different realizations of static disorder are associated with the observed spectral changes of LH2 (Rutkauskas, *et al.* 2005, Rutkauskas, *et al.* 2004). (1) We find here that spectral fluctuations reflect realizations of the disorder in the B850 ring with different degrees of exciton delocalization and different effective coupling of excitons to phonon modes. (2) The positions and spectral shapes of the main exciton components are determined by the disorder-induced shift of the exciton eigenvalues in combination with a phonon-induced shift and broadening. Being dependent on the realization of the disorder, these factors produce different shapes of the emission profile. (3) In addition, different delocalization and effective coupling to phonons determine a different type of excitation dynamics for each of these realizations. We conclude that experimentally observed quasi-stable conformational states are characterized by different excitation energy transfer regimes varying from a wave-like motion of a delocalized exciton to a non-coherent hopping of a localized wavepacket and an immobile self-trapped excitation.

THEORY

We employ the cumulant-expansion method (Mukamel 1995) to calculate spectral responses in the presence of strong exciton-phonon coupling. This method allows for an exact solution of spectral line shapes and excitation energy dynamics in a molecule with a single

electronic transition (Mukamel 1995). In a generalization for molecular aggregates (Zhang, *et al.* 1998) the line shapes are calculated including explicitly a diagonal coupling of nuclear modes to one-exciton states (inducing fluctuations of the energies of excitonic transitions), whereas off-diagonal coupling (inducing relaxation between the exciton eigenstates) is taken into account perturbatively. Linear spectra, *i.e.*, absorption and non-selective steady-state FL can be expressed as:

$$\begin{aligned} \text{OD}(\omega) &= \omega \sum_k \mathbf{d}_k^2 \text{Re} \int_0^\infty e^{i(\omega - \omega_k)t - \mathbf{g}_{kkkk}(t) - R_{kkkk}t} dt \\ \text{FL}(\omega) &= \omega \sum_k P_k \mathbf{d}_k^2 \text{Re} \int_0^\infty e^{i(\omega - \omega_k)t + i2\lambda_{kkkk}t - \mathbf{g}_{kkkk}^*(t) - R_{kkkk}t} dt \end{aligned} \quad (1)$$

$$\mathbf{d}_k = \sum_n c_n^k \mathbf{d}_n$$

$$R_{kkkk} = - \sum_{k' \neq k} R_{k'k'kk}$$

where P_k , \mathbf{d}_k , and ω_k denote the steady-state population, transition dipole moment and frequency (first moment of the absorption spectrum) of the k th one-exciton state, \mathbf{g}_{kkkk} is the line-broadening function, λ_{kkkk} is the reorganization energy value for the k th state. The wavefunction amplitude c_n^k (participation of the n th site in the k th exciton state) associates the transition dipole of the exciton state with the molecular transition dipole \mathbf{d}_n . It is important to note that our expressions for the linear spectra take into account a relaxation-induced broadening of the exciton states given by their inverse lifetimes, *i.e.*, R_{kkkk} . This term was not present in the original theory of Zhang *et al.* (Zhang, *et al.* 1998), but applications of the theory demonstrated its importance in order to fit quantitatively the spectra of molecular assemblies such as J-aggregates (Ohta, *et al.* 2001), the FMO-complex (Wendling, *et al.* 2002), the PSII reaction center (Novoderezhkin, *et al.* 2005, Raszewski, *et al.* 2005, Renger and Marcus 2002), bacterial LH2 antenna (Rutkauskas, *et al.* 2005, Rutkauskas, *et al.* 2004) and the LHCII complex from higher plants (Novoderezhkin, *et al.* 2004, Novoderezhkin, *et al.* 2005). The inverse lifetime of the k th state is given by a sum of the relaxation rates within the one-exciton manifold (Equation 1). The rate of the $k' \rightarrow k$ population transfer is given by (Zhang, *et al.* 1998):

$$\begin{aligned}
R_{kkk'k'} = & \tag{2} \\
& -2\text{Re} \int_0^{\infty} \hat{W}(\omega_{kk'}, t) \{ \mathbf{g}''_{kk'k'k}(t) - \{ \mathbf{g}'_{k'kk'k}(t) - \mathbf{g}'_{k'kkk}(t) + 2i\lambda_{k'kk'k'} \} \\
& \times \{ \mathbf{g}'_{k'k'kk'}(t) - \mathbf{g}'_{kkkk'}(t) + 2i\lambda_{k'k'kk'} \} \} dt \\
\hat{W}(\omega_{kk'}, t) = & \\
& \exp \{ -i\omega_{kk'}t - \mathbf{g}_{kkkk}(t) - \mathbf{g}_{k'k'k'k'}(t) + 2\mathbf{g}_{k'k'kk}(t) + 2i(\lambda_{k'k'kk} - \lambda_{k'k'k'k'})t \}
\end{aligned}$$

where $\omega_{kk'} = \omega_k - \omega_{k'}$. The relaxation tensor in the form of Equation 2 is denoted as the modified Redfield tensor (Yang and Fleming 2002) to distinguish it from the standard Redfield tensor obtained in the limit of weak exciton-phonon coupling. The g-functions and λ values in Equations 1 and 2 are:

$$\begin{aligned}
\mathbf{g}_{kk'k''k'''}(t) = & \\
& - \int_{-\infty}^{\infty} \frac{1}{2\pi\omega} C_{kk'k''k'''}(\omega) \left[\coth \frac{\omega}{2k_B T} (\cos \omega t - 1) - i(\sin \omega t - \omega t) \right] d\omega \\
\lambda_{kk'k''k'''} = & - \lim_{t \rightarrow \infty} \frac{d}{dt} \text{Im} \{ \mathbf{g}_{kk'k''k'''}(t) \} = \int_{-\infty}^{\infty} \frac{1}{2\pi\omega} C_{kk'k''k'''}(\omega) d\omega \tag{3}
\end{aligned}$$

where $C_{kk'k''k'''}(\omega)$ is the matrix of the spectral densities in the eigenstate (exciton) representation, which reflects coupling of one-exciton states to a manifold of nuclear modes (see next section). In principle, coupling to nuclear motions with arbitrary time scales can be included explicitly in the g-function. But it is convenient to consider separately the action of fast and slow nuclear motions.

Fast modes

Electronic transitions in a pigment molecule (or collective excitonic transitions in a cluster of strongly coupled pigment molecules) are affected by fast intra- and inter-molecular vibrations, phonon modes of the protein environment, etc., *i.e.*, all these factors cause the so-called dynamic disorder. In the frequency range of 10-2000 cm^{-1} (as revealed by FL line-narrowing (FLN) (Peterman, *et al.* 1997), hole-burning (Pieper, *et al.* 1999), and molecular

dynamic simulations (Damjanovic, *et al.* 2002) these modes determine the homogeneous line-broadening (represented by g_{kkkk}) of the exciton transitions, a red shift of the zero phonon lines (ZPL) (which is equal to the reorganization energy value λ_{kkkk}), and the Stokes shift of the emission maximum of the k th exciton state (equal to $2\lambda_{kkkk}$). Equation 3 relates these quantities to the spectral density in the eigenstate basis $C_{kkkk}(\omega)$. The latter (as well as the $C_{kk'k''k'''}(\omega)$ quantities needed to calculate the relaxation tensor) can be obtained from the matrix of the spectral densities in the site representation $C_{nmn'm'}(\omega)$.

To simplify the matter we assume only a diagonal electron-phonon coupling in the site representation, *i.e.*, nuclear modes induce fluctuations of the pigment site energies without acting on the intermolecular couplings. Generally, there may be some correlations between fluctuations acting on different sites, but we restrict to the simplest case of uncorrelated dynamic disorder. This model implies that each molecule has its own independent thermal bath. We further suppose that the spectral density function of each such bath is site-independent, *i.e.*, spectral density in the site representation is $C_{nmn'm'}(\omega) = \delta_{nm}\delta_{nn'}\delta_{mm'}C(\omega)$. Transformation to the eigenstate representation yields:

$$C_{kk'k''k'''}(\omega) = \sum_n c_n^k c_n^{k'} c_n^{k''} c_n^{k'''} C(\omega) \quad (4)$$

Equation 4 shows that diagonal phonon coupling in the site representation results in both diagonal and off-diagonal couplings in the exciton basis. To construct the spectral density profile we use the sum of an overdamped Brownian oscillator and resonance contributions due to high-frequency modes:

$$C(\omega) = 2\lambda_0 \frac{\omega\gamma_0}{\omega^2 + \gamma_0^2} + \sum_{j=1,2,\dots} 2\lambda_j \omega_j^2 \frac{\omega\gamma_j}{(\omega_j^2 - \omega^2)^2 + \omega^2 \gamma_j^2}$$

$$\lambda_j = S_j \omega_j \quad (5)$$

$$\lambda = \int_{-\infty}^{\infty} \frac{1}{2\pi\omega} C(\omega) d\omega = \lambda_0 + \sum_{j=1,2,\dots} \lambda_j$$

where λ is the reorganization energy in the site representation, S_j is the Huang-Rhys factor of the j th vibrational mode in the site representation. Parameters of the temperature-independent spectral density (frequencies ω_j , couplings λ_j , and damping constants γ_j for high-frequency vibrations together with the coupling λ_0 , and damping γ_0 for Brownian oscillator) are obtained from the FLN, and further adjusted from the simultaneous fit of absorption/FL spectra at different temperatures.

Note that according to Equations 3-5 the line-broadening functions and reorganization energies of the k th exciton state in the eigenstate representation (g_{kkkk} and λ_{kkkk}) are smaller than in the site representation by a factor of $1/\sum(c_n^k)^4$ (this factor connects $C_{kkkk}(\omega)$ and $C(\omega)$ in Equation 4). The latter quantity is known as the inverse participation

ratio (PR) and is equal to the delocalization length of individual exciton state (Fidder, *et al.* 1991, Meier, *et al.* 1997, Novoderezhkin, *et al.* 1999). In the literature there exist many other definitions of delocalization length reflecting different aspects of the exciton dynamics, and therefore yielding different “exciton sizes” for the same system. The relation between them has been studied in great detail (Dahlbom, *et al.* 2001, Meier, *et al.* 1997, Novoderezhkin, *et al.* 1999).

Slow modes

Slow nuclear motions associated with conformational changes of the pigment-protein in a native membrane or when immobilized in a gel, on a mica surface, etc., and occurring on the microsecond to second time scale, result in the so-called static disorder of the pigment electronic transition energies (*i.e.*, the non-equivalence of pigment site energies – transition energy of each pigment in the complex deviates from some average value by an amount specific to that pigment) manifested as inhomogeneous broadening in conventional bulk spectroscopic experiments or the time-dependence of FL spectral parameter traces in single-molecule measurements (Rutkauskas, *et al.* 2005, Rutkauskas, *et al.* 2004).

We model different realizations of the static disorder (combinations of pigment site energy deviations from the non-disordered value), corresponding to different complexes measured simultaneously in bulk, or one complex at different moments in time in single-molecule experiments, by random uncorrelated shifts of the site energies (diagonal disorder). Numerical diagonalization of the one-exciton Hamiltonian yields eigenstate energies ω_k and eigenfunctions c_n^k , required to calculate absorption/FL spectra for one realization of the static disorder. Such calculations with a number of realizations of static disorder allows for a statistical characterization and comparison of the resulting spectra with the results of single-molecule experiment or with the bulk spectra after averaging of spectra calculated for different realizations of the disorder.

Combined action of slow and fast modes

Note that in the absence of exciton-phonon coupling the ω_k value corresponds to ZPL position of the k th exciton level. In the weak coupling limit ZPLs are slightly broadened due to bath-induced exciton relaxation but the ω_k value still corresponds to the ZPL position and coincides with the maximum of the absorption and emission of the k th state.

In the case of strong coupling with phonons (Equation 1) the ZPL position is $\omega_k - \lambda_{kkkk}$, *i.e.*, red-shifted with respect to the eigenvalues of a free-exciton Hamiltonian ω_k . The first moment of the absorption is at ω_k , whereas the first moment of FL is $\omega_k - 2\lambda_{kkkk}$. Static disorder induces random shifts of the eigenvalues ω_k . In their turn, the line-broadening function g_{kkkk} (*i.e.*, phonon-induced broadening) and reorganization energy λ_{kkkk} (together with the Stokes shift of the k th level, *i.e.*, $2\lambda_{kkkk}$) are also affected by the static disorder being proportional (see Equations 3 and 4) to a disorder-dependent $PR_k = \sum_n (c_n^k)^4$ (PR_k value is dependent on the specific realization of the static disorder through the wavefunction amplitudes c_n^k). It has been well established (Fidder, *et al.* 1991, Meier, *et al.*

1997, Novoderezhkin, *et al.* 1999) that an increase in static disorder (given by the fwhm of the Gaussian distribution from which the pigment site energy shifts are drawn) on the average increases the PR_k values for different realizations of the static disorder, thus increasing the effective dynamic disorder value, *i.e.*, the phonon induced broadening of the exciton states and reorganization shift. Furthermore, an increase in static disorder induces a larger spread of the PR_k values corresponding to different realizations, thus increasing the spread of the line-broadenings and reorganization shifts.

Thus, both the positions of the exciton levels (given by $\omega_k - \lambda_{kkkk}$) and the line widths (determined by g_{kkkk}) depend on a combined action of static and dynamic disorder. In particular, the experimentally measured distribution of the ZPL positions (as obtained from a hole-burning experiment for $k = 0$, or studied by a single-molecule technique) includes the disorder of the exciton eigenvalues ω_k , in combination with the variation of reorganization-induced shifts λ_{kkkk} . The amount of this additional reorganization-induced disorder increases in proportion to the exciton-phonon coupling strength λ_j and the amount of static disorder that makes the reorganization effects more pronounced in a more disordered system with larger site inhomogeneity.

In the case of the LH1 antenna or the B850 ring from LH2 the static disorder has its most prominent effect on the lowest exciton states, especially $k = 0$ (Novoderezhkin, *et al.* 1999, Novoderezhkin, *et al.* 1999, Novoderezhkin, *et al.* 2003), (and examples given below). Realizations of strong disorder produce more localized and more red-shifted states. The reorganization energy for these realizations is also larger, inducing a further red shift. Moreover, these red-shifted states feature a more pronounced phonon/vibrational wing (because the line-broadening function g_{kkkk} increases for localized states with bigger PR_k value). Thus, the character of the slow conformational changes of the complex significantly influences the effective coupling of the exciton states with the fast nuclear motions (given by Equations 4), producing different phonon-induced broadening and reorganization energy effects. Thus one can expect a red shift and broadening of the FL spectrum for conformations of the complex with broken symmetry that are associated with a large disorder of the site energies.

Complexes in a more symmetric configuration are expected to conform with the classical excitonic picture (no static disorder). The corresponding spectral profiles are not shifted and as will be shown later are broadened predominantly due to exciton relaxation.

These described spectral trends were observed in our study of FL fluctuations of single LH2 (Rutkauskas, *et al.* 2005, Rutkauskas, *et al.* 2004). Single complex FL spectra exhibited large red and blue shifts occurring on a second time scale that were accompanied by spectral broadening. These observations are interpreted on the basis of the proposed model.

Model of LH2 antenna

The LH2 spectral line shapes and their dynamics are determined by the coupling of electronic excitations to a manifold of nuclear modes (both fast and slow). The optical line shapes as observed both in conventional (Mukamel 1995) and in single-molecule

spectroscopy (Jung, *et al.* 2002) are defined by fast nuclear modes. Slow nuclear motions associated with conformational changes of the pigment-protein on a microsecond to second time scale are responsible for the change of realizations of static disorder. It is reasonable to suppose that the experimentally observed quasi-stable states of single LH2 FL spectral traces, characterized by different line shape and peak position, can be treated as different equilibrium positions of the nuclear coordinates, *i.e.*, different realizations of the static disorder (Dempster, *et al.* 2001, Jang and Silbey 2003). We hypothesize that transitions between these states occur due to thermal nuclear motion. We do not consider here the dynamics of such transitions but rather restrict ourselves to a modeling of FL line shapes for different realizations of the static disorder. Our model takes into account excitonic interactions within the B850 ring, the presence of static disorder of pigment site energies, and strong coupling of electronic excitations to phonons.

To construct a one-exciton Hamiltonian, the unperturbed transition energies of BChl 850(α) and BChl 850(β) were taken as 12275 and 12125 cm^{-1} , respectively. The energies of the $1\alpha1\beta$, $1\beta2\alpha$, $1\alpha2\alpha$, $1\beta2\beta$, and $1\alpha2\beta$ pigment-pigment interactions were taken to be 291, 273, -50, -36, and 12 cm^{-1} , respectively, according to (Sauer *et al.* 1996). The static disorder was described by uncorrelated perturbations of the transition energies randomly chosen from a Gaussian distribution with the fwhm of σ . Numerical diagonalization of the Hamiltonian (for each realization of the disorder) gives the energies of the exciton states ω_k and the wavefunction amplitudes c_n^k (participation of the n th site in the k th exciton state).

The absorption and FL line shapes are calculated using Equations 1-5. To reproduce the peak positions and the low-frequency wings of the absorption/FL spectra, it is not necessary to include the high-frequency part of the spectral density function (second term in Equation 5). Thus, we assume that the spectral density function $C(\omega)$ has the form of a single overdamped Brownian oscillator with coupling parameter $\lambda = \lambda_0$ and relaxation time $\tau = 1/\gamma_0$ (keeping just the first term in Equation 5). In our model λ and τ (as well as σ) are site-independent parameters adjusted from the fit of the bulk absorption and FL spectra. All experimental data presented below were acquired at RT and the simulation of the data was performed with the corresponding parameters.

RESULTS AND DISCUSSION

Experimental results are obtained by acquiring series of FL spectra of individual LH2 complexes. Figure 1 presents an average of single-molecule FL spectra over time and over particles as well as the distribution of the FL peak positions together with corresponding results of the modeling. The averaged FL profile has a maximum near 870 nm. Realizations with the FL peak near this wavelength occur with the highest probability. The data is reproduced with parameters $\sigma = 370 \text{ cm}^{-1}$, $\lambda = 390 \text{ cm}^{-1}$, and $\tau = 50 \text{ fs}$. Note that the absorption spectrum of the B850 ring of LH2 complex *in vivo* can be reproduced with the same σ and τ , and $\lambda = 220 \text{ cm}^{-1}$ (data not shown). Most probably, this difference in λ reflects the different strength of exciton-phonon coupling for immobilized and *in vivo*

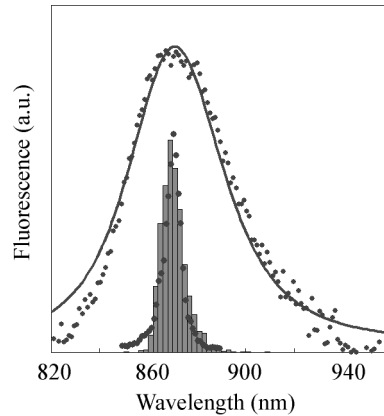


Figure 1. Experimental FL profile averaged in time and over particles (points) and calculated FL spectrum averaged over realizations of the static disorder (solid line). The histogram shows the distribution of peak positions of the experimental FL spectra (points) and the same distribution for the calculated FL spectra (bars).

complexes but is still within the acceptable range of the variation of the parameter values.

Single-molecule spectra of different complexes measured under the same experimental conditions are collected into groups with their peak wavelengths within narrow intervals. Figure 2 shows averages of experimental and calculated FL profile occurrences with the

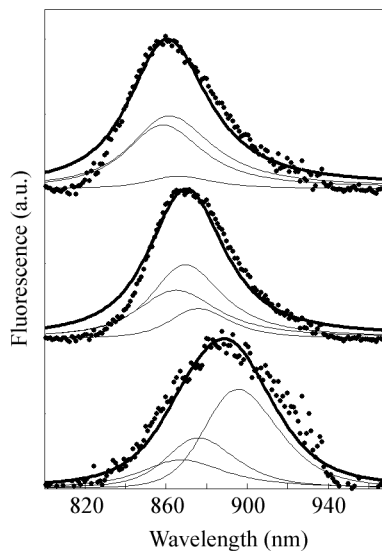


Figure 2. Experimental (points) and calculated (solid lines) FL profiles averaged over realizations with peak positions in the ranges 859-861 nm (top), 869-871 nm (middle), and 889-891 nm (bottom). The calculated emission spectra are shown together with the contributions from the three lowest exciton components (thin solid lines). Both measured and calculated spectra are normalized to unity. The value of uncorrelated diagonal disorder is 370 cm^{-1} .

peak positions within 859-861 nm, 869-871 nm, and 889-891 nm. Red-shifted single-molecule profiles on the average are significantly broadened and display a specific shape with a more pronounced short-wavelength wing. Spectra with intermediate and blue-shifted peak position feature regular FL asymmetry, *i.e.*, a more pronounced long-wavelength tail. Notice that the blue-shifted spectra are also broader than those with intermediate peak wavelength. All these spectral features are satisfactorily reproduced by our model.

Our modeling of the spectra shows that the line shapes associated with the various peak positions are determined by a specific exciton structure corresponding to specific realizations of static disorder. Figure 2 shows contributions of three lowest exciton components ($k = 0, \pm 1$) to the red-shifted, intermediate, and blue-shifted FL profiles (these components are averaged over realizations that result in the corresponding peak position). The contributions from the higher exciton states ($k = \pm 2$) can be neglected due to their small dipole strength and insignificant population (but they are still included in the calculation of the whole FL profiles). The three types of exciton structure shown in Figure 2 correspond to different degrees of delocalization of exciton states. To study this relationship in more detail we have calculated the PR_k values for all the realizations of static disorder (Figure 3) and separated them into groups corresponding to blue-shifted, intermediate, and red-shifted spectral profile peak positions (Figure 4).

Delocalization of the exciton states contributing to the steady-state FL can be characterized by the thermally averaged PR, $\langle PR \rangle$, defined as an average of PR_k values of the individual exciton states weighted with the steady-state populations of those states. $\langle PR \rangle$ values corresponding to the blue, intermediate and red-shifted FL positions shown in Figure 2 are 0.098, 0.118 and 0.245, respectively, reflecting the increasingly localized character of the exciton states contributing to the redder FL spectrum.

Participation ratio for different realizations of static disorder

Figure 3 shows the $PR_k = \sum_n (c_n^k)^4$ values for the 5 lowest exciton levels (*i.e.*, $k = 0, \pm 1, \pm 2$) of LH2 calculated for 2000 realizations of the disorder. Each point corresponds to the PR_k value of one exciton state for one realization of the static disorder as a function of the wavelength of the ZPL of this state (the position of ZPL is $\omega_k - \lambda_{kkkk}$ on the energy scale). Averaging of the PR values corresponding to exciton states with ZPLs within a narrow wavelength intervals results in a smooth PR curve well known for LH2/LH1 complexes, *i.e.*, almost constant in the middle of the long-wavelength absorption band with an increase on the red side (Alden, *et al.* 1997, Novoderezhkin, *et al.* 1999, Novoderezhkin, *et al.* 1999, Novoderezhkin, *et al.* 2003). Figure 4 shows the distributions of PR_k values for each of the exciton states taken from the 2000 realizations shown in Figure 3 corresponding to spectral profiles with peak wavelengths in the ranges 858-862 nm, 869-871 nm, and 887-894 nm. Note, that this is a statistical representation of data similar to Figure 2 although the intervals of blue- and red-shifted spectral profile maxima are wider in order to collect more occurrences.

The PR values of the exciton states corresponding to blue-shifted FL spectra are 0.085-

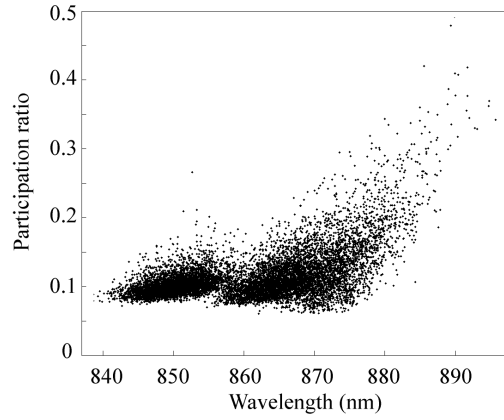


Figure 3. The PR_k values for the 5 lowest exciton levels (*i.e.*, $k=0, \pm 1, \pm 2$) calculated for 2000 realizations of the disorder. Each point shows the PR value for certain one-exciton state as a function of the wavelength of the ZPL of this state.

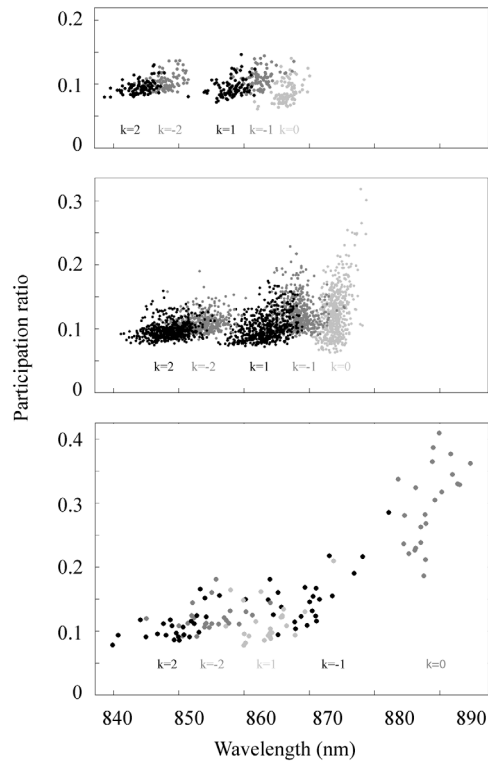


Figure 4. The PR values for realizations with the fluorescence peaks within 858-862 nm (top), 869-871 nm (middle), and 887-894 nm (bottom) taken from realizations shown in Figure 3. For each group of realizations the PR values for the 5 lowest exciton levels are marked by different grey tones. The position of each point on the wavelength-axis is given by the ZPL of the corresponding exciton state.

0.13 for the higher states ($k = \pm 1, \pm 2$) and 0.065-0.12 for the lowest one ($k = 0$) (Figure 4). These values are close to the homogeneous limit. That is, for a circular aggregate of N molecules $PR = 1/N$ for the lowest and $3/2N$ for the higher states in the absence of the static disorder. For LH2 with $N = 18$ this results in 0.056, and 0.083, respectively. So, we conclude that the exciton states that result from realizations of static disorder corresponding to blue-shifted spectra are not significantly destroyed by the disorder. As a result in this case the exciton structure is also not too different from that of the homogeneous ring, *i.e.*, most of the dipole strength is concentrated in two degenerate levels ($k = \pm 1$), whereas the lowest state ($k = 0$) is almost forbidden due to the symmetry of the ring. The RT emission originates mostly from the degenerate $k = \pm 1$ pair giving rise to a blue-shifted FL (Figure 2, top frame).

FL profiles with an intermediate peak position result from realizations of stronger static disorder (Figure 4, middle frame). This situation corresponds to an increase in the splitting between the exciton levels and a more localized character of the exciton states yielding PR_k values which have increased up to 0.15-0.20 for the $k = \pm 1$ and up to 0.30 for the lowest $k = 0$ state. This red-shifted and more localized $k = 0$ state also becomes more radiant borrowing some of the dipole strength from higher levels so its contribution to the FL profile becomes more significant (Figure 2, middle frame).

The bottom frame of Figure 4 illustrates PR_k values of exciton states corresponding to red-shifted FL profiles. In this case the exciton structure is very strongly perturbed by the disorder, which induces a large splitting between the energy levels, in particular, the splitting between the $k = \pm 1$ and the lowest $k = 0$ state is increased significantly (as compared with the blue-shifted and intermediate spectral profiles). Due to this large splitting between excitonic energy levels FL mostly originates from the lowest state, which is now strongly allowed and red-shifted. Its localized character ($PR = 0.2-0.4$) gives rise to an increased strength of the effective exciton-phonon coupling (proportional to the PR_k value). Such an increased coupling results in the broadening of the FL profile together with an additional red shift (Figure 2, bottom frame).

Relaxation-induced broadening

We have seen that an increase in the red shift (because of the low exciton eigenvalue and reorganization shift) is accompanied by enhanced exciton-phonon coupling in the exciton representation (Equation 4) which produces an increasingly larger broadening of the FL spectra. Another line-broadening factor that determines the width of the blue-shifted FL spectra is exciton relaxation. Typically due to predominant downhill relaxation the inverse lifetime increases for the higher levels. In our model $R_k = 16, 29, 44,$ and 57 ps^{-1} for the $k = 0, -1, 1, -2$ levels, respectively. The more pronounced relaxation broadening of the $k = \pm 1$ levels results in a larger width of the blue-shifted FL spectra (determined mostly by the $k = \pm 1$ emission). Note that in the absence of relaxation a blue shift would be always accompanied by a narrowing of the FL line because the $k = \pm 1$ levels are always narrower than the lowest one (for a disordered complex) due to their smaller PR values and, as a

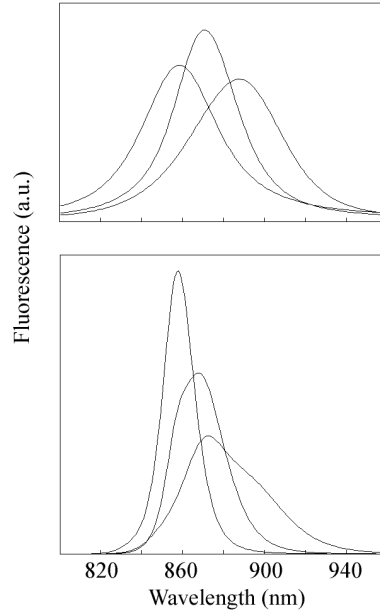


Figure 5. Top frame: calculated FL profiles averaged over realizations peaking near 860, 870, and 890 nm. The spectra are not normalized and shown in the same (arbitrary) units. Bottom frame: the FL profiles for the same realizations as in top frame (and in the same units), but calculated without taking into account the relaxation-induced broadening. Note that the reddest FL profile in this case has the opposite asymmetry and the peak position shifted from 890 to 873 nm.

result, a smaller value of the line-broadening function. Disregarding exciton relaxation it would be impossible to explain the observed broadening of the blue-shifted FL spectra (Figure 5).

Thus, we conclude that the blue-shifted FL line shape is determined by delocalized exciton states broadened due to fast exciton relaxation, whereas the broadening of the red-shifted FL profiles originates from a localized excitation dressed by phonons. Switching between these two limits is driven by slow nuclear motions.

Exciton wavefunctions in the site representation

Analysis of the PR_k values suggests a different degree of delocalization for each of the three spectral profiles shown in Figures 2. This can also be illustrated by a straightforward visualization of the corresponding exciton wavefunctions. As an example we selected one typical realization of the static disorder with a blue-shifted FL peak position at 858 nm, an intermediate one at 871 nm, and two red-shifted ones at 894 nm. The corresponding thermally averaged $\langle \text{PR} \rangle$ values are 0.087, 0.14, 0.25, and 0.35, corresponding to a delocalization over 11, 7, 4, and 3 pigment molecules, respectively. Figure 6 (left frames) shows the shifts of the transition energies of the sites from $n = 1$ to $n = 18$ for these realizations. For the same realizations we show the squared wavefunction amplitudes $(c_n^k)^2$ for $k = 0$, *i.e.*, the participation of the n th site in the lowest $k = 0$ exciton state (Figure 6,

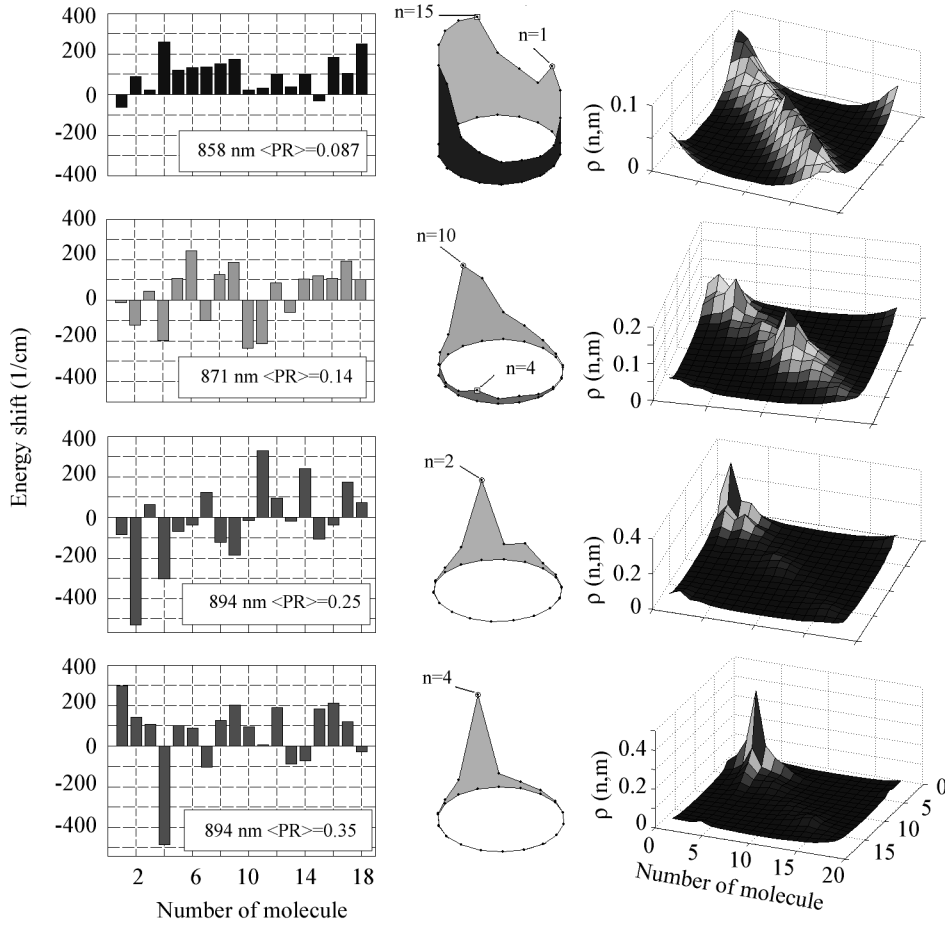


Figure 6. Site energies, exciton wavefunctions, and density matrices for the four different realizations of the disorder with the FL peaking at 858, 871, 894, and 894 nm and $\langle PR \rangle$ values of 0.087, 0.14, 0.25, and 0.35, respectively. Left column: the shifts of the transition energies (from the unperturbed values) of the sites from $n = 1$ to $n = 18$. Middle column: participation of the n th site in the lowest exciton state, given by the squared wavefunction amplitude $(c_n^k)^2$ for $k = 0$. The circle in the horizontal plane corresponds to the plane of the B850 ring, the points mark the positions of the sites from $n = 1$ to $n = 18$. For each case the site corresponding to maxima of the wavefunctions is indicated. Numbering of the sites is clockwise. Right column: steady-state density matrix in the site representation $\rho(n,m)$ at RT.

middle frames). To visualize the shapes of the exciton wavepacket (given by a superposition of the exciton wavefunctions) we calculate the density matrix in the site representation, *i.e.*, $\rho_{nm} = \sum_{kk'} \rho_{kk} c_n^k c_m^{k'}$. In the steady-state limit (after exciton relaxation) $\rho_{kk'} = \delta_{kk'} P_k$, where P_k is the Boltzmann distribution of the exciton populations. In Figure 6 (right frames) we show the steady-state density matrices at RT for the chosen realizations. The distribution in the diagonal direction, *i.e.*, ρ_{nn} shows the area of a non-coherent delocalization of the excitation. The width of the density matrix in the anti-diagonal direction gives the coherence length of the exciton (which is always less than the width of

the distribution in the diagonal direction).

The first, most delocalized exciton is characterized by relatively small shifts of the site energies, which are all less than the inter-pigment interaction energy ($M = 270\text{-}290\text{ cm}^{-1}$). Moreover these shifts have a partially correlated character, *i.e.*, the pigments $n = 5\text{-}9$ are almost uniformly blue-shifted by $100\text{-}150\text{ cm}^{-1}$, pigments $n = 10\text{-}14$ – by $30\text{-}100\text{ cm}^{-1}$, etc., so that in most cases the relative shift between neighboring pigments is much less than the interaction between them. This amount of disorder does not destroy significantly the unperturbed (delocalized) states. Thus, the lowest exciton state is delocalized over the whole ring, but due to disorder the distribution of the wavefunction amplitudes is not uniform (as it must be in the homogeneous limit). Although each of the individual wavefunctions is delocalized, their superposition at RT results in a more localized wavepacket. The density matrix displays a coherence length (fwhm in the anti-diagonal direction) of about 5-6 molecules due to thermal mixing of the states. The distribution along the diagonal direction shows no preferred localization site on the ring. So, for the dynamics we can expect the motion of a wavepacket delocalized over 5-6 pigments around the whole ring (as we will show below).

In the case of the second realization of static disorder (intermediate FL peak) the site energy shifts are not significantly larger, but they are less correlated. For example, there is a number of neighboring pigments (like $n = 4\text{-}5$, $6\text{-}7$, $9\text{-}10$, and $11\text{-}12$ in this example) with opposite signs of the shift. The difference in energies starts to exceed the coupling M between these sites. For these intermediate realizations the lowest exciton state becomes more localized. The corresponding wavefunction has a pronounced maximum at the red-most pigment, $n = 10$. In the steady-state limit the wavepacket (with a coherence length of about 3-4 molecules) is localized near the sites $n = 10$ or $n = 4$.

The third realization (red FL peak) is similar to the second one, but with larger and uncorrelated site shifts that exceed significantly the M value. The $k = 0$ wavefunction is localized with a main peak at $n = 2$ and a smaller one at $n = 4$. The wavepacket is localized near $n = 2$ with some small coherence between the $n = 2$ and $n = 4$ sites.

The fourth realization demonstrates yet another scenario of localization. In this case the major part of the pigments exhibits a correlated shift (as in the first realization), but one pigment ($n = 4$) has a very large red shift. This determines the almost complete localization of the $k = 0$ state on the $n = 4$ site and localization of the wavepacket on that same site without sizable coherence with other sites.

Coherent dynamics of the density matrix

The diagonal elements of the steady-state density matrix ρ_{nn} (Figure 6) display the probability of population of the n th site of the B850 ring. The population distribution is different for different realizations of the disorder. Thus, a small amount of disorder is characterized by a more or less uniform distribution, *i.e.*, the excitation (coherently delocalized over a few molecules) can be found on any part of the ring. On the other hand, a larger amount of disorder leads to predominant localization of the excitation on a group

of pigments, or even on a single site.

We wish to study the dynamics of the excitation for these limiting cases. To this end we calculate the time evolution of the density matrix for the same realizations as in Figure 6. We restrict to coherent dynamics, *i.e.*, we calculate the motion of the initially prepared wavepacket without taking into account the relaxation of the one-exciton populations and the decay of coherences between one-exciton states. The coherent dynamics in the eigenstate basis is calculated using the Liouville equation for $\rho_{kk'}(t)$ (without including a relaxation tensor), with the initial conditions corresponding to the coherent wavepacket $\rho_{kk'}(t=0) = (P_k P_{k'})^{1/2} \exp(i\phi_k - i\phi_{k'})$, with the steady-state populations $\rho_{kk}(t=0) = P_k$ and arbitrarily fixed phases ϕ_k of the exciton states (in principle such a wavepacket could be created using a specially shaped laser pulse). The time evolution of the density matrix in the site representation is $\rho_{nn}(t) = \sum_{kk'} \rho_{kk'}(t) c_n^k c_m^{k'}$. Note that the initial phases determine the location of the wavepacket within the ring at $t = 0$, but do not influence the character of its time evolution. The time evolution of the site populations $\rho_{nn}(t)$ during the 0-1.1 ps and 0-200 fs time intervals is shown in Figure 7 and 8, respectively.

For the first realization with insignificant disorder the wavepacket that is delocalized over 4-6 molecules moves in a wavelike fashion around the ring. The initially created

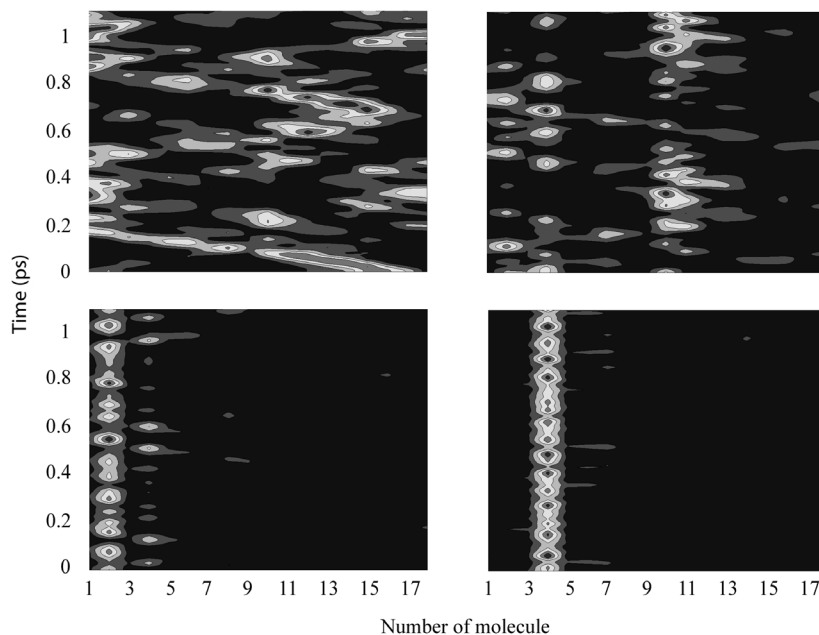


Figure 7. Coherent dynamics of the density matrix, *i.e.*, calculated without relaxation of populations and coherences. Initial ($t = 0$) populations correspond to a thermally equilibrated wavepacket at RT, initial coherences have arbitrary fixed phases. Diagonal elements of the density matrix in the site representation $\rho(n,n)$ are shown as a function of time for the same realizations as in Figures 6, *i.e.*, for realizations with the $\langle PR \rangle$ values of 0.087 (left top), 0.14 (right top), 0.25 (left bottom), and 0.35 (right bottom).

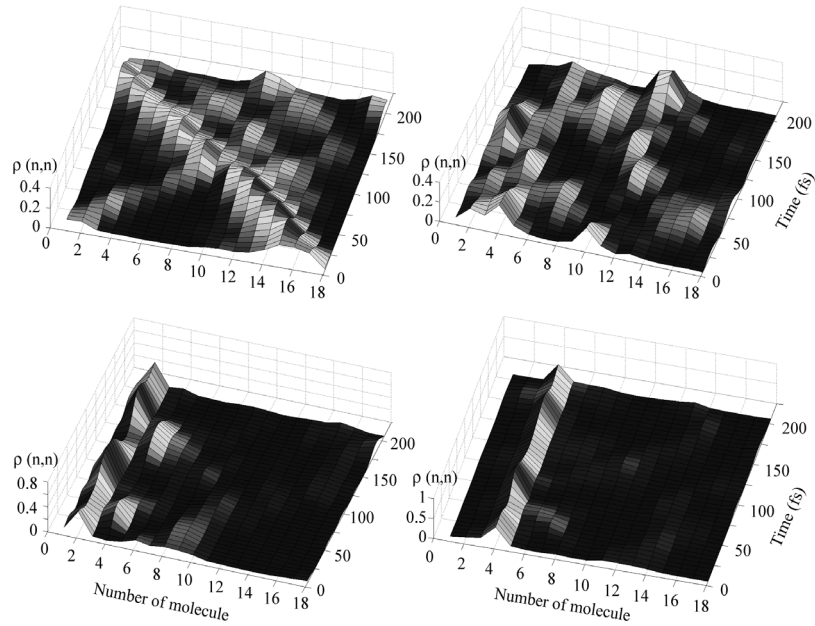


Figure 8. The same as in Figure 7, but for a time scale of 0-200 fs.

wavepacket has its maximum population amplitude at sites $n = 15-16$ (see Figure 9) with an additional smaller maximum at $n = 2$. The full passage of the main maximum around the whole ring occurs in 200 fs. Note that a second maximum moves in the opposite direction (this dynamics is clearly seen during first 100 fs, when the two maxima move towards each other). At 100 fs they meet, and after that the motion of the smaller maximum is hardly distinguishable. If we look at the dynamics on the 1 ps time scale it becomes clear that the wavelike motion is more pronounced during the first 200 fs (Figure 7). For larger delays the

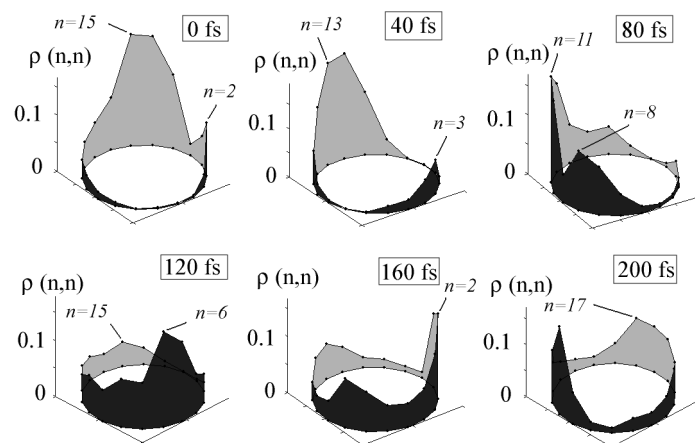


Figure 9. The shapes of the exciton wavepacket (distribution of diagonal elements of the density matrix $\rho(n,n)$ over N sites of the ring) at fixed delays for the 858 nm realization shown in Figures 6-8.

coherent dynamics looks more like the interference of the waves destroyed by their scattering on impurities. First of all it should be noticed that the dynamics of the coherences $\rho_{kk'}(t) = \rho_{kk'}(0)\exp(i\omega_k t - i\omega_{k'} t)$, induces increasingly large dephasing at large delays. Due to this additional maxima can appear at larger delays instead of a single main maximum at $t = 0$. Secondly, even without such dephasing, the distribution of the site populations $\rho_{nn}(t)$ may have a complicated form (with a lot of maxima) due to the disorder that destroys the shape of the exciton wavefunctions. As a result we obtain a complex time-dependent redistribution of the excitation density between many maxima instead of a perfect aberration-free motion of a single wave. But some wavelike features are still clearly distinguishable even at larger delays. Some maxima exhibit a well-pronounced motion around the ring (in both directions) with the same time constant (about 100 fs to pass over half of the ring).

For the second realization the excitation is delocalized over the sites $n = 2-4$ or $n = 10-13$. The calculated dynamics strongly resembles the hopping of the excitation from one group to the other with a time constant of about 350 fs. Thus, between 0 and 150 fs the excitation is on the $n = 2-4$ group, then from 150 to 500 fs the sites $n = 10-13$ are populated, between 500 and 850 fs the excitation is again on the $n = 2-4$ group. Within the $n = 2-4$ group there are oscillations between the sites $n = 2$ and $n = 4$ with a time constant of about 50 fs (corresponding to a jump from $n = 2$ to $n = 4$ or vice versa). Similar oscillations occur between the site $n = 10$ and sites $n = 11-13$. The wavelike motion observed for the first realization with small disorder is almost absent in this case, but it is possible to recognize some wavelike flow of excitation density from one group to another through the intermediate site $n = 7$. Due to the much stronger disorder the wavelike motion is destroyed by scattering on impurities, producing a lot of secondary waves moving in both directions. This results in a complicated non-uniform standing-wave pattern with oscillating populations of some sites (whereas other sites are almost not populated). Generally for a disordered system we always get a superposition of propagating waves and standing waves. For example, in the first realization besides the pronounced wavelike motion one can see some oscillations between the $n = 10-16$ and $n = 17-18-1-2-3$ group with the time constant (half of period) of 350 fs.

In an ensemble experiment the combination of the wave-like motion and the hopping-type dynamics with time constants of 100 and 350 fs should give rise to similar components in the anisotropy decay kinetics. This prediction is in surprisingly good agreement with the observed bi-exponential polarization decay with 100 and 400 fs components in FL up-conversion experiments for LH1 (Bradforth, *et al.* 1995) and the B850 ring of LH2 (Jimenez, *et al.* 1996).

In the third realization of static disorder the excitation stays on the $n = 2$ site with some hopping to the $n = 4$ site. But the average population of the $n = 4$ site remains relatively small.

For the fourth realization the excitation is completely localized at one site, *i.e.*, $n = 4$ without any migration to the other sites. But there is still some oscillatory modulation of the

$n = 4$ population due to small coherences between the $n = 4$ and neighboring sites.

All of these excitation dynamics scenarios are associated with specific realizations of the static disorder. Thus, in a single-molecule experiment we observe realizations corresponding to physically different limits of the excitation dynamics, *i.e.*, coherent wavelike motion of a delocalized exciton (with a 100 fs pass over half of the ring), hopping-type motion of the wavepacket (with 350 fs jumps between separated groups of 3-4 molecules), and self-trapping of an excitation that does not move from its localization site (Figures 7-9).

Disordered ring vs. elliptical deformations

Finally we wish to compare the model with uncorrelated energetic disorder (which enables us to explain the observed spectral fluctuations as shown in Figures 1 and 2) with alternative models that assume elliptical deformations of the ring producing a correlated shift of the site energies and pigment-pigment couplings.

First of all it should be noticed that the disordered model (with uncorrelated disorder of the site energies) requires relatively large disorder values in order to obtain the splitting between the main exciton components necessary to simulate the absorption spectrum. In our model with the uncorrelated disorder value of $\sigma = 370 \text{ cm}^{-1}$ the splitting between the $k = \pm 1$ energy levels is 40, 65, and 100 cm^{-1} for realizations with the FL peak at 860, 870, and 890 nm, respectively (Figure 2). The important feature is the increasingly bigger splitting between the $k = \pm 1$ levels and the intense $k = 0$ transition for more disordered realizations producing the specific shape of the red-shifted FL spectra.

The low-temperature polarized FL excitation spectra gave splitting values between the k

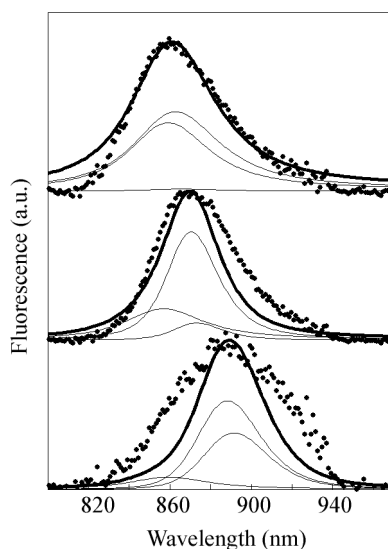


Figure 10. The same as in Figure 2, but for the model with elliptical deformation. The values of the correlated and random (uncorrelated) disorder of the site energies are 275 and 125 cm^{-1} , respectively.

= ± 1 levels distributed within the 50-175 cm^{-1} range with a maximum at 110 cm^{-1} (van Oijen, *et al.* 1999), which is larger than the 65 cm^{-1} value predicted by the disordered model. This anomalously large splitting was explained by supposing a modulation of the coupling strength associated with an elliptical deformation in combination with random (uncorrelated) disorder of about 125 cm^{-1} (Ketelaars, *et al.* 2001, Matsushita, *et al.* 2001, Mostovoy and Knoester 2000, van Oijen, *et al.* 1999). Generally the ellipticity can produce also a correlated shift of the site energies $\sim \sin(4\pi n/N)$ giving rise to a similar mixing of the $k = \pm 1$ levels (Jang and Silbey 2003) accompanied by an increase in the splitting between them.

We have applied this alternative model to our single-molecule data. We restrict ourselves to the case of the deformation-induced modulation of the site energies ΔE_n in combination of the reduced amount of random (uncorrelated) disorder of the site energies σ . We suppose that $\Delta E_n = \Delta E \sin(4\pi(n-n_0)/N)$, where ΔE is taken from a Gaussian distribution with the fwhm of σ_{corr} and with $\langle \Delta E \rangle = 0$. Generally the first moment $\langle \Delta E \rangle$ can be non-zero, but this does not change significantly the results discussed below. Since we do not consider the polarization of the emission, the n_0 value (that determines the principle axes of ellipses) is taken arbitrary. Generally, both the n_0 and ΔE values are fluctuating according to experimental observations (Bopp *et al.* 1999). With such a model the bulk absorption and averaged FL spectra can be explained by taking $\sigma_{\text{corr}} = 275 \text{ cm}^{-1}$ and $\sigma = 125 \text{ cm}^{-1}$ (instead of $\sigma_{\text{corr}} = 0$ and $\sigma = 370 \text{ cm}^{-1}$ in the disordered model). The averaged $k = \pm 1$ splitting is now increased up to 120 cm^{-1} . The emission profiles calculated for occurrences with different FL peak positions are shown in Figure 10.

Comparison of the disordered (Figure 2) and elliptical model (Figure 10) shows that in the latter case we have a larger $k = \pm 1$ splitting (due to ellipticity), but lower intensities of the lowest $k = 0$ level (due to lower values of uncorrelated disorder). Moreover, the disorder-induced red shift of the $k = 0$ transition (responsible for the broadened and specifically shaped red-shifted FL profiles in the disordered model) is absent in the elliptical model with the reduced disorder value.

In the elliptical model the blue-shifted (860 nm) emission originates from the B850 ring weakly perturbed both by random and correlated shifts of the site energies. In this case the $k = \pm 1$ levels are almost degenerate and contribute equally to the emission (Figure 10, top).

Realizations with a bigger elliptical deformation produce an increased splitting between the $k = \pm 1$ levels, so that the emission is determined mostly by the lower, $k = -1$ state giving FL profiles peaking at 870 nm (Figure 10, middle). Due to the anomalously big $k = \pm 1$ splitting the $k = 1$ level is only weakly populated, whereas the lowest $k = 0$ state is almost forbidden. Thus, the contribution of the $k = 1$ and $k = 0$ states to the emission is much lower (as compared with the disordered model), thus producing narrower FL profiles at 870 nm.

The $k = 0$ level becomes more intense for the red-shifted realizations, but its relative contribution is still not so much pronounced as in the disordered model (as well as its shift from the $k = -1$ level is not as large). Thus, the FL spectra peaking at 890 nm are

determined mostly by the $k = -1$ level with some contribution of the almost non-shifted $k = 0$ level. Such a configuration of the exciton levels makes it impossible to reproduce the broad experimental FL profile (Figure 10, bottom).

We conclude that the exciton structure predicted by the elliptical model considered here (which is in fact typical for all the models with elliptical deformations) is not consistent with the observed changes in FL spectra. The most serious contradiction between the disordered and elliptical model is connected with different predictions about the intensities and spectral positions of the $k = 0$ transition. Note in this respect that direct measurements (Monshouwer, *et al.* 1997) suggested that the $k = 0$ level is strongly superradiant in agreement with the disordered model.

CONCLUSIONS

We show that the model of the disordered ring allows a quantitative interpretation of the single-molecule spectroscopic data for LH2. The positions and spectral shapes of the main exciton components of the B850 ring are determined in this model by the disorder-induced shift of the exciton eigenvalues in combination with phonon-induced effects (*i.e.*, reorganization shift and broadening, that increase in proportion to the inverse delocalization length of the exciton state). Being dependent on the realization of the disorder, these factors produce different forms of the emission profile. In addition, different delocalization degrees and effective couplings to phonons determine different types of the excitation dynamics in these realizations. We demonstrate that experimentally observed quasi-stable conformational states are characterized by the excitation energy transfer regimes varying from a coherent wavelike motion of a delocalized exciton to a hopping-type motion of a wavepacket (with jumps between separated groups of 3-4 molecules) and self-trapping of a localized excitation.

The alternative models that assume elliptical deformations of the ring fail to explain the spectral shapes of the experimentally observed emission profiles corresponding to different FL peak positions.

REFERENCES

- Alden, R. G., Johnson, E., Nagarajan, V., Parson, W. W., Law, C. J., and Cogdell, R. J. (1997) Calculations of spectroscopic properties of the LH2 bacteriochlorophyll-protein antenna complex from *Rhodospseudomonas acidophila*. *J. Phys. Chem. B.* 101, 4667-4680.
- Bopp, M. A., Sytnik, A., Howard, T. D., Cogdell, R. J., and Hochstrasser, R. M. (1999) The dynamics of structural deformations of immobilized single light-harvesting complexes. *Proc. Natl. Acad. Sci. U.S.A.* 96, 11271-11276.
- Bradforth, S. E., Jimenez, R., van Mourik, F., van Grondelle, R., and Fleming, G. R. (1995) Excitation transfer in the core light-harvesting complex (LH1) of *Rhodobacter sphaeroides*: an ultrafast fluorescence depolarization and annihilation study. *J. Phys. Chem.* 99, 16179-16191.
- Dahlbom, M., Pullerits, T., Mukamel, S., and Sundström, V. (2001) Exciton delocalization in the B850

- light-harvesting complex: comparison of different measures. *J. Phys. Chem. B.* 105, 5515-5524.
- Damjanovic, A., Kosztin, I., Kleinekathoefer, U., and Schulten, K. (2002) Excitons in a photosynthetic light-harvesting system: a combined molecular dynamics, quantum chemistry, and polaron model study. *Phys. Rev. (E)*. 65, 031919.
- Dempster, S. E., Jang, S. J., and Silbey, R. J. (2001) Single molecule spectroscopy of disordered circular aggregates: a perturbation analysis. *J. Chem. Phys.* 114, 10015-10023.
- Fidder, H., Knoester, J., and Wiersma, D. A. (1991) Optical properties of disordered molecular aggregates – a numerical study. *J. Chem. Phys.* 95, 7880-7890.
- Hofmann, C., Aartsma, T. J., Michel, H., and Köhler, J. (2003) Direct observation of tiers in the energy landscape of a chromoprotein: a single-molecule study. *Proc. Natl. Acad. Sci. U.S.A.* 100, 15534-15538.
- Hu, X. C., Ritz, T., Damjanovic, A., Autenrieth, F., and Schulten, K. (2002) Photosynthetic apparatus of purple bacteria. *Q. Rev. Biophys.* 35, 1-62.
- Yang, M., and Fleming, G. R. (2002) Influence of phonons on exciton transfer dynamics: comparison of the Redfield, Förster, and modified Redfield equations. *Chem. Phys.* 275, 355-372.
- Jang, S., and Silbey, R. J. (2003) Single complex line shapes of the B850 band of LH2. *J. Chem. Phys.* 118, 9324-9336.
- Jimenez, R., Dikshit, S. N., Bradforth, S. E., and Fleming, G. R. (1996) Electronic excitation transfer in the LH2 complex of *Rhodobacter sphaeroides*. *J. Phys. Chem.* 100, 6825-6834.
- Jung, Y., Barkai, E., and Silbey, R. J. (2002) Current status of single-molecule spectroscopy: theoretical aspects. *J. Chem. Phys.* 117, 10980-10995.
- Ketelaars, M., van Oijen, A. M., Matsushita, M., Köhler, J., Schmidt, J., and Aartsma, T. J. (2001) Spectroscopy on the B850 band of individual light-harvesting 2 complexes of *Rhodospseudomonas acidophila* I. Experiments and Monte Carlo simulations. *Biophys. J.* 80, 1591-1603.
- Matsushita, M., Ketelaars, M., van Oijen, A. M., Köhler, J., Aartsma, T. J., and Schmidt, J. (2001) Spectroscopy on the B850 band of individual light-harvesting 2 complexes of *Rhodospseudomonas acidophila* II. Exciton states of an elliptically deformed ring aggregate. *Biophys. J.* 80, 1604-1614.
- McDermott, G., Prince, S. M., Freer, A. A., Hawthornthwaite, A. M., Papiz, M. Z., Cogdell, R. J., and Isaacs, N. W. (1995) Crystal structure of an integral membrane light-harvesting complex from photosynthetic bacteria. *Nature.* 374, 517-521.
- Meier, T., Chernyak, V., and Mukamel, S. (1997) Multiple exciton coherence sizes in photosynthetic antenna complexes viewed by pump-probe spectroscopy. *J. Phys. Chem. B.* 101, 7332-7342.
- Meier, T., Zhao, Y., Chernyak, V., and Mukamel, S. (1997) Polarons, localization, and excitonic coherence in superradiance of biological antenna complexes. *J. Chem. Phys.* 107, 3876-3893.
- Monshouwer, R., Abrahamsson, M., van Mourik, F., and van Grondelle, R. (1997) Superradiance and exciton delocalization in bacterial photosynthetic light-harvesting systems. *J. Phys. Chem. B.* 101, 7241-7248.
- Mostovoy, M. V., and Knoester, J. (2000) Statistics of optical spectra from single-ring aggregates and its application to LH2. *J. Phys. Chem. B.* 104, 12355-12364.
- Mukamel, S. (1995) Principles of Nonlinear Optical Spectroscopy, Oxford University Press, New York.
- Novoderezhkin, V., Monshouwer, R., and van Grondelle, R. (1999) Disordered exciton model for the core light-harvesting antenna of *Rhodospseudomonas viridis*. *Biophys. J.* 77, 666-681.
- Novoderezhkin, V., Monshouwer, R., and van Grondelle, R. (1999) Exciton (de)localization in the

- LH2 antenna of *Rhodobacter sphaeroides* as revealed by relative difference absorption measurements of the LH2 antenna and the B820 subunit. *J. Phys. Chem. B.* 103, 10540-10548.
- Novoderezhkin, V., Wendling, M., and van Grondelle, R. (2003) Intra- and interband transfers in the B800-B850 antenna of *Rhodospirillum rubrum*: Redfield theory modeling of polarized pump-probe kinetics. *J. Phys. Chem. B.* 107, 11534-11548.
- Novoderezhkin, V. I., Andriyevskaya, E. G., Dekker, J. P., and van Grondelle, R. (2005) Pathways and timescales of primary charge separation in the photosystem II reaction center as revealed by a simultaneous fit of time-resolved fluorescence and transient absorption. *Biophys. J.* 89.
- Novoderezhkin, V. I., Palacios, M. A., van Amerongen, H., and van Grondelle, R. (2004) Energy-transfer dynamics in the LHCII complex of higher plants: modified Redfield approach. *J. Phys. Chem. B.* 108, 10363-10375.
- Novoderezhkin, V. I., Palacios, M. A., van Amerongen, H., and van Grondelle, R. (2005) Excitation dynamics in the LHCII complex of higher plants: modeling based on the 2.72 angstrom crystal structure. *J. Phys. Chem. B.* 109, 10493-10504.
- Ohta, K., Yang, M., and Fleming, G. R. (2001) Ultrafast exciton dynamics of J-aggregates in room temperature solution studied by third-order nonlinear optical spectroscopy and numerical simulation based on exciton theory. *J. Chem. Phys.* 115, 7609-7621.
- Papiz, M. Z., Prince, S. M., Howard, T., Cogdell, R. J., and Isaacs, N. W. (2003) The structure and thermal motion of the B800-850 LH2 complex from *Rps. acidophila* at 2.0 Å over-circle resolution and 100 K: new structural features and functionally relevant motions. *J. Mol. Biol.* 326, 1523-1538.
- Peterman, E. J. G., Pullerits, T., van Grondelle, R., and van Amerongen, H. (1997) Electron-phonon coupling and vibronic fine structure of light-harvesting complex II of green plants: temperature dependent absorption and high-resolution fluorescence spectroscopy. *J. Phys. Chem. B.* 101, 4448-4457.
- Pieper, J., Voigt, J., and Small, G. J. (1999) Chlorophyll a Franck-Condon factors and excitation energy transfer. *J. Phys. Chem. B.* 103, 2319-2322.
- Raszewski, G., Saenger, W., and Renger, T. (2005) Theory of optical spectra of photosystem II reaction centers: location of the triplet state and the identity of the primary electron donor. *Biophys. J.* 88, 986-998.
- Renger, T., and Marcus, R. A. (2002) Photophysical properties of PS-2 reaction centers and a discrepancy in exciton relaxation times. *J. Phys. Chem. B.* 106, 1809-1819.
- Rutkauskas, D., Novoderezhkin, V., Cogdell, R. J., and van Grondelle, R. (2005) Fluorescence spectroscopy of conformational changes of single LH2 complexes. *Biophys. J.* 88, 422-435.
- Rutkauskas, D., Novoderezhkin, V., Cogdell, R. J., and van Grondelle, R. (2004) Fluorescence spectral fluctuations of single LH2 complexes from *Rhodospseudomonas acidophila* strain 10050. *Biochemistry.* 43, 4431-4438.
- Sauer, K., Cogdell, R. J., Prince, S. M., Freer, A., Isaacs, N. W., and Scheer, H. (1996) Structure-based calculations of the optical spectra of the LH2 bacteriochlorophyll-protein complex from *Rhodospseudomonas acidophila*. *Photochem. Photobiol.* 64, 564-576.
- Scheuring, S., Reiss-Husson, F., Engel, A., Rigaud, J. L., and Ranck, J. L. (2001) High-resolution AFM topographs of *Rubrivivax gelatinosus* light-harvesting complex LH2. *EMBO J.* 20, 3029-3035.
- Sundström, V., Pullerits, T., and van Grondelle, R. (1999) Photosynthetic light-harvesting: reconciling dynamics and structure of purple bacterial LH2 reveals function of photosynthetic unit. *J. Phys. Chem. B.* 103, 2327-2346.
- van Grondelle, R., Dekker, J. P., Gillbro, T., and Sundström, V. (1994) Energy-transfer and trapping

- in photosynthesis. *Biochim. Biophys. Acta.* 1187, 1-65.
- van Grondelle, R., and Novoderezhkin, V. (2001) Dynamics of excitation energy transfer in the LH1 and LH2 light-harvesting complexes of photosynthetic bacteria. *Biochemistry.* 40, 15057-15068.
- van Oijen, A. M., Ketelaars, M., Köhler, J., Aartsma, T. J., and Schmidt, J. (1999) Unraveling the electronic structure of individual photosynthetic pigment-protein complexes. *Science.* 285, 400-402.
- Wendling, M., Przyjalowski, M. A., Gullen, D., Vulto, S. I. E., Aartsma, T. J., van Grondelle, R., and van Amerongen, H. (2002) The quantitative relationship between structure and polarized spectroscopy in the FMO complex of *Prosthecochloris aestuarii*: refining experiments and simulations. *Photosynth. Res.* 71, 99-123.
- Zhang, W. M., Meier, T., Chernyak, V., and Mukamel, S. (1998) Exciton-migration and three-pulse femtosecond optical spectroscopies of photosynthetic antenna complexes. *J. Chem. Phys.* 108, 7763-7774.

Comparative study of spectral flexibilities of bacterial light-harvesting complexes: structural implications

Danielis Rutkauskas, John Olsen, Andrew Gall, Richard J. Cogdell, C. Neil Hunter, and Rienk van Grondelle

ABSTRACT

This paper presents a comparative study of the frequencies of spectral jumping of individual light-harvesting complexes of six different types: LH2 of *Rhodospseudomonas acidophila*, *Rhodobacter sphaeroides*, *Rhodospirillum rubrum*, LH1 of *Rhodobacter sphaeroides*, and two “domain swap mutants” of LH2 of *Rhodobacter sphaeroides*: PACLH1 and PACLH2mol, in which the α -polypeptide C-terminus is exchanged with the corresponding sequence from LH1 of *Rhodobacter sphaeroides* or LH2 of *Rhodospirillum rubrum*, respectively (Olsen, *et al.* 2003). The quasi-stable states of fluorescence peak wavelength that were previously observed for the LH2 of *Rhodospseudomonas acidophila* were confirmed for other species. We also observed occurrences of extremely blue-shifted spectra, which were associated with reversible bleaching of one of the chromophore rings. Different jumping behaviour is observed for single complexes of different types investigated with the same equivalent excitation intensity. The differences in spectral diffusion is associated with subtle differences of the binding pocket of B850 pigments and the structural flexibility of the different types of complexes.

INTRODUCTION

In photosynthesis, bacterial light-harvesting pigment-protein complexes capture solar light thereby initiating a complicated chain of reactions leading to the conservation of energy in form of stable chemical potential (van Grondelle, *et al.* 1994). The discovery of high-resolution crystallographic structures of two peripheral light-harvesting complexes (LHCs) of type 2 (LH2) from the purple bacteria *Rhodospseudomonas (Rps.) acidophila* and *Rhodospirillum (Rs.) molischianum* (Koepeke, *et al.* 1996, McDermott, *et al.* 1995, Papiz, *et al.* 2003) has put the previously available biochemical and physical information into a proper structural perspective and, consequently, has resulted in a better physical understanding of the photosynthetic light-harvesting mechanism (Cogdell, *et al.* 1996, Hu, *et al.* 2002, Robert, *et al.* 2003, Sundström, *et al.* 1999, Novoderezhkin and van Grondelle submitted to the PCCP). The LH2 of *Rps. acidophila* is a highly symmetric ring of nine protein-pigment subunits, each containing two α helical transmembrane polypeptides: the α -polypeptide on the inner and the β -polypeptide on the outer side of the ring. Close to the C-terminal end of these transmembrane helices a highly conserved His residue forms a ligand to a bacteriochlorophyll *a* (BChl *a*) molecule, resulting in a ring of 18 tightly coupled BChls *a* with a center-to-center distances of slightly less than 1 nm between neighboring pigments. This ring is responsible for the intense absorption of LH2 at around 850 nm (B850 ring). A second ring of nine weakly interacting BChls *a* is located closer to the N-terminus of the polypeptides and is largely responsible for the absorption around 800 nm (B800 ring). The LH2 of *Rs. molischianum* exhibits a similar structure overall with two pigment rings in a protein scaffold similar to that of LH2 of *Rps. acidophila*, but it has eightfold symmetry, and a somewhat different pigment arrangement particularly with respect to the B800 BChls *a*. Although there are no crystal structures of either LH2 or LH1 of *Rhodobacter (Rb.) sphaeroides*, an accurate model of a monomeric LH1 of *Rb. sphaeroides* (without PufX) has been constructed (Fotiadis, *et al.* 2004) based upon the NMR structure of the β -polypeptide (Conroy, *et al.* 2000), the low-resolution projection map of LH1 of *Rs. rubrum* (Karrasch, *et al.* 1995), and the structure of the LH2 of *Rs. molischianum* which shares many protein motifs in common with LH1. The homology of the LH2 of *Rb. sphaeroides* to that of *Rps. acidophila* in the light of the cryo-EM structural information (Walz, *et al.* 1998) allowed to use the atomic structure of the latter to model the interactions of the polypeptides with the BChl *a* pigments.

Abundant theoretical and experimental effort has resulted in a detailed model of electronic and energy transfer properties of LHCs (Alden, *et al.* 1997, Hu, *et al.* 1997, Novoderezhkin, *et al.* 1999, Novoderezhkin, *et al.* 2003, Scholes and Fleming 2000, van Grondelle and Novoderezhkin 2001, Wu, *et al.* 1997). The two basic features of this model are the excitonic coupling between pigments and the static disorder of the pigment electronic transition energies. Energetic disorder arises from the fact that a protein is intrinsically a disordered system occurring in a number of conformational substates. As a consequence the electronic transition energies of the different sites are not identical due to

the interaction of each chromophore with the surrounding protein.

At physiological and even at cryogenic temperatures a protein is not a rigid entity; it moves in its conformational landscape probing different substates. This was observed in low temperature single-molecule experiments on LH2, where the spectral diffusion of the B800 band was attributed to structural alterations (van Oijen, *et al.* 2000). In later work, spectral fluctuations of varying magnitude occurring on different time scales were associated with the hierarchical structure of protein conformational landscape (Hofmann, *et al.* 2003). We have observed changes of the realization of energetic disorder in single-molecule fluorescence (FL) experiments on LH2 of *Rps. acidophila* manifested by spectral changes on the time scale of a second. Calculations, based on the disordered exciton model using the modified Redfield theory to describe exciton relaxation, related these changes to conformational changes of the pigment-protein on a phenomenological level without considering the underlying microscopic detail (Rutkauskas, *et al.* 2004).

Although such an analysis adequately describes the electronic changes of the system, the related microscopic structural alterations are also of interest. It has been suggested that for some proteins, for example, myoglobin (Frauenfelder, *et al.* 1989), conformational changes may be functionally important. The functional role of structural changes in LH2 is open to speculation at this time; one possibility is that the photosynthetic system must be dynamically reorganized in a densely crowded membrane to maintain close ring-to-ring contact. In this work we investigate the possible structural changes by monitoring the FL spectral evolution of individual complexes. The microscopic parameters of protein-pigment interaction, such as hydrogen bonding (H-bonding) between chromophores and the protein, allow us to establish a connection between the observable spectral and structural changes.

Although a large part of the red shift of the B850 ring absorption relative to that of a monomeric BChl *a* is due to excitonic interaction between neighbouring BChls *a*, it has been demonstrated that an almost equally significant contribution to this spectral shift originates from protein-pigment interactions (Cogdell, *et al.* 2002, Robert, *et al.* 2003). Even in the absence of precise structural information, evidence of the role of the protein in chromophore absorption was suggested by comparison of polypeptide sequences of LH2 from different species (Zuber and Brunisholz 1991). In LH2s absorbing at 850 nm the primary sequence of the α -polypeptide contains a recurring motif of either Tyr-Trp or Tyr-Tyr residues at positions 43 and 44 (or +13 and +14 counting from the conserved His residue). In a natural variant of LH2 of *Rps. acidophila* absorbing at 820 nm, these two residues are Phe-Leu, whilst the rest of the sequence is very similar. This implied that these conserved residues might be spectroscopically significant. Replacement of either α Tyr+13 or α Tyr+14 with Phe and Leu, respectively, in the LH2 of *Rb. sphaeroides* caused a progressive blue shifting of the absorption (Fowler, *et al.* 1992, Fowler, *et al.* 1994), and this was associated with the disruption of H-bonds to acetyl carbonyl groups of the B850 BChls *a*. Similar factors were found for the other species based on sequence homology (Zuber and Brunisholz 1991) and available structures and models (Hu and Schulten 1998, Koepke, *et al.*

1996, McDermott, *et al.* 1995, Papiz, *et al.* 2003). Summarizing, the following residues form H-bonds to acetyl carbonyl groups of BChls *a* in the B850 (or B870 in case of LH1) ring: LH2 *Rps. acidophila* α Tyr+13(43) and α Trp+14(44), LH2 *Rb. sphaeroides* α Tyr+13(44) and α Tyr+14(45), LH2 *Rs. molischianum* α Trp+11(45) and β Trp+9(44), and LH1 of *Rb. sphaeroides* α Trp+11(43) and β Trp+9(48). It is noteworthy that in the LH2 of *Rps. acidophila* and *Rb. sphaeroides*, the α -polypeptide donates one H-bond to the acetyl carbonyl of BChl *a* in the same dimeric subunit and a second one to the BChl *a* in the adjacent subunit whereas in the LH2 *Rs. molischianum* and LH1 of *Rb. sphaeroides* both H-bonds are intra-subunit.

Other factors of the pigment interaction with its protein environment that might have an impact on the pigment site energy are the rotation of the acetyl group from the molecular plane (Gudowskanowak, *et al.* 1990, Hanson, *et al.* 1987), a deformation of the porphyrin ring (Gudowskanowak, *et al.* 1990), its close proximity to point charges (Eccles and Honig 1983, Hanson, *et al.* 1987), the ligation state of the central Mg²⁺ ion (Hanson, *et al.* 1987).

The aforementioned protein-pigment interaction modes connect the microscopic structural detail to the electronic and associated spectroscopic properties of the complex. Changes of these interactions caused by structural fluctuations are associated with the observed temporal evolution of the FL spectrum. Here we study jumps in the emission spectrum upon continuous illumination for different kinds of LHCs. The investigated proteins exhibit a high sequence homology in general but also subtle differences in their B850 pigment binding pocket. We discuss the observed variation of the frequency and size of spectral jumps (spectral flexibility) with the reference to structural diversity of the complexes.

MATERIALS AND METHODS

LH2 complexes of *Rps. acidophila* 10050 and *Rs. molischianum* DSM120 were grown anaerobically at 30° C in Pfenning's medium (Pfenning 1969) and modified *Rhodospirillaceae* medium (Evans, *et al.* 1990), respectively. Cells were harvested by centrifugation. After rupturing the cells in a French press, photosynthetic membranes were obtained by centrifugation. The membranes were solubilized using N,N-dimethyldodecylamine-N-oxide (LDAO), and the LH2 proteins were purified as described previously (Olsen, *et al.* 2003).

LH2 complexes of *Rb. sphaeroides* and domain swap mutants PACLH1 and PACLH2mol were purified as in (Olsen, *et al.* 2003) in the DD13 deletion strain.

LH1 membranes were purified according to (Olsen, *et al.* 1994). The membranes were diluted with a buffer of 1 mM Tris (pH 7.5) and 1 mM EDTA to less than 5% of sucrose by volume and concentrated by centrifugation for 4 hours at 40 krpm in a Beckman Ti 45 rotor. The membrane pellet was resuspended in ~ 1 ml of buffer of 20 mM HEPES (pH 8). Approximately 500 units of resuspended membranes with OD = 875 were solubilised with 4% β -DDM, in buffer of 20 mM HEPES (pH 8) and NaCl to a final concentration of 155 mM in 10 ml total volume. The β -DDM was added drip-wise to the resuspended membranes with gentle stirring and left to solubilise for 30 minutes with stirring at 4° C.

The solubilised membranes were centrifuged at 48 krpm for 1 hour in a Beckman Ti70.1 rotor to remove any unsolubilised material. The solubilised membranes were then loaded onto a pre-equilibrated DEAE Sepharose column (155 mM NaCl, 20 mM HEPES (pH 8) and 0.03% β -DDM), 15 ml bed volume, and washed for 90 minutes at 155 mM NaCl concentration and then at 170 mM NaCl for a further 90 minutes. The purified complexes were then eluted using a 170-400 mM NaCl salt gradient over 60 minutes and 4 ml fractions collected for analysis. The purest fractions, as ascertained by the 875:280 nm absorbance ratio, were used in a final purification step on a Superose 200 size exclusion column pre-equilibrated to 155 mM NaCl, 20 mM HEPES (pH 8) and 0.03% β -DDM. The fraction at the peak of the elution profile was used for a single-molecule spectroscopy.

Stock solutions of all samples were divided into small aliquots and kept at -80° C until thawed and were used only once, thus avoiding repetitive freezing and thawing. For the actual measurement the samples of LH2 of *Rps. acidophila*, *Rb. sphaeroides*, and *R. molischanum* were diluted with the buffer of 20 mM Tris (pH 8.0) and 0.1% LDAO. The mutants and LH1 of *Rb. sphaeroides* were diluted in a buffer containing 1% of n-octyl- β -D-glucopyranoside (β -OG) without buffer exchange. All the samples were flushed and kept in the deoxygenated buffer, the same as the one used for dilution. The oxygen in the buffers used for flushing was removed by means of a three component oxygen scavenger: 100-times concentrated water stock solutions containing 20 mg/ml of glucose oxidase and 3.5 mg/ml of catalase were kept at -80° C before use. For deoxygenation 1 ml of stock solution of each component together with 750 mg of glucose were added to 40 ml of buffer thus fully removing dissolved oxygen. Deoxygenated buffer was kept under N_2 atmosphere prior to flushing. All the measurements were conducted at 5° C to prolong the survival time of less stable species.

Isolated LH2 and LH1 complexes were immobilized on a standard microscope coverslip as described previously (Rutkauskas, *et al.* 2005). The confocal setup utilized to acquire sequences of single-molecule FL spectra was based on a commercial biological microscope described earlier (Rutkauskas, *et al.* 2004). This setup has the option of 594 nm excitation with a constant power and random polarization He-Ne laser (Melles Griot, 05SYR810-230). With this wavelength, the LHCs were excited in their Q_x absorption band allowing the use of the longpass glass filter RG715 (Edmund Optics Ltd, 46065) with transmission extended further to the blue as compared to the previously utilized broadband interference filter for 800 nm excitation. The effect of the objective achromatism on the excitation and signal collection efficiency was compensated for by decollimating the 594 nm beam before the objective.

RESULTS

In earlier work (Rutkauskas, *et al.* 2005, Rutkauskas, *et al.* 2004) we obtained FL time series of spectra for LH2 of *Rps. acidophila* with different excitation intensities at 800 nm. A significant fraction of the complexes evolved between distinctly different and relatively

constant quasi-stable levels of the spectral FL peak wavelength (FLP), and the frequency and size of spectral jumps increased with the excitation intensity. We also assessed the changes of the FL spectral line shape associated with these spectral jumps. The goal of the present work is to compare the spectral flexibilities for a set of different species and to associate the observed differences with variations in the molecular structure. To do so we need consistent datasets: different species were measured at the same temperature of 5° C, upon 594 nm excitation, using a level of absorbed energy equivalent to 2 μ W of 800 nm excitation for LH2 of *Rps. acidophila*, which is an intermediate level of excitation intensity compared with the range we probed previously (Rutkauskas, *et al.* 2005, Rutkauskas, *et al.* 2004). Higher excitation intensities at 594 nm were not feasible due to the increased FL background (see below). The corresponding intensities were calculated from the known absorption extinction coefficients (Alden, *et al.* 1997, Sturgis, *et al.* 1988) and the bulk absorption spectra. The following LHCs were investigated: LH2 of *Rps. acidophila*, *Rb. sphaeroides*, *Rs. molischianum*, and LH1 of *Rb. sphaeroides*. We obtained 240 spectra for about 200 molecules of each species. Exciting at 594 nm instead of 800 nm allowed for the extension of the detection to the blue, since a more blue-shifted emission long-pass filter could be used. In particular this helped the investigation of the changes of the FL profile shape (Rutkauskas *et al.*, submitted manuscript). Furthermore, the use of 594 nm excitation enabled us to detect the occurrence of extreme blue spectral jumping and to draw conclusions as to which species are capable of undergoing such drastic transformation.

A second dataset with 800 nm excitation was obtained to verify the reproducibility of the relative extent of spectral jumping between different species. The excitation intensity for each type of LHC was again adjusted from the known absorption extinction coefficients and the bulk absorption spectra to be equivalent to 2 μ W of 800 nm for LH2 of *Rps. acidophila*. The difference in the size of the focal area for the two wavelengths was not taken into account. Thus, a direct comparison of the two datasets must be done with caution, although the relation between different species within a single dataset can in principle be compared with that for a different excitation wavelength. In addition to the four species for which we obtained spectral traces at 594 nm excitation, we measured the domain swap mutants of *Rb. sphaeroides* LH2 – PACLH1 and PACLH2mol using only 800 nm excitation light. These mutants have the C-terminal part of the α -polypeptide altered from that of the wild type (WT) to the same sequence of LH1 of *Rb. sphaeroides* and LH2 of *Rs. molischianum*, respectively (Olsen, *et al.* 2003), which has impaired the FL efficiency. It was not possible to investigate these mutants with 594 nm excitation, since at this wavelength there was significant background FL originating from the glass coverslip in the spectral region of interest which could not be removed by filtering. For the systems other than these mutants the signal-to-noise ratio (S/N) was sufficient to analyze the FL images and obtain the coordinates of single particles while the FL spectra were corrected by subtracting the background spectrum measured on an area of the coverslip free of fluorescent complexes. However, for 800 nm excitation the background is virtually limited to the dark current of the avalanche photo diode (APD) and the readout noise of charge-coupled device (CCD)

camera allowing the accumulation of data also from species with a relatively low FL efficiency.

Quasi-stable FLP levels for different species

Recently we made a rather surprising observation that the FLP of a single LH2 of *Rps. acidophila*, of a significant fraction of the complexes measured, evolved through a number of quasi-stable levels (Rutkauskas, *et al.* 2005, Rutkauskas, *et al.* 2004). This led us to question whether this behaviour is characteristic for this particular species or if it is a property of pigment-protein complexes in general. To distinguish such quasi-stable levels we relied on a qualitative visual assessment that the variation of the averages of such levels was significantly larger than the fluctuations within the levels. Although less pronounced as in the LH2 of *Rps. acidophila* the spectra of the other species also showed quasi-stable levels of FLP, which often interchanged without intervening non-radiative periods: examples of spectral traces are shown in Figure 1. Depending on the excitation wavelength (594 or 800 nm) for LH2 of *Rps. acidophila* between 3 and 10%, respectively, of the measured complexes exhibited quasi-stable levels of FLP. The corresponding figure for LH2 of *Rb. sphaeroides* was found to be about 11%. The domain swap mutant of LH2 of *Rb. sphaeroides*, PACLH1, featured quasi-stable behaviour in 9% of the cases, while for PACLH2mol this was about 8%. It is also noteworthy that for the two domain swap mutants the spectral shift that

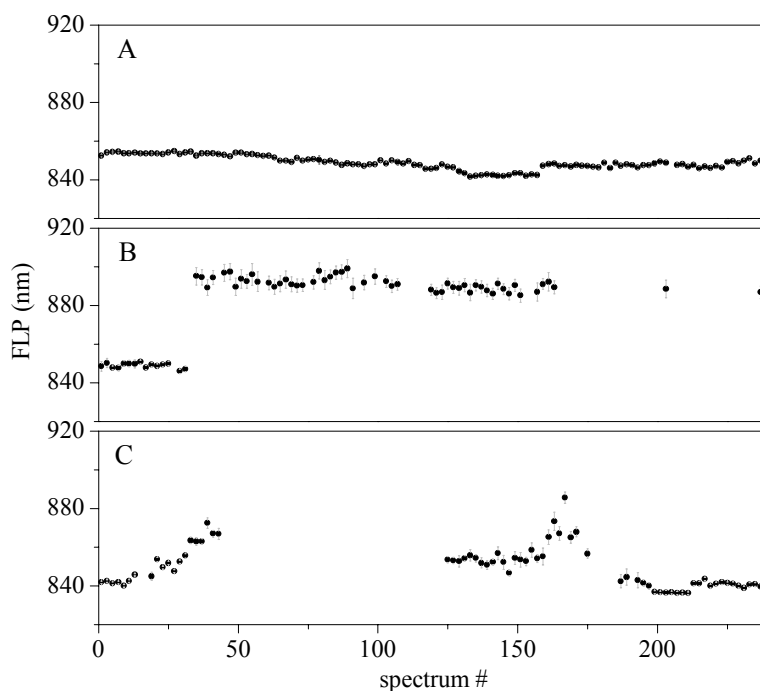


Figure 1. Characteristic FLP time traces of three different species of LH2 complexes: (A) *Rb. sphaeroides*, (B) PACLH2mol, (C) PACLH1. Only every third data point is shown to improve clarity.

occurred most was to an FLP at around 880-890 nm. This red-shifted level appeared to be very stable, as once in this state most of the complexes remained there until the end of the trace. This does not imply that spectral changes only occurred to the red, but for these mutants we were not able to observe spectral jumps to the blue. This was a consequence of using 800 nm excitation and the FL barrier filter which effectively eliminated jumps to the blue from the average position which is already blue-shifted relative to the WT (FLP distributions for both mutants peak at around 845 nm). The LH2 of *Rs. molischanum* and the LH1 of *Rb. sphaeroides* exhibited much less evidence of such quasi-stable levels: 0.5-1.7% and 0-6%, respectively, for the different datasets with two different excitation wavelengths.

Extreme blue jumps

Excitation at 594 nm instead of 800 nm allowed us to observe extreme blue spectra that were already apparent from the experiment with 800 nm excitation, but could not be visualized to their fullest extent because of the FL filter. It appeared that roughly 10% of the measured complexes of LH2 of *Rps. acidophila* and *Rb. sphaeroides* (but not *Rs. molischanum*) exhibited transitions to states with spectra peaking at around 810 nm and significantly narrower than the average. An example of such a spectral evolution is shown in Figures 2 and 3. The peak wavelength of the initial spectrum is around 870 nm; in the course of time the spectrum decreases in intensity, broadens and its peak wavelength shifts to the blue. Before the spectrum finally narrows down and settles to an emission maximum around 810 nm, it moves through a state that appears to be a superposition of two fluorescent species with different spectral maxima. Surprisingly, after a number of spectra with a peak position around 810 nm, the emission spectrum returns to a wavelength close to the initial one at about 870 nm, albeit with the lower intensity. The most surprising finding is that in a remarkably large number of cases (50-90%) the intermediate FLP value of about 810 nm is regained after a period of 810 nm FL.

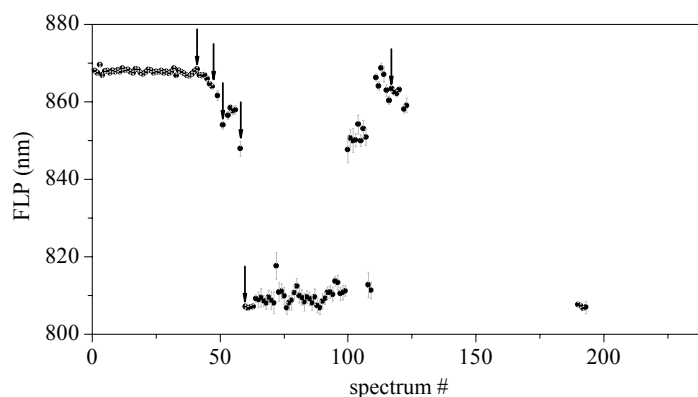


Figure 2. FLP trace of a single LH2 of *Rps. acidophila* with an extreme jump to around 810 nm. The arrowed spectra are depicted in the Figure 3.

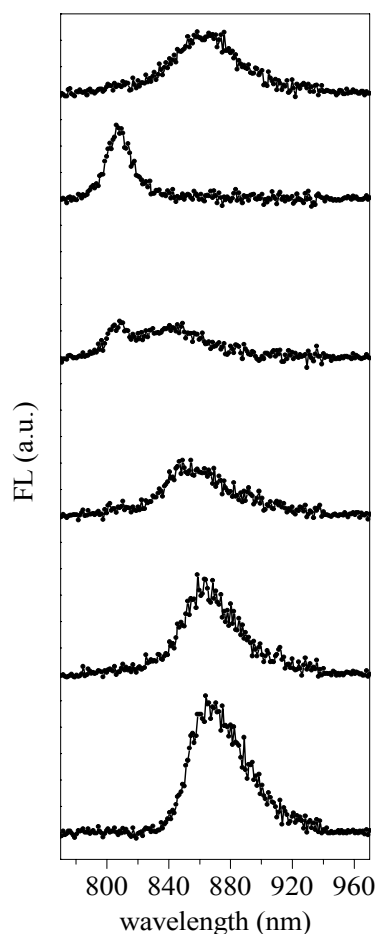


Figure 3. Selected spectra from Figure 2: from bottom to top in increasing spectrum number (#).

Comparison of the frequency of spectral jumping

A number of different criteria can be defined to assess the extent of spectral jumping of either individual complexes or populations of complexes from different species. In the latter case we pool the occurrences of spectral jumps from particular complexes to obtain the characteristics pertaining to a species under certain experimental conditions. Examples of possible criteria are: the distribution of standard deviation (STD) values of FLP time traces; distribution of FLP of all spectra from all particles constituting the experimental population; distribution of FLP differences between adjacent points in the time trace; distribution of FLP differences relative to the beginning of the time trace. The first criterion allows for a comparison of the extent of spectral jumping between different experimental populations but it does not convey the details of spectral jumping. The latter three are criteria that deal with changes in the FLP value between subsequent points in the FLP time trace. Thus they are sensitive to the immediate (with the limited time resolution of the

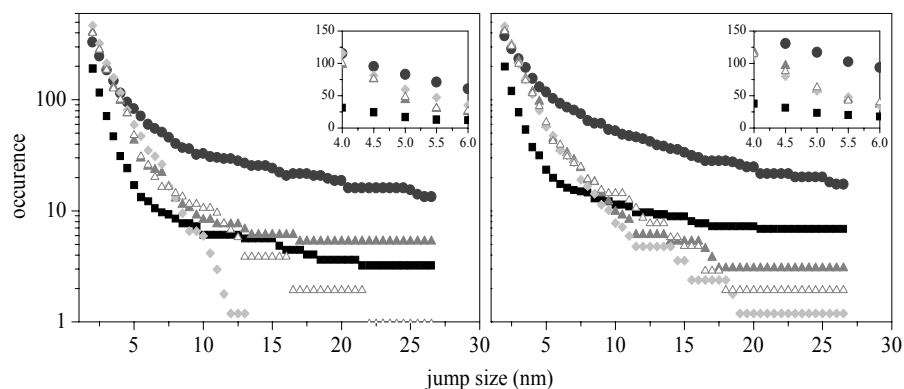


Figure 4. Cumulative histograms of positive (left panel) and negative (right panel) jumps with the sliding point definition for different species at 594 nm excitation. Plot legend is the same as in Figure 5: LH2 of *Rps. acidophila* – black squares, *Rb. sphaeroides* – dark grey circles, *R. molischianum* – grey full and empty triangles, LH1 of *Rb. sphaeroides* – light grey diamonds. Insets magnify the area around 5 nm jump size.

experiment) but overlook overall spectral changes occurring over a few points in the time trace. The criterion we opt for in this work is the distribution of FLP changes using the sliding point definition. In this definition a spectral jump exceeding a certain threshold is recorded as follows: for the initial point of reference we take the first point in the time trace and search for the next point in the trace that deviates from the reference by more than a specified threshold. Once this happens, the jump is recorded, and the reference is transferred to the point where the jump occurred. This is repeated until the end of the trace for all the complexes (different time traces) in the population and for different threshold values. Such a procedure results in a distribution where each point indicates the number of jumps that are larger than the corresponding value of the threshold (Figure 4). Although it does not provide the numbers of jumps of a specific size, the difference between two points

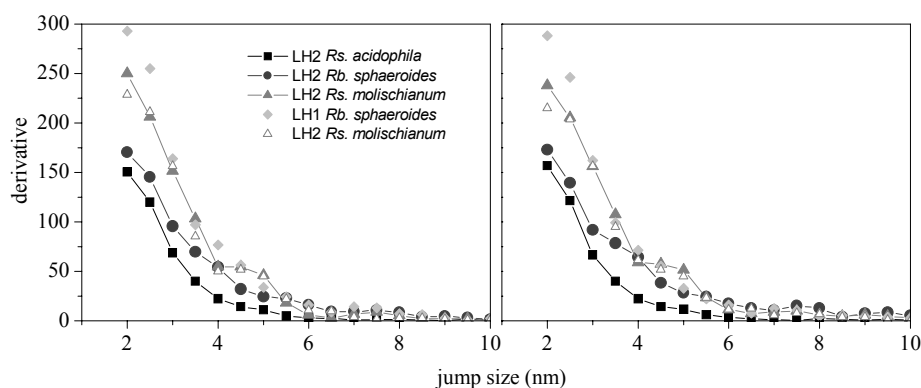


Figure 5. Derivatives of distributions of a number of jumps with the sliding point definition at 594 nm excitation. Left panel – positive, right – negative jumps.

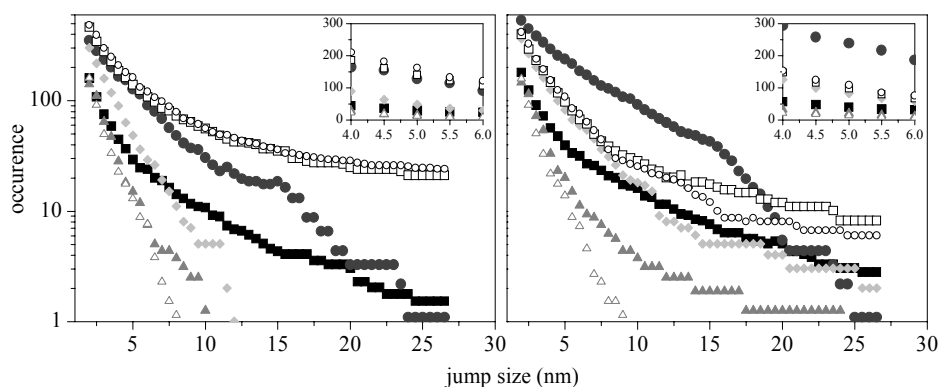


Figure 6. Cumulative histograms of positive (upper panel) and negative (lower panel) jumps with the sliding point definition for different species at 800 nm excitation. Plot legend is the same as in Figure 7: LH2 of *Rps. acidophila* – black squares, *Rb. sphaeroides* – dark grey circles, *Rs. molischanium* – grey full and empty triangles, LH1 of *Rb. sphaeroides* – light grey diamonds, PACLH1 – hollow black squares, PACLH2mol – hollow black circles. Insets magnify the area around 5 nm jump size.

in the histogram is the number of jumps of the size within the range set by the corresponding thresholds. In Figure 4, at large values of the jump size the curves exhibit stretches of constant magnitude. That is because, due to the generally low occurrence of large spectral changes, there are jump size intervals corresponding to zero occurrence.

These cumulative distributions are weighted with the total number of non-zero spectra in the experimental population and some common multiplication factor to preserve realistic numbers of jumps. Such a normalization has to be done since different experimental populations contain unequal numbers of measured complexes with a varying percentage of non zero spectra (note that spectral time traces consist of alternating emissive and dark periods).

One advantage of such a calculation in comparison with the other criteria is that it

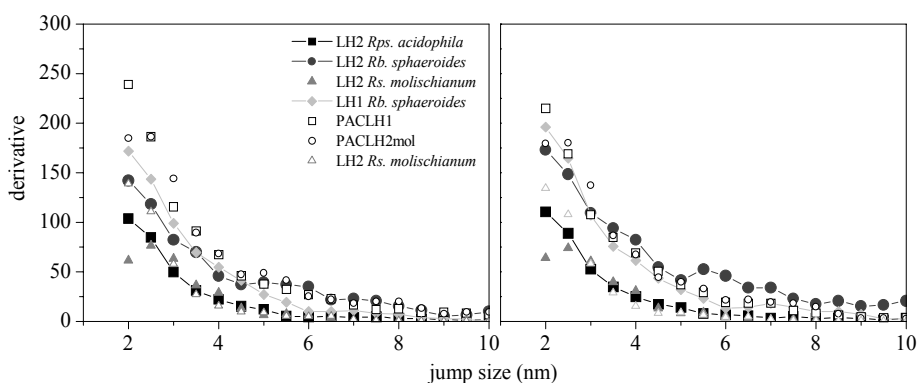


Figure 7. Derivatives of distributions of number of jumps with the sliding point definition at 800 nm excitation. Left panel – positive, right – negative jumps.

contains information about the overall spectral evolution (due to the definition of a jump by means of a “sliding point”) and at the same time it is sensitive to immediate spectral changes since a jump is also recorded in the cases when the difference between adjacent points in the trace is larger than a set threshold.

Since such a cumulative distribution does not directly convey information about the number of jumps of a certain size, we calculate the derivative of the distribution because it is equal to the number of jumps within a unit interval of the jump sizes. A comparison of the number of positive and negative jumps of different size occurring for all the different species with the same equivalent excitation intensity at 594 nm is shown in Figure 5. The jump size scale upper limit is set to only 10 nm to emphasize the occurrence of jumps of intermediate magnitude, *i.e.*, jumps that are larger than random spectral fluctuations and smaller than those with occurrence is too small to make a sensible inter-species comparison. It appears from Figure 5 that the general spectral jumping behaviour of the different species is not strikingly divergent. The ratio between the most different occurrences of jumps of the same size for different species is not more than 3. Moreover, the limited statistics of the data raise the question of how reliable and reproducible such differences are. To examine the reproducibility of such data, we have collected two data sets under identical experimental conditions for LH2 of *Rs. molischianum*. The difference between these datasets indicates the confidence margins of the frequency of spectral jumping for other species. It appears that the derivative curves of the positive and negative spectral jumps up to 5 nm can be separated in the ascending order: LH2 of *Rps. acidophila*, *Rb. sphaeroides*, and LH2 of *Rs. molischianum* and LH1 of *Rb. sphaeroides*. At jumps larger than 5 nm the relationship between the extents of the spectral changes for the different species becomes ambiguous due to the limited statistics of the available data.

Unfortunately we have to make this arbitrary separation between “intermediate” and “large” jumps at one value of the jump size of 5 nm due to the limited statistics of the jumps. Ideally we would extend the derivative dependence also into the range of large jumps of tens of nanometers. This would provide us with a means for a more detailed and specific distinction between the different species in terms of their conformational landscape that can be probed by monitoring spectroscopic changes. We also recognize the fact that the distinction of large and intermediate spectral jumps with the threshold of 5 nm is highly arbitrary and is caused merely by statistical considerations. It has probably little or no relevance to the actual hierarchy of potential energy barriers in the conformational landscape of the pigment-proteins.

The numbers of positive and negative spectral jumps larger than 5 nm in the case of LH2 of *Rps. acidophila* and *Rb. sphaeroides* also contain occurrences of extreme spectral jumping, since, as mentioned earlier, for these species FLP sometimes shifts to around 810 nm. Such dramatic changes do not occur for LH1 of *Rb. sphaeroides* nor for LH2 of *Rs. molischianum* (as mentioned earlier). Consequently, a comparison of frequencies of large spectral jumps (excluding extremities) for the different species should be done with somewhat lower values of jumps for the two species of LH2 of *Rps. acidophila* and *Rb.*

sphaeroides. Taking this into account, this comparison is made from the cumulative distributions that around 5 nm are shown as insets of the cumulative histograms in Figure 4. In order of ascending number of positive and negative jumps larger than 5 nm different complexes occur as: LH2 of *Rps. acidophila*, LH2 of *Rs. molischianum* and LH1 of *Rb. sphaeroides*, and LH2 of *Rb. sphaeroides*.

The cumulative curves of LH1 of *Rb. sphaeroides* and LH2 of *Rps. acidophila* intersect at around 8 nm jump size indicating that the ratio of jumps larger than 8 nm is reversed compared to that at 5 nm demanding a more detailed classification of the sizes of jumps at least for these two species. However, the occurrence of jumps larger than 8 nm is too scarce to conduct such detailed comparison.

Summarizing, LH2 of *Rps. acidophila* features the smallest number of both positive and negative spectral jumps of all sizes; LH2 of *Rs. molischianum* and LH1 of *Rb. sphaeroides* are similar to each other and exhibit the largest number of intermediate jumps and are in the second place for large jumps; LH2 of *Rb. sphaeroides* exhibits the biggest number of the large jumps and is in the second place for intermediate jumps.

Cumulative histograms and corresponding derivative curves resulting from an analogous measurement with 800 nm excitation for the different species are shown in Figures 6 and 7, respectively. The derivative curves of the positive and negative jumps can be roughly divided into two groups: LH2 and LH1 of *Rb. sphaeroides* and the LH2 domain swap mutants jump more than LH2 of *Rps. acidophila* and *Rs. molischianum*. It is difficult to separate LH2 and LH1 of *Rb. sphaeroides* since the corresponding curves change their relative position both for positive and negative jumps even up to a jump size of 5 nm. The extent of positive spectral jumping of the two mutants of LH2 of *Rb. sphaeroides*, PACLH1 and PACLH2mol, is closer to the higher end of the observable jumping frequency for the different species, which is probably not too surprising, since the significant alteration of the native protein structure may be expected to destabilize these complexes. The corresponding negative jumps are less frequent in the dataset probably due to the fact that the average spectrum of the mutants is strongly blue-shifted relative to the WT so that blue spectral occurrences are not visible due to the FL filter.

One distinct difference from the equivalent results with 594 nm excitation is that LH2 of *Rs. molischianum* has relatively few occurrences of jumps upon 800 nm excitation, and this result is reproducible for at least one more dataset obtained under identical experimental conditions. A possible explanation of this apparent discrepancy is that we overestimate the number of absorbed photons upon 800 nm excitation, which is probably due to a partial bleaching of the B800 ring under intense excitation. So in the following we will rely on the 594 nm excitation dataset.

In terms of the large jumps upon 800 nm excitation, the various complexes are distributed in a similar manner as for 594 nm excitation with the exception of LH2 of *Rs. molischianum*. In ascending order of positive and negative jumps: LH2 of *Rps. acidophila*, LH1, and LH2 of *Rb. sphaeroides* (Figure 6). The two mutants exhibit the largest occurrence not only of intermediate but also of large positive spectral jumps.

DISCUSSION

In this section we summarize the occurrence of quasi-stable behaviour and frequency of spectral jumping for different species, and discuss the intriguing observation of the extreme blue spectral shifts. Then we investigate the microscopic origin of the inter-species variation of spectroscopic flexibility.

Extreme blue jumps

We observed that, in a number of cases, upon 594 nm excitation LH2 of *Rps. acidophila* and *Rb. sphaeroides* exhibited extreme blue spectral shifts down to FLP around 810 nm, but this was not the case for the LH2 of *Rs. molischanum* or LH1 of *Rb. sphaeroides*. From the trace shown in Figure 3 it appears that states with a moderately blue-shifted spectral peak wavelength serve as precursors for the final state with the FLP around 810 nm (note that this does not imply that in all cases of spectral diffusion, each pigment-protein complex eventually arrives to this state). This spectral shift occurs through an intermediate spectrum that appears to be a superposition of spectral line shapes with the FLP value strongly blue-shifted relative to the intermediate one. It is unclear what the origin of this blue-shifted spectroscopic intermediate is, as it is not compatible with an intact B850 ring within the context of the proposed disordered exciton model. We propose that the emission spectrum peaking at 810 nm originates from the B800 ring in the absence of an efficient energy transfer to the B850. The absence of B800-850 transfer step implies that the B850 is bleached, indicating extreme changes in the electronic structure of the ring that are probably associated with sizeable spatial rearrangement. It is rather surprising then that such a bleaching is reversible. The formation of an excitation trap in the B850 ring was used to explain the long non-radiative periods of LH2 of *Rps. acidophila* (Bopp, *et al.* 1997). This, however, cannot be used to explain our observations since, even in the presence of the trap, the B850 BChls *a* would still accept energy from the B800 BChls *a*. Thus these remarkable observations remain to be clarified in future investigations.

The above analysis demonstrates that in this experiment we exercise rather harsh excitation levels that can seriously destabilize the pigment-protein structure and in some cases to such an extent that one of the pigment rings is, at least temporarily, “spectroscopically” disabled. However, even if such a state is attained, it does not necessarily imply an irreparable damage of the pigment-protein, since in most cases the change appears to be reversible. This demonstrates the extreme robustness and flexibility of photosynthetic pigment-proteins allowing them to sustain activity even under excitation conditions that are remote from native and may represent an evolved stability to cope with abrupt large changes in illumination levels.

Quasi-stable FLP levels for different species

In terms of the occurrence and also of how distinctly different the observed quasi-stable states are, the different species are distributed in the following descending order: LH2 of *Rps. acidophila*, LH2 domain swap mutants of *Rb. sphaeroides*, LH2 of *Rb. sphaeroides*, LH1 of *Rb. sphaeroides* and LH2 of *Rs. molischianum*. It has to be noted that the quasi-stable states of the domain swap mutants occurred mostly with an FLP around 880-890 nm, which indicates the existence of a well-defined stable conformation with this spectroscopic signature. In terms of an excitonic model, such red spectral shift can be associated with the red-shifting of just one pigment in the B850 ring (Novoderezhkin *et al.*, submitted manuscript), which can be due to the strengthening of the H-bond to the acetyl group of the BChl *a* (see below) caused by structural deformation. Consequently, this state is probably associated with a local structural change of the proteic surroundings of one pigment. The LH2 domain swap mutants of *Rb. sphaeroides* have their C-terminal part of the α -polypeptide exchanged for corresponding sequences from the LH2 of *Rs. molischianum* or the LH1 of *Rb. sphaeroides* (Olsen, *et al.* 2003). These manipulations have altered the α Tyr+13 and α Tyr+14 residues, which in the native complex form H-bonds to the B850 BChls *a* and instead introduce only one candidate for H-bond formation, α Trp+11, which shifts the FL spectrum of the mutants to the blue. However, in that work the authors reported a red-shifted species as a minor component of the absorbance spectrum for both domain swap mutants. It is possible that these species reflected one of these long lived quasi-stable states *in vivo*. The introduction of amino acids that are different to those in the LH2 WT structure appears to introduce conformational substates that are difficult to escape from, leading to the observed stable, strongly red-shifted, spectral states.


Our observations also allow us to approach the question of the hierarchical organization of the conformational landscape of the bacterial LHCs that was ascertained for the LH2 complex of *Rs. molischianum* in (Hofmann, *et al.* 2003) following the proposed hierarchy of energy barriers for myoglobin (Frauenfelder, *et al.* 1989). In the case where the energy barriers separating different conformations are organized in tiers according to their height, we should observe changes between spectroscopically different states associated with transitions over large energy barriers and smaller spectral fluctuations within those states corresponding to transitions over smaller barriers. In the case where the energy barriers are organized randomly, we should observe transitions between the different spectroscopic states perturbed only by the statistical fluctuations, alternating with smaller spectroscopic fluctuations associated with the crossing of smaller energy barriers. Our observation of the quasi-stable states indicates large energy barriers separating spectroscopically different states. We also observed fluctuations within those states. However, the spectral evolution also involves small spectral changes linking the large ones. Thus we can conclude that the actual conformational landscape of bacterial LHCs exhibits some hierarchical organization character, but with additional complexity that prevents its description purely in terms of the tier model of the energy barriers.

Comparison of the frequency of spectral jumping

A comparison of the frequency of spectral jumping for different species at two excitation wavelengths is made in Table 1. It appears that some observations are not reproduced between datasets with different excitation wavelengths. Thus, for example, we observed that the LH2 of *Rb. sphaeroides* with 594 nm excitation exhibits fewer intermediate and more large spectral jumps than the LH1 of *Rb. sphaeroides* or LH2 of *Rs. molischianum*. However in the dataset at 800 nm excitation we could not make a distinction between the two groups in terms of intermediate jumps and at the same time the relationship between the numbers of large jumps remained the same as in the 594 nm dataset. We must conclude that the two species are similar in their frequency of intermediate jumps given the limited statistics of our data. Perhaps with better measurement statistics a distinction might be made.

From the combination of both datasets we can make the following observations: for both positive and negative jumps of intermediate size, the LH2 of *Rps. acidophila* is spectroscopically the least flexible; the LH2 and LH1 of *Rb. sphaeroides* and the LH2 of *Rs. molischianum* exhibit similar levels of larger jumps. In terms of large positive and negative jumps the complexes are distributed in the following ascending order: LH2 of *Rps. acidophila*, LH1 of *Rb. sphaeroides* and LH2 of *Rs. molischianum*, and LH2 from *Rb. sphaeroides*. The two domain swap mutants feature the largest number of red jumps of all sizes. If we put more emphasis on the large spectral jumps then the corresponding list is: LH2 of *Rps. acidophila*, LH2 of *Rs. molischianum* and LH1 of *Rb. sphaeroides*, and LH2 of *Rb. sphaeroides* in the order of increasing spectral flexibility.

Table 1. Experimental frequencies of positive and negative spectral jumps of intermediate and large size for different species.

	Intermediate jumps (594 nm)	Intermediate jumps (800 nm)	Large jumps (594 nm)	Large jumps (800 nm)
				LH2 <i>Rs. molischianum</i>
	LH2 <i>Rps. acidophila</i>	LH2 <i>Rs. molischianum</i> & <i>Rps. acidophila</i>	LH2 <i>Rps. acidophila</i>	LH2 <i>Rps. acidophila</i>
	LH2 <i>Rb. sphaeroides</i>	LH2 <i>Rb. sphaeroides</i> & LH1 <i>Rb. sphaeroides</i>	LH1 <i>Rb. sphaeroides</i> & LH2 <i>Rs. molischianum</i>	LH1 <i>Rb. sphaeroides</i>
	LH2 <i>Rs. molischianum</i> & LH1 <i>Rb. sphaeroides</i>		LH2 <i>Rb. sphaeroides</i>	LH2 <i>Rb. sphaeroides</i>
		Mutants (red jumps)		Mutants (red jumps)

The microscopic origin of spectral jumps

In this section we will discuss the microscopic parameters, determining the spectral properties of the B850 BChl *a* and structural flexibility of the complexes. We assume that structural changes induce alterations of those microscopic factors that are associated with the observed spectroscopic shifts. We further suggest that subtle differences in the chromophore binding pocket in different complexes determine their different spectroscopic response. In combination with differing structural flexibility this allows us to interpret the diversity of spectral flexibility among complexes.

The factors that have been considered as important in determining the pigment-protein electronic structure can be divided into two groups:

- 1) pigment-pigment exciton coupling (Alden, *et al.* 1997, Hu, *et al.* 1997, Novoderezhkin, *et al.* 1999, Novoderezhkin, *et al.* 2003, Scholes and Fleming 2000, van Grondelle and Novoderezhkin 2001, Wu, *et al.* 1997);
 - 2) the tuning of the individual pigment site energy due to:
 - a) local protein environment:
 - i) point charges;
 - ii) H-bonding;
 - iii) axial ligation of Mg²⁺.
 - b) structural changes of the chromophore itself:
 - i) rotation of the C2 acetyl carbonyl group;
 - ii) distortion of porphyrin macrocycle.
- (Cogdell, *et al.* 1997, He, *et al.* 2002, McLuskey, *et al.* 2001).

The second set of factors determines the so-called pigment site energy, *i.e.*, the electronic transition energy of the pigment in the absence of other pigments. Changes of these site energies are propagated by excitonic coupling over the delocalized electronic system of the ring of chromophores and are reflected in the absorption and FL properties.

Since the actual pigment site energy is a result of all the effects mentioned in 2), a comparison of the spectral properties of different species can only be made after a systematic analysis of the contribution of each parameter. Furthermore, the assessment of the relative spectral flexibility requires a detailed knowledge of the distance dependence of each factor and the trajectory of structural changes. In short, a complete model would require molecular dynamics simulations over long times that are not feasible at the moment and fall beyond the scope of this work. For this reason, the effect of the above factors on the observed spectroscopic flexibility of the different species will only be assessed qualitatively.

To determine how each of the factors listed above influences the site energy and the spectroscopic properties of an individual pigment in a protein is a major problem in itself. Molecular orbital calculations indicate that placing point charges at 3.5 Å from rings A and C of a bacteriochlorin system produce Q_y absorption shifts in the order of 100 nm depending on the position and sign of the charge (Eccles and Honig 1983, Hanson, *et al.* 1987). And even in the case when such point charges are absent, the electric field emanating

from the more distant parts of the surrounding protein must have an effect on the absorption (Stark effect). Formation of an H-bond to the acetyl group of BChl *a* has been calculated to red-shift the absorption of Q_y by 6 nm, while an H-bond to the keto group causes a blue shift of the same magnitude (Hanson, *et al.* 1987). The latter are “pure” effects of H-bonding, *i.e.*, they are due to the interaction of the ligand with the conjugated electronic system of the BChl *a* macrocycle. The rotation of the acetyl group out of the plane of the BChl *a* molecule causes a blue shift of the absorption of up to 20 nm for the Q_y transition, if the torsion angle assumes values of $\pm 90^\circ$ (Gudowskanowak, *et al.* 1990, Hanson, *et al.* 1987). The effect of a Mg^{2+} ligation is illustrated by the calculation of the exchange of the imidazole ligand (His) to a water molecule producing a blue shift of the Q_y absorption of 3 nm (Hanson, *et al.* 1987). Calculations suggest that distortions of the porphyrin macrocycle may lead to the absorption red shifts in the order of 100 nm in extreme cases (Barkigia, *et al.* 1988). All of these contributions to BChl red shifts were discussed extensively in (Gall, *et al.* 1997).

From the comparison of the above numbers it appears that point charges, the rotation of the acetyl group, and the deformation of the porphyrin ring have the largest spectroscopic impact. In the B850 ring of the complexes investigated there are no point charges in the proximity of the BChl *a* macrocycles. The macrocycle of at least one of the B850 BChl *a* molecules is strongly distorted in a number of different LHCs (Lapouge, *et al.* 1999), and the acetyl carbonyl group is rotated out of the molecular plane (McLuskey, *et al.* 2001).

Deformation of the porphyrin ring is thought to be due to the H-bonding of its peripheral groups and ligation of the central Mg^{2+} ion (Scheidt and Lee 1987). H-bonding also determines the position of the acetyl carbonyl group relative to the molecular plane (McLuskey, *et al.* 2001). The structural configuration of the pigment must also be influenced by mechanical effects such as van der Waals interactions within the pigment-protein. However, accounting for such an effect can only be done by molecular dynamics simulations and will not be considered here.

Thus we have narrowed down the list of all the microscopic factors to those which are spectroscopically most significant: the porphyrin macrocycle deformation and the acetyl group rotation, which are at least partly accounted for by the H-bonding to the acetyl carbonyl. Furthermore, systematic mutational studies have revealed a linear relationship between the H-bonding strength to the acetyl carbonyls of the B850 BChls *a* and the absorption peak wavelength (Sturgis, *et al.* 1997, Sturgis and Robert 1997). This allows us to correlate the observable spectroscopic jumps to structural changes by means of the changes in the H-bonding strength. The weakening of the H-bond to the acetyl carbonyl allows its rotation further out of the molecular plane (McLuskey, *et al.* 2001) and probably relaxes the deformation of the porphyrin ring, which together leads to a blue spectral shift, whereas the strengthening of the bond has an opposite effect, causing a red shift. This way the observed blue and red spectral shifts can be interpreted.

The relative structural flexibility of different species is assessed based on the network of H-bonds described above. In the LH2 of *Rps. acidophila* and *Rb. sphaeroides*, the α -

Table 2. The strength of H-bonding to carbonyl acetyls of B850 BChls *a* and structural flexibility of different complexes.

Species	Acetyl downshift (cm^{-1})	Reference	Flexible
LH2 <i>Rps. acidophila</i>	30 (degenerate)	(Robert, <i>et al.</i> 1988)	no
LH2 <i>Rb. sphaeroides</i>	30 & 25	(Fowler, <i>et al.</i> 1994)	no
LH2 <i>Rs. molischanum</i>	18 (degenerate)	(Germeroth, <i>et al.</i> 1993)	yes
LH1 <i>Rb. sphaeroides</i>	18 (degenerate)	(Olsen, <i>et al.</i> 1994)	yes

polypeptide donates one H-bond to the acetyl carbonyl of BChl *a* in the same dimeric subunit and a second one to the BChl *a* in the adjacent subunit; H-bonds between different subunits contribute to the structural stabilization of the complex as a whole. However, in LH2 of *Rs. molischanum* and LH1 of *Rb. sphaeroides*, the H-bonds to the acetyl carbonyl as well as to the keto groups of the BChls *a* are internal to the subunit. This difference in the H-bonding pattern is proposed to be associated with the different structural flexibility of the LH2 of *Rb. sphaeroides* and the LH1 of *Rb. sphaeroides*: the former is considered to be less flexible than the latter (Bahatyrova, *et al.* 2004). In addition to this, LH1 is thought to be more flexible partly due to its larger size.

The acetyl carbonyl H-bonding strength is experimentally assessed by the downshift of a corresponding spectral Raman peak (which in the absence of H-bonding is around 1660 cm^{-1}); together with proposed structural flexibilities these strengths for different species are summarized in Table 2.

In the following we interpret the inter-complex variation of spectroscopic flexibility based on differences in the structural flexibility and the H-bonding strength. The possible structural changes are presumed to be associated with changes in the H-bonding strength. It is assumed that the stronger the H-bond, the larger its change may be in response to structural alteration. Since the spectral change and that of the H-bonding strength are proportional, the former is also larger in the case where a strong H-bond is perturbed. Thus, for example, LH1 of *Rb. sphaeroides* and LH2 of *Rs. molischanum* are structurally flexible, but their H-bonding to the acetyl carbonyl is associated with only an 18 cm^{-1} downshift of the corresponding Raman peak. This implies frequent structural changes with little spectroscopic consequence, which results in a similar intermediate spectroscopic flexibility of the two complexes as was observed experimentally. The absence of stable conformations complies with the observed absence of quasi-stable FLP states.

The LH2 of *Rb. sphaeroides* is less flexible but its H-bonding corresponds on the average to a downshift of the Raman peak of $\sim 29 \text{ cm}^{-1}$. Consequently, structural changes, although less frequent, will result in larger spectroscopic alterations, leading to a large observed spectral flexibility. Intermediate occurrence of quasi-stability is associated with some conformations from which it is difficult to escape.

Finally, LH2 of *Rps. acidophila* exhibits H-bonding as strong as that of *Rb. sphaeroides*, which means that the same structural changes will be associated with similar spectral alterations for both complexes. However, the spectroscopic flexibility of LH2 of *Rps. acidophila* is observed to be the lowest of all complexes investigated. Since there is no quantitative criterion of structural flexibility, it might be that although both LH2 of *Rps. acidophila* and *Rb. sphaeroides* are rather structurally rigid the former is more inflexible than the latter due to other differences in their protein backbones, resulting in fewer structural changes, which leads to a lower spectral flexibility. This also implies that the LH2 of *Rps. acidophila* must exhibit more stable conformations, which is corroborated by the observed multitude of quasi-stable states of FLP.

Although rather qualitative, the above speculations allow us to interpret the observed differences in spectroscopic flexibility among the various complexes. This analysis is instructive as it shows that structural flexibility, although related, is not identical to the experimentally observable frequency of spectral jumping. For example, LH1 is supposed to be more flexible than any of the LH2 complexes due to its larger size; however, its spectral flexibility is of an intermediate magnitude probably due to the weaker connection between structural and spectroscopic changes. Thus, when considering flexibilities one should be careful as to exactly which issue is addressed.

CONCLUSIONS

In this work we have conducted a comparative study of FL spectral evolution of different kinds of single bacterial LHCs. We previously observed that the FLP of single LH2 of *Rps. acidophila* evolved through different quasi-stable states. Here we found that to various extent this is a property of other types of bacterial LHCs.

Moreover, an improved experimental arrangement allowed the observation of extreme spectral jumps to the blue that we associated with bleaching of one of the pigment rings, which is probably connected to a sizable structural rearrangement. It is surprising that such transitions are often reversible implying the recovery of the destabilized ring.

The measurement of FL spectral traces of a number of individual complexes allowed us to build the statistics of spectral jumping. The investigated pigment-proteins are rather complex systems, and an unambiguous connection between the experimentally observable FL spectral change and corresponding structural deformation cannot be made at the moment. However, we conclude that the observed variation of frequency and size of spectral jumping of different LHCs must be associated with different structural flexibilities of the pigment-proteins and a variation of the strength of the factors determining the electronic transition (site) energies of the chromophores.

REFERENCES

Alden, R. G., Johnson, E., Nagarajan, V., Parson, W. W., Law, C. J., and Cogdell, R. J. (1997) Calculations of spectroscopic properties of the LH2 bacteriochlorophyll-protein antenna complex

- from *Rhodospseudomonas acidophila*. *J. Phys. Chem. B* 101, 4667-4680.
- Bahatyrova, S., Frese, R. N., van der Werf, K. O., Otto, C., Hunter, C. N., and Olsen, J. D. (2004) Flexibility and size heterogeneity of the LH1 light harvesting complex revealed by atomic force microscopy - functional significance for bacterial photosynthesis. *J. Biol. Chem.* 279, 21327-21333.
- Barkigia, K. M., Chantranupong, L., Smith, K. M., and Fajer, J. (1988) Structural and theoretical models of photosynthetic chromophores - implications for redox, light-absorption properties and vectorial electron flow. *J. Am. Chem. Soc.* 110, 7566-7567.
- Bopp, M. A., Jia, Y. W., Li, L. Q., Cogdell, R. J., and Hochstrasser, R. M. (1997) Fluorescence and photobleaching dynamics of single light-harvesting complexes. *Proc. Natl. Acad. Sci. U.S.A.* 94, 10630-10635.
- Cogdell, R. J., Fyfe, P. K., Barrett, S. J., Prince, S. M., Freer, A. A., Isaacs, N. W., McGlynn, P., and Hunter, C. N. (1996) The purple bacterial photosynthetic unit. *Photosynth. Res.* 48, 55-63.
- Cogdell, R. J., Howard, T. D., Isaacs, N. W., McLuskey, K., and Gardiner, A. T. (2002) Structural factors which control the position of the Q_y absorption band of bacteriochlorophyll a in purple bacterial antenna complexes. *Photosynth. Res.* 74, 135-141.
- Cogdell, R. J., Isaacs, N. W., Freer, A. A., Arrelano, J., Howard, T. D., Papiz, M. Z., Hawthornthwaite, A. M., and Prince, S. (1997) The structure and function of the LH2 (B800-850) complex from the purple photosynthetic bacterium *Rhodospseudomonas acidophila* strain 10050. *Prog. Biophys. Mol. Biol.* 68, 1-27.
- Conroy, M. J., Westerhuis, W. H. J., Parkes-Loach, P. S., Loach, P. A., Hunter, C. N., and Williamson, M. P. (2000) The solution structure of *Rhodobacter sphaeroides* LH1 beta reveals two helical domains separated by a more flexible region: structural consequences for the LH1 complex. *J. Mol. Biol.* 298, 83-94.
- Eccles, J., and Honig, B. (1983) Charged amino-acids as spectroscopic determinants for chlorophyll *in vivo*. *Proc. Natl. Acad. Sci. U.S.A.* 80, 4959-4962.
- Evans, M. B., Hawthornthwaite, A. M., and Cogdell, R. J. (1990) Isolation and characterisation of the different B800-850 light-harvesting complexes from low- and high-light grown cells of *Rhodospseudomonas palustris*, strain 2.1.6. *Biochim. Biophys. Acta.* 1016, 71-76.
- Fotiadis, D., Qian, P., Philippsen, A., Bullough, P. A., Engel, A., and Hunter, C. N. (2004) Structural analysis of the reaction center light-harvesting complex I photosynthetic core complex of *Rhodospirillum rubrum* using atomic force microscopy. *J. Biol. Chem.* 279, 2063-2068.
- Fowler, G. J. S., Visschers, R. W., Grief, G. G., van Grondelle, R., and Hunter, C. N. (1992) Genetically modified photosynthetic antenna complexes with blueshifted absorbency bands. *Nature.* 355, 848-850.
- Fowler, G. J. S., Sockalingum, G. D., Robert, B., and Hunter, C. N. (1994) Blue shifts in bacteriochlorophyll absorbance correlate with changed hydrogen-bonding patterns in light-harvesting LH2 mutants of *Rhodobacter sphaeroides* with alterations at α Tyr44 and α Tyr45. *Biochem. J.* 299, 695-700.
- Frauenfelder, H., Steinbach, P. J., and Young, R. D. (1989) Conformational relaxation in proteins. *Chem. Scripta.* 29A, 145-150.
- Gall, A., Sturgis, J. D., Fowler, G. J. S., Hunter, C. N., and Robert, B. (1997) Influence of the protein binding site on the absorption properties of the monomeric bacteriochlorophyll in *Rhodobacter sphaeroides* LH2 complex. *Biochemistry.* 36, 16282-16287.
- Gall, A., and Robert, B. (1999) Characterization of the different peripheral light-harvesting complexes from high- and low-light grown cells from *Rhodospseudomonas palustris*. *Biochemistry.* 38, 5185-

5190.

Germeroth, L., Lottspeich, F., Robert, B., and Michel, H. (1993) Unexpected similarities of the B800-850 light-harvesting complex from *Rhodospirillum rubrum* to the B870 light-harvesting complexes from other purple photosynthetic bacteria. *Biochemistry*. 32, 5615-5621.

Gudowskanowak, E., Newton, M. D., and Fajer, J. (1990) Conformational and environmental effects on bacteriochlorophyll optical spectra - correlations of calculated spectra with structural results. *J. Phys. Chem.* 94, 5795-5801.

Hanson, L. K., Thompson, M. A., and Fajer, J. (1987) Environmental effect of properties of chlorophylls *in vivo*. Theoretical models. In Progress in photosynthesis research. Biggins, J., Ed., Martinus Nijhoff, Dordrecht.

He, Z., Sundström, V., and Pullerits, T. (2002) Influence of the protein binding site on the excited states of bacteriochlorophyll: DFT calculations of B800 in LH2. *J. Phys. Chem. B*. 106, 11606-11612.

Hofmann, C., Aartsma, T. J., Michel, H., and Köhler, J. (2003) Direct observation of tiers in the energy landscape of a chromoprotein: a single-molecule study. *Proc. Natl. Acad. Sci. U.S.A.* 100, 15534-15538.

Hu, X., and Schulten, K. (1998) Model for the light-harvesting complex I (B875) of *Rhodobacter sphaeroides*. *Biophys. J.* 75, 683-694.

Hu, X. C., Ritz, T., Damjanovic, A., Autenrieth, F., and Schulten, K. (2002) Photosynthetic apparatus of purple bacteria. *Q. Rev. Biophys.* 35, 1-62.

Hu, X. C., Ritz, T., Damjanovic, A., and Schulten, K. (1997) Pigment organization and transfer of electronic excitation in the photosynthetic unit of purple bacteria. *J. Phys. Chem. B*. 101, 3854-3871.

Karrasch, S., Bullough, P. A., and Ghosh, R. (1995) The 8.5 Å projection map of the light-harvesting complex-I from *Rhodospirillum rubrum* reveals a ring composed of 16 subunits. *EMBO J.* 14, 631-638.

Koepke, J., Hu, X. C., Muenke, C., Schulten, K., and Michel, H. (1996) The crystal structure of the light-harvesting complex II (B800-850) from *Rhodospirillum rubrum*. *Structure*. 4, 581-597.

Lapouge, K., Naveke, A., Gall, A., Ivancich, A., Seguin, J., Scheer, H., Sturgis, J. N., Mattioli, T. A., and Robert, B. (1999) Conformation of bacteriochlorophyll molecules in photosynthetic proteins from purple bacteria. *Biochemistry*. 38, 11115-11121.

McDermott, G., Prince, S. M., Freer, A. A., Hawthornthwaite, A. M., Papiz, M. Z., Cogdell, R. J., and Isaacs, N. W. (1995) Crystal structure of an integral membrane light-harvesting complex from photosynthetic bacteria. *Nature*. 374, 517-521.

McLuskey, K., Prince, S. M., Cogdell, R. J., and Isaacs, N. W. (2001) The crystallographic structure of the B800-820 LH3 light-harvesting complex from the purple bacteria *Rhodospseudomonas acidophila* strain 7050. *Biochemistry*. 40, 8783-8789.

Novoderezhkin, V., Monshouwer, R., and van Grondelle, R. (1999) Exciton (de)localization in the LH2 antenna of *Rhodobacter sphaeroides* as revealed by relative difference absorption measurements of the LH2 antenna and the B820 subunit. *J. Phys. Chem. B*. 103, 10540-10548.

Novoderezhkin, V., Wendling, M., and van Grondelle, R. (2003) Intra- and interband transfers in the B800-B850 antenna of *Rhodospirillum rubrum*. Redfield theory modeling of polarized pump-probe kinetics. *J. Phys. Chem. B*. 107, 11534-11548.

Olsen, J. D., Robert, B., Siebert, A., Bullough, P. A., and Hunter, C. N. (2003) Role of the c-terminal extrinsic region of the alpha polypeptide of the light-harvesting 2 complex of *Rhodobacter sphaeroides*: a domain swap study. *Biochemistry*. 42, 15114-15123.

Olsen, J. D., Sockalingum, G. D., Robert, B., and Hunter, C. N. (1994) Modification of a hydrogen bond to a bacteriochlorophyll a molecule in the light-harvesting 1 antenna of *Rhodobacter sphaeroides*.

- Proc. Natl. Acad. Sci. U.S.A.* 91, 7124-7128.
- Papiz, M. Z., Prince, S. M., Howard, T., Cogdell, R. J., and Isaacs, N. W. (2003) The structure and thermal motion of the B800-850 LH2 complex from *Rps. acidophila* at 2.0 Å resolution and 100 K: new structural features and functionally relevant motions. *J. Mol. Biol.* 326, 1523-1538.
- Pfenning, N. (1969) *Rhodospseudomonas acidophila*, a new species of the budding purple non-sulfur bacteria. *J. Bacteriol.* 99, 597-602.
- Robert, B., Cogdell, R. J., and van Grondelle, R. (2003) The light-harvesting system of purple bacteria. In Light-harvesting antennas in photosynthesis. Green, B. R. and Parson, W. W., Eds., Vol. 13, Kluwer academic publishers, Dordrecht, Netherlands.
- Robert, B., Vermeglio, A., Steiner, R., Scheer, H., and Lutz, M. (1988). In Photosynthetic light harvesting systems, de Gryuter & Co., Berlin and New York.
- Rutkauskas, D., Novoderezhkin, V., Cogdell, R. J., and van Grondelle, R. (2005) Fluorescence spectroscopy of conformational changes of single LH2 complexes. *Biophys. J.* 88, 422-435.
- Rutkauskas, D., Novoderezhkin, V., Cogdell, R. J., and van Grondelle, R. (2004) Fluorescence spectral fluctuations of single LH2 complexes from *Rhodospseudomonas acidophila* strain 10050. *Biochemistry.* 43, 4431-4438.
- Scheidt, W. R., and Lee, Y. J. (1987) Recent advances in the stereochemistry of metallotetrapyrroles. In Structure and bonding. Buchler, J. W., Ed., Vol. 64, Springer-Verlag, Berlin.
- Scholes, G. D., and Fleming, G. R. (2000) On the mechanism of light harvesting in photosynthetic purple bacteria: B800 to B850 energy transfer. *J. Phys. Chem. B.* 104, 1854-1868.
- Sturgis, J. N., Hunter, C. N., and Niederman, R. A. (1988) Spectra and extinction coefficients of near infrared absorption bands in membranes of *Rhodobacter sphaeroides* mutants lacking light-harvesting and reaction center complexes. *Photochem. Photobiol.* 48, 243-247.
- Sturgis, J. N., Olsen, J. D., Robert, B., and Hunter, C. N. (1997) Functions of conserved tryptophan residues of the core light-harvesting complex of *Rhodobacter sphaeroides*. *Biochemistry.* 36, 2772-2778.
- Sturgis, J. N., and Robert, B. (1997) Pigment binding-site and electronic properties in light-harvesting proteins of purple bacteria. *J. Phys. Chem. B.* 101, 7227-7231.
- Sundström, V., Pullerits, T., and van Grondelle, R. (1999) Photosynthetic light-harvesting: reconciling dynamics and structure of purple bacterial LH2 reveals function of photosynthetic unit. *J. Phys. Chem. B.* 103, 2327-2346.
- van Grondelle, R., Dekker, J. P., Gillbro, T., and Sundström, V. (1994) Energy-transfer and trapping in photosynthesis. *Biochim. Biophys. Acta.* 1187, 1-65.
- van Grondelle, R., and Novoderezhkin, V. (2001) Dynamics of excitation energy transfer in the LH1 and LH2 light-harvesting complexes of photosynthetic bacteria. *Biochemistry.* 40, 15057-15068.
- van Oijen, A. M., Ketelaars, M., Köhler, J., Aartsma, T. J., and Schmidt, J. (2000) Spectroscopy of individual light-harvesting 2 complexes of *Rhodospseudomonas acidophila*: diagonal disorder, intercomplex heterogeneity, spectral diffusion, and energy transfer in the B800 band. *Biophys. J.* 78, 1570-1577.
- Walz, T., Jamieson, S. J., Bowers, C. M., Bullough, P. A., and Hunter, C. N. (1998) Projection structures of three photosynthetic complexes from *Rhodobacter sphaeroides*: LH2 at 6 Å LH1 and RC-LH1 at 25 Å. *J. Mol. Biol.* 282, 833-845.
- Wu, H. M., Rätsep, M., Lee, I. J., Cogdell, R. J., and Small, G. J. (1997) Exciton level structure and energy disorder of the B850 ring and the LH2 antenna complex. *J. Phys. Chem. B.* 101, 7654-7663.
- Zuber, H., and Brunisholz, R. A. (1991) Structure and function of antenna polypeptides and

chlorophyll-protein complexes: principles and variability. In Chlorophylls. Sheer, H., Ed., CRC, Boca Raton, FL.

Spectral trends in the fluorescence of single bacterial light-harvesting complexes: experiments and modified Redfield simulations

Danielis Rutkauskas, Vladimir Novoderezhkin, Andrew Gall, John Olsen, Richard J. Cogdell, C. Neil Hunter, and Rienk van Grondelle

ABSTRACT

In this work we present and discuss the single-molecule fluorescence spectra of a variety of species of light-harvesting complexes: LH2 of *Rhodospseudomonas acidophila*, *Rhodobacter sphaeroides*, *Rhodospirillum rubrum*, and LH1 of *Rhodobacter sphaeroides*. The emission spectrum of these complexes varies as a function of time as was described in earlier work (Rutkauskas, *et al.* 2005, Rutkauskas, *et al.* 2004). For each type of complex, we observe a pronounced and well reproducible characteristic relationship between the fluorescence spectral parameters of the peak wavelength, width and asymmetry. This dependence for the LH2 complexes can be quantitatively explained on the basis of a disordered exciton model by varying the static disorder and phonon coupling parameters. In addition, a correlation of the pigment site energies has to be assumed to interpret the behavior of the LH1 complex.

INTRODUCTION

In purple non-sulphur photosynthetic bacteria, but also in plants and algae, light-harvesting complexes (LHCs) are mediators of the initial stages of a complex sequence of events involving multiple redox reactions, creation of a proton gradient across the thylakoid membrane, and culminating in the synthesis of carbohydrates in the Calvin cycle. The function of the LHCs is to absorb light energy and funnel it to the reaction center (RC) wherein the turnover and subsequent transfer of electrons to the quinone initiates this chain of events (Whitmarsh and Govindjee 1999).

High-resolution 3D crystal structures of two peripheral LHCs of type 2 (LH2) from the purple bacteria *Rhodospseudomonas (Rps.) acidophila* and *Rhodospirillum (Rs.) rubrum* (Koepke, *et al.* 1996, McDermott, *et al.* 1995, Papiz, *et al.* 2003) show that both complexes consist of two rings of bacteriochlorophyll (BChl) *a* molecules in a protein scaffold; and that these are responsible for the absorption bands around 800 and 850 nm, referred to as B800 and B850, respectively. Cryo electron microscopy has shown that the structure of LH2 of *Rhodobacter (Rb.) sphaeroides* is similar to that of *Rps. acidophila* (Walz, *et al.* 1998) whilst LH1 of *Rb. sphaeroides* contains only one pigment ring, with maximum absorption around 875 nm, which is similar to the B850 ring in the LH2 complexes.

The electronic and energy-transfer properties of the LHCs have been successfully described in terms of a model including the excitonic coupling between pigments, static disorder of the pigment electronic transition energies, and dynamic disorder arising from the electronic transition coupling to a phonon bath (Alden, *et al.* 1997, Hu, *et al.* 1997, Novoderezhkin, *et al.* 1999, Novoderezhkin, *et al.* 2003, Sauer, *et al.* 1996, Scholes and Fleming 2000, van Grondelle and Novoderezhkin 2001, Wu, *et al.* 1997). Excitonic coupling leads to the coherent delocalization of a single excitation over a number of pigments in the ring. At the same time the two kinds of disorder destroy the coherence and make the excitation more localized. Most generally, the excitation dynamics in the system of pigments is described using the density matrix formalism. However, in the case where the static disorder prevails over the exciton coupling, this description can be simplified to an incoherent Förster hopping; in the opposite case, the excitation evolves due to the exciton relaxation which is adequately described by the modified Redfield theory.

We have recently observed fluorescence (FL) spectral diffusion of individual LH2 complexes of *Rps. acidophila* accompanied by changes of the spectral profile shape at room temperature (RT). The FL spectrum was observed to broaden upon a shift of the peak wavelength from the intermediate value. Furthermore, the blue-shifted and intermediate spectral line shapes feature a conventional asymmetry – a marked long wavelength tail, while the red-shifted profiles exhibit a clear short wavelength wing. We associate these spectral changes with possible structural deformations of the antenna ring that induce the observed spectral evolution through the protein-pigment interactions. Our results are in line with the earlier room- (Bopp, *et al.* 1999) and low-temperature single-molecule FL experiments (van Oijen, *et al.* 2000) that were interpreted in terms of dynamic structural

deformations and they conform with the generally accepted notion of proteins as mobile entities, undergoing a variety of structural deformations on a number of time-scales (Frauenfelder, *et al.* 1991).

We quantitatively explained the observed FL profile shapes in the framework of the modified Redfield theory by varying the realization of the static energetic disorder taken from a random Gaussian distribution. An alternative model of partially correlated static disorder in combination with a smaller amount of random disorder was ascertained to interpret low-temperature single-molecule FL excitation experiments (Ketelaars, *et al.* 2001, Matsushita, *et al.* 2001, van Oijen, *et al.* 2000, van Oijen, *et al.* 1999). However, such a model results in a weakly allowed lowest excitonic state, which is in contradiction with the observed superradiance of bacterial LHCs at low temperature (Monshouwer, *et al.* 1997). We recently demonstrated that this model does not reproduce the observed changes of a single LH2 FL spectral shape at RT (Novoderezhkin, *et al.*, submitted).

The different FL profile shapes of LH2 of *Rps. acidophila* are due to a subtle interplay between static and dynamic disorder. The static disorder determines the eigenvalues of the exciton states and consequently their splitting and the equilibrium thermal population. It also redistributes the oscillator strength between the states. The dynamic disorder red shifts the exciton components of the emission due to phonon-induced reorganization effects, thus changing the splitting between exciton levels, and also broadening them. The higher exciton states are additionally broadened due to dynamic disorder causing the ultrafast relaxation between the exciton states, as observed in time-resolved experiments (Novoderezhkin, *et al.* 1999). Thus, the extent to which dynamic disorder influences the spectral profiles of the exciton states depends on the particular realization of the static disorder, which for each exciton level is characterized by the participation ratio (PR), with $PR = \sum_n (c_n^k)^4$, where c_n^k are wavefunction amplitudes. Note that the value of PR (dependent on the realization of the static disorder) is the inverse of the coherent delocalisation length of the exciton state. In this view, the exciton state localization (determined by the static disorder) is a measure of the effective phonon bath coupling to an exciton state and consequently of the phonon-induced broadening and reorganization shift (Novoderezhkin, *et al.*, submitted).

In the present study we further extend our previous work of interpreting the FL spectral profile shape and underlying electronic structure of single LHCs. Here we investigate a variety of different bacterial LHCs, for which either crystal structures or accurate structural models exist enabling the modelling of the FL profile. With this we demonstrate the general applicability of the proposed model for different types of bacterial LHCs.

MATERIALS AND METHODS

LH2 complexes of *Rps. acidophila* 10050 and *Rs. molischianum* DSM120 were purified as described previously (Gall and Robert 1999). LH2 complexes of *Rb. sphaeroides* were purified as in (Olsen, *et al.* 2003). LH1 membranes were purified according to (Olsen, *et al.* 1994) and

complexes extracted as described elsewhere (Rutkauskas, *et al.*, submitted).

The preparation of the diluted sample for the actual measurement and the procedure of the oxygen removal from the sample was described previously (Rutkauskas, *et al.*, submitted). All the measurements were conducted at 5° C to prolong the survival time of less stable species.

Isolated LH2 and LH1 complexes were immobilized on a glass microscope coverslip as described previously (Rutkauskas, *et al.* 2005). The confocal setup utilized to acquire sequences of single-molecule FL spectra is based on a commercial biological microscope described earlier (Rutkauskas, *et al.* 2005). It has an option of 594 nm excitation with a constant power and random polarization He-Ne laser (Melles Griot, 05SYR810-230). With this wavelength, the LHCs are excited in their Q_x absorption band allowing the use of the longpass glass filter RG715 (Edmund Optics Ltd, 46065) with transmission extended further to the blue as compared to the previously utilized broadband interference filter for 800 nm excitation. The effect of the objective achromatism on the excitation and signal collection efficiency is compensated for by decollimating the 594 nm beam before the objective.

RESULTS

Previously we obtained FL time series of spectra of individual LH2 complexes of *Rps. acidophila* with the aim of observing the spectral dynamics as a signature of possible underlying structural changes. We observed FL spectra with various peak wavelengths and widths, and the characteristic relationship between these spectroscopic parameters was interpreted on the basis of the disordered exciton model of the B850 ring in combination with the Redfield theory that describes excitation relaxation in the excitonic manifold (Rutkauskas, *et al.* 2005, Rutkauskas, *et al.* 2004). Various peak wavelengths were connected to different realizations of static energetic disorder of pigment site energies that in turn were associated with conformational substates of pigment protein.

In the present work several bacterial LHCs were measured upon 594 nm excitation, using a level of absorbed energy equivalent to 2 μ W of 800 nm excitation for LH2 of *Rps. acidophila*. Compared to the previous data analysis, where we investigated averaged single-molecule FL profiles in a few selected peak wavelength intervals, here we consider distributions of peak wavelength and averages of corresponding distributions of spectral width and asymmetry (see below). This results in a characteristic continuous dependency between these spectral parameters, which allows for a more detailed and specific inter-species comparison.

Figure 1 displays a greyscale-coded distribution of spectral full width at half of the maximum (fwhm) values corresponding to values of FL peak wavelength (FLP) for LH2 of *Rps. acidophila*. Similar histograms were obtained for LH2 of *Rb. sphaeroides*, and *Rs. molischianum* and for LH1 of *Rb. sphaeroides*. The histogram in Figure 1 is constructed by

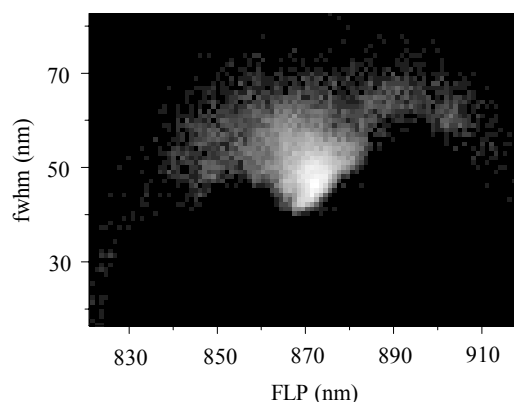


Figure 1. Logarithmic greyscale distribution of single-molecule FL spectral fwhm depending on FLP. The histogram resulted from the data set obtained for LH2 of *Rps. acidophila* acquired with 6 μ W at 800 nm excitation at 20° C and containing about 21000 spectra.

fitting all spectra obtained under the same experimental conditions, collecting spectra with their FLP within selected narrow intervals and building distributions of the corresponding values of fwhm. This is done throughout the range of occurring FLPs so that we obtain distributions of fwhm corresponding for each value of FLP. Figure 1 is generated by combining all of these distributions and applying a greyscale-coding for the frequency of occurrence of fwhms corresponding to a defined FLP interval. It does not demonstrate a one-to-one relationship between the FLP and the fwhm, *i.e.*, individual spectra with the same FLP exhibit a distribution of fwhm values. However, averaging of fwhms corresponding to each FLP results in a relation between \langle fwhm \rangle and FLP with a characteristic and fully reproducible shape.

A number of such dependences calculated from datasets obtained for LH2 of *Rps. acidophila* with different excitation intensities is displayed in Figure 2A. It appears that, notwithstanding the broad distribution in the vertical direction in Figure 1, the essential features of the \langle fwhm \rangle -FLP relation are very well reproducible between the different datasets. The curve has a conspicuous dip at intermediate values of FLP (corresponding to the maximum of the FLP distribution) and rises on each side. This implies that on the average the spectrum is broader for FLP values deviating from the intermediate value around 870 nm. The decline of the curve on each side is an experimental artefact of the FL filter applied to the experiments upon 800 nm excitation, which is apparent from a comparison with the data obtained upon 594 nm excitation (Figure 2B). At FLPs moderately deviating from 870 nm, the curves are relatively smooth, but they become noisier in the wings due to the limited statistics of the strongly shifted spectral occurrences. The experiment applying intense excitation (1-6 μ W) was aimed at probing these occurrences which may be associated with naturally existing, but less accessible conformational substates of the pigment-protein. Below we will show that in our calculations, similar strongly shifted spectra are generated only in the case when a large

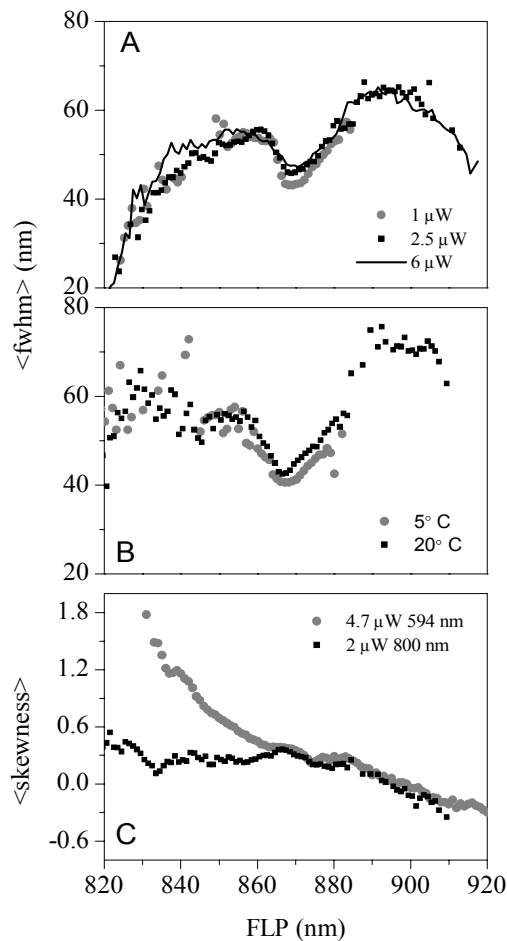


Figure 2. LH2 of *Rps. acidophila*. Top panel: <fwhm>-FLP dependences at different excitation intensities at 800 nm at 20° C; middle panel: <fwhm>-FLP relations at two different temperatures and the same excitation intensity of 4.7 μW at 594 nm; lower panel: <skewness>-FLP curves with two different excitation wavelengths at 20° C.

number of the static disorder realizations are sampled. This implies that such strongly shifted spectra are not necessarily associated with conformational substates that are difficult to access, but that they correspond to rare realizations of the disorder.

With the increased excitation intensity the <fwhm>-FLP curve lifts (Figure 2A) for a subset of spectra with peak wavelength between 865 and 875 nm. This indicates an overall broadening of the spectrum, which is probably due to an increased spectral diffusion that is fast compared to the spectral integration time and which is not observed as a spectral jumping but contributes to the spectral width.

The average spectral width also depends on the temperature of the measurement: spectra at 5° C are generally slightly narrower than those at 20° C (Figure 2B), which is again probably related to a faster spectral diffusion at 20° C as in the case of the increased

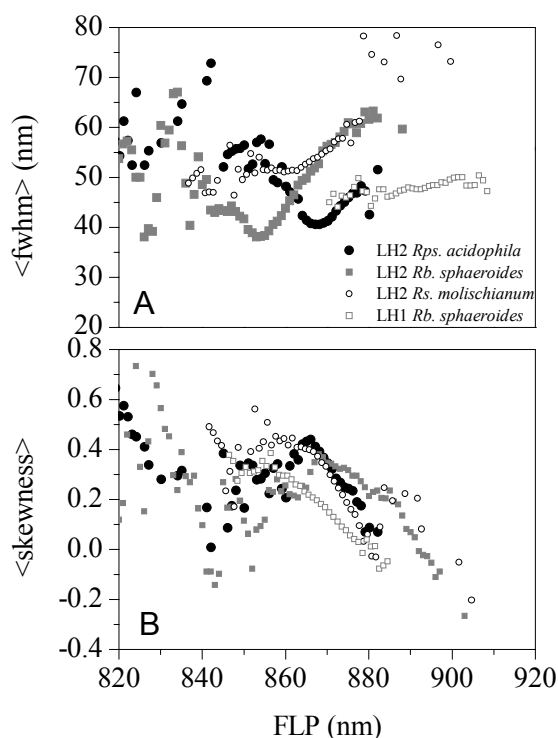


Figure 3. Top panel: <fwhm>-FLP, lower panel: <skewness>-FLP relations for different bacterial light-harvesting complexes. Different complexes are denoted by: LH2 of *Rps. acidophila* black circles, *Rb. sphaeroides* grey squares, *Rs. molischianum* hollow circles, and LH1 of *Rb. sphaeroides* hollow squares. All measurements were conducted at 5° C with 594 nm excitation.

excitation intensity.

Since the spectral width does not fully characterize the spectral profile, we also trace the dependence of the average spectral skewness as a function of FLP (Figure 2C). A simple relationship connects the skewness as a fit parameter of the skewed Gaussian function and the half widths at half of the maximum on both sides of the maximum: fit parameter $b = \ln(\delta_2 / \delta_1)$, where δ_2 (δ_1) is the long-(short-)wavelength half width. In the case of a slight asymmetry ($b \ll 1$), this yields $b \approx 2(\delta_2 - \delta_1) / \delta$, where $\delta = \delta_2 + \delta_1$ is the fwhm. From a comparison of the <skewness>-FLP curves obtained with different excitation wavelengths (for LH2 of *Rps. acidophila* shown in Figure 2C) it appears that the 800 nm FL filter distorts the experimental FL profiles bluer than 860 nm. At the same time, the two curves overlay very well to the red of 860 nm demonstrating the reproducibility of this dependency. Generally the spectral asymmetry is rather constant for blue and intermediate FLPs and diminishes for the red-shifted profiles.

The <fwhm>-FLP curves for the LH2 of *Rps. acidophila*, *Rb. sphaeroides*, *Rs. molischianum* and LH1 of *Rb. sphaeroides* are compared in Figure 3A. The four species were measured with the same equivalent excitation intensity at 594 nm, which enables a direct comparison of the

spectral correlations. The curves obtained for LH2 of *Rps. acidophila* and *Rb. sphaeroides* have a similar general shape, although the position of the dip is different along both axes: spectra of *Rb. sphaeroides* with intermediate FLP are narrower and shifted to the blue relative to those of *Rps. acidophila*. The positions of these dips are close to the respective bulk FL maxima. At the same time both curves display a similar rise slope at both sides of the dip.

The curve for LH2 of *Rs. molischianum* has only a small discernible minimum, and it displays a rising wing on the red side but is rather flat in the blue. LH1 of *Rb. sphaeroides* exhibits only a weak dependence of the spectral profile width on the peak wavelength. It should be noted that spectra of LH2 of *Rs. molischianum* with intermediate peak wavelength (around 860 nm) are broader than those of any of the remaining three complexes. In that sense LH1 with the most recurring FLP around 890 nm comes second: broader than LH2 of *Rps. acidophila* and *Rb. sphaeroides*, and narrower than LH2 of *Rs. molischianum*.

Figure 3B demonstrates the <skewness>-FLP dependences for all four LHC species investigated. The curves obtained for LH2 of *Rb. sphaeroides*, *Rs. molischianum*, and LH1 of *Rb. sphaeroides* are offset along the FLP axis to match their FLP distribution maxima to that of *Rps. acidophila*. All dependences exhibit the same trend: the spectrum is more symmetric when shifting to the red and features a negative asymmetry at strongly red-shifted FLP values. It also appears that for the same corresponding FLP, LH2 of *Rb. sphaeroides* exhibits the largest asymmetry, *Rps. acidophila* and *Rs. molischianum* are of similar skewness with intermediate magnitude, while LH1 is the most symmetric.

MODELLING AND DISCUSSION

In the following we do not attempt to interpret the temperature and excitation intensity dependences of the <fwhm>-FLP curves since these are rather subtle effects which are much less pronounced than the inter-species variation. However, the curves shown in Figures 2A-C demonstrate that in general the dependence of the average spectral fwhm and skewness on the FLP of a single complex is very reproducible for different experimental datasets. Thus in the following we calculate the <fwhm>-FLP and <skewness>-FLP dependences for different types of complexes with the aim of explaining these general trends.

Modelling the B850 ring

The model of the B850 antenna is the same as used for LH2 of *Rps. acidophila* in previous work (Rutkauskas, *et al.* 2005, Rutkauskas, *et al.* 2004, Novoderezhkin, *et al.*, submitted). In the B850 ring Coulombic interactions between the pigments lead to an excitonic coupling that coherently delocalizes a single excitation over a number of pigments in the ring. The eigenvalues (exciton energy levels) and eigentstates (exciton wavefunctions) of the system are obtained by diagonalizing the one exciton Hamiltonian and assuming the presence of a random Gaussian static energetic disorder. The spectral profiles of the exciton states are acquired based on the modified Redfield theory (Mukamel 1995, Zhang, *et al.* 1998) by

taking into account the dynamic disorder associated with the phonon coupling to the electronic transition of a chromophore. A subtle interplay between the two types of disorder determines the overall FL profile as described in the Introduction.

The line-broadening function and the reorganization shift of an exciton state are expressed in terms of a spectral density in the site representation and are proportional to the PR of the exciton state. Compared to the previous work (Rutkauskas, *et al.* 2005, Rutkauskas, *et al.* 2004) this spectral density in the site representation $C(\omega)$ is approximated by a sum of four (instead of just one) Brownian oscillators:

$$C(\omega) = \sum_{m=1-4} 2\lambda_{0m} \frac{\omega\gamma_{0m}}{\omega^2 + \gamma_{0m}^2}$$

with characteristic frequencies $\gamma_{0m} = [70 \ 160 \ 450 \ 1200] \text{ cm}^{-1}$ and couplings $\lambda_{0m} = [80 \ 170 \ 300 \ 400] \text{ cm}^{-1}$. This form of the spectral density yields more realistic values of phonon-induced line-broadening and reorganization shift. As a result, we have obtained a better quantitative fit of the average FL profiles with different peak wavelengths for LH2 of *Rps. acidophila* (Figure 4). FL profiles, blue- or red-shifted from the intermediate peak wavelength of 870 nm, are characterized by specific changes of the exciton structure and are accompanied by changes in the spectral width and asymmetry as was described in detail

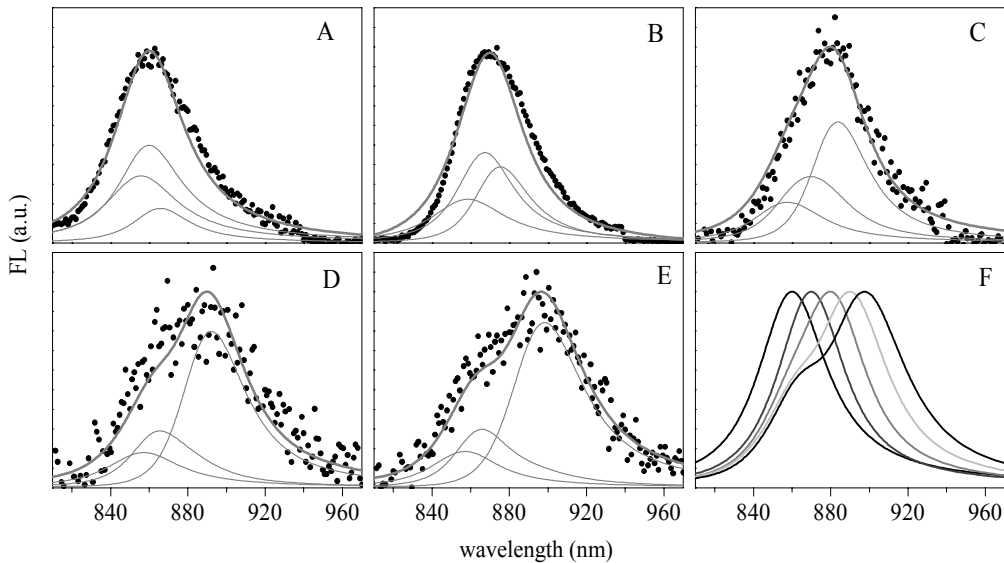


Figure 4. FL profiles for the LH2 complex of *Rps. acidophila* at 20° C averaged over realizations with peak wavelengths around: (A) 860, (B) 870, (C) 880, (D) 890, and (E) 900 nm. Experimental data is represented by black points; calculated spectra (thick grey solid lines) are shown together with the contributions from the three lowest exciton components (thin grey solid lines). The static disorder $\sigma = 350 \text{ cm}^{-1}$. In (F) calculated FL profiles with different peak positions from (A-E) are put together; thermally averaged PR values of 0.1, 0.14, 0.18, 0.22, 0.27 correspond to the increasingly red-shifted fluorescence profiles.

previously (Rutkauskas, *et al.* 2005, Rutkauskas, *et al.* 2004).

Since the FL spectral profile is determined by the interplay of the static disorder and the phonon-induced shifts and broadenings, we hypothesize that the differences in the <fwhm>-FLP and <skewness>-FLP curves observed for different species can be reproduced by varying the width of the disorder distribution and the magnitude of the phonon coupling. In the following we present the variation of the relations between the spectral parameters depending on the static and dynamic disorder. Additionally we investigate the effect of the size of the antenna ring, opening of the ring, and partially correlated disorder due to elliptical deformation. These model calculations are for the B850 ring of the LH2 of *Rps. acidophila* consisting of 9 dimeric subunits with the model parameters as specified above unless stated otherwise. Subsequently experimental and calculated <fwhm>-FLP and <skewness>-FLP dependences are compared for different types of complexes.

Variation of the model parameters

The simulated effects of the static and dynamic energetic disorder on the spectral properties are presented in Figures 5A and B, respectively. It appears that increasing the amount of static disorder, on the average, increases the spectral width, flattens the characteristic dip in the <fwhm>-FLP dependency at intermediate FLP (around 870 nm for the LH2 of *Rps. acidophila*) and shifts it to the red. It also diminishes the spectral asymmetry. Larger dynamic disorder has a similar and even more pronounced effect on the overall spectral width, induces a larger dip in the <fwhm>-FLP relationship and shifts it strongly to the red, Figure 5B. It also reduces the spectral asymmetry. Thus both types of disorder exert similar effects on the spectral properties except that the larger static disorder flattens the <fwhm>-FLP dependency while increasing the dynamic disorder makes the dip more noticeable.

The effects of the ring size and deletion of a few dimeric subunits are shown in Figures 5C and D, respectively. Increasing the antenna size from 9 to 16 dimeric subunits somewhat flattens the <fwhm>-FLP dependency, shifts it to the blue, and on the average narrows down the spectrum noticeably. At the same time the spectral asymmetry alters insignificantly. Opening of the ring by removing 4 dimeric subunits from an antenna containing 16 dimers does not significantly influence either the <fwhm>-FLP or <skewness>-FLP relationships (Figure 5D).

The result of the partially correlated disorder due to the elliptical deformation of the ring is presented in Figure 5E. The applied ellipticity model and its consequences for the electronic structure of the ring are described in more detail in (Novoderezhkin, *et al.*, submitted). The increased contribution of this disorder lowers the <fwhm>-FLP curve, deepens the characteristic minimum while the general shape of the curve remains similar to that in the absence of the correlation. The spectral asymmetry is lowered although at even larger values of the correlated disorder the skewness of the red-shifted profiles increases.

Having observed the general trends of the <fwhm>-FLP and <skewness>-FLP relations depending on the model parameters we may now define the sets of parameters

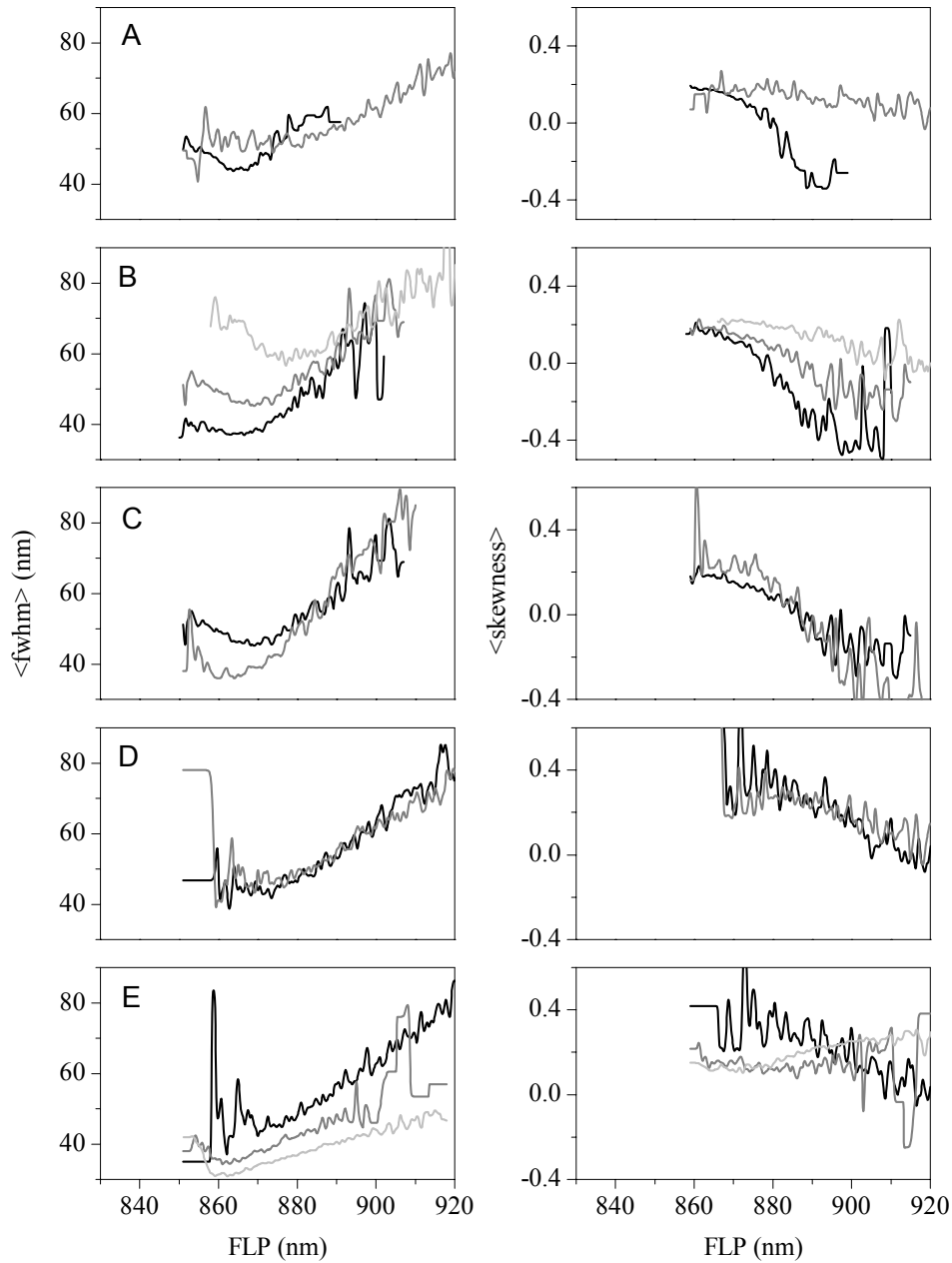


Figure 5. The effect of the variation of different model parameters. A: the static disorder, black curves correspond to $\sigma = 270 \text{ cm}^{-1}$ and grey curves to $\sigma = 630 \text{ cm}^{-1}$; B: the dynamic disorder, $\sigma = 370 \text{ cm}^{-1}$, different curves correspond to the couplings to phonons multiplied by a factor of 0.7 (black), 1 (grey), and 1.5 (light grey); C: the antenna size, $\sigma = 370 \text{ cm}^{-1}$, black is a ring of 9 dimeric subunits, and grey 16; D: opening of the ring, $\sigma = 630 \text{ cm}^{-1}$, black is a full ring of 16 dimeric subunits, and grey is an incomplete ring of 12 subunits; E: partially correlated disorder, the ring consists of 16 dimeric subunits, black corresponds to a ratio of the random static (cm^{-1}) and correlated disorder (cm^{-1}) of 630/0, grey to 250/330, light grey to 80/500.

that best reproduce the spectral correlations for different types of complexes.

LH2 of *Rps. acidophila*

The pigment site energies and inter-pigment couplings in the B850 antenna of LH2 of *Rps. acidophila* are the same as in the previous work (Rutkauskas, *et al.* 2005, Rutkauskas, *et al.* 2004), (Novoderezhkin, *et al.*, submitted). Figure 6 contrasts the experimental and simulated $\langle \text{fwhm} \rangle$ -FLP and $\langle \text{skewness} \rangle$ -FLP dependences for this complex. The simulation reproduces the experimentally observable trends, although the calculated values of the spectral asymmetry are somewhat lower than the measured ones. This is probably because the relaxation-induced broadening of the $k = \pm 1$ states introduces broad Lorentzian wings to these exciton components. It might be that in reality the relaxation cannot be described by a simple exponential decay (as supposed in a modified Redfield theory) and the actual line shapes are closer to Gaussian.

For the FLP near the intermediate value of 870 nm, the spectra feature a minimal fwhm (43-45 nm) (Figure 6) and a regular asymmetry with a sharp blue wing and a broader red tail ($b > 0$) (Figures 4B, 6). Such asymmetry is determined by the more intense long wavelength phonon wing in the emission of each of the exciton levels (Figure 4B).

Blue-shifted spectra exhibit almost the same asymmetry, but larger fwhm (up to 52-56 nm) (Figure 4A). They correspond to a realization of the disorder for which the splitting between the exciton levels is relatively small so that the $k = \pm 1$ levels are populated and this dominates the whole profile. As the emitting levels are mainly the higher energy exciton states, they are broadened due to the predominantly downhill relaxation, giving rise to a broadened overall spectrum.

Red-shifted profiles are determined by a disorder pattern associated with an increased splitting and red shift of the exciton energy levels. The coherence of the exciton states is significantly perturbed, all exciton states and especially the lowest $k = 0$ are strongly localized. An increase of the gap between the exciton states leads to a more populated

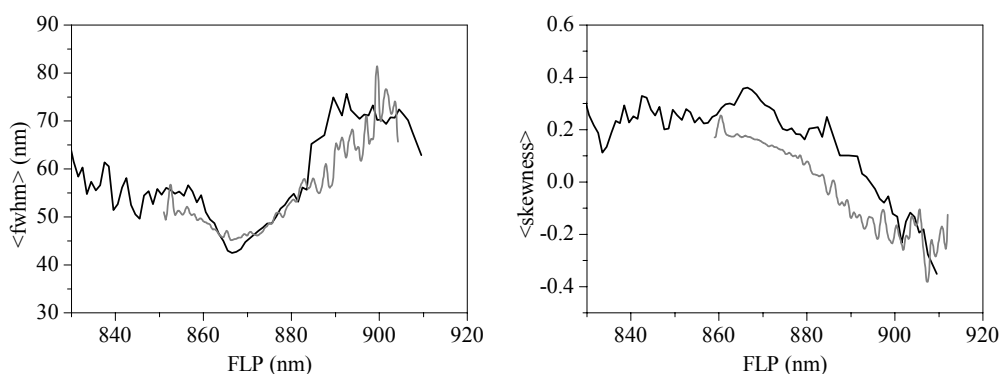


Figure 6. Comparison of the experimental and simulated $\langle \text{fwhm} \rangle$ -FLP and $\langle \text{skewness} \rangle$ -FLP dependences for the LH2 of *Rps. acidophila* at 20°C. The experimental data is represented by black and the calculation by gray curves. The static disorder $\sigma = 350 \text{ cm}^{-1}$.

lowest $k = 0$ state so that even at RT it starts to dominate the overall FL profile. Localization of the lowest state increases its effective coupling to the phonons: the energy level is further broadened and additionally red-shifted due to reorganization effects. As a result, the FL profile, with the FLP value increasing from 890 to 900 nm, broadens and even changes the sign of the asymmetry parameter. Such extremely red-shifted spectra have a shoulder around 860 nm (seen both in the experimental and calculated spectra, Figure 4D, E) due to contributions from the higher exciton states, whereas the intense emission from the lowest exciton state determines the peak at 890-900 nm. Note, that individual exciton components still have their “normal” asymmetry, but the whole FL profile becomes sharper in the red, giving rise to a negative value of the skewness starting from FLP of 885 nm in the calculation and 890-895 nm in the measurement.

LH2 of *Rs. molischianum*

For LH2 of *Rs. molischianum* the pigment-pigment couplings are the same as those in the previous modelling of this complex (Novoderezhkin, *et al.* 2003): the energies of the $1\alpha1\beta$, $1\beta,2\alpha$, $1\alpha2\alpha$, $1\beta,2\beta$, and $1\alpha2\beta$ interactions are +273, +249, -38, -26, and +10 cm^{-1} , respectively.

The site energies are blue-shifted by 10 nm relative to those of LH2 of *Rps. acidophila* to reproduce the overall shift of the bulk absorption spectrum. We found that the differences between LH2 of *Rps. acidophila* and *Rs. molischianum* in inter-pigment coupling and/or antenna size (9 and 8 dimeric subunits, respectively) do not significantly influence the structure of the lowest exciton band. Instead, the broader FL spectrum of *Rs. molischianum* (Figure 3A) could be explained by an increase of the static and/or dynamic (phonon-induced) disorder. As was shown above the increase in the static disorder generally broadens the FL spectrum and diminishes the dip in the $\langle \text{fwhm} \rangle$ -FLP relationship. Thus, the $\langle \text{fwhm} \rangle$ -FLP and $\langle \text{skewness} \rangle$ -FLP dependences could be reproduced with the same

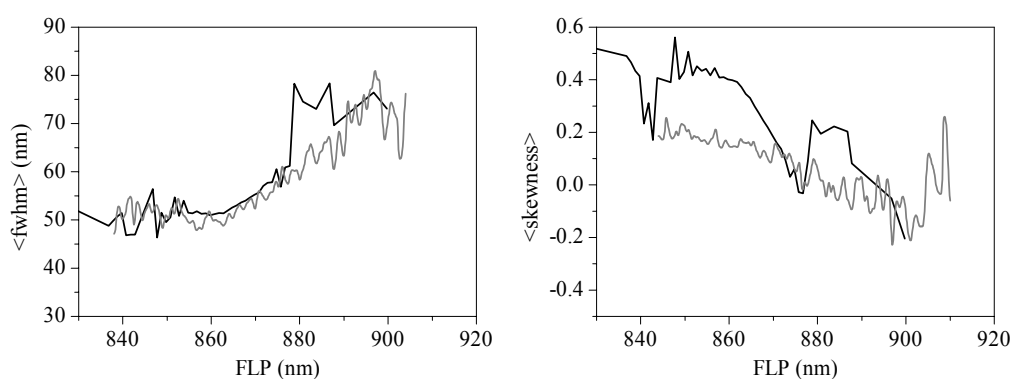


Figure 7. Comparison of the experimental and simulated $\langle \text{fwhm} \rangle$ -FLP and $\langle \text{skewness} \rangle$ -FLP dependences for the LH2 of *Rs. molischianum* at 5° C. Spectral density is the same as for *Rps. acidophila*, but the static disorder is increased to $\sigma = 500 \text{ cm}^{-1}$. The experimental data is represented by black and the calculation by grey curves.

spectral density as for the *Rps. acidophila*, but with the static disorder distribution broadened from 350 to 500 cm^{-1} (Figure 7).

The broadened static disorder distribution produces fewer realizations of the delocalized exciton structure (the “blue” realizations in the case of LH2 of *Rps. acidophila*). Generally speaking this has a dramatic effect on the dynamics of the most delocalized blue-shifted realizations. The rate of the relaxation between the exciton states (proportional to their delocalisation length) is significantly reduced, diminishing the relaxation-induced broadening of the blue-shifted FL profiles. The result is a flatter $\langle \text{fwhm} \rangle$ -FLP dependence at shorter wavelengths (compare Figures 6 and 7).

A second consequence of the smaller delocalization is an increase in the effective phonon coupling to the exciton states. This lifts the $\langle \text{fwhm} \rangle$ -FLP dependence so that the $\langle \text{fwhm} \rangle$ corresponding to the intermediate FLP value of 860 nm is 50-52 nm for *R. molischianum* instead of 43-45 nm at around 870 nm for *Rps. acidophila*.

LH2 of *Rb. sphaeroides*

In the model calculations above it was demonstrated that the decrease of the static or dynamic disorder has a similar effect on the average spectral width but for the former the dip in the $\langle \text{fwhm} \rangle$ -FLP dependency increases while it decreases for the latter. The curve can be lowered by scaling both types of disorder simultaneously thus preserving its general shape. Indeed, the data for LH2 of *Rb. sphaeroides* can be explained by proportionally reducing the values of the static and dynamic disorder for LH2 of *Rps. acidophila* (i.e., the site inhomogeneity σ and the couplings λ_{0m}) by a factor of 1.2 (Figure 8). The average FLP was adjusted by introducing an 8 nm blue shift of the unperturbed site energies of *Rb. sphaeroides* compared to *Rps. acidophila*. The character of the $\langle \text{fwhm} \rangle$ -FLP and $\langle \text{skewness} \rangle$ -FLP dependences is the same as for the LH2 of *Rps. acidophila* (compare Figures 6 and 8), which is related to the fact that the ratio between the static and dynamic disorder values is the

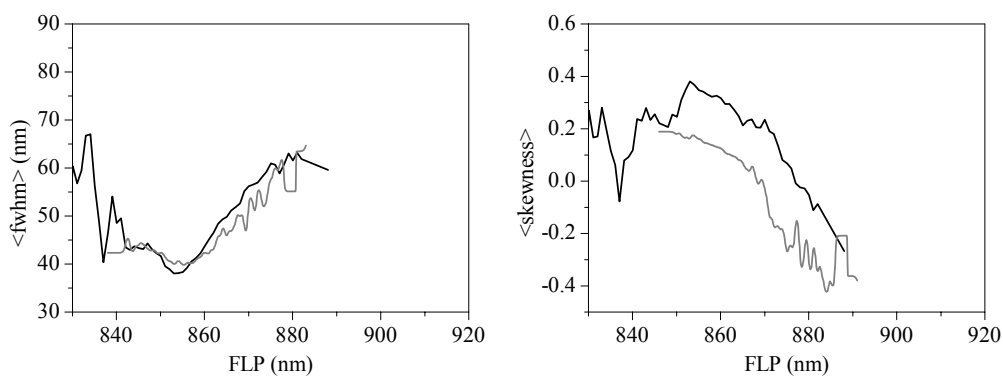


Figure 8. Analogous to Figure 6, but for the LH2 of *Rb. sphaeroides* at 5° C. Spectral density is the same as for *Rps. acidophila*, but the exciton-phonon couplings λ_{0m} are reduced by a factor of 1.2 and the static disorder is decreased to $\sigma = 300 \text{ cm}^{-1}$. The experimental data is represented by black and the calculation by grey curves.

same for both species. At the same time, the decrease of the absolute value of the static disorder results in a generally narrower FL spectral profile for LH2 of *Rb. sphaeroides*.

LH1 of *Rb. sphaeroides*

Within the range of the observable FLP values (870-910 nm), the $\langle \text{fwhm} \rangle$ of the LH1 complex varies less than for any of the investigated complexes. This dependence is to some extent similar to that of the LH2 of *Rps. molischianum*: the $\langle \text{fwhm} \rangle$ is rather constant at relatively blue FLPs for both complexes. This resemblance probably stems from the similarity of the binding pocket of the B850 (B870) BChls *a* in the two complexes (Germeroth, *et al.* 1993), implying a similar character of the protein-pigment interactions determining the electronic structure and the associated FL spectrum of the ring (Robert, *et al.* 2003, Cogdell, *et al.* 2002). Thus, the general trend of only a weakly rising $\langle \text{fwhm} \rangle$ -FLP relationship can be obtained by increasing the static disorder value as in the case of LH2 of *Rs. molischianum*. At the same time other factors that were found to influence the spectral properties of the antenna have to be considered for a better fit.

The LH1 complex has been recognized to be remarkably heterogeneous, exhibiting a variety of different shapes and ring sizes, especially in the absence of the reaction center complex which is normally enclosed by LH1 (Bahatyrova, *et al.* 2004). It is not unreasonable to expect that even an additional purification step with the size-exclusion column did not result in a completely homogeneous sample consisting of particles of the same ring size and/or shape. Thus what we observe may correspond to the spectral response of a mixture of different structural fractions. However, it was demonstrated above that the variation of the B850 ring size from 9 to 16 dimeric subunits increases the slope of the $\langle \text{fwhm} \rangle$ -FLP curve at the edges (Figure 5C), whereas removal of up to 4 dimeric subunits from the intact ring of 16 dimers does not noticeably affect the spectral properties (Figure 5D).

Introducing the partially correlated disorder due to the elliptical deformation decreases

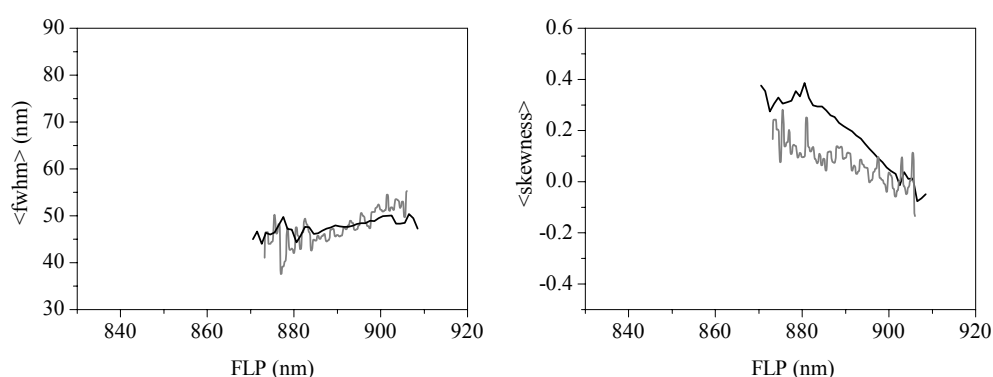


Figure 9. LH1 of *Rb. sphaeroides* at 5° C. The ring contains 32 pigments, the spectral density is the same as for *Rps. acidophila*, but the exciton-phonon couplings λ_{0m} are increased by a factor of 1.28, and site energies of every 5th pigment are obtained from a Gaussian distribution of the width of 380 cm⁻¹. The experimental data is represented by black and the calculation by grey curves.

the slope of the dependence on the red side but significantly lowers the curve and introduces its steeper rise in the blue (Figure 5E). In addition the <skewness>-FLP dependence becomes rather flat, which is unlike the measured relationship.

Thus it appears that making allowances for either the larger size of the LH1 ring or its opening or elliptical deformation do not improve the overlay of the measurement and simulation.

We also investigated the possibility of the correlation of the site energies of a certain number of neighboring pigments. Figure 9 demonstrates the best fit between the experimental and calculated curves in the case of the correlation radius of 5 pigments, which implies that the site energies of every 5th pigment in the ring are obtained at random from the Gaussian distribution whereas the site energies of the intermediate sites are calculated from a cubic spline dependence connecting those points. Such refinement of the model allows to reproduce a very slight rise of the FLP-<fwhm> dependence and the descent of the FLP-<skewness> relationship.

It is possible that after some modification the model will allow us to further refine the interpretation of the behavior of the LHCs. This could be a more complicated heterogeneity of the site energies, in case of LH1 – an alternative spectral density function taking into account the coupling to the low-frequency vibrations that have been determined experimentally (Novoderezhkin, *et al.* 2000), or generalization of the modified Redfield approach by including 1-2 vibrational coordinates yielding different relaxation dynamics and different spectral line shapes. However, these possibilities deserve a separate study and will be explored in a following manuscript.

CONCLUSIONS

We have obtained collections of FL spectra of individual bacterial LHCs of several different types. Every dataset exhibited a distribution of the spectral peak wavelength and a corresponding spectral width and asymmetry. Each species exhibited a characteristic dependence between the average spectral width and asymmetry and the corresponding peak wavelength that was highly reproducible for different datasets of the same type of complex. Ensemble averaging was circumvented by acquiring spectra of individual complexes, which allowed the direct comparison of the experimental and simulated spectra, as calculated with different realizations of static disorder to reproduce the occurrence of different spectral peak wavelengths. By varying the amount of the static disorder and the strength of the phonon coupling to the electronic transitions, the same basic model of a disordered excitonically coupled pigment ring quantitatively reproduced the dependences between the spectral parameters for the LH2 ring of different complexes. At the same time, a correlation between the pigment site energies has to be assumed to interpret the corresponding dependences for the LH1 complex.

REFERENCES

- Alden, R. G., Johnson, E., Nagarajan, V., Parson, W. W., Law, C. J., and Cogdell, R. J. (1997) Calculations of spectroscopic properties of the LH2 bacteriochlorophyll-protein antenna complex from *Rhodospseudomonas acidophila*. *J. Phys. Chem. B.* 101, 4667-4680.
- Bahatyrova, S., Frese, R. N., van der Werf, K. O., Otto, C., Hunter, C. N., and Olsen, J. D. (2004) Flexibility and size heterogeneity of the LH1 light harvesting complex revealed by atomic force microscopy - functional significance for bacterial photosynthesis. *J. Biol. Chem.* 279, 21327-21333.
- Bopp, M. A., Sytnik, A., Howard, T. D., Cogdell, R. J., and Hochstrasser, R. M. (1999) The dynamics of structural deformations of immobilized single light-harvesting complexes. *Proc. Natl. Acad. Sci. U.S.A.* 96, 11271-11276.
- Cogdell, R. J., Howard, T. D., Isaacs, N. W., McLuskey, K., and Gardiner, A. T. (2002) Structural factors which control the position of the Q_y absorption band of bacteriochlorophyll a in purple bacterial antenna complexes. *Photosynth. Res.* 74, 135-141.
- Frauenfelder, H., Sligar, S. G., and Wolynes, P. G. (1991) The energy landscapes and motions of proteins. *Science.* 254, 1598-1603.
- Gall, A., and Robert, B. (1999) Characterization of the different peripheral light-harvesting complexes from high- and low-light grown cells from *Rhodospseudomonas palustris*. *Biochemistry.* 38, 5185-5190.
- Germeroth, L., Lottspeich, F., Robert, B., and Michel, H. (1993) Unexpected similarities of the B800-850 light-harvesting complex from *Rhodospirillum rubrum* to the B870 light-harvesting complexes from other purple photosynthetic bacteria. *Biochemistry.* 32, 5615-5621.
- Hu, X. C., Ritz, T., Damjanovic, A., and Schulten, K. (1997) Pigment organization and transfer of electronic excitation in the photosynthetic unit of purple bacteria. *J. Phys. Chem. B.* 101, 3854-3871.
- Ketelaars, M., van Oijen, A. M., Matsushita, M., Köhler, J., Schmidt, J., and Aartsma, T. J. (2001) Spectroscopy on the B850 band of individual light-harvesting 2 complexes of *Rhodospseudomonas acidophila* I. Experiments and Monte Carlo simulations. *Biophys. J.* 80, 1591-1603.
- Koepke, J., Hu, X. C., Muenke, C., Schulten, K., and Michel, H. (1996) The crystal structure of the light-harvesting complex II (B800-850) from *Rhodospirillum rubrum*. *Structure.* 4, 581-597.
- Matsushita, M., Ketelaars, M., van Oijen, A. M., Köhler, J., Aartsma, T. J., and Schmidt, J. (2001) Spectroscopy on the B850 band of individual light-harvesting 2 complexes of *Rhodospseudomonas acidophila* II. Exciton states of an elliptically deformed ring aggregate. *Biophys. J.* 80, 1604-1614.
- McDermott, G., Prince, S. M., Freer, A. A., Hawthornthwaite, A. M., Papiz, M. Z., Cogdell, R. J., and Isaacs, N. W. (1995) Crystal structure of an integral membrane light-harvesting complex from photosynthetic bacteria. *Nature.* 374, 517-521.
- Monshouwer, R., Abrahamsson, M., van Mourik, F., and van Grondelle, R. (1997) Superradiance and exciton delocalization in bacterial photosynthetic light-harvesting systems. *J. Phys. Chem. B.* 101, 7241-7248.
- Mukamel, S. (1995) Principles of Nonlinear Optical Spectroscopy, Oxford University Press, New York.
- Novoderezhkin, V., Monshouwer, R., and van Grondelle, R. (1999) Disordered exciton model for the core light-harvesting antenna of *Rhodospseudomonas viridis*. *Biophys. J.* 77, 666-681.
- Novoderezhkin, V., Monshouwer, R., and van Grondelle, R. (2000) Electronic and vibrational coherence in the core light-harvesting antenna of *Rhodospseudomonas viridis*. *J. Phys. Chem. B.* 104, 12056-12071.

- Novoderezhkin, V., Monshouwer, R., and van Grondelle, R. (1999) Exciton (de)localization in the LH2 antenna of *Rhodobacter sphaeroides* as revealed by relative difference absorption measurements of the LH2 antenna and the B820 subunit. *J. Phys. Chem. B.* 103, 10540-10548.
- Novoderezhkin, V., Wendling, M., and van Grondelle, R. (2003) Intra- and interband transfers in the B800-B850 antenna of *Rhodospirillum rubrum*: Redfield theory modeling of polarized pump-probe kinetics. *J. Phys. Chem. B.* 107, 11534-11548.
- Olsen, J. D., Robert, B., Siebert, A., Bullough, P. A., and Hunter, C. N. (2003) Role of the C-terminal extrinsic region of the alpha polypeptide of the light-harvesting 2 complex of *Rhodobacter sphaeroides*: a domain swap study. *Biochemistry.* 42, 15114-15123.
- Olsen, J. D., Sockalingum, G. D., Robert, B., and Hunter, C. N. (1994) Modification of a hydrogen bond to a bacteriochlorophyll a molecule in the light-harvesting 1 antenna of *Rhodobacter sphaeroides*. *Proc. Natl. Acad. Sci. U.S.A.* 91, 7124-7128.
- Papiz, M. Z., Prince, S. M., Howard, T., Cogdell, R. J., and Isaacs, N. W. (2003) The structure and thermal motion of the B800-850 LH2 complex from *Rps. acidophila* at 2.0 Å resolution and 100 K: new structural features and functionally relevant motions. *J. Mol. Biol.* 326, 1523-1538.
- Robert, B., Cogdell, R. J., and van Grondelle, R. (2003) The light-harvesting system of purple bacteria. In Light-harvesting antennas in photosynthesis. Green, B. R. and Parson, W. W., Eds., Vol. 13, Kluwer academic publishers, Dordrecht, Netherlands.
- Rutkauskas, D., Novoderezhkin, V., Cogdell, R. J., and van Grondelle, R. (2005) Fluorescence spectroscopy of conformational changes of single LH2 complexes. *Biophys. J.* 88, 422-435.
- Rutkauskas, D., Novoderezhkin, V., Cogdell, R. J., and van Grondelle, R. (2004) Fluorescence spectral fluctuations of single LH2 complexes from *Rhodospseudomonas acidophila* strain 10050. *Biochemistry.* 43, 4431-4438.
- Sauer, K., Cogdell, R. J., Prince, S. M., Freer, A., Isaacs, N. W., and Scheer, H. (1996) Structure-based calculations of the optical spectra of the LH2 bacteriochlorophyll-protein complex from *Rhodospseudomonas acidophila*. *Photochem. Photobiol.* 64, 564-576.
- Scholes, G. D., and Fleming, G. R. (2000) On the mechanism of light harvesting in photosynthetic purple bacteria: B800 to B850 energy transfer. *J. Phys. Chem. B.* 104, 1854-1868.
- van Grondelle, R., and Novoderezhkin, V. (2001) Dynamics of excitation energy transfer in the LH1 and LH2 light-harvesting complexes of photosynthetic bacteria. *Biochemistry.* 40, 15057-15068.
- van Oijen, A. M., Ketelaars, M., Köhler, J., Aartsma, T. J., and Schmidt, J. (2000) Spectroscopy of individual light-harvesting 2 complexes of *Rhodospseudomonas acidophila*: diagonal disorder, intercomplex heterogeneity, spectral diffusion, and energy transfer in the B800 band. *Biophys. J.* 78, 1570-1577.
- van Oijen, A. M., Ketelaars, M., Köhler, J., Aartsma, T. J., and Schmidt, J. (1999) Unraveling the electronic structure of individual photosynthetic pigment-protein complexes. *Science.* 285, 400-402.
- Walz, T., Jamieson, S. J., Bowers, C. M., Bullough, P. A., and Hunter, C. N. (1998) Projection structures of three photosynthetic complexes from *Rhodobacter sphaeroides*: LH2 at 6 Å LH1 and RC-LH1 at 25 Å. *J. Mol. Biol.* 282, 833-845.
- Whitmarsh, J., and Govindjee (1999) The photosynthetic process. In Concepts in photobiology: photosynthesis and photomorphogenesis. Singhal, G., Renger, G., Sopory, S., Irrgang, K.-D. and Govindjee, Eds., Narosa Publishers, New Delhi.
- Wu, H. M., Rätsep, M., Lee, I. J., Cogdell, R. J., and Small, G. J. (1997) Exciton level structure and energy disorder of the B850 ring and the LH2 antenna complex. *J. Phys. Chem. B.* 101, 7654-7663.

Zhang, W. M., Meier, T., Chernyak, V., and Mukamel, S. (1998) Exciton-migration and three-pulse femtosecond optical spectroscopies of photosynthetic antenna complexes. *J. Chem. Phys.* 108, 7763-7774.

Conformational relaxation of single bacterial light-harvesting complexes

Danielis Rutkauskas, and Rienk van Grondelle

ABSTRACT

In this work we investigate “natural” (occurring in the absence of excitation) spectral diffusion after a spectral jump of individual peripheral light-harvesting complexes 2 of a purple bacterium *Rhodospirillum rubrum*. After about a quarter of all the observed spectral jumps a complex spontaneously evolves in the absence of the agitating excitation light resulting in a different spectroscopic state. This we associated with the natural conformational development of the pigment-protein which so far has not been observed for this type of complexes on a single-molecule level. The functional significance of such structural rearrangements is probably associated with the necessity for a light-harvesting complexes to adjust in the densely packed photosynthetic membrane. It also raises an intriguing question as to what are the implications of the concurrent changes of the spectral properties.

INTRODUCTION

Although textbooks frequently picture proteins as static structures, in reality, this is an oversimplification. Experimental evidence of protein motions (Careri, *et al.* 1979, Wagner 1983) has led to their characterization as “screaming and kicking” (Weber 1975). Despite this awareness, the study of protein motions, their classification and characterization, and investigation of their biological function is still at an embryonic stage because of the bewildering variety of possible protein motions and intrinsic complexity of even the simplest molecules. Even a relatively short chain of amino acids is characterized by a large number of degrees of freedom and exhibits an enormous variety of different sets of coordinates of protein atoms. These are called conformations or conformational substates and are associated with variations of the potential energy of the system. In a sense conformations are analogous to energy levels of much simpler systems such as atoms. In the protein world the concept of a one dimensional energy level scheme is substituted for a much more imaginative idea of a conformational energy hypersurface or landscape which is a function of all degrees of freedom in the system. For illustration usually a one dimensional cross section of this conformational landscape is presented to demonstrate an arrangement of interchanging energy barriers and minima in between them. Each conformation corresponds to a minimum while a transition to a different conformation is associated with crossing of an energy barrier (Frauenfelder, *et al.* 1991).

Despite this developing conceptual framework little is known about the conformational landscape and dynamics in it of any actual protein. In that sense probably one of the best studied proteins is the relatively small protein myoglobin the biological function of which is to reversibly bind molecular oxygen. Its properties have been investigated extensively during the last few decades with an array of different techniques, which resulted in a model for the energy landscape and ensuing dynamics of the complex protein behavior (Ansari, *et al.* 1985, Austin, *et al.* 1975, Bourgeois, *et al.* 2003). In this model all the relevant conformational states are classified into a hierarchy of tiers according to the size of the energy barriers separating different conformations and consequently also according to the extent of the structural rearrangement required to alter the conformation. The zero tier consists of a limited number of well characterized so-called taxonomic states with well-defined biological function. Furthermore, each of these states can be subdivided into a number of substates that are no longer characterized individually but treated as a statistical distribution. It is suggested that this hierarchical structure can be further extended by structuring each minimum of a higher tier into a number of minima of the subsequent tier. While protein movements between conformations in the higher tiers are thought to be functionally significant, the function of the small conformational changes in the lower tiers is not clear.

The aim of the present study in combination with the previous work (Hofmann, *et al.* 2003, Rutkauskas, *et al.* 2005) is to obtain a glimpse of the natural protein motions of a membrane protein, the peripheral light-harvesting complex 2 (LH2) of the photosynthetic

purple bacterium *Rhodospseudomonas (Rps.) acidophila*. The function of LH2 is to capture solar light and transfer its energy to the reaction center protein, which initiates the charge separation reaction eventually leading to fixation of the absorbed energy in a stable chemical form (van Grondelle, *et al.* 1994).

The structure of LH2 has been resolved with atomic resolution (McDermott, *et al.* 1995): the complex is a highly symmetric ring of nine pigment-protein subunits, each containing two helical transmembrane polypeptides: the α -polypeptide on the inner and the β -polypeptide on the outer side of the ring. Closer to the C-terminal the protein binds a ring of 18 tightly coupled bacteriochlorophyll (BChl) *a* molecules with a center-to-center distance of less than 1 nm between neighboring pigments. This ring is responsible for the intense absorption of LH2 around 850 nm (B850 ring). A second ring of nine weakly interacting BChls *a* is located closer to the protein N-terminus and is largely responsible for the absorption peaking at 800 nm (B800 ring).

Thorough investigation of the electronic and energy transfer properties resulted in a consistent physical model of LH2 (Alden, *et al.* 1997, Hu, *et al.* 1997, Novoderezhkin, *et al.* 1999, Novoderezhkin, *et al.* 2003, Scholes and Fleming 2000, van Grondelle and Novoderezhkin 2001, Wu, *et al.* 1997). The two basic features of this model are the excitonic coupling between pigments and the static disorder of the pigment electronic transition energies, which arises from an intrinsic disorder of the protein.

The available crystal structure of LH2 is an average of many different conformations, and little is known about the dynamics of this complex on a slow (ms-s) time scale. Due to the protein-pigment interactions (Cogdell, *et al.* 2002, Robert, *et al.* 2003), changes of the pigment site energies and consequently fluorescence (FL) spectral properties are expected to be associated with the protein movements. Thus, an observable FL spectrum is indicative of the protein movements.

In our previous work we observed spontaneous and light-induced conformational changes; at present we aim to remove a complex from its initial state and to monitor the result of the subsequent natural spectral evolution, which is similar to the flash photolysis measurement on myoglobin (Frauenfelder, *et al.* 1989). However, since our experiment is conducted on individual light-harvesting complexes (LHCs), we avoid ensemble averaging that complicates the analysis and interpretation of the relevant kinetic traces. In this way, we gain direct information about the spontaneous pigment-protein motions.

MATERIALS AND METHODS

Purified LH2 complexes of *Rps. acidophila* 10050 were prepared as described earlier (Cogdell and Hawthornthwaite 1993, Halloren, *et al.* 1995). Stock solution of the sample in buffer (20 mM Tris-HCl (pH 8.0) and 0.1% lauryldimethylamine oxide (LDAO)) was divided into aliquots and kept at -80°C until thawed and used only once thus avoiding repetitive thawing and freezing. For immobilization of the complexes the stock solution was diluted with the same buffer to pM concentration. The buffer was deoxygenated and used to flush the

immobilized complexes. Dissolved oxygen was removed by first ventilating the buffer with nitrogen gas and at the same time stirring with a magnetic spinner for at least 0.5 h; the remaining oxygen was chemically removed by adding small amount of sodium dithionite without opening the deoxygenation chamber. Isolated LH2 complexes were immobilized on a standard microscope coverslip as described previously (Rutkauskas, *et al.* 2005). The confocal setup utilized to acquire sequences of single-molecule FL spectra was based on a commercial biological microscope as described earlier (Rutkauskas, *et al.* 2005).

RESULTS AND DISCUSSION

In our earlier work we obtained sequences of FL spectra of continuously illuminated individual bacterial LHCs (Rutkauskas, *et al.* 2005). For most complexes the spectral trace starts with the FL peak wavelength (FLP) close to 870 nm. This wavelength is the peak wavelength of the bulk spectrum and the most recurrent value in the FLP distribution of the single complexes. In the course of time the trace develops according to various scenarios. Transitions between different FLP values are associated with spontaneous and light-induced conformational changes of the pigment-protein. The light effect is due to the non-radiative relaxation of the excitation energy, which is transformed into vibrational modes and facilitates the potential energy barrier crossing in the conformational landscape.

FLP deviations from 870 nm are accompanied by the spectral broadening and the change of the spectral asymmetry. To explain these spectral variations we applied the disordered exciton model (Alden, *et al.* 1997, Hu, *et al.* 1997, Novoderezhkin, *et al.* 1999, Novoderezhkin, *et al.* 2003, Scholes and Fleming 2000, van Grondelle and Novoderezhkin 2001, Wu, *et al.* 1997), in which both the excitonic coupling between the pigments and the static disorder of the pigment electronic transition energies are taken into account. In this model, the observable spectral occurrences are associated with different realizations of the static disorder which are linked to structural conformations by means of the microscopic parameters such as hydrogen bonds to the functional groups of the BChl molecule. Although phenomenological, the model satisfactorily interprets the detected changes of the FLP and profile shape.

Furthermore, a significant fraction of the measured complexes exhibits FLP evolution through a number of quasi-stable states, *i.e.*, levels of distinctly different and relatively constant magnitude in the time trace. These surprisingly long-lived states (tens of seconds) we associated with conformations that are difficult to access but also difficult to escape from, and the applied high excitation intensity facilitates the transitions to and from these states. The duration of the quasi-stable states varies probably due to different heights of the conformational energy barriers and the probabilistic nature of the barrier crossing.

Introducing excitation at 594 nm instead of 800 nm allowed us to make a surprising observation of extremely blue-shifted states around 810 nm which we associated with the B850 ring being temporarily bleached and the B800 emitting the FL in the absence of the excitation energy transfer step (Rutkauskas, *et al.*, submitted). Such situation must be related

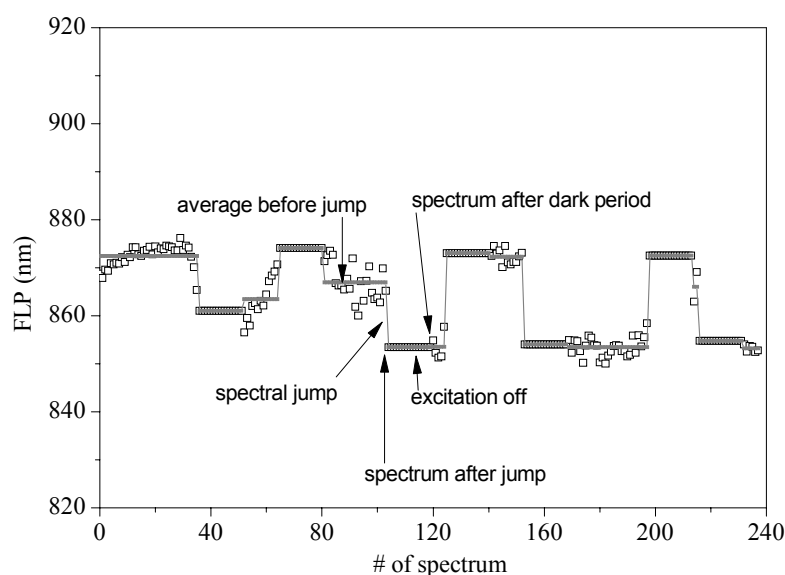


Figure 1. Example of FLP temporal trace with excitation switched off after the spectral jump larger than 10 nm. Grey trace marks average levels and periods with excitation blocked.

to the sizable structural rearrangement of the B850 ring. It is furthermore surprising as the bleaching of the B850 is often reversible.

The intense excitation accelerates conformational transitions into states that are difficult to access, but at the same time it will reinforce further evolution. The aim of the present work is to observe the natural conformational relaxation. To this end, excitation is blocked after a spectral jump (meaning conformational change has occurred) to allow the spontaneous evolution of the complex. Thus, a measurement consists of the acquisition of a FL spectrum, its fitting to obtain a value of FLP, which is then compared with the average of FLP values of the previous spectra. A spectral jump is detected if the difference between the newly acquired point in the FLP time trace and the average of the values of the previous points is larger than a selected threshold; in this way immediate (between subsequent spectra) and overall spectral changes are monitored. After a dark period the laser light is switched on again and the whole cycle is repeated: FLP of each collected spectrum is compared with the average of the preceding FLP values starting from the end of the last “dark” period and in case of a new spectral jump, the excitation is blocked again. An example of a resulting spectral time trace is presented in Figure 1. For clarity, periods of the FLP time trace in the absence of the excitation are filled with the value of the last spectrum acquired before the switch-off.

This experimental procedure allows the comparison of the spectral state before the laser light is switched off and the state immediately after the excitation is switched on again. Thus it yields information about the result of a natural conformational evolution during a period

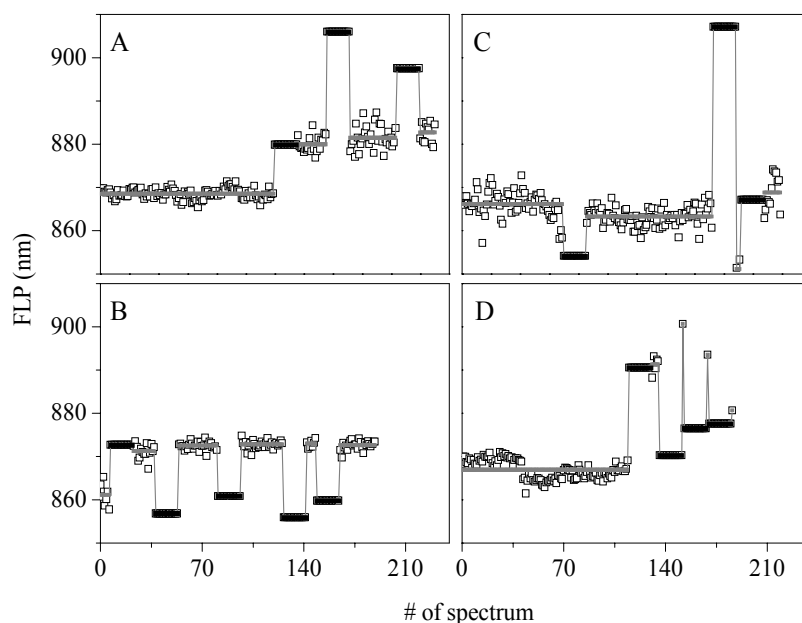


Figure 2. Examples of different scenarios of FLP traces. Traces A-C measured with $1 \mu\text{W}$ at 800 nm excitation, dark period of 15 spectra and threshold of the jump of 10 nm . Trace D – $3 \mu\text{W}$ and the rest of the parameters the same as for A-C. Dark periods are marked by black thick bar.

without excitation. We observed, as is not surprising given the complexity of the conformational landscape, a multitude of scenarios of this evolution. Figure 1 contains a trace with periods without excitation followed by a spectrum deviating insignificantly from the state before the switch off. This shows that during a dark period (equivalent to the duration of 15 spectra) the complex does not undergo a significant spontaneous development. Figure 2 shows some characteristic cases of changes among the conformational (spectral) substates. The complex in Figure 2A evolves through at least three states: while in the first state with FLP around 880 nm the complex does not change in the absence of the excitation although it is driven to a different state when the excitation is applied for some time. The other two states around 905 nm and 890 nm switch to the first state if left in the dark. Thus it appears that the conformational energy barriers separating the 880 nm state from the 890 nm and 905 nm states are asymmetric so that the forward transition is more difficult than the backward. At the same time once in the 880 nm state the complex is in a conformational energy minimum from which the transition to the initial 870 nm state is more difficult than a further evolution to redder states. Figure 2B is a surprising example of a complex cycling between a state with an intermediate FLP value around 870 nm and states around 860 nm ; transitions from 870 nm to 860 nm occur in the presence of the excitation light whereas the transition from 860 nm back to 870 nm occurs spontaneously (in the absence of the excitation light) again indicating the asymmetric character of the energy barrier between the states. The latter two are examples of spectral jumping to the red

and to the blue, respectively. However, they are not sufficient to draw conclusions about the general character of spontaneous evolution from the red or blue states. Figure 2C demonstrates the possibility of a drastic spontaneous change: the second state with an FLP value around 910 nm spontaneously moves to a state around 850 nm, and is driven back to the intermediate position by continuing excitation. Such scenario is at variance with the first example implying that the conformational energy landscape of the complex exhibits a multitude of routes for natural evolution. Finally, Figure 2D shows an example of a state with an intermediate value of FLP around 870 nm (second state in the trace) that spontaneously moves to a very short-lived state around 900 nm that is then driven by light to a different spectral position. This demonstrates that even from the initial conformation with the FLP around 870 nm a complex can spontaneously move to a state with a different spectral peak wavelength.

The general trends of the natural spectral evolution of different conformations are envisaged from the statistics of the FLP values before and after the dark period for all such periods. Figure 3 presents an example of a scattered distribution of such pairs of FLP values demonstrating the extent of spontaneous spectral diffusion of conformations with various FLPs. The two diagonal lines confine conformations that change by less than the value of the spectral jump threshold. Dots outside this area represent conformations spontaneously evolving into significantly different spectral states. Points above the confined area denote states that are relatively blue and change to relatively red. Points below this area indicate the opposite relationship between the initial and final states. The total number of conformations of these two types is of a comparable magnitude. Probably due to the limited statistics we do not observe a preferential FLP value of spectrally diffusive states: the points outside the confined area do not exhibit any clustering. However, most of those states are to the blue of 870 nm. This means that they are rather blue and exhibit a possibility of further evolution even more to the blue or on the contrary – to the red.

On the other hand, spectral states that diffuse insignificantly exhibit a distribution of

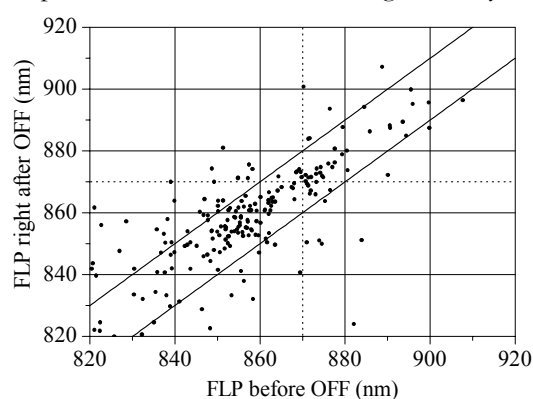


Figure 3. Distribution of pairs of FLP values before the excitation is blocked and after it is switched on. The measurement is with 3 μW excitation intensity, duration of the dark period is 15 spectra, and spectral jump threshold is 10 nm.

Table 1. Percentage of spontaneously evolving conformations.

Excitation intensity (μW)	# of measured molecules	Duration of the dark period [§]	Jump threshold (nm)	% of jumpy states in the dark [#]
3	118	15	10	29
3	170	15	20	21
3	138	30	20	22
1	147	15	10	27

[§]Duration of the dark period in the absence of the excitation is measured in a number of spectra.

[#]“% jumpy states in the dark” indicates a fraction of dark periods after which FLP value is different from that before blocking the excitation by more than the threshold value.

FLP values similar to that of the diffusive states. It also appears that conformations with the same value of FLP evolve rather differently since there is a wide spread of FLP values along the ordinate axis. Thus, the FLP value does not unambiguously determine the conformational evolution of a complex. This is probably related to the complexity of the potential energy hypersurface: from particular conformation a complex can move to a number of other conformations and a probabilistic character of the barrier crossing then results in different final states. Or it is possible that due to the complexity of the LH2 structure some of the spectroscopic states are degenerate, *i.e.*, multiple structural conformations correspond to the same spectroscopic state. In that case different initial conditions set diverse evolutionary pathways resulting in various final states.

It is further to be noticed that some conformations with an FLP either to the blue or to the red of 870 nm evolve to a state with FLP close to 820 nm. With 800 nm excitation a spectrum peaking at 820 nm is, in fact, just a wing of an even bluer spectrum strongly distorted by the FL filter. From the comparison of the datasets acquired with 800 and 594 nm excitation it appears that corresponding spectrum peaks around 810 nm and is associated with the temporary bleaching of the B850 ring, as was explained above. It is an astonishing observation that in a number of cases an intact light-harvesting antenna spontaneously moves to a state with a bleached B850 ring.

The overall statistics of spectrally diffusive conformations for the measurements with different excitation intensities and durations of the applied dark period is summarized in Table 1. The conformation is considered to be evolving if corresponding FLP values differ by more than a set threshold of the spectral jump. In general about 20-30% of the conformations evolve in the dark into significantly different spectral substates. For example, with an excitation intensity of 3 μW , a dark period duration of 15 spectra, and a jump threshold of 10 nm, 29% of the observed conformational substates move into conformations with an FLP value that differs from the FLP before the dark period by more than 10 nm. Therefore, spontaneous spectral diffusion is significant compared to the light-

induced effects.

Within the framework of the disordered exciton model spectra blue-shifted relative to the intermediate position of 870 nm correspond to coherently delocalized excitation relatively unperturbed by the static disorder when pigment site energies are of similar magnitude (Rutkauskas, *et al.* 2005, Rutkauskas, *et al.* 2004), (Novoderezhkin, *et al.*, submitted). Spectral blue shift also occurs when electronic transition energies are uniformly shifted to the blue. This can be due to such microscopic factors as breakage of hydrogen bonds to the acetyl carbonyl group of the BChls (Fowler, *et al.* 1994, Olsen, *et al.* 1994, Olsen, *et al.* 1997, Rutkauskas, *et al.*, submitted). The red-shifted spectral states correspond to a localized excitation seriously perturbed by the energetic disorder. A red shift of just one pigment site energy can significantly shift the whole spectrum to the red. This might be caused by the strengthening of the hydrogen bonding. Therefore transitions between the conformations of various FLP must be associated with significant and in some cases possibly correlated structural rearrangement of the binding pocket of one or a number of chromophores. Apparently at room temperature the protein lattice of a bacterial light-harvesting pigment-protein possesses sufficient vibrational energy to induce such changes.

CONCLUDING REMARKS

In this work we observed the spontaneous non-equilibrium relaxation of individual bacterial light-harvesting pigment-protein complexes from spectral states arbitrarily prepared by the excitation light. Application of a single-molecule technique is paramount since it allows the detection of spectral changes that otherwise would be masked by the ensemble averaging. The natural spectral development is associated with the transitions of the pigment-protein in its conformational potential energy landscape. To the best of our knowledge, these spontaneous pigment-protein motions, unaffected by the probe of the excitation light have, not been observed previously on a single-molecule level for the light-harvesting complexes. Transitions among spectral forms differing by tens of nanometers occur in the absence of the illumination. We discovered that a multitude of different spectral evolutionary scenarios are possible indicating an anticipated complexity of the conformational landscape. Such changes must be associated with significant structural rearrangements leading to an alteration of microscopic factors such as hydrogen bonding strength to the side groups of the BChls in the complex. That these alterations occur naturally is a consequence of an intriguing structural flexibility of the light-harvesting ring, which probably has some functional significance. One possibility is that complexes have to readjust in a densely packed photosynthetic membrane. It then remains open to speculation as to what are the implications of the changes of the spectral properties corresponding to these structural rearrangements.

REFERENCES

- Alden, R. G., Johnson, E., Nagarajan, V., Parson, W. W., Law, C. J., and Cogdell, R. J. (1997) Calculations of spectroscopic properties of the LH2 bacteriochlorophyll-protein antenna complex from *Rhodospseudomonas acidophila*. *J. Phys. Chem. B.* 101, 4667-4680.
- Ansari, A., Berendzen, J., Bowne, S. F., Frauenfelder, H., Iben, I. E. T., Sauke, T. B., Shyamsunder, E., and Young, R. D. (1985) Protein states and protein quakes. *Proc. Natl. Acad. Sci. U.S.A.* 82, 5000-5004.
- Austin, R. H., Beeson, K. W., Eisenstein, L., Frauenfelder, H., and Gunsalus, I. C. (1975) Dynamics of ligand-binding to myoglobin. *Biochemistry.* 14, 5355-5373.
- Bourgeois, D., Vallone, B., Schotte, F., Arcovito, A., Miele, A. E., Sciara, G., Wulff, M., Anfinrud, P., and Brunori, M. (2003) Complex landscape of protein structural dynamics unveiled by nanosecond Laue crystallography. *Proc. Natl. Acad. Sci. U.S.A.* 100, 8704-8709.
- Careri, G., Fasella, P., and Gratton, E. (1979) Enzyme dynamics – statistical physics approach. *Ann. Rev. Biophys. Bioeng.* 8, 69-97.
- Cogdell, R. J., and Hawthornthwaite, A. M. (1993) Preparation, purification and crystallization of purple bacterial antenna complexes. Vol. 1, Academic Press, New York.
- Cogdell, R. J., Howard, T. D., Isaacs, N. W., McLuskey, K., and Gardiner, A. T. (2002) Structural factors which control the position of the Q_y absorption band of bacteriochlorophyll a in purple bacterial antenna complexes. *Photosynth. Res.* 74, 135-141.
- Fowler, G. J. S., Sockalingum, G. D., Robert, B., and Hunter, C. N. (1994) Blue shifts in bacteriochlorophyll absorbency correlate with changed hydrogen-bonding patterns in light-harvesting 2 mutants of *Rhodobacter sphaeroides* with alterations at alpha-Tyr-44 and alpha-Tyr-45. *Biochem. J.* 299, 695-700.
- Frauenfelder, H., Sligar, S. G., and Wolynes, P. G. (1991) The energy landscapes and motions of proteins. *Science.* 254, 1598-1603.
- Frauenfelder, H., Steinbach, P. J., and Young, R. D. (1989) Conformational relaxation in proteins. *Chem. Scripta.* 29A, 145-150.
- Halloren, E., McDermott, G., Lindsay, J. G., Miller, C., Freer, A. A., Isaacs, N. W., and Cogdell, R. J. (1995) Studies on the light-harvesting complexes from the thermotolerant purple bacterium *Rhodospseudomonas cryptolactis*. *Photosynth. Res.* 44, 149-155.
- Hofmann, C., Aartsma, T. J., Michel, H., and Köhler, J. (2003) Direct observation of tiers in the energy landscape of a chromoprotein: a single-molecule study. *Proc. Natl. Acad. Sci. U.S.A.* 100, 15534-15538.
- Hu, X. C., Ritz, T., Damjanovic, A., and Schulten, K. (1997) Pigment organization and transfer of electronic excitation in the photosynthetic unit of purple bacteria. *J. Phys. Chem. B.* 101, 3854-3871.
- McDermott, G., Prince, S. M., Freer, A. A., Hawthornthwaite, A. M., Papiz, M. Z., Cogdell, R. J., and Isaacs, N. W. (1995) Crystal structure of an integral membrane light-harvesting complex from photosynthetic bacteria. *Nature.* 374, 517-521.
- Novoderezhkin, V., Monshouwer, R., and van Grondelle, R. (1999) Exciton (de)localization in the LH2 antenna of *Rhodobacter sphaeroides* as revealed by relative difference absorption measurements of the LH2 antenna and the B820 subunit. *J. Phys. Chem. B.* 103, 10540-10548.
- Novoderezhkin, V., Wendling, M., and van Grondelle, R. (2003) Intra- and interband transfers in the B800-B850 antenna of *Rhodospirillum rubrum*. Redfield theory modeling of polarized pump-probe kinetics. *J. Phys. Chem. B.* 107, 11534-11548.

- Olsen, J. D., Sockalingum, G. D., Robert, B., and Hunter, C. N. (1994) Modification of a hydrogen bond to a bacteriochlorophyll a molecule in the light-harvesting 1 antenna of *Rhodobacter sphaeroides*. *Proc. Natl. Acad. Sci. U.S.A.* 91, 7124-7128.
- Olsen, J. D., Sturgis, J. N., Westerhuis, W. H. J., Fowler, G. J. S., Hunter, C. N., and Robert, B. (1997) Site-directed modification of the ligands to the bacteriochlorophylls of the light-harvesting LH1 and LH2 complexes of *Rhodobacter sphaeroides*. *Biochemistry*. 36, 12625-12632.
- Robert, B., Cogdell, R. J., and van Grondelle, R. (2003) The light-harvesting system of purple bacteria. In Light-harvesting antennas in photosynthesis. Green, B. R. and Parson, W. W., Eds., Vol. 13, Kluwer academic publishers, Dordrecht, Netherlands.
- Rutkauskas, D., Novoderezhkin, V., Cogdell, R. J., and van Grondelle, R. (2005) Fluorescence spectroscopy of conformational changes of single LH2 complexes. *Biophys. J.* 88, 422-435.
- Rutkauskas, D., Novoderezhkin, V., Cogdell, R. J., and van Grondelle, R. (2004) Fluorescence spectral fluctuations of single LH2 complexes from *Rhodospirillum rubrum* strain 10050. *Biochemistry*. 43, 4431-4438.
- Scholes, G. D., and Fleming, G. R. (2000) On the mechanism of light harvesting in photosynthetic purple bacteria: B800 to B850 energy transfer. *J. Phys. Chem. B.* 104, 1854-1868.
- van Grondelle, R., Dekker, J. P., Gillbro, T., and Sundström, V. (1994) Energy-transfer and trapping in photosynthesis. *Biochim. Biophys. Acta.* 1187, 1-65.
- van Grondelle, R., and Novoderezhkin, V. (2001) Dynamics of excitation energy transfer in the LH1 and LH2 light-harvesting complexes of photosynthetic bacteria. *Biochemistry*. 40, 15057-15068.
- Wagner, G. (1983) Characterization of the distribution of internal motions in the basic pancreatic trypsin-inhibitor using a large number of internal NMR probes. *Q. Rev. Biophys.* 16, 1-57.
- Weber, G. (1975) Energetics of ligand binding to proteins. *Adv. Protein Chem.* 29, 1-83.
- Wu, H. M., Rätsep, M., Lee, I. J., Cogdell, R. J., and Small, G. J. (1997) Exciton level structure and energy disorder of the B850 ring and the LH2 antennal complex. *J. Phys. Chem. B.* 101, 7654-7663.

Summary

In this thesis we present the study of spectral fluorescence properties of individual photosynthetic bacterial light-harvesting complexes in physiological conditions with the aim of investigating spontaneous structural fluctuations. The crystal structures of two types of these complexes are known with atomic resolution, revealing a surprisingly symmetric arrangement of the light-absorbing pigment molecules (bacteriochlorophylls and carotenoids) coordinated by the protein scaffold. In photosynthesis the function of the light-harvesting complexes is to capture the solar light and transfer its energy to the other components of the photosynthetic machinery, which ultimately results in the synthesis of the life-sustaining carbohydrates.

A fluorescence spectrum of a ring of chromophores in close proximity is predominantly determined by two factors: inter-pigment excitonic interaction, which is dependent on the geometrical arrangement of the chromophores, and also pigment site energies that are tuned by the surrounding protein. Thus the key idea in this work is that the conformational (structural) condition of the light-harvesting complex is associated with the observable fluorescence spectrum. Therefore also the changes of the fluorescence spectrum are indicative of the structural permutations in the complex.

In an ensemble of complexes structural changes are not synchronized. Thus corresponding spectral fluctuations are averaged out. This ensemble averaging is nevertheless circumvented in the single-molecule experiment, where we obtain sequences of fluorescence spectra of single light-harvesting complexes, immobilized and immersed in a buffer, at constant excitation power and ambient conditions. Earlier experiments have demonstrated that at room temperature pigment-protein complexes are permanently bleached within a few seconds in the presence of the atmospheric oxygen. Therefore we take great care to remove the dissolved oxygen in order to prolong the fluorescent time of the complexes.

Chapters 3 and 4 present the initial results on the LH2 complex of *Rhodospseudomonas acidophila* bacterium. We observe correlated changes of the fluorescence spectral peak wavelength, width and asymmetry on a second time scale. The spectrum was found to broaden when shifting either to the blue or to the red from the intermediate peak wavelength and become more symmetric for redder peak wavelengths. These alterations are indicative of corresponding slow structural changes. We also make a remarkable observation of distinctly different and long-living (tens of seconds) spectral states, which we associate with conformations of the pigment-protein that are difficult to escape from. The link between the spectral and structural changes is established by the phenomenological model,

which takes into account the excitonic interaction between the pigments, the static disorder of the pigment electronic transition (site) energies, and the excitonic relaxation described by the modified Redfield theory. The observable spectral shapes and peak wavelengths are explained by assuming different realizations of the static disorder.

Although we aim at observing “natural” structural changes, the necessity of exciting a complex with laser light interferes with its spontaneous evolution due to a significant amount of thermal energy released through the non-radiative relaxation of the absorbed excitation. The light-induced effect is noticeable in the increase of the number of spectral jumps with the higher excitation intensity. Thus what we observe is a consequence of natural and light-induced conformational changes.

Spontaneous spectral evolution was obtained in a modified experiment, where the laser excitation is blocked after a spectral jump occurs thus allowing the natural development as described in Chapter 8. It appears that in the dark about a quarter of the spectral states evolves into significantly different spectral states indicating spontaneous conformational changes. This demonstrates that the fraction of spontaneous changes is rather significant.

A more detailed account of electronic configurations of light-harvesting complexes corresponding to various spectral line shapes is given in Chapter 5. A spectral profile is determined by the interplay of the static and dynamic disorder. The aforementioned observable correlation between the spectral parameters of the peak wavelength, width and asymmetry is explained on the basis of this interplay. In Chapter 7 it is demonstrated that the same basic model adequately explains spectral correlations for different types of complexes. It appears that realizations of the weak static disorder, where pigment site energies differ little, correspond to a blue-shifted fluorescence profile. Realizations of stronger disorder with the site energies deviating from the average value in a partially correlated manner and by less than the coupling between pigments result in spectra with intermediate peak wavelength. A strongly red-shifted spectrum is associated with the pigment site energies perturbed in uncorrelated manner by more than the inter-pigment coupling. It can also result from a strong red shift of an electronic transition of just one pigment.

We try to approach the problem of the microscopic basis of the observed spectral changes by comparing the frequency of spectral jumping for a few types of light-harvesting complexes with available structural models as explained in Chapter 6. Spectral fluctuations are associated with structural changes by assuming the strengthening or weakening of the hydrogen bonds between the protein scaffold and the functional groups of bacteriochlorophylls. Differences in the spectral flexibility of various complexes are due to different strengths of this hydrogen bonding and also different structural flexibility associated with the size of the antenna ring and hydrogen bonding network stabilizing the macromolecule.

Summarizing, we have observed the anticipated spectral fluctuations which reinforces the idea of a protein being a mobile entity. Accompanying correlations of spectral parameters could be explained based on the disordered exciton model in accordance with the previous

measurements on ensembles of complexes. Different spectral realizations were associated with various patterns of static disorder of pigment site energies that were suggested to be due to the strengthening or weakening of the relevant hydrogen bonds. However, due to an intrinsic complexity of the investigated pigment-proteins the relation between the structural conformation and the corresponding fluorescence spectrum is ambiguous thus leaving open to discussion the question as to what are the precise structural configurations observed in our experiments.

Samenvatting

De dynamische organisatie van bacteriële fotosynthetische licht-verzamelende complexen: fluorescentie microscopie

In dit proefschrift presenteren wij de studie van de spectrale fluorescentie eigenschappen van individuele bacteriële licht-verzamelende complexen onder physiologische omstandigheden, met als doel spontane structurele fluctuaties te onderzoeken. De kristalstructuren van twee typen van dit soort complexen zijn bekend met atomaire resolutie, en onthullen dat er een verbazingwekkende symmetrische ordening bestaat van de licht absorberende pigment molekulen (bacterichlorophyllen en carotenoiden) en dat zij gecoördineerd/gecontroleerd worden door het omringend eiwit. De functie van de licht-verzamelende complexen in het fotosynthetische proces is om zonlicht in te vangen en deze energie over te dragen naar de andere componenten van de fotosynthetische machine, om uiteindelijk levensonderhoudende koolhydraten te produceren.

Een fluorescentiespectrum van een ring van chromoforen die dicht op elkaar zitten wordt voornamelijk veroorzaakt door twee factoren: inter-pigment excitonische interactie, wat afhankelijk is van de ruimtelijke ordening van de chromoforen, en de pigment site-energieën die door het omringende eiwit worden bepaald. De hoofdgedachte in dit werk is daarom dat de structurele toestand van het licht-verzamelend complex direct verbonden is met het meetbare fluorescentiespectrum. De veranderingen in het fluorescentiespectrum zijn daarom ook een aanwijzing voor de structurele permutaties in het complex.

Structurele veranderingen in een ensemble van complexen lopen niet synchroon. De corresponderende spectrale fluctuaties komen daarom gemiddeld op hetzelfde uit. Dit gemiddeld over het ensemble op hetzelfde uitkomen wordt hoe dan ook omzeild door het één-molekuul-experiment, waarmee we opeenvolgende fluorescentiespectra kunnen verkrijgen van afzonderlijke licht-verzamelende complexen, geïmmobiliseerd en ondergedompeld in een buffer, geëxciteerd met constant vermogen en bij kamer temperatuur. Eerdere experimenten hebben aangetoond dat bij kamer temperatuur binnen een paar seconden pigment-eiwit complexen permanent gebleekt worden in de aanwezigheid van omgevings-zuurstof. Daarom wordt er nadrukkelijk zorg voor gedragen om al het opgeloste zuurstof te verwijderen om de fluorescentietijd van de complexen de verlengen.

In hoofdstuk 3 en 4 worden de eerste/voorlopige resultaten van het LH2 complex van de *Rhodospseudomonas acidophila* bacterie gepresenteerd. Wij observeren gecorreleerde veranderingen tussen de piek-golflengte, wijde en symmetrie van het fluorescentiespectrum op een seconde tijdsschaal. Het spectrum werd breder als er zowel naar het blauw als naar

het rood van de tussenliggende piek-golflengte werd verschoven, en werd meer symmetrisch voor meer rode piek-golflengtes. Deze wijzigingen zijn indicaties van daarmee corresponderende langzame structurele veranderingen. Tevens maken we een opmerkelijke observatie van duidelijk verschillende en lang levende (tientallen seconden) spectrale toestanden, die we associëren met pigment-eiwit conformaties waaruit moeilijk te ontsnappen is. De verbinding tussen de spectrale en structurele veranderingen wordt gemaakt met het fenomenologische model, wat de excitonische interactie tussen pigmenten, de statische wanorde van de pigment elektronische overgangs (site) energie, en de excitonische relaxatie die wordt beschreven door de aangepaste Redfield theorie in het model meenemen. De meetbare spectrale vormen en piek-golflentes worden verklaard door verschillende realisaties van statische wanorde te veronderstellen.

Alhoewel we ernaar streven om "natuurlijke" structurele veranderingen te zien, is er de noodzaak om een complex aan te slaan met laserlicht, wat interfereert met haar spontane evolutie, veroorzaakt door een significante hoeveelheid thermische energie wat vrijkomt bij de niet-stralingsovergangen van de geabsorbeerde excitatie. Het licht-geïnduceerde effect is waar te nemen door een toename van het aantal spectrale sprongen met toenemende excitatie intensiteit. Wat wij observeren is daardoor een gevolg van natuurlijke en licht-geïnduceerde vormveranderingen.

Spontane spectrale evolutie werd verkregen middels een aangepast experiment, waarbij de laser-excitatie geblokkeerd wordt na een spectrale sprong, dus door het toestaan van de natuurlijke ontwikkeling zoals beschreven in hoofdstuk 8. Het blijkt dat in de donkere toestand ongeveer een kwart van de spectrale toestanden evolueert in significant andere spectrale toestanden, wijzend op spontane vormveranderingen. Dit demonstreert dat de fractie van spontane veranderingen nogal beduidend is.

Een meer gedetailleerde benadering van de elektronische toestanden van licht-verzamelande complexen behorende bij verscheidene spectrale lijn-vormen wordt gegeven in hoofdstuk 5. Een spectraal profiel wordt vastgesteld door de interactie tussen de statische en dynamische wanorde. De eerder genoemde meetbare correlatie tussen de spectrale parameters van de piek-golflengte, wijde en asymmetrie wordt uitgelegd op basis van deze interactie. In hoofdstuk 7 wordt aangetoond dat hetzelfde basismodel deze spectrale correlaties voor verschillende typen complexen toereikend uitlegd. Het lijkt erop dat realisaties van de zwakke statische wanorde, waarbij de koppeling tussen de pigment site energien weinig verschilt, overeenkomen met een blauwverschuiving van het fluorescentieprofiel. Realisaties van sterkere wanorde waarbij de site-energien op een gedeeltelijk gecorreleerde afwijking van de gemiddelde waarde, maar minder dan de koppeling tussen de pigmenten, resulteert in spectra met een tussenliggende piek-golflengte. Een sterk rood verschoven spectrum wordt geassocieerd met de pigment site-energien die op een onafhankelijke wijze verstoord worden door meer dan de inter-pigment koppeling. Het kan ook veroorzaakt worden door een sterke rood verschuiving van de elektronische overgang van slechts één pigment.

We proberen om het probleem van de mikroskopische basis van de geobserveerde spectrale verandering te benaderen door de frequentie van de spectrale sprongen voor een paar typen

licht-verzamelande complexen met de beschikbare modellen zoals besproken in hoofdstuk 6. Spectrale veranderingen worden geassocieerd met structurele veranderingen door het aannemen van een versterking of verzwakking van de waterstofbruggen tussen het omringende eiwit en de functionele groepen bacteriochlorofyllen. Verschillen in spectrale flexibiliteit tussen verscheidene complexen worden veroorzaakt door verschillende sterkten van deze waterstofbruggen, verschillende structurele flexibiliteit die geassocieerd wordt met de grootte van de antenne-ring, en het waterstofbruggen netwerk wat het makromolekuul stabiliseert.

Samenvattend, hebben we de verwachte spectrale fluctuaties geobserveerd die het beeld van het eiwit als een flexibele eenheid versterken. Samenvallende correlaties tussen spectrale parameters kunnen uitgelegd worden door het wanordelijke excitonische model in overeenkomst met eerder gedane experimenten op ensembles van complexen. Verschillende spectrale realisaties werden geassocieerd met verscheidene patronen van statische wanorde van pigment site-energien die verondersteld waren te worden veroorzaakt door de versterking of verzwakking van de betreffende waterstofbruggen. Echter, de intrinsieke complexiteit van de onderzochte pigment-eiwitten veroorzaakt een dubbelzinnige relatie tussen de structurele conformatie en het daarmee corresponderende fluorescentiespectrum, waardoor de discussie over de vraag wat de exacte structurele configuraties die geobserveerd worden in onze experimenten open blijft.

Nawoord

According to a certain luminary “one does not remember his own life any better than the novel he has read”, and on a different occasion it has been remarked that everything is connected to everything else, then an attempt of adequately depicting the reasons culminating in the present circumstances, which appears to be an implication of this very last section, is rather futile. However, I genuinely desire to acknowledge and thank *people* who or whose presence possibly without them even knowing it helped me to produce this thesis.

Rienk, the professor of the group and my supervisor, to whom I feel indebted for having had the possibility of doing this project, and who facilitated a relaxed and creative atmosphere providing an incentive for a productive work.

Jos, an irreplaceable intermediary with the world of the mechanical workshop, whose cooperation to a large extent undermined the success of the project.

John Olsen, who not only provided the sample, but was patient and responsive to give invaluable biochemical advise as to how to properly treat it.

Erwin Peterman, from the very beginning counselling me in technical matters, which helped to avoid making too many trials and errors.

Vladimir Novoderezhkin, capable of envisaging regularity in the midst of apparent chaos, his involvement has initiated a new turn in the interpretation of the experimental data.

Julius Janušonis, with whom discussions have triggered a number of improvements in the analysis and presentation of the measurement observations.

Leonas Valkunas, so enthusiastic about the subject that it seduced me to visit Amsterdam as an exchange student for the first time and stay for a longer while afterwards.

Virgis Barzda, whom I owe having had the opportunity of a one-month experience in his lab, which was both great fun but also taught me the subtleties of the microscopy know-how.

Special thanks to Luuk who kindly agreed to translate the Summary to Dutch.

My present co-workers Kinga, Mariangela, Eli, Alisa, Daniel, Maxim, Cosimo, Jason, Sandrine, Toh, Magda, Kate, Rudi, Denitsa, Chantal, Olga, Elena, Dmitrij, Marloes, John, Jan, Henny and the former members of the group Bas, Lavanya, Stefania, Janne, Jante, Claudiu, Olaf, Frank, Markus, Anjali, Herbert, Miguel with some of whom our cooperation went beyond the cofferoom sit-ins.

Mikas, who provided a rare and very much needed feedback in the work discussions, but was also a cheerful company in extracurricular activities, bursting with pieces of folk wisdom in every mundane situation.

Manolis, a faithful referee of my manuscripts that imminently lacked articles, was a mindful company in so many after-conference trips and also encouraged me to somewhat soften the sharp “nude-brutality” edges; Nina, who did a brilliant work designing the cover for the thesis. And I am grateful to both of them for their friendly company.

Sofia, who kindly lent me a hand polishing the Introductions and thanks to whom I finally realized that the separation between the vague acquaintances and the lifetime friends has an infinitely more subtle gradation.

Jolanda and Raoul, who helped me to tame the stranger city of Amsterdam when I just started here.

Ruti, each time with a warm welcome whenever I went for a visit to Israel making it a totally different and more memorable experience.

Friends from OS: Liova, Jasas, Marius, Gitana, Aušra, Vika, Raselė, Irka, Žilvis, Edva, Aurutė who are all so different and yet an interaction with whom made me realize that I probably will never really travel further away than within a few kilometers from my home place.

Tomas, whom I could always count on for a company to go and explore Lithuanian nature beauty.

Julija, who challenged the world of the black-and-white dichotomy.

Lolita, whom I am grateful for that “moment in a half lit world”.

Lithuanian friends in Amsterdam: Akvilė, Martynas, Vida, André, Jolita, with whom I shared so many fun times.

At last and that only to emphasize the importance of it, I thank my family: my sister Lina, who hosted me during my returns to Vilnius and who managed to tolerate the accompanying outbursts of vocational debauchery, my parents, who were the ones to instill me with the idea of trespassing the imaginary and geographical boundaries and who remained a true support once I did, and my grandparents who were keen spectators of my successes.